1-1-1971

A theoretical and experimental investigation of deflections and bending moments in cantilever plates: With application to helical gear design.

Omer L. Hageniers
University of Windsor

INFORMATION TO USERS

This manuscript has been reproduced from the microfilm master. UMI films the text directly from the original or copy submitted. Thus, some thesis and dissertation copies are in typewriter face, while others may be from any type of computer printer.

The quality of this reproduction is dependent upon the quality of the copy submitted. Broken or indistinct print, colored or poor quality illustrations and photographs, print bleedthrough, substandard margins, and improper alignment can adversely affect reproduction.

In the unlikely event that the author did not send UMI a complete manuscript and there are missing pages, these will be noted. Also, if unauthorized copyright material had to be removed, a note will indicate the deletion.

Oversize materials (e.g., maps, drawings, charts) are reproduced by sectioning the original, beginning at the upper left-hand corner and continuing from left to right in equal sections with small overlaps.

ProQuest Information and Learning
300 North Zeeb Road, Ann Arbor, MI 48106-1346 USA
800-521-0600

A THEORETICAL AND EXPERIMENTAL INVESTIGATION OF DEFLECTIONS AND BENDING MOMENTS IN CANTILEVER PLATES: WITH APPLICATION TO HELICAL GEAR DESIGN

A Thesis
Submitted to the Faculty of Graduate Studies through the Department of Mechanical Engineering in Partial Fulfilment of the Requirements for the Degree of Doctor of Philosophy of Applied Science at the University of Windsor

by

Omer L. Hageniers

Windsor, Ontario

1971

APPROVED BY: J. R. Cooper

Gonsoton

L. Rai

A. L. Hamel.

W North

365381

ABSTRACT

A theoretical and experimental study of the deflections and bending moments in cantilever plates of various aspect ratios under point loadings is presented. Good agreement between theory and experiment is shown. Deflection information is obtained holographically and bending moment information at the fixed edge of the cantilever plate is obtained using strain gages. Bending moment distribution factors are obtained which can be used to predict the maximum moment in a cantilever plate under point loading.

The results are extended by superposition to the case of line loaded cantilever plates. This information is shown to be suitable for prediction of the bending moment distribution factors in helical and Novikov gear profiles. This information is therefore suitable for use in gear design.

ACKNOWLEDGMENT

I would like to express my thanks to Dr. W. P. T. North whose support made this project possible. As well, I thank the National Research Council of Canada for their aid in the form of Grant number A3360. In particular, I would like to express my thanks to my wife, Marilyn, whose patience, encouragement and support has made this work possible.

This manuscript was typed by Mrs. E. Miner , whose aid and patience were instrumental in bringing it to completion.

TABLE OF CONTENTS

LIST OF FIGURES

NOMENCLATURE

a	plate half width
a_i	deflection coefficient
A_{imn}	coefficient in deflection series
α	nondimensional load position in y direction
b	plate length
β	nondimensional load position in x direction
β_m	line load angle
γ	coefficient
γ_{xy}	shear strain
D	plate stiffness
δ	plate deflection
E	modulus of elasticity
ϵ_x	strain in the x direction
ϵ_y	strain in the y direction
F	face width
ϕ_n	pressure angle
h	plate thickness
H	potential energy
K_m	moment distribution factor
K_t	stress concentration factor
l_m	load line length
L	work done by a load
λ	wavelength of light
m	index
M	moment
M_x	moment in the x direction

M_y moment in the y direction

M_{xy} shearing moment

M_{st} matrix of coefficients

M_{max} Maximum bending moment at the wall

M_{nom} nominal bending moment at the wall

n index

N fringe order

η non dimensional intersection point of line load with free edge of plate

ν Poisson's ratio

P load

P_d Diametral pitch

ψ helix angle

q load intensity

σ stress

σ_x stress in the x direction

σ_y stress in the y direction at tangency point

t width of Lewis parabola

τ_{xy} shear stress

θ_1 angle between illuminating beam and normal to plate

θ_2 angle between viewing direction and normal to plate

V strain energy

W_t transmitted load

W_{st} matrix of coefficients

x coordinate system normal to wall

y coordinate system parallel to wall

Y_n Lewis factor

1. INTRODUCTION

1.1 Subject of Investigation

This study is concerned with the deflections and maximum stresses in cantilever plates under the action of transverse loading. In particular, it is concerned with obtaining this information in a form which is suitable for use in gear design. Since gear teeth of the helical or Novikov form are not uniformly loaded, the application of plate theory in determining the stress distribution in them is necessary. However, there is no simple formula relating the plate dimensions, the type of loading, and the stress distribution; therefore, it is desirable to present this information in the form of charts to make it more readily useful to a designer. While the information on stresses is the most important, when the load is being shared between two adjacent teeth on a gear, the deflection characteristics of the teeth determine how much load each carries and therefore the stresses in each. The deflection information is therefore of interest to the designer when axial overlap is occurring during the contact cycle of the gear being considered.

1.2 Importance of Bending Moment Distribution Information in Gear Design

The maximum static load carrying capacity of a gear tooth is determined by either the contact stresses or the bending stresses occurring in it during operation. Whichever of

these two stresses exceeds the allowable maximum will determine the allowable loading on the gear tooth. This investigation will make no attempt to study contact stresses, but will be concerned with bending stresses only. Factors limiting the magnitude of this stress are either the yield point of the material or its fatigue life, which is usually based on infinite life design. Several authors (1) (2) have shown that bending moment distribution information, when used in conjunction with stress concentration information, can predict the stresses in non uniformly loaded gear teeth. A great deal of work has been done to determine two dimensional stress concentration factors for gear tooth profiles using two dimensional photoelasticity. The application of this data to spur gears is relatively straight forward; however, for helical gear teeth, knowledge of the moment distribution is also necessary to obtain the value of the maximum stress. Therefore, the design of helical gear teeth would be much simpler if moment distribution information (or maximum moment information) was available.

1.3 Plan of Investigation

As previously stated, the subject of this investigation is the deflections and bending moments in cantilever plates and their application to gear design. It was decided that the deflections of plates would be obtained by holography which yields full field information; this is especially important in plates since the location of the maximum deflection value is not known beforehand. The moments (maximum) would be

determined by strain gages located at the fixed edge of the plate, in the direction normal to the fixed edge.

Due to the difficulties in applying line loads to cantilever plates only point loads were considered in the experimental study. Each plate, however, was loaded at various points so that superposition could be used to approximate line loads. It is quite likely that the errors in superposition are less than those in trying to establish a uniformly distributed line load.

A theoretical solution will also be presented based on a paper by J. Szmelter et al (3), which will be extended to include a solution for bending moments. This solution will consider the different types of loading commonly encountered in helical gear design, i. e: line loads at various angles across the face of the plate. These results will then be compared to work done by Wellauer and Seireg (4) on line loaded cantilever plates.

2. LITERATURE REVIEW

2.1 Bending Moment and Deflection Studies on Gear Teeth

The stressing of gear teeth has long been a subject of investigation, and in 1893, Wilfred Lewis laid the foundations for the modern concept of gear design. His approach was dictated by the spur gears in use at that time which had symmetry of loading (in theory, at any rate); resulting in a two dimensional approach to the problem. His hypothesis was that the weakest point in the profile was the point of tangency between an inscribed parabola and the fillets at the base of the tooth. A parabolic beam loaded at its tip is a constant stress section, and its stress is given by:

$$\sigma = \frac{W_t P_d \, 6h}{F \, t^2} = \frac{W_t \, P_d}{F \, Y_n} \quad \ldots.(2.1)$$

where: σ = maximum stress in section

W_t = applied tangential load

F = face width

P_d = Diametral pitch

h = height of Lewis parabola

t = width of Lewis parabola at tangency point

Y_n = Lewis Factor

This approach to determining the stress in gear teeth had one big advantage in that it was easy to apply, but it also had the disadvantage that it did not predict the actual stresses. This shortcoming was hard to overlook; therefore, a great deal of experimentation was carried out using strain gages and

photoelasticity to obtain stress concentration factors based on the Lewis Factor. The AGMA (American Gear Manufacturers Association) still uses a modified Lewis equation for gear design at this time (5), which includes factors for the stress concentration, material (fatigue life), flexibility of mountings, shock loading, operating temperature, etc.

So much for the simple spur gear system; in helical gear systems the loading is not uniform and a two dimensional approach, as suggested by Lewis, is no longer applicable. The type of loading in spur, helical involute and Novikov gear teeth is shown in Figure 1. The helical involute system is the most widely used in high speed and high power applications; however, the newly introduced Novikov system is replacing it in many applications in Russia and England (6) (7) (8) (9) (10) (11). The Novikov or Circarc system was first developed by Ernest Wildhaber in 1923 in the U. S. A. (12) (13); however, subsequent testing showed no significant improvement over the helical involute system and development was dropped. In 1954, this system of gearing was reintroduced by Col. M. L. Novikov in Russia and has since received wide acceptance there (14). Work on these gear profiles has shown the need for, and desirability of a new approach to design of these gears, due to the localized loading effect (see Figure 1). This localized loading effect completely violates Lewis' premises and a new version of his equation can be written as:

$$\sigma = K_m K_t \frac{W_t P_d}{F Y_n} \qquad \ldots\ldots (2.2)$$

where: K_m = Moment Distribution Factor

K_t = Stress Concentration Factor from two dimensional studies.

This type of approach was first applied to the Novikov system by Fediankan and Tschechanow (15) in 1958 when they presented some design information for Novikov profiles, the values of K_m they introduced were based on tests of several gear sets. In 1961, Wellauer and Seireg (4) applied this approach to helical gear loading by testing a thick plate, with an aspect ratio of 0.188 and deriving quasi-theoretical moment distribution curves based on a semi-emperical method for the same aspect ratio. Also, my own work in 1969 (1) showed the validity of this approach in predicting the stresses in Novikov gear profiles.

Very little work has been done on obtaining bending moment distribution factors for gear teeth, even though the usefulness of it has been proven. The first person to consider the problem of moment distribution in long gear teeth was MacGregor in 1935 (16). He studied, both experimentally and theoretically, the deflections of a wide cantilever plate (aspect ratio 0.167) under a central load at the free edge. His theoretical solution assumed that the plate was infinitely wide in order to evaluate the Fourier integrals which appeared in his solution. He also evaluated the bending moment at the

wall for the point immediately adjacent to the load.

In 1937, D. L. Holl (17), using a finite difference approach, solved for the deflections and moments in a plate with an aspect ratio of 0.250, under a point load located at the centre of the free edge. He considered 41 points in his solution which limited the accuracy, but left the solution manageable. He points out the limitations of the difference method; however, he also indicates that it is possible to solve plates of finite length by this method.

Then in 1948, Jaramillo (18), worked out an exact solution for a cantilever plate of infinite length loaded by a point load at any distance from the wall. Because the plate was infinitely long, he was able to express the deflection in terms of improper integrals and avoid the difficult boundary conditions at the free corners. He was then able to evaluate these integrals by numerical methods in order to obtain the deflections and moments in the plate. His solution, of course, is valid only for infinite cantilever plates, but since the effects of the load are quickly dissipated, it is possible to apply it as an approximation to long plates under central loading.

Vartak, in 1957, experimentally studied two thin cantilever plates with point loading at various points along the free edge. He determined the bending moments along the fixed edge for plates with aspect ratios of 0.250 and 0.167; however,

the deflection of the 0.250 plate was more than $3\frac{1}{2}$ times its thickness which puts the results for it in doubt. His experiments were the first to consider loading of the free corner, which is the critical position for a cantilever plate.

Also in 1948, J. W. Dalley tested a point loaded cantilever square plate (20) and determined deflection contours for several loading points. His study was the first to consider loading at points not at the boundary of the plate. He also determined stresses in the plate; however, the points he chose to study were not at the maximum moment points, therefore their value is very limited. A dial gage was used in his experiment to traverse the plate and obtain the deflection contours for loading at a given point.

Then in 1959, Wellauer and Seireg (4) made the first and only serious attempt to obtain moment distribution factors for gear teeth. They tested two thick plates with aspect ratios of 0.188 (2" x $2\frac{1}{4}$" x 12"), one of which was tapered to simulate a gear tooth shape. Their study showed no significant effect of taper on moment distribution at the base of the tooth for the profile they tested. Bending moment distributions were determined for various line loads, representative of spur, helical involute and Novikov gears. They also suggested a semi-emperical bending moment solution, based on the work of Jaramillo and a moment image technique they proposed. Their theoretical results compared very well with their experimental results; this could be because the plate they were considering

had a low aspect ratio which would tend to minimize the errors in their theoretical approach.

In 1966, Kugimiya (2) determined the stresses in an involute helical gear set, rotating slowly, using strain gages. Then, employing an approach similar to that of Wellauer and Seireg, he also calculated the theoretical stresses in the gears. His experiment showed very good agreement between theory and experiment.

Szmelter, Sulikowski and Lipinski, in 1961, (3), applied a Ritz approach to the problem of cantilever plates using a polynomial to represent the deflected surface. In their paper they presented results for a corner loaded rectangular cantilever plate, as well as a plate with a uniformly distributed load. A numerical evaluation of the coefficients is necessary, but this need be done only once for a plate with Poisson's ratio and aspect ratio specified. Then it is possible to specify many different types of loadings and evaluate the deflections produced. Their solution offers a relatively simple approach to the deflections in cantilever plates; however, a large amount of calculation is necessary, but a high speed digital computer does make the calculations easy.

3. PROBLEM AS STUDIED

3.1 Theoretical Considerations

3.1.1 Selection of Method

From a consideration of the problem at hand i. e: a cantilever plate of a given aspect ratio, loaded by an arbitrary transverse loading; it is necessary to make certain assumptions to simplify the problem. In fact, these assumptions are specifically those outlined in Chapter One of "Theory of Plates and Shells" by Timoshenko and Woinowsky-Krieger (21). These are the typical specifications that the plate thickness is small in comparison with its other dimensions, the deflections are small in comparison to the thickness, the material has linear properties, it is elastic, etc.

First, let us specify the geometry involved in describing a cantilever plate, and for the sake of similarity and convenience we will define our system of coordinates in a manner similar to that of Szmetler et al (3). This is shown in Figure 2, where the aspect ratio is, of course, defined as (b/2a) and the thickness as h. If one were to consider the problem of a point load somewhere on the plate using the classical approach to thin plate problems, it becomes necessary to establish the boundary conditions on the four sides such that the deflection and slope are zero at the fixed edge and the shear and normal moment are zero on the three free edges. This represents eight boundary conditions to be satisfied. Also

the load must be represented as a Fourier Series in order to have continuous load function. In order to get an estimate of how complex and, indeed, almost impossible such a theoretical solution is, one need only refer to Jaramillo (18) who solved the case of the infinite plate which avoids several of the problems: there are no difficult corners to consider, the load is symmetric, and the infinite Fourier series can be replaced by improper integrals which can be evaluated numerically. The exact solution for a finite length plate, having no such advantages is quite likely impossible (at least for me).

Now that exact solution has been ruled out, it is necessary to consider some of the approximate techniques available for solving the present problem. Basically, there are three methods available, finite difference, finite element and energy. Each of these has its own advantages and disadvantages which must be considered in light of the specific problem to be solved. In the cantilever plate problem, it seems that deflection contours would be of great interest, as well as the bending moments at the clamped edge, which will intuitively be the largest moments in the plate. Also, since all of these methods are numerical in nature and require a great deal of computation, this becomes an important factor in choosing the method of solution. In fact, this becomes a primary consideration when accuracy of solution is considered important, since these three techniques give improved accuracy as either more points, elements, or terms are considered.

In a finite difference solution for plate deflections, one equation is generated for each point considered; as well, those familiar with the technique will realize that fictitious points outside the boundary of the plate must also be considered, which also generate an equation each. One will then have an equation for every point in the plate being considered, where these equations are linear algebraic ones with the number of unknowns equal to the number of points being considered. For the details of this approach, one can refer to "Theory of Plates and Shells", pg. 351 (reference 21). This set of linear algebraic equations must then be solved for the deflections of all points considered. The quality of solution rests, as can be easily guessed, upon the number of points considered in the net, i. e: more points, better accuracy; but at the same time a larger system of equations. This larger system of equations results, of course, in more error due to round-off in computations, and at some point a balance exists between increased possible accuracy due to more points (and equations) and decreased accuracy due to round-off errors in the computations. So much for deflections which only generate a single equation per point considered. Now, if bending moments are also desired, a change in technique is required. This finite difference method is outlined by Holl (17) in his paper, which was previously mentioned, where he uses 15 points to represent a symmetrically loaded (i. e: 15 points are only half the plate, if the load were not symmetric, he

would require 27 points) cantilever plate. He then generates 41 equations in 41 unknowns, i. e: almost three times as many as the number of points being considered, from the difference equations and his boundary conditions. It can easily be concluded that a better solution requires more points to increase the possibility of true plate action, while this also causes the calculations required to increase at a greater rate.

In considering finite element techniques, the choice of the element type, as well as the number of elements must be considered; this is discussed extensively in "Finite Elements Methods in Stress Analysis" by Holand and Bell (reference 22). The number of degress of freedom which an element has, determines how well it can approximate plate action, and elements have been proposed with 12 and more degrees of freedom. Basically, the finite element technique consists of replacing the continuous plate by an array of elements whose stiffness and means of connection is specified, which converts a statically indeterminate problem into a determinate one. In classical finite element techniques, a structural matrix of influence coefficients is established, which, after inclusion of boundary conditions, has to be inverted, resulting in a great deal of difficulty, as well as numeric errors, (i. e: computational). More recently, the Rayleigh-Ritz finite element method has been developed which avoids the inversion problem; this technique is described by Walker (23)

who works out the deflections of a simply supported, uniformly loaded plate. This method is, however, very complex, especially when it is extended to include bending moment determination as well.

An energy method, as its name implies, is concerned with the energy stored in a plate when it is loaded. The essential steps in the solution are to choose a deflection function (usually a finite series of terms) capable of satisfying the boundary conditions, evaluate the stored energy in the plate, and by making the contribution of each term a minimum, determine its coefficients. A complete treatment of this approach is given by Timoshenko and Woinowsky-Krieger (21) who indicate that the method was first applied to plate problems by Ritz. This method was used by Szmelter et al. (3) in working out the deflections of a cantilever plate, loaded by a point load at the free corner, as well as a uniformly loaded plate. Their technique is the one which I plan to use as the basis for my theoretical formulation. The reasons for which this has been done are as follows:

(1) the solution is machine solution oriented

(2) the accuracy of solution at a point does not depend upon the absence or presence of nearby points

(3) the solution can be extended to moment prediction

(4) the number of points at which calculations are being preformed can be easily changed.

3.1.2 Deflection and Moment Determination

As mentioned in the previous section, the theoretical prediction of deflection will be based directly on the paper entitled, "Bending of a Rectangular Plate Clamped at One Edge", by J. Szmelter, T. Sulikowski and J. Lipinski (3). It seems helpful to present the pertinent parts of their paper here, in order to more clearly define the limitations and scope of this technique.

Referring again to Figure 2, we see that the edge $x = 0$ is clamped with the edges $x = b$ and $y = \pm a$ free. Now let the unknown displacement function $w(x,y)$ be assumed in the following form:

$$w(x,y) = \sum_{i=0}^{\infty} a_i \, w_i(x,y) \qquad \ldots (3.1)$$

where $w_i(x,y)$ are known functions satisfying the boundary conditions at the clamped edge, which are:

$$w_i(0,y) = \partial w_i(0,y)/\partial x = 0 \qquad \ldots (3.2)$$

The strain energy of the bent plate is given by (see reference 21 for example):

$$V = \frac{D}{2} \int_0^b \int_{-a}^{a} \left\{ w_{,xx}^2 + 2\nu w_{,xx} w_{,yy} + w_{,yy}^2 + 2(1-\nu) w_{,xy}^2 \right\} dxdy \qquad \ldots (3.3)$$

where D denotes the plate rigidity, ν is Poisson's ratio, and $w_{,xx}$ means the second derivative of w with respect to x.
Now substituting (3.1) in (3.3) we have:

$$V = \frac{D}{2} \sum_{i,k=0}^{\infty} a_i \, a_k \, V_{ik} \qquad \ldots (3.4)$$

where the coefficients V_{ik} are determined from the following integral

$$V_{ik} = \int_{o}^{b} \int_{-a}^{a} \left\{ w_{i,xx}\, w_{k,xx} + \nu \left(w_{i,xx} w_{k,yy} + w_{i,yy}\, w_{k,xx} \right) \right.$$

$$\left. + w_{i,yy} w_{k,yy} + 2\,(1-\nu)\, w_{i,xy} w_{k,xy} \right\} dxdy \qquad \ldots (3.5)$$

At the same time, we now assume that the functions $w_i\,(x,y)$ satisfy the following condition of orthogonality:

$$V_{ik} \left\{ \frac{b^3}{2a} \right\} = \begin{cases} 1 & \text{when } i = k \\ 0 & \text{when } i \neq k \end{cases} \qquad \ldots (3.6)$$

Equation (3.4) then becomes

$$V = \frac{Da}{b^3} \sum_{i=0}^{\infty} a_i^{\,2} \qquad \ldots (3.7)$$

Let L_i denote the work of a given load on the displacement $w_i(x,y)$. We then see from (3.1) and the superposition principle that the work L of the load performed on the displacement w is equal to

$$L = \sum_{i=0}^{\infty} a_i\, L_i$$

The potential energy of the plate then can be given as

$$H = V - L = \frac{Da}{b^3} \sum_{i=0}^{\infty} a_i^2 - \sum_{i=0}^{\infty} a_i \, L_i \qquad \ldots (3.9)$$

The plate is in equilibrium when its potential energy reaches a minimum, i. e. when

$$\frac{\partial H}{\partial a_k} = \frac{2Da}{b^3} a_k - L_k = 0 \qquad \ldots (3.10)$$

which leads to

$$a_k = \frac{b^3 L_k}{2Da} \qquad \ldots (3.11)$$

Now substituting (3.11) in (3.1), the displacement w can be expressed as

$$w(x,y) = (b^3/2Da) \sum_{i=0}^{\infty} L_i \, w_i(x,y) \qquad \ldots (3.12)$$

If we now assume that the functions $w_i(x,y)$ have the form of polynomials, i. e:

$$w_i(x,y) = \sum_{n,m} A_{imn} \, (x/b)^n (y/a)^m \qquad \ldots (3.13)$$

Where the coefficients A_{imn} are determined in such a way that the boundary conditions (3.2) and the orthogonality conditions (3.6) are satisfied. From (3.2), it follows that

$$n = 2,3,4, \ldots \qquad m = 0,1,2,\ldots \qquad \ldots (3.14)$$

Substituting (3.13) in (3.5) we obtain

$$V_{ik} = \frac{2a}{b^3} \sum_{mnpq} A_{imn} A_{kpq} W_{nmpq} \qquad \ldots (3.15)$$

where:

$$W_{mnpq} = \begin{cases} 0 & \text{when } (m+q) \text{ is odd} \\ \dfrac{n(n-1)p(p-1)}{(n+p-3)(m+q+1)} + \left\{\dfrac{b}{a}\right\}^4 \dfrac{m(m-1)q(q-1)}{(m+q-3)(n+p+1)} & \\ + \left\{\dfrac{b}{a}\right\}^2 \dfrac{\nu n(n-1)q(q-1) + \nu m(m-1)p(p-1) + 2(1-\nu)nmpq}{(n+p-1)(m+q-1)} & \text{when } (m+q) \text{ is even} \end{cases} \qquad \ldots (3.16)$$

The groups of indices mn or pq in equations (3.15) and (3.16) may be replaced by a single index s or r according to the following table:

n(or p) =	m (or q) = 0	1	2	3	4	5	6	7	8	9
2	r (or s) = 0	1	4	5	10	11	18	19	28	29
3	2	3	8	9	16	17	26	27		
4	6	7	14	15	24	25				
5	12	13	22	23						
6	20	21								

etc.

Now we can rewrite the coefficients used above in a new form

$$A_{imn} = A_{is}, \quad A_{kpq} = A_{kr}, \quad W_{nmpq} = W_{sr} = W_{rs} \qquad \ldots (3.17)$$

and (3.15) becomes

$$V_{ik} = \frac{2a}{b^3} \sum_{r,s} A_{is} A_{kr} W_{sr} \qquad \ldots (3.18)$$

The matrix of coefficients V_{ik} may be resolved into a product of two triangular matrices of coefficients M_{st}, according to the following formulas

$$\sum_{t} M_{ts} M_{tr} = W_{sr}, \quad M_{st} = 0 \qquad \text{for } s>t \qquad \ldots (3.19)$$

These equations can be used for the successive calculation of all the coefficients M_{rt}. The matrix M_{rt} is the square root of the matrix $W_{sr}(3)$. The matrix W_{sr} is defined positive and therefore all the coefficients M_{rt} are real.

The coefficients $A_{ir} = A_{ipq}$ can easily be calculated from the equations

$$\sum_{r} A_{ir} M_{rt} = \begin{cases} 0 & \text{when } i = t \\ 1 & \text{when } i \neq t \end{cases} \qquad \ldots (3.20)$$

The calculation of A_{ir} is simple because the matrix M_{rt} is triangular. Also, if we substitute (3.19) and (3.20) in (3.18) we can verify that the functions $w_i(x,y)$ containing the coefficients of A_{ir}, calculated above, satisfy the condition of orthogonality (3.16).

This is where Szmetler et al (3) left their derivation and calculated results for two examples they presented in their paper. To summarize their method, one must first establish W_{sr} using equation (3.16) and the table which follows it, then

calculate M_{st} using equation (3.19), and subsequently determine A_{ir} from equation (3.20).

Since expressions for the deflection, w (x,y), have been developed as outlined above, it is only logical to extend the results to determination of the bending moments in the plate. The relations between the bending moments and deflection are (See reference 21 for example);

$$M_x = D\,(w_{,xx} + \nu\, w_{,yy})$$
$$M_y = D\,(w_{,yy} + \nu\, w_{,xx}) \qquad \ldots (3.21)$$
$$M_{xy} = D\,(1 - \nu)\, w_{,xy}$$

Referring to equations (3.12) and (3.13) we see that w (x,y) can be written as:

$$w\,(x,y) = \frac{b^3}{2Da} \sum_{i}^{\infty} \sum_{m,n} A_{imn} \left(\frac{x}{b}\right)^{n} \left(\frac{y}{a}\right)^{m} L_i \qquad \ldots (3.22)$$

Differentiating (3.22) to obtain $w_{,xx}$, w_{yy} and $w_{,xy}$ these become:

$$w_{,xx}\,(x,y) = \frac{1}{2D} \left(\frac{b}{a}\right) \sum_{i}^{\infty} \sum_{mn} A_{imn}\, n(n-1) \left(\frac{x}{b}\right)^{n-2} \left(\frac{y}{a}\right)^{m} L_i$$

$$w_{,yy}(x,y) = \frac{1}{2D} \left(\frac{b}{a}\right)^{3} \sum_{i}^{\infty} \sum_{mn} A_{imn}\, m(m-1) \left(\frac{x}{b}\right)^{n} \left(\frac{y}{a}\right)^{m-2} L_i \qquad \ldots (3.23)$$

$$w_{,xy}\,(x,y) = \frac{1}{2D} \left(\frac{b}{a}\right)^{2} \sum_{i}^{\infty} \sum_{mn} A_{imn}\, mn \left(\frac{x}{b}\right)^{n-1} \left(\frac{y}{a}\right)^{m-1} L_i$$

Now if we substitute (3.23) into (3.21) we have the following expressions for the moments.

$$M_x(x,y) = \sum_i^{\infty} M_{xi}(x,y)\, L_i$$

$$= \frac{1}{2}\left(\frac{b}{a}\right) \sum_i^{\infty} \sum_{m,n} A_{imn} \left\{ n(n-1) \left(\frac{x}{b}\right)^{n-2} \left(\frac{y}{a}\right)^{m} \right.$$

$$\left. + \nu \left(\frac{b}{a}\right)^{2} m(m-1) \left(\frac{x}{b}\right)^{n} \left(\frac{y}{a}\right)^{m-2} \right\} L_i$$

$$M_y(x,y) = \sum_i^{\infty} M_{yi}(x,y)\, L_i$$

$$= \frac{1}{2}\left(\frac{b}{a}\right) \sum_i^{\infty} \sum_{mn} A_{imn} \left\{ \left(\frac{b}{a}\right)^{2} m(m-1) \left(\frac{x}{b}\right)^{n} \left(\frac{y}{a}\right)^{m-2} \right. \qquad \ldots (3.24)$$

$$\left. + \nu\, n(n-1) \left(\frac{x}{b}\right)^{n-2} \left(\frac{y}{a}\right)^{m} \right\} L_i$$

$$M_{xy}(x,y) = \sum_i^{\infty} M_{xyi}(x,y)\, L_i$$

$$= \frac{1}{2}\left(\frac{b}{a}\right)^{2} \sum_i^{\infty} \sum_{mn} A_{imn}\, mn \left(\frac{x}{b}\right)^{n-1} \left(\frac{y}{a}\right)^{m-1} L_i \quad (1-\nu)$$

These expressions can be used to predict the moments in a cantilever plate of a particular aspect ratio (b/2a), particular material (ν), and at a given point (x,y).

3.1.3 Moment Distribution Factor

The Moment Distribution factor (K_m) is here defined as the ratio of the maximum bending moment at the fixed edge of the plate to the nominal moment at the fixed edge. Referring to Figure 3 this can be expressed as:

$$K_m = \frac{M_{max}}{M_{nom}} \qquad \ldots (3.25)$$

where: M_{max} = maximum moment at the fixed edge

M_{nom} = nominal moment at the fixed edge which is defined as

$$M_{nom} = \frac{1}{2a}\int_{-a}^{a} M \, dy \qquad \ldots (3.26)$$

where M is the value of the bending moment at the wall. The nominal moment can also be computed in terms of the load being applied to the plate. The two types of loads applied to plates in this study are point loads and line loads. A point load is shown in Figure 3, acting on a plate of aspect ratio (b/2a), at the point (βb, αa). The value of M_{nom} for the plate shown is:

$$M_{nom} = \frac{\beta P b}{2a} \qquad \ldots (3.27)$$

An arbitrary line load is shown in Figure 4; it is not completely arbitrary, however, in that it is assumed that the load intersects the free edge (at η) and then extends at some angle (β_m) till it

intersects another edge. The value of M_{nom} for this plate is:

$$M_{nom} = \frac{P}{2a}\left\{ b - \frac{(a+\eta)}{2} \tan \beta_m \right\} \quad \ldots (3.28)$$

These values of the nominal moments will be used in determining the bending moment distribution factors.

3.2 Details of Computer Program

The method of determining deflections and moments, as outlined in Section 3.1.2, is a computational technique which involves a great deal of calculation, i. e: solving a large set of linear algebraic equations, etc. To do this by hand would be next to impossible (it seems, however, that Szmetler et al (3) did so for two aspect ratios) if a large number of plates and loadings are considered. It was therefore considered desirable to write a computer program which would calculate the deflections and moments in a cantilever plate, of a given aspect ratio, under a particular point load.

A listing of the final program is given in Appendix A; there are 12 subroutines in the program which are called sequentially by the main program. The program was written in subroutine form to allow overlays which would save core space; as well as break the program into logical segments to allow easier programming and debugging.

The subroutines are:

1 ESTISR

2 SETW

3 SETM

4 SETA

5 SHIFT

6 SORT

7 ESTW

8 ESTMXY

9 SETL

10 DETW

11 DETM

12 MMAX

and as mentioned before, they are listed in Appendix A.

The program is written to allow for a maximum of 140 coefficients in the series for the deflection; this was done in 200K of available core storage. The limitation on core storage required added complexity in the program which would not have been necessary if a larger computer had been available (not to say that 200K is small). Since the completion of this program, more core storage has become available which would have made the added complexity unnecessary.

In the main program Poisson's ratio is chosen, the aspect ratio is set, and the number of terms in the series is set. Poisson's ratio was set at 0.3 for all of the computer runs since this is a suitable value for steel and most aluminum alloys.

In subroutine ESTISR, the table relating the coefficients used in equation 3.17 is established. This table is necessary to derive the matrix W_{sr} from the coefficients mnpq. The matrix W_{sr} is then set up in subroutine SETW using equation 3.16 and

and the table of coefficients established in ESTISR. The values of W_{sr} are stored in W(I,J); however, since W_{sr} is symmetric (equation 3.17) it will be necessary to save only the upper triangular portion of the matrix. The values of W_{sr} are calculated as double precision numbers; this, of course, requires twice as much storage space as single precision numbers would. This was done since using single precision numbers allows only 30 terms in the series of coefficients for deflection to be calculated due to loss of accuracy in the equations.

The next subroutine called is SETM, and in this subroutine the coefficients M_{st} are calculated using equation 3.19. The terms in M_{st} are also double precision, and are stored in the lower triangular portion of W(I,J) since the matrix M_{st} is triangular (i. e: all terms above the diagonal term are zero). In order to accomplish this, it was necessary to store the diagonal elements of W_{sr} in the vector A (I), thus leaving the diagonal of matrix W(I,J) available for storing M_{st}.

Subroutine SETA determines the coefficients A_{ir} from equation 3.20, these are also double precision numbers. The necessity for double precision numbers is evident here, since all of the previously calculated terms in A_{ir} must be used to calculate each succeeding term. The terms in A_{ir} are stored in the upper triangular portion of W(I,J) which was previously occupied by W_{sr}. Vector A(I) was used in this phase to store the diagonal elements in M_{st}; this is necessary so that the diagonal terms in A_{ir} can be generated in these positions.

After A_{ir} is calculated, it is transferred to the lower triangular half of W(I,J) with all the above diagonal elements set to zero. Subroutine SHIFT is then called, and its sole function is to rearrange the terms in W(I,J) into a more convenient sequence for the following subroutine.

The next subroutine called is subroutine SORT, and in this subroutine the matrix of coefficients, A_{ir}, is sorted into its even and odd terms. These are defined in the following manner; a term will be considered even when its y exponent (m in equation 3.13) is even and odd when its y exponent is odd. The reason for this will become more evident later; let it be adequate now to say that it is necessary to do this. The even terms will be placed in AE(I,J) and the odd terms in AO(I,J). In order to once again conserve space, these matrices will be equivalenced with W(I,J). The matrices AE(I,J) and AO(I,J) need to be dimensioned only half the size (i. e: one quarter as many terms) as W(I,J) since many of the A_{ir} terms (75%) are zero and can be deleted. Also, since the remaining calculations are simple multiplications and additions, AE(I,J) and AO(I,J) will be in single precision format. Having the matrices equivalenced with W(I,J) could cause some problems since they will contain numbers already stored in W(I,J). The subroutine SHIFT was called to rearrange the A_{ir} terms so that this would not be a problem.

In subroutine ESTW, which is called next, the grid points are chosen at which coefficients will be calculated. These points are then those where loads can be placed and deflection

and moment information determined. The coordinates (x,y) of the points are stored in X(I) and Y(I); they are chosen, however, in terms of x/b and y/a, in order to make them compatable with equation 3.13. These coordinates are chosen only in the region $y \geqslant 0$ and $x \geqslant 0$ since it will be possible to consider points for $y < 0$ by a type of reflection about the axis as outlined later. Two new matrices are defined in this subroutine: RE(I,J,K) and RO(I,J,K) which are also equivalenced with W(I,J) in order to save space. These matrices are dimensioned 6x6x70, each 6x6 (of both the odd and even matrices) group represents the value of $w_i(x,y)$ at 36 points represented by the values of X(I) and Y(I). As mentioned, they represent the values of $w_i(x,y)$, with the terms generated by AE (I,J) going into RE(I,J,K) and those generated by AO(I,J) going into RO(I,J,K).

Next in subroutine ESTMXY, the same thing that was done for w_i (x,y) in ESTW is done for $M_x(x,y)$, $M_y(x,y)$ and $M_{xy}(x,y)$. That is to say that M_{xi} is computed by equation 3.24 and stored in ROX(I,J,K) and REX (I,J,K) and M_{xyi} is stored in ROYX(I,J,K) and REXY(I,J,K). These matrices are all equivalenced with W(I,J) to reduce core storage.

Now it only remains to sum up the terms as indicated in equations 3.13 and 3.24 to obtain the moments and deflection of the plate at the points specified; however, before this can be done, it is first necessary to evaluate L_i. The work done by a force P on the displacement w_i (x,y) is given by:

$$L_i = \int_0^b \int_{-a}^{a} P\, w_i(x,y)\, dxdy \qquad \ldots (3.29)$$

If the load is acting at point (a_1,b_1), and it is a true point load, then it has a value at this point only (i. e: $P = 0$ if $x \neq a_1$ and $y \neq b_1$). The value of the integral is then:

$$L_i = P\, w_i\,(a_1, b_1) \qquad \ldots (3.30)$$

Then in order to apply a load at a point it is only necessary to select the values of $w_i(a_1,b_1)$as the work vector L_i. This is done in subroutine SETL where the vector C(I) is loaded with the values of L_i, chosen by the main program to represent a given loading from the terms in RO(I,J,K) and RE(I,J,K). In this subroutine, an error vector is also generated. This is outlined by Szmetler et al: they show that the influence of the nth component on the sum (i. e. deflection) is given by:

$$\xi_m = L_n^2 \Big/ \sum_{i=o}^{n} L_i^2 \qquad \ldots (3.31)$$

This error vector is useful in indicating how many terms should be taken in the solution for deflections. These values are stored in ERROR(I).

Subroutine DETW is called next and this subroutine determines the deflection of the plate under the point loading chosen. This is done by taking the sum of the products $w_i(x,y)\, L_i$;

this is, in effect, evaluating equation 3.12 for w(x,y). The values of w(x,y) are stored in D(I,J) which in the scheme used here is dimensioned 6x11. In determining w(x,y) the even components (i. e. terms RE(I,J,K) x C(K)) are symmetric about the x axis; however, the odd components (i. e: terms RO(I,J,K) x C(K)) are skew symmetric, which is to say they are added in the region $y \geq 0$ and subtracted in the region $y < 0$. The values of D(I,J) are printed out in a suitable format to give the deflections of the plate under the loading chosen.

Subroutine DETM is then called, and it determines $M_x(x,y)$, $M_y(x,y)$ and $M_{xy}(x,y)$ in the same manner as DETW determined w(x,y). The resulting moments at the chosen points in the plate are stored in DX(I,J), DY(I,J) and DXY(I,J) which are all dimensioned 6x11. These values are all printed out in matrix format. The last subroutine called is MMAX which computes the maximum and minimum moment at the chosen points from M_x, M_y and M_{xy} at each of these points. The equation used is:

$$M_{\max, \min} = \frac{M_x + M_y}{2} \pm \sqrt{\left\{\frac{M_x - M_y}{2}\right\}^2 + M_{xy}^2} \qquad \ldots (3.32)$$

for the maximum and minimum moments, while the angle at which the maximum moment acts is determined from (See reference 24 for their derivation),

$$\theta = \frac{1}{2}\arctan\left\{\frac{2 M_{xy}}{M_y - M_x}\right\} \qquad \ldots (3.33)$$

The values of the principal moments and their angle are printed out in matrix form as well, since these may prove useful in determining the accuracy of the solution by noting the directions of the free boundary moments.

This completes the description of the inner workings of the program as well as the concepts behind it. The program, as presented here, is suitable for single point loads on plates; as well, it will be used to study the effects of line loads. This will require some modifications since the line load will be simulated by a series of point loads, with the point load solutions being superimposed to generate the required moment information. Since these modifications are simple and self evident, no detailed description of them will be given.

3.3 Details of Plates Tested

The plates tested were cut from a single sheet of $\frac{1}{4}$ inch thick, low carbon, hot rolled steel sheet. The surface of this plate was rather poor (i. e: loose scale was present) but no attempt was made to improve its conditions (other than painting). A total of 10 aspect ratios were tested, even though only 3 plates were used; this was accomplished by cutting strips off the top of each plate after it was tested, thereby resulting in a new aspect ratio. This process is outlined in Figure 5, where plate I attains aspect ratios of (3,2,1.5), plate II attains aspect ratios of (1.00, 0.75, 0.50) and plate III attains aspect ratios of (0.33, 0.25, 0.167, 0.10). The reason for doing this becomes clear when one considers that strain gages are mounted near the clamped edge of the plate.

Plate I has 5 gages, Plate II has 7 gages, and Plate III has 9 gages; mounting this number of gages on 10 different plates (one for each aspect ratio) would be both expensive and a large amount of labour, which can be avoided by using the method outlined here.

The aspect ratios chosen were selected to adequately cover the range between the cantilever beam (high aspect ratios) and the quasi infinite plate (low aspect ratios). They were chosen to do so in a logarithmic fashion, since preliminary theoretical results indicated this was desirable. Aspect ratios were also chosen to correspond to those tested by previous investigators: i. e: 1.0 (Dalley, reference 20); 0.25, 0.33 (Vartak, reference 19 and Holl, reference 17).

The thickness of the plates was chosen great enough to provide holographic stability against air currents and table vibrations. In most cases studied, the $\frac{1}{4}$ inch thickness was adequate; however, the 12" x 4" (aspect ratio 3.0) plate could not be studied holographically since its length made it too sensitive to vibration.

In order to calculate the deflections and moments from the experimental information, it was first necessary to obtain modulus (E) and Poisson's Ratio (γ) information. This was done by testing tension specimens cut from the same piece of steel plate as the test plates. The resulting values were $E=30.2 \times 10^6$ and $r= 0.276$; this resulted in the value of 4.62×10^4 for the plate stiffness (D). The details of this determination are outlined in Appendix B.

3.4 Major Assumptions Involved

The following is a list of assumptions which may affect the generality of the experimental results obtained.

(1) That the method of clamping the plates is a reasonable approximation to a fixed end condition. This has been a subject of concern in many studies, and it seems to be likely from their comments that for deflections it is not adequate (in fact machining from a solid block may not be) but for moments, excellent results can be obtained. However, some effect can still be expected.

(2) The strain gages used on the plates were of finite length and width (1/8 inch by 1/16 inch) which introduces some error due to averaging, but they must also be placed a finite distance away from the clamped edge. This will result in a lower moment reading than actually exists at the clamped edge; however, since the gage length is small (and therefore the closeness of its centre to the clamped edge of the plate) this error is assumed negligible (particularly since the plate lengths are at least 9 times the gage length).

4. Experimental Arrangement and Procedure

4.1 Deflection Determination

The deflections were determined using holographic interferometry to obtain the full field deflection contours of the plates under load. This method was chosen because it lends itself so readily to plate deflection determination as the point of maximum deflection, as well as the deflected surface, is immediately evident. This method has obvious advantages over point sensors such as dial gages - where a large number of readings, as well as a plot of the deflected surface, must be made before the maximum point becomes evident.

The basic elements of holography are described in a host of papers; even though this is a new technique, there has been a vast amount of research done to apply it in many areas. The basic elements and advantages of the technique are well described by Stetson and Powell (25). Also the application of the technique to plate deflections is described by Boone and Verbiest (26). The basic arrangement of the holographic system used in this experiment is shown in Figure 6. This system is slightly different from that commonly used in holography in that one beam is used to illuminate both the object and the reference beam mirror, whereas most systems use two separate beams. The primary advantage of such a system is that it is inherently more stable; therefore, since the stability of the table being used was marginal for two beam systems, the single illumination beam was used. One of the greatest limitations of the holographic technique is the requirement of interferometric stability, which requires a special table as a working base.

The construction of the table used in this study is described in Appendix C. where the stability required is also discussed. The construction of the other optical elements used is also described in the same appendix.

Hologram interferometry relies on the comparison of two nearly identical holograms of the object (or a hologram and the real object). This is done by double exposure of the film (with a change taking place between exposures) or by viewing the changed object through a developed hologram plate. When either of these techniques is used, fringes are produced which are related to movements away from the hologram plate. The equation for the formation of such fringes is explained by A. E. Ennos (27) and is given by:

$$\delta = \frac{\lambda N}{(\cos \theta_1 + \cos \theta_2)} \qquad \ldots (4.1)$$

where: δ is the deflection of the plate

λ is the wavelength of the light used (6328 A^{o})

N is the fringe order

θ_1 is the angle between the illuminating beam and the normal to the plate

θ_2 is the angle between the normal to the plate and the viewing direction

The angles θ_1 and θ_2 are shown in Figure 6. The angles θ_1 and θ_2 of course vary across the specimen; however, looking at equation (4.1), it is easy to see that if the angles θ_1 and θ_2 are small, any small change in them will result in only a small change in the equation for δ. The conditions in the experiment were such, that neglecting the angle variation results in an error

of only 2% across the plate. This was therefore done in the data reduction to reduce the amount of work involved. As well, the angles θ_1 and θ_2 were kept equal, since this results in a diffuse reflection of light from the plate onto the film which helps improve beam balance (for optimum recording, the reference beam should be 5 times the intensity of the object beam). Therefore θ_1 and θ_2 are equal in the present arrangement, with both of them being set equal to 14 degrees. Using these angles and substituting for λ, equation (4.1) becomes:

$$\delta = 12.8 \times 10^{-6} N \qquad \ldots (4.2)$$

where δ is now given in inches. This indicates the fantastic sensitivity available - which can be a disadvantage, since correspondingly small loads must be used which can be difficult to apply.

In the testing of a particular plate, the first step was to mount it in the plate holder (which is described in Appendix D). The plate holder was then clamped to the table to prevent its movement during the rest of the experiment. Then, using the arrangement shown in Figure 7, a hologram was made by exposing the film for 3 seconds. The film used was Scientia 10E70 by Agfa Gaveart and it was illuminated by a 5 mw Spectra Physics He-Ne Gas Laser. Holography requires the use of film with high resolution (28) and the film used here is capable of resolving 2800 lines/mm (regular photographic film, i. e: Kodak Tri-X can resolve only 40 lines/mm). The hologram was then developed in Agfa developer Metinol U for 4 minutes, fixed in Agfa Acido Fix for 4 minutes, and washed in running water for 10 minutes.

An attempt was made to keep the wash water at room temperature in order to prevent emulsion shrinkage or expansion. As well, during the exposure of the film and subsequent testing period, the ventilation system was shut down to eliminate air currents which might result in fringe movement.

After the hologram was allowed to air dry (which usually took about one hour), it was replaced in the film holder. The Scientia 10E70 emulsion was on 4" and 5" glass plates, which makes it possible to replace the film easily in the holder, as described in Appendix C. When this is done, a series of equally spaced fringes is usually seen on the plate; these can be removed by carefully adjusting the position of the film against the positioning pins. When the plate appears uniformly bright, the hologram has been properly repositioned. If, however, the fringes are curved and cannot be completely nulled out, it is quite likely that emulsion shrinkage has occurred, and a new hologram must be made. Once a satisfactory hologram had been made, repositioned, and nulled, the loading sequence of the plate was carried out.

Before the plate was put in the loading frame, it was painted with a diffusely reflective aluminum paint. The paint used was made by Magnaflux Corporation and is used as an undercoat in Brittle Coating experiments. A grid of lines was then drawn on the painted surface of the plate, such that its width was divided into 10 equal segments and its length into 5 equal segments (see Figure 8). As is shown in Figure 8, the loads were applied where the grid lines intersected and at the edges of the plate. The load selected was such that a maximum of about 30 to 40 fringes appeared on the plate.

The deflection data was recorded by photographing the live holographic fringes as observed through the holographic plate. This was done using a 35 mm camera and Panatomic - X film with a one second exposure. This sequence was repeated at each of the points marked in Figure 8. Because of the sensitivity of the technique, the loads were all less than 5 lbs., with some ranging down to 0.1 lbs. on the more flexible plates.

The photographs of the holographic fringes then contain all the information necessary to obtain deflection contours for the plate, as well as locating the point of maximum deflection. The photographs may be printed before information is taken from them, or they may be projected on a screen for interpretation.

4.2 Bending Moment Determination

The bending moment distribution along the clamped edge of the plate was determined by using a series of strain gages distributed along the edge of the plate. It is possible to relate the bending moment to the strain at the surface of the plate if one assumes that at the clamped edge only strains normal to the wall can exist. This means that ϵ_y (the strain parallel to the wall) must be zero, as is the shear strain (γ_{xy}). Therefore, the only strain is that measured by the gage, ϵ_x. The stresses computed from such a strain distribution are (see reference 29, Timoshenko and Goodier, for instance):

$$\sigma_x = \frac{E\epsilon_x}{(1-\nu^2)}, \quad \sigma_y = \frac{\epsilon_x E \nu}{(1-\nu^2)}, \quad \tau_{xy} = 0 \qquad \ldots (4.3)$$

The relation between the bending moment in a given direction in a plate and the surface stress in the same direction is given by (see reference 24 for example):

$$M = \frac{h^2\sigma}{6} \qquad \ldots (4.4)$$

where the moment M is given in lb. - in./in. The moments at the clamped edge of the plate then become after substituting (4.3) in (4.4):

$$M_x = \frac{E h^2 \epsilon_x}{6 (1 - \nu^2)} \quad , \quad M_y = \frac{\nu E h^2 \epsilon_x}{6 (1 - \nu^2)} \quad , \quad M_{xy} = 0 \qquad \ldots (4.5)$$

By this means, it is possible to calculate the bending moments from the strain readings.

The strain gages were placed symmetrically along the clamped edge, on the side of the plate opposite the load. This results in all of the strains being compressive. There was a gage placed along the centre line of the plate ($y = 0$) and one at either end of the plate ($y = \pm 1$); this is illustrated in Figure 9 where the locations of other gages are listed.

The procedure involved loading the plate at each of the grid points shown in Figure 8 and then recording the strain reading at each of the gage positions. The load used was up to 130 lbs. in dead weights depending upon the stiffness of the plate, with the maximum strains to 500 μ in/in. The strains were read out on a Budd P-350 strain indicator, used in conjunction with a Budd SB-1 switch and balance unit which allows a maximum of 10 gages to be used. The internal dummy in the switch and balance unit was used, which means that no temperature compensation is available; however, over the period of the experiment no measurable changes were noticed.

5. Results and Discussion

5.1 Plate Deflections

5.1.1 Theoretical Results

The first results calculated were those which corresponded to the work of previous investigators. This was done to check the validity of the approach being used on plates of different aspect ratios. There is, however, very little to compare to; the only work being that of MacGregor (16), Holl (17), Jaramillo (18) and Dalley (20).

First we will compare the theoretical results and the work of MacGregor (16) who tested a plate with a central point load on its free edge and an aspect ratio of 0.147. He also presented theoretical results which he had obtained for an infinite plate. His results, experimental and theoretical, are shown in Figure 10. The plate he tested was steel, with $E = 30 \times 10^6$ and Poisson's ratio 0.3, also it was $8\frac{1}{2}$ inches wide, 1.25 inches long and 0.125 inches thick. Based on these dimensions, the deflections expected were calculated using the theory presented in section 3.1.2. These are shown in the same figure as MacGregor's results. Agreement is good with the theory comparing within 1.3% of MacGregor's theory and within 0.5% of his experimental results at the point of maximum deflection. Agreement is also good along the whole length of the plate.

Figure 11 shows a comparison between the free edge deflections of a cantilever plate with a point load centrally applied on its free edge. These results were obtained by Holl(17) who used a finite difference technique to obtain the deflections of a cantilever

plate with an aspect ratio of 0.250. Also shown in the same figure are the results obtained from the present theoretical solution to the same problem. The two curves agree quite well in terms of general shape; however, there is a 12% difference between them at the point of maximum deflection. Holl's results were obtained from a finite difference technique which used only 16 elements to represent the plate; the reason his deflections are larger than those predicted by the theory is likely due to the limited number of elements he used.

Jaramillo (18) derived the deflections of an infinite plate under various point loading. In Figure 12, the free edge deflection of an infinite plate under the action of a free edge load, as calculated by Jaramillo, is shown. As well, the free edge deflections of a plate with an aspect ratio of 0.167 with a load at $\alpha = 0$, $\beta = 1$ (see Figure 3 for nomenclature). It is not expected that these should agree perfectly; however, excellent agreement is shown over most of the plate length, with poorest agreement occurring at the centre of the plate edge (under the load). Here the maximum difference is 5.5%, which is still reasonable considering that Jaramillo's solution is for an infinite plate.

Dalley (20) tested a square plate with point loads at different locations on the plate. Figure 13 shows the deflection contours he obtained for the plate loaded with a point load at the centre of its free edge. Also shown are values calculated by the theory being used here; they are shown listed at the grid points marked. There is excellent agreement between Dalley's experimental and the theoretical results (1% at maximum deflection point).

Figure 14 shows Dalley's results for a corner loaded square plate, as well as the theoretical values. Again, agreement is almost perfect with a maximum difference of about 1% at the maximum deflection point. Dalley is the only investigator to give deflection contours, and the ability of the theoretical results to compare to his over the surface of the whole plate, indicates the validity of the approach chosen.

In fact, the high degree of agreement between the theoretical approach being employed here (i. e: that of Szmetler et. al.) and the work of the four authors cited, establishes the accuracy of the method. For this reason, the method was considered suitable for use as a basis for comparison with the experimental results.

The theoretical results for twelve aspect ratios, with a Poisson's ratio of 0.3, were calculated using the technique outlined in section 3.2. The deflection information from the program run, for an aspect ratio of 0.25, is shown in Table I. The program calculates the deflections at all of the grid points shown in Figure 8 for loading at each of the points marked by a star in the same picture. This results in 30 unique loadings, each generating a matrix of deflections at 66 points. Looking at one of the deflection matrices, the fixed edge is at the left side of the page and the free edge at the right side. The point at which the load is applied is underlined, with the values of α and β written beside the matrix giving the location of the load as well. This method of generating a deflection matrix quickly pinpoints the location of the maximum deflection point in relation to the maximum load point. As can be seen from the table, the

maximum deflection is always at the free edge and also on a normal from the wall through the load point or between the normal and the closest free corner. This has been observed in all of the plates considered under point loads anywhere on the plates. Using these matrices, it is possible to draw deflection contours for the plates, which should correspond to the results of the holographic interferometry experiments. This will be discussed in greater detail in the following section, where the theory and experiment will be compared.

5.1.2 Experimental Results

A total of ten plates were tested, as was previously mentioned. Three of these, with aspect ratios of 1.0, 0.50 and 0.25, will be discussed in detail here. These three plates are representative of the others tested, and have been selected since they cover a large portion of the aspect ratio range tested.

Figures 15, 16 and 17 show live fringe holograms of the three plates mentioned for loading at various points along the free edge. These photographs of the loaded plates were taken through the hologram made while the plate was unloaded, thus producing the fringes shown. The illumination of the plates is nonuniform since insufficient laser power was available for the field size being used; this tends to be a bit of a problem when examining the photographs. The experimental deflection values were taken visually from the negatives in an enlarger, and since the human eye has far more latitude than photographic paper, no serious problems were encountered due to this nonuniformity.

Figure 15 shows the holographic deflection contours for the

square plate tested. All photographs were taken using the same load of 0.55 lbs, which produces a varying amount of maximum deflection depending upon the position of the load. The loadings shown are for free edge location of the load (i. e: $\beta = 1$ and $0 \leq \alpha \leq 1$), other values of α and β were tested of course, but the results will be presented in a summarized form only. It is interesting to note here that the fringes on the plate tend to remain relatively straight; (truly straight fringes would indicate that the deflection is not too localized). Rather, the effect of the load is reaching all points of the clamped edge with an approximately equal effect. In Figure 16, which shows the deflection contours for a similar loading scheme on a plate with aspect ratio of 0.5, the curvature of the fringes is very pronounced. Also in loading this plate, it was necessary to use higher loads near the centre of the plate than at the corner to produce a suitable number of fringes. Here the effect previously mentioned becomes evident, that is to say that the maximum deflection occurs at the free edge between the load point and the nearest free corner. This effect is more evident in Figure 17 where the deflection contours are shown for a plate with aspect ratio of 0.25. Here the deflection can be seen to be relatively localized; in fact, so much so that all loadings for $0 \leq \alpha \leq .8$ appear to produce approximately equal maximum deflections. The loading here produces such large variations in deflection that approximately twice the load had to be used at the centre of the plate as at the free corner to give equal maximum deflection.

Figures 18 through 20 compare the theoretical and

experimental deflection contours (i. e: lines of constant $\frac{\delta D}{P b^2}$) obtained for the square plate tested. The agreement between theory and experiment is excellent for all the loadings shown; (these being the same as those shown in Figure 15). In fact, the maximum differences between the two are about 2%. This agreement was to be expected, of course, because of the good agreement shown between the theoretical results and the experimental results of Dalley (Figures 13 and 14).

Figures 21 through 23 compare the theoretical and experimental deflection contours obtained for the plate with aspect ratio of 0.50. The agreement for this plate is not quite as good, with some differences up to 5%; however, most contours agree to a greater accuracy than that. The contours are in all cases of the same shape and merely displaced or slightly less curved.

In Figures 24 through 26 the theoretical and experimental deflection contours are shown for the plate with aspect ratio of 0.25 tested (the experimental contours being shown in Figure 17). The agreement here is also within about 5% in the worst cases, with very good agreement in terms of contour shape and location. There are several points which seem to come out of the nine figures just mentioned (i.e: 18 through 26). And they are:

1) theoretical and experimental contours are similar in shape
2) maximum differences between the two are less than 5%
3) maximum deflection is always indicated by both contour sets to be in the same place
4) as the aspect ratio decreases, the value of $\frac{\delta_{max} D}{P b^2}$ decreases.

Up to this point, no mention has been made of any loadings other than those which are on the free edge. However, many other

loadings (i. e: at interior points) were tested and calculated theoretically, but due to space limitations they will only be summarized in terms of the maximum deflection produced. These results will be presented in the next 5 figues; however, it is first necessary to explain the dotted line which appears in all of the figures. This line represents the elementary maximum deflection of a point loaded cantilever. This is equivalent to saying that this would be the maximum deflection produced if the plate were infinitely stiff in the y direction and could therefore only bend in the x direction. This approach will of course result in lower deflections than those which actually do occur. Since the curves are plotted in terms of $\frac{\delta_{max} D}{P b^2}$ vs. Aspect Ratio, it is necessary to derive this relationship for the cantilever beam. Shigley (5) gives the relation between the maximum deflection and other variables as

$$\delta_{max} = \frac{P}{6 E I} (3 x^2 b - x^3) \quad \ldots \quad (5.1)$$

where the arrangement is shown in the small figure (a) to the right, also this maximum deflection occurs at the free end of the beam. The moment of inertia, I, is given by (refer to Figure (b))

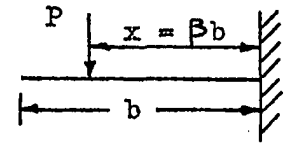

(a)

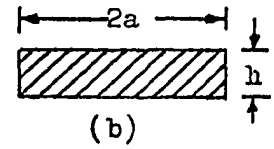

(b)

$$I = \frac{1}{12} (\text{base}) (\text{height})^3$$

$$= \frac{a h^3}{6} \quad \ldots \quad (5.2)$$

The distance x between the load point and the fixed end of the cantilever is given by $x = \beta b$. Now if we substitute this value for x and the value of I given by (5.2), equation (5.1) becomes

$$\delta_{max} = \frac{P b^3}{a h^3 E} (3\beta^2 - \beta^3) \qquad \ldots (5.3)$$

The plate rigidity, D, is given by

$$D = \frac{E h^3}{12 (1 - \nu^2)}$$

from which

$$E h^3 = 12 D (1 - \nu^2)$$

substituting this equation in (5.3) we have

$$\delta_{max} = \frac{P b^3 (3\beta^2 - \beta^3)}{12 D a (1 - \nu^2)} \qquad \ldots (5.4)$$

rearranging we have

$$\frac{\delta_{max} D}{P b^2} = \left(\frac{b}{2a}\right) \left(\frac{3\beta^2 - \beta^3}{(1 - \nu^2)}\right) \qquad \ldots (5.5)$$

or:

$$\frac{\delta_{max} D}{P b^2} = m \left(\frac{b}{2a}\right) \qquad \ldots (5.6)$$

where m is a constant which depends on the location of the load point (β). The values of m corresponding to the β values which were considered experimentally are given in the following table:

β	m
0.2	.0202
0.4	.0790
0.6	.158
0.8	.258
1.0	.367

Equation (5.6) predicts a linear relation between the maximum deflection and aspect ratio for the ideal cantilever beam.

Figure 27 shows the variation of maximum plate deflection as a function of aspect ratio, for cantilever plates loaded at various points along the free edge. The solid curves indicate the values predicted by theory, and several points relating to these curves are immediately evident. First, as the aspect ratio becomes small, (i. e: short, stubby plates) the maximum deflection reaches a constant value which depends upon the load position (α). Second, as the aspect ratio becomes large (i. e: long, narrow plates) the value of α becomes insignificant and all of the curves converge on the value predicted by the elementary cantilever approach which was outlined previously. As can be seen, the curve for central loading ($\alpha = 0$) approaches this value (i. e: cantilever value) for far smaller values of aspect ratio than the curves for larger values of α. A fourth point is that all curves for values of α other than 1 will become asymptotic to the curve for $\alpha = 0$ as the aspect ratio decreases. These four points are true for all values of β considered and the maximum theoretical deflection variation as a function of aspect ratio is shown in Figures 28 through 31 for β values of 0.8, 0.6, 0.4 and 0.2.

The experimental maximum deflections obtained from the holographic experiments are also shown in the figures just mentioned, as are the results of several other investigators. Referring again to Figure 27, it can be seen that agreement between theory and experiment is excellent for corner loading of the plate. In fact, agreement for all values of α is good, with some scatter shown for the 0.8 and 0.6 curves. This scatter can best be explained in terms of load point location on the plate, since the values of

$\frac{\delta_{max}\, D}{P\ b^2}$ are changing rapidly in this region as a function of α; any small error in α (i. e: load position) will result in large scatter. The experimental points for $\alpha = 0$ (central loading of the free edge) are in excellent agreement with the theoretical values for high aspect ratio; however, they tend towards a higher value as the aspect ratio becomes smaller. This is, however, in agreement with the results of MacGregor (16), whose experimental point is shown for the plate he tested (aspect ratio = 0.147). Also shown at the extreme left hand side of the figure is the infinite plate value of MacGregor, which should be equal to the value predicted by theory. There is a difference between the two of 10%, however, and the most reasonable explanation of this difference is to attribute it to errors in the energy solution being used. Also shown in this figure is the result of Holl (17) who used a finite element solution, but agreement here is poor, as was mentioned previously in section 5.1.1. Two investigators, who studied cantilever square plate deflections experimentally, have their results shown in this figure. They are Palmer (30) and Dalley (20). Agreement with Dalley's results are so good that his points are not visible since they are identical to the present experimental results. Palmer's point, however, for a corner loaded plate, tested using projected moiré fringes shows a larger deflection resulting than is predicted here.

Figure 28 shows the variation of the maximum plate deflection with aspect ratio for point loads at $\beta = 0.8$ and $\alpha = 0$, 0.2, 0.4, 0.6, 0.8 and 1.0. These curves are strikingly similar to those shown in Figure 27 for $\beta = 1.0$. Experiment and theory

agree to within 5% everywhere, with more scatter in the points for $\alpha = 0.8$ and 0.6, for the same reason as mentioned before. There are no other experimenters to compare results with, for loadings within the plate boundaries. However, the agreement between theory and the present experiment is adequate to serve as a verification of the theoretical approach.

Figure 29 shows the variation of the maximum plate deflection with aspect ratio for point loads along $\beta = 0.6$ for various values of α. Agreement is again quite good, with a general tendency for the experimental values to be above the theoretical curves for low aspect ratios. The percent difference between the two (experiment and theory) is approximately 5% maximum for $\alpha = 1.0$, 0.2 and 0, and 10% maximum for $\alpha = 0.4$, 0.6 and 0.8. These differences occur only for aspect ratios less than 0.50, while for aspect ratios greater than this agreement is excellent.

However, if we now look at Figure 30 which shows the variation of the maximum plate deflection as a function of aspect ratio for $\beta = 0.4$ and various values of α, a new effect is in evidence. The theoretical and experimental (if they had been drawn) curves arrive at different constant maximum deflection values as the aspect ratio approaches zero. The difference between these values is about 10%. For higher aspect ratios, the agreement is still very good. This discrepency between theory and experiment will be discussed later.

In Figure 31, the variation of the maximum plate deflection as a function of aspect ratio is shown for $\beta = 0.2$ and various values of α. Here the spread between theory and experiment is huge,

(40% for $\alpha = 1$); however, the general shape of the curves is similar. This loading ($\beta = 0.2$) is closer to the clamped edge than the previous loading ($\beta = 0.4$) and the discrepency between theory and experiment is larger; this would tend to indicate that either the theory is inadequate near the clamped edge or the experiment is inadequate there.

In order to get a better indication of what is happening as β varies, Figure 32 was constructed. This figure shows the variation of the maximum plate deflection $(\frac{\delta_{max} D}{P b^2})$ as a function of load position (β) for a plate of low aspect ratio (≤ 0.25). Two theoretical curves are shown, one for $\alpha = 1.0$ (corner loading) and one for $\alpha = 0.0$ (central loading). The theory and experimental points for $\alpha = 0$ are seen to agree well; also shown is Jaramillo's curve (18) for the infinite plate. The experimental points for $\alpha = 0$ are seen to lie between Jaramillo's curve and the theory curve, with the difference between the two theory curves being about 10%. The curve for $\alpha = 1.0$ shows a much higher deflection than that for $\alpha = 0.0$; in fact, it is about 2.8 times as great. The experimental points shown indicate good agreement with theory for β greater than 0.6. However, for lower values of β the experiemtnal points show a higher deflection than was indicated by theory. This effect can be explained on the basis of one or both of the following considerations:

1) as the load is applied nearer the fixed edge, shear deflections which the theory ignores may become important

2) fixed edge rotations which may be insignificant when the

load is far from the edge (and producing more deflection per pound) could easily amount to an increase in deflection of 40%.

5.2 Plate Bending Moments

5.2.1 Theoretical Results

In order to check the accuracy of the theoretical approach, the theoretical bending moments were first calculated which corresponded to the work which had been done by other investigators. There are four investigators who have bending moment information for cantilever plates available. They are: Holl (17), Jaramillo (18), Vartak (19) and Wellauer and Seireg (4).

Holl, as was mentioned before, used a finite difference technique to calculate the moments and deflections for a cantilever plate with a central free edge point load, with an aspect ratio of 0.25. His moment results are shown in Figure 33, as are the values predicted by the theory being used here. The comparison between the two methods is extremely good, with the difference at the maximum moment point being only 2%. The area under both curves is identical, which is, of course, a necessary situation since the integral of the moment along the fixed edge must equal the applied moment to the plate. The distribution of the fixed edge bending moment is slightly different, however, with Holl's results being higher near the edge of the plate and lower at the centre.

In Figure 34, the bending moments predicted by Jaramillo (18) for an infinite plate loaded by a point load at its free edge are compared to those predicted by the present theory for a plate with aspect ratio of 0.167. That this comparison is justified will be made evident at a future time. Comparison between the two curves is very good, with the poorest agreement occurring at the centre of

the plate where the difference is 4%. This agreement is still quite good considering that the difference in aspect ratio should account for some part of this difference.

Vartak (19) tested two plates, under point loadings at the free edge, with aspect ratios of 0.167 and 0.250. The deflections of the 0.250 plate were about 3.5 times the thickness, which is beyond the region where small deflection theory can be expected to hold. This plate was not considered here for that reason, and comparison is made only to his results for the 0.167 plate he tested. His results for corner and middle free edge loading are shown in Figure 35, where they are compared to the values predicted by the theory developed here. As is easily seen, the comparison is very good for both mid point and corner loading of the free edge. Under corner load, the theory is 10% lower than the experimental value predicted by Vartak. For mid point loading, the comparison is much better with the theory 3% higher than Vartak's value. This agreement is very encouraging since the theory shows good comparison with experimental data.

Wellauer and Seireg (4) tested a thick cantilever plate; this plate was 2 inches thick, 12 inches long and projected 2.25 inches from the wall. This corresponds to an aspect ratio of 0.187. The plate had $\frac{1}{4}$ inch fillets; these, of course, lead to some problems when it comes to placing the strain gages near the wall. The fillets are necessary since the plate was machined from a solid block, and in order to avoid infinite stresses at the corners where the plate and wall are joined, some fillet radius is required. The gage length of the gages used by them was 1/8 inch; this means

then, that the point at which the moment is being measured is at least 0.375 inches away from the wall. This corresponds to 16.7% of the plate length and lower moments must therefore be measured for this reason, than actually occur at the fixed edge. In Figure 36, their experimental and theoretical results are compared with the theoretical approach being used here. A few words about the theory advocated by Wellauer and Seireg would appear to be in order here, since this approach of theirs will be mentioned many times in subsequent sections. Their approach is semi empirical (their term) in that it uses as its basis the theoretical results of Jaramillo and manipulates them to obtain a solution which compares to their experimental results. The basic premise is that Jaramillo's infinite plate result is valid for finite length plates of low aspect ratio (this is borne out by the present research). Therefore, for loading along the plate centreline, their solution is identical to that of Jaramillo. However, for off centre loading, some of the fixed edge bending moment would have no plate to act upon (as it is symmetric with respect to the load point). Here they introduce a concept which they call the moment image technique, whereby the extra moment (beyond the end of the plate) is reflected about the plate end and added to the moment already there. This method is illustrated in the figure at the right. It is easy to see that using this concept will result in M_{max} for corner loading being 2 M_{max} for mid point loading.

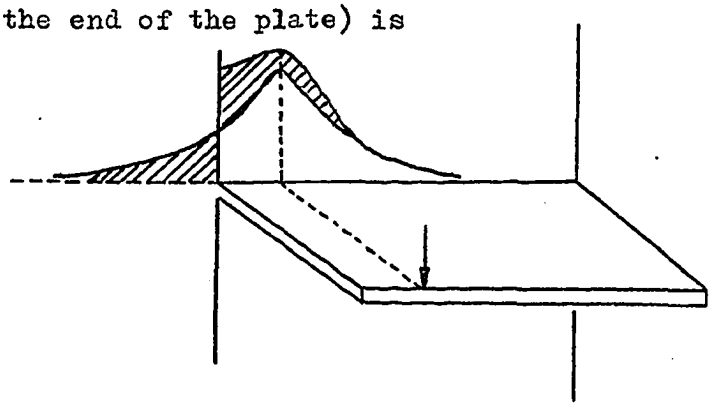

Referring to Figure 36 again, we see that for central loading of the free edge ($\alpha = 0$, $\beta = 1$) agreement between the two theoretical curves shown and the experimental points is good with the difference at the maximum point being about 3%. For corner loading, it is a different story altogether, with the present theory giving $\frac{M_{max}}{P} = 1.22$, the theory of Wellauer and Seireg giving $\frac{M_{max}}{P} = 1.00$, and their experiment giving $\frac{M_{max}}{P} = 0.90$. That their theory could give poor results is evident from the description of it which was just given. Their experimental data could be in some error as well due to fillet radius which existed at the wall. As was mentioned, the gages had to be located at least 16.7% of the plate length away from the wall. The values indicated from my theory for these locations and loadings are $\frac{M_{max}}{P} = 0.98$ for corner loading and $\frac{M_{max}}{P} = 0.45$ for mid point loading of the free edge. This tends to explain some of the differences between Wellauer and Seireg's experiment and the theory being presented here, since this reduces the percentage differences to about 10% for both of the loadings being considered here.

Based on the comparison between the theory and the results presented by the four authors mentioned above, the theory derived in section 3.1.2 was judged a satisfactory solution to the problem. The bending moments at various points (66 of them) were then calculated for different point loadings (30 of them) as shown in Figure 8 for plates with various aspect ratios. This results in the generation of a large amount of information which is impossible to present totally. The maximum bending moments at the fixed edge will be presented at a later time (in section 5.2.2) as will several bending moment distribution curves. For the moment, let

us look at the principal moment distribution in the whole plate for several loadings.

Figure 37 shows in a top view the principal moments and their direction for a point loaded (β = 1.0, α = 0.0) cantilever plate with aspect ratio of 1.0. The moments are drawn to scale, with the arrows indicating their sign. As can be seen in the figure, it is quite easy to visualize the stress flow from a diagram such as this. As well, by observing the moments at the free boundaries, a judgment of the solution validity (at the boundaries anyway) can be made, since the principal moment directions are known a priori there. For the plate being considered here, the free boundary moments of any significant value are seen to conform quite well to the directions which are allowed by the boundary conditions (i. e: parallel to the boundary a moment may exist but normal to it none can exist).

In Figure 38 the same plate is shown under the action of a corner load. The stress trajectories are seen here to begin normal to the wall and curve over towards the corner where the load is being applied. Here, there are moments of obviously wrong directions at the free boundaries in the region of the load. The deviation from the expected direction becomes worse as the point of load application is approached. This means that the bending moment theory used to predict these moments must be in error at these points. While this does hurt the general application of this method, it was to be expected that using an energy technique would result in a little less than perfect results. The results at the fixed edge, where the maximum moments result, do conform to the expected

direction and therefore are not suspect as those at the free boundary are.

The theoretical principal bending moments in a centrally loaded (β = 1.0, α = 0.0) cantilever plate of aspect ratio 0.25 are shown in Figure 39. The moments are drawn to the scale shown there, with the arrows indicating their sign. Comparing the moments in this plate to those in Figure 37 (where the same loading is applied to a plate with an aspect ratio of 1.0) two points are evident. First, as a plate becomes wider (i. e: lower aspect ratio), the stress trajectories must curve more severely since they originate normal to the wall and must curve toward the load point. Second, the effect of the load is more isolated in plates of low aspect ratio, which is to say that the moment is unable to distribute itself uniformly along the clamped edge.

In Figure 40 the same plate (aspect ratio = 0.25) is shown with a point load at a free corner. The resulting bending moments in this case are seen to be extremely localized with one half of the plate almost stress free. Here it becomes evident that any lengthening of this plate would not reduce the stress introduced in it at all; in fact even in the case shown, the plate could be significantly shortened (in the clamped direction) and no increase in stress would occur. The moments at the free edge are obviously in error with regard to direction and the reasoning here is the same as mentioned previously for Figure 38.

Based on the foregoing figures and discussion, it is reasonable to say that the moment calculation technique used for point loaded cantilever plates gives a satisfactory means for

predicting the bending moments. The moments indicated by this means are questionable at the free edges of the plate in the region of the load, but satisfy the boundary condition at the clamped edge, which is the region of major importance.

5.2.2 Experimental Results

As was outlined in section 4.2, ten different plates were tested under 30 unique loadings each, or 300 different point loadings. For each of these cases, a bending moment profile was obtained at the fixed edge using several strain gages located along the fixed edge. A detailed comparison of the bending moment profiles obtained experimentally to those predicted by theory will be made only for free edge loading (β = 1.0) of the plates tested. This is done for the sake of brevity and since these moments represent the most severe that can occur in the plate. A discussion on the maximum moments produced for loadings where β is less than 1.0 will be carried out, however, later in this section.

Figure 41 shows the theoretical and experimental bending moment distributions at the clamped edge of a cantilever plate of aspect ratio 0.10 under various point loads at the free edge (β = 1.0, various values of α). The general trend is that the theory is predicting higher values than those indicated experimentally. The curves are very similar in shape, with only small differences notable in this respect. Since only nine strain gages were used on this plate and the moments are very localized, (as can be seen in the figure), a certain amount of imagination is necessary to draw the experimental curve. For this reason it is possible that a slightly different interpretation of how this curve

should have been drawn would have resulted in a better comparison of the theory and experiment. The difference between theory and experiment is about 7% at the maximum moment point for all values of α except -0.8 where the difference is about 14%. For central loading only $\frac{1}{2}$ of the plate sees any load effect (i. e: moment) and under the action of a corner load, only 1/3 of the plate sees any load effect. This localized nature of the bending moment at the root of the plate is of great significance. This is, of course, the effect predicted by Jaramillo (18) in his theoretical solution for the infinite plate.

Figure 42 shows the theoretical and experimental bending moment distributions at the clamped edge of a cantilever plate of aspect ratio 0.167 under several free edge loadings ($\beta = 1.0$, $0 \geqslant \alpha \geqslant -1.0$). The theoretical curves are again higher than the experimental curves with the theory being about 10% higher than experiment, in most cases. The similarity of shape of the curves (theory and experiment) is excellent with the exception of the curves for $\alpha = -0.8$. In this case the theory indicates a maximum directly opposite the load point, while the experiment indicates a maximum at the edge of the plate. No explanation of this will be attempted here, as it will be discussed later. Here it can be seen that the whole length of the plate sees bending moments under central loading, while for corner loading $\frac{1}{2}$ of the plate sees the effect of the load. This is far less localized than the moments for the plate of aspect ratio 0.100.

The bending moments predicted theoretically and obtained experimentally for a plate of aspect ratio 0.250 are shown in

Figure 43 for various free edge point loads. Once more the theoretical curves predict higher and slightly more localized moments than the experiment produces. An obvious reason for some of this difference is the fact that the strain gages must be a small distance from the wall and take an average reading over their length. A 1/8 inch gage length was chosen to alleviate this problem as much as possible. However, in the case of the 0.100 plate, the gage centre was still about one tenth of the plate length away from the wall. This factor of course diminishes as the aspect ratio increases because of the way the experiment was carried out (see section 3.3). Returning to Figure 43, it is evident that the curves all agree in shape, except the curve for $\alpha = -0.8$. The curve for corner loading ($\alpha = -1.0$) shows that about three-quarters of the plate fixed edge is stressed by the loading. Agreement between the maximum values of bending moment (theory and experiment) is very good for the corner loading; the difference being only 4%.

The results for the plate with aspect ratio of 0.333 are shown in Figure 44. Also shown there are the theoretical root bending moment distributions for various point loadings on the free edge. Agreement is good with about 10% difference resulting at the maximum values for the different loadings shown. In comparing these moment distribution curves with the previous curves presented, it becomes evident that as the aspect ratio increases, a larger percentage of the plate length is being used to effectively resist the load being applied. Another way of putting this is to say that only a certain length of a plate with low aspect ratio sees any bending moment at the fixed edge under a point load. This is verified by Jaramillo (18)

for the infinite plate.

All four of the plates mentioned in this section had very good shape agreement between the theoretical and experimental curves except for the curve for $\alpha = -0.8$. In all the cases studied, with aspect ratio 0.333 or less, the experiment shows that the maximum bending moment for $\alpha = -0.8$ loading occurs at the edge of the plate (i. e: $y = 1.0$). The theory, however, predicts that the maximum moment will occur at the clamped edge directly opposite the load point (i. e: $y = -0.8$) for $\alpha = -0.8$ loading. These two cases obviously cannot both be correct and one of them must be in error. It is most likely that the theory is correct while the experiment suffers at this point due to clamping problems. It is easy to see that any slight curvature changes at the clamped edge in the y direction can easily cause this shift in moment distribution to occur.

Moving on to Figure 45, where the fixed edge bending moments for a plate of aspect ratio 0.50 under various free edge loadings are shown, a new factor is evident. For central loading the bending moment distribution is shown to be essentially constant across the width of the plate. This is a significant departure from the previous plates shown where the fixed edge bending moments were more localized. However, for corner loading ($\alpha = -1.0$) a significant non uniformity of bending moment results. There are not the severe localizations shown by the previous plates, but corner loading does result in a maximum moment which is twice as high as that obtained for central loading. Agreement between theory and experiment is within 4% for central loading and differs by about 10% for corner

loading.

In Figure 46, the theoretical and experimental fixed edge bending moments are shown for a cantilever plate of aspect ratio 0.75, loaded at various points along its free edge. Comparing this plate to the previous one, (aspect ratio = 0.50), it is interesting to note that for central loading the 0.75 plate shows a much higher maximum moment than the 0.50 plate ($\frac{M}{P}$ = 0.87 vs. 0.64) while for corner loading, the maximum moments are quite comparable ($\frac{M}{P}$ = 1.32 vs. 1.30). The comparison between theory and experiment is quite good with the maximum differences being about 10% for all loadings shown. The theory now indicates that for corner loading the maximum bending moment will not occur opposite the load, but will be displaced towards the centre of the plate.

A comparison of the theoretical and experimental fixed edge bending moments for a cantilever plate of aspect ratio 1.00 for point loading at various free edge positions is shown in Figure 47. The agreement between theory and experiment is excellent with the difference being only 2% for central loading. For corner loading, the difference between the two is 10% at the maximum loadpoint. This plate, as well as the previous two tested, represent a second grouping. The first group consisted of plates with aspect ratios less than 0.333 and the second group plates with aspect ratios between 0.333 and 1.00. In this second group, the moment distribution for central loading is uniform (approximately), while for corner loadings, the distributions are anything but uniform.

The next three figures: 48, 49 and 50 show the distributions (theoretical and experimental) for cantilever plates with aspect

ratios of 1.5, 2.0 and 3.0. These are collected into a third group of plates, those with aspect ratio greater than 1.5. This group consists of plates which show very little variation in fixed edge bending moment, for different positions of the load point (i. e: α). Very little will be said of these plates, except that for the 1.5 and 2.0 plates the theory predicts maximum moments at interior points of the plate, while the experimental work indicates the maximum moments at the edge of the plate. The explanation of this is the same as that indicated previously for the plates of lower aspect ratio. Also the theoretical curves for the 3.0 plate are not shown since they are essentially equivalent to the experimental curves shown.

The maximum moments from all of the foregoing cases, as well as loadings at different points on the plates are summarized in the following graphs. These maximum moments are particularly important since they represent the bending moments which will cause failure in a practical cantilever plate application. In order to establish a criteria for comparison of the maximum moments to a commonly known case, the elementary cantilever moment will be written here in a suitable format. For a load P located a distance $x = \beta b$ away from the fixed edge, the total bending moment at the fixed edge is:

$$M = P \beta b \qquad \ldots (5.7)$$

for a simple cantilever beam. This is the moment for the total width of the beam; therefore, in order to reduce this to the bending moment per unit width (as is the usual convention), the moment must be divided by the plate width of 2a giving:

$$M = P \beta \left(\frac{b}{2a} \right) \qquad \ldots (5.8)$$

In order to obtain a nondimensional form, the moment (in in. -lb./in.)

is divided by P (the load), also in the cantilever the maximum moment is merely the moment anywhere across the width and we obtain:

$$\left(\frac{M_{max}}{P}\right) = \beta \left(\frac{b}{2a}\right) \qquad \ldots \quad (5.9)$$

The non dimensional maximum moment for the cantilever beam is therefore merely a product of the load position β and the plate aspect ratio (b/2a). The cantilever curves are plotted in Figures 51 through 55, as dotted lines. The relationship between maximum moment and aspect ratio is linear, therefore straight lines result in these figures.

In Figure 51, the theoretical and experimental maximum bending moments are plotted as a function of aspect ratio for point loadings at various points along the free edge ($\beta = 1.0$, $0 \leq \alpha \leq 1.0$). It is evident that all of the theoretical curves lie above the cantilever curve. This in effect states that for the aspect ratios shown, the moment distributions are non uniform and result in a higher value than the ideal cantilever beam would produce. Several general comments on the theoretical curves are in order and these will apply to all of the figures in this group (51 through 55). First, as the aspect ratio decreases all of the curves (for all values of α) approach a constant value. Second, for high aspect ratios (greater than 1.0) the maximum moment values approach the cantilever value, and the position of the load (α) becomes unimportant. Third, as the aspect ratio decreases ($\leq .04$) loading for any value of α less than 0.8 results in the same value of $\frac{M_{max}}{P}$. The agreement between theory and experiment is very good overall. The trend is that the experimental results are lower than the theoretical values; this was already mentioned in the previous

ten figures. It can be seen that the experimental results for central loading tend to a much lower (10%) value than the theory predicts. Also shown are the results of the other authors cited. Both of the plates tested by Vartak (19) are shown here, and while his 0.167 plate agrees well with the present experiment, the results for his 0.250 plate are extremely high for corner loading and much lower for central loading. The results of Wellauer and Siereg (4) are also shown (aspect ratio 0.187) and their results indicate a much lower moment for corner loading, and a much higher value for mid point loading. Holl's (17) theoretical point is also shown for the aspect ratio of 0.250. At the extreme left of the graph is MacGregor's (16) theoretical value for the case of the infinite plate; this theory indicates a higher value (10% difference) than the present theory. The theory and experiment are in good agreement with regards to predicting the shape of the curves to be expected, since they both indicate the same form of curves.

Figure 52 shows the theoretical and experimental variation in the maximum moment in cantilever plates of various aspect ratios loaded at $\beta = 0.8$ with various values of α. The shape of the theoretical curves is very similar to those for $\beta = 1.0$, the main difference being that they indicate lower values. Again the experiment indicates a much lower (10%) value than the theory for low aspect ratios, for all values of α other than 1.0. The curves for corner loading show much better agreement for lower aspect ratios.

In Figure 53, which shows the variation in maximum moment vs.

aspect ratio for various values of α and $\beta = 0.6$, it is interesting to note that the curve for $\alpha = 1.0$ is asymptotic to almost the same value for low aspect ratios as it was for $\beta = 0.8$ and 1.0. However, the value which the $\alpha = 0.0$ curve approaches is much lower (0.3 as compared to 0.42 for $\beta = 0.8$) The experimental results for $\alpha = 1.0$ show a much lower value (15%) than the theory predicts, but for central loading ($\alpha = 0.0$) the theory and experiment approach the same value for low aspect ratios. This figure, as well as the previous ones, shows very good agreement for high aspect ratios (i. e: values greater than 1.0) between the theory and experiment.

The curves for $\beta = 0.4$ are shown in Figure 54. The agreement between theory and experiment is still reasonable (10%) for all values of α except 1.0. For this loading there is a 25% difference between theory and experiment for all values of aspect ratio less than 1.0. All experimental points are lower than the corresponding theoretical points in this figure.

Extremely poor agreement is shown in Figure 55 between theory and experiment especially for $\alpha = 1.0$ where the experimental points fluctuate wildly. This figure shows the results for loading along $\beta = 0.2$, which means that the load is very close to the fixed edge. Any small errors in β (i. e: positioning of the loading apparatus) will result in a larger fluctuation in the maximum moment produced.

In order to get a better indication of what is happening as the load point approaches the fixed edge, Figure 56 was drawn. This figure shows the variation in maximum moment for a plate of low

aspect ratio (≤ 0.25) as a function of the distance of the load from the fixed edge for corner loading ($\alpha = 1.0$) and mid point loading ($\alpha = 0.0$). Jaramillo's (18) results for the infinite plate are shown as a dashed line in that figure and the theoretical curve is also shown there. The theoretical curve is 10% lower than Jaramillo's result for $\beta = 1.0$ and agreement becomes poorer as $\beta \rightarrow 0$. The experimental results for $\alpha = 0$ are lower than the theory (10% for 1.0, but only 6% for $0.8 \geq \beta \geq 0.4$). For corner loading ($\alpha = 1.0$) the experiment drops off much faster than the theory as $\beta \rightarrow 0$. Agreement is within 10% only for $\beta = 1.0$ and 0.8, while for lower values of β divergence is rapid. An explanation of what is happening in this case appears to be a difficult problem. However, the plate being clamped in the loading jig as it is cannot be rigidly fixed. In fact, the absolutely rigid fixed edge is an impossibility, since no matter how stiff the material of the wall is, or how massive it is, some deformation will take place. This deformation will tend to decrease the maximum moments in the plate and tend towards a more uniform distribution. This effect has been noted by several of the other investigators mentioned here, including Wellauer and Seireg (4) who tested plates machined from a solid block of material. A recent study including the effects of fixed edge flexibility on the deflections of thick cantilever plates has been carried out by Umezewa, Ishikawa and Hayashi (31). Their investigation shows that the fixed edge actually distorts. This will, or course, result in moment redistribution of the sort mentioned earlier. It is, therefore, a shortcoming of the present theory that it cannot

account for fixed edge flexibility easily. However, agreement between theory and experiment at about 10% is still a suitable comparison for engineering purposes.

In section 3.1.3 the moment distribution factor was defined as the ratio of the maximum moment in the plate to the nominal moment in the plate as defined by equation (3.27) for point loaded cantilever plates. The fact that this equation is identical to equation (5.9) is hardly surprising. Therefore, in order to obtain the moment distribution factor, K_m, one must simply divide the value of $\frac{M_{max}}{P}$ from any of the Figures 51 through 55 by the value given by the dotted line (cantilever value) at that aspect ratio. This was done here, resulting in Figures 57 through 61.

Figure 57 shows the variation of K_m with aspect ratio for cantilever plates loaded along the free edge ($\beta = 1.0$) with a point load at various values of α. The curves all converge to the value of 1.0 for high aspect ratios, since the maximum moments approach the cantilever moments in that case. For low aspect ratios (≤ 0.25) the moment distribution factor becomes inversely proportional to aspect ratio, and the equation can be written in the form:

$$K_m = \gamma / (\text{aspect ratio}) \quad \ldots \quad (5.10)$$

where $\gamma = 1.23$ for $\beta = 1.0$ and $\alpha = 1.0$ and $\gamma = 0.475$ for $\beta = 1.0$ and $\alpha = 0.0$. For plates between the two cases mentioned, (i. e: aspect ratios greater than 0.25 and less than 4.0, it is necessary to refer to the figure to obtain K_m values. The experimental points shown were also transferred from Figure 51 and the same agreement shown there is shown here also.

The K_m values for $\beta = 0.8$ and various values of α are shown in Figure 58. These curves are very similar to those shown in Figure 59, with the curves converging to 1.0 for high aspect ratios (≥ 4.0) and increasing as the aspect ratio decreases. The values of γ as defined by equation (5.10) are: $\gamma = 1.50$ for $\beta = 0.8$ and $\alpha = 1.0$ and $\gamma = 0.510$ for $\beta = 0.8$ and $\alpha = 0.0$. The experimental values show a trend towards predicting slightly lower values than the theory does.

In Figure 59, the theoretical and experimental variation of K_m with aspect ratio is shown for point loaded cantilever plates, loaded at $\beta = 0.6$ and various values of α. The γ values for this figure are: $\gamma = 1.92$ for $\beta = 0.6$ and $\alpha = 1.0$ and $\gamma = 0.550$ for $\beta = 0.6$ and $\alpha = 0.0$. Theory and experiment agree quite well. The agreement is not as good for Figures 60 and 61 where the K_m curves for $\beta = 0.4$ and 0.2 are given. The shape of the theoretical curves in these figures is quite similar to the ones mentioned previously.

In summary, it is possible to say that for aspect ratios greater than 6.0 the value of K_m is essentially 1.0 for all values of β and α. For values aspect ratio between 6.0 and 0.250, the curves presented in Figures 57 through 61 must be consulted to determine K_m. For values of aspect ratio less than 0.250, it is possible to use equation (5.10) to calculate K_m. The values of γ are listed in the following table:

β	α	
	0.0	1.0
1.0	0.475	1.23
0.8	0.510	1.50
0.6	0.550	1.92
0.4	0.630	3.10
0.2	0.980	4.96

The values listed under $\alpha = 0.0$ can also be used for other values of α if the curve for that value of α has converged to the mid point curve ($\alpha = 0.0$). These values of aspect ratio at which this happens are: 0.200 for $\beta = 0.2$, 0.100 for $\beta = 0.4$, 0.100 for $\beta = 0.6$, and 0.050 for $\beta = 0.8$.

5.3 Effect of Poisson's Ratio

In order to determine the magnitude and type of effect Poisson's ratio has on cantilever plate deflections and moments, several runs of the program shown in appendix A were made with different values of Poisson's ratio. The aspect ratio chosen for this study of Poisson's ratio effect was 0.25. Figure 62 shows the free edge deflections of two cantilever plates of aspect ratio 0.25 under the action of both a mid point load and a corner load. These plates have Poisson's ratios of 0.0 and 0.5, these being the two extreme values possible. The plate with the largest Poisson's ratio has the largest deflection for both loadings shown. Similarly, Figure 63 shows the moments resulting in the same plates for the same loadings. For mid point loading, the maximum moment is greater for $\nu = 0.5$; however, for corner loading, the

maximum moment is greater for $\nu = 0.0$. This is because the moment for $\nu = 0.5$ peaks within the plate; this is not what was expected, but it does occur.

In Figure 64, the maximum deflection and moment in a cantilever plate of aspect ratio 0.25, with mid point loading and corner loading are shown as a function of Poisson's ratio. The maximum deflection of a cantilever plate under a point load is seen to increase as Poisson's ratio of the plate does. In going from $\nu = 0.0$ to $\nu = 0.5$, for corner loading $\frac{\delta_{max} D}{Pb^2}$ goes from 0.351 to 0.483; while for $\nu = 0.3$, the value is 0.415. This means that if the value at $\nu = 0.3$ is taken as a base value, an increase in deflection of 14.4% occurs for $\nu = 0.5$, while a decrease in deflection of 15.4% occurs for $\nu = 0.0$. For mid point loading ($\beta = 1.0, \alpha = 0.0$) if we again take the value at 0.3 as the base value; an increase in deflection of 18.7% occurs for $\nu = 0.5$, while a decrease in deflection of 9.7% occurs for $\nu = 0.0$. The effect of Poisson's ratio on deflection is very important for the extremes mentioned; and an effect of a few percent can be expected even in going from $\nu = 0.25$ to 0.3.

For mid point loading, the maximum bending moment in the plate increases with increasing Poisson's ratio. If the value for $\nu = 0.3$ is chosen as the base value, a 10% increase in $\frac{M_{max}}{P}$ is noted for $\nu = 0.5$, while a 10% decrease in the maximum moment results for $\nu = 0.0$. However, for corner loading, the maximum bending moment in the plate decreases with increasing Poisson's ratio. Taking the value of maximum moment for $\nu = 0.3$ as the base value; a decrease in moment of 19.1% results for $\nu = 0.5$, while

an increase of 13.2% results for $\nu = 0.0$.

No experimental work has been done on studying this variation in cantilever plate bending moments and deflections with Poisson's ratio. The theory employed here indicates that a certain amount of caution is necessary in model studies to ensure that Poisson's ratio is accounted for. In particular, the testing of models made of rubber like materials (certain photoelastic materials fall in this category) is to be avoided due to the way in which the maximum bending moment for corner loading moves from the free edge towards the centre of the clamped edge.

5.4 Extension of Bending Moment Theory to Helical Tooth Loading

All of the discussion up to this point has dealt with cantilever plates under the action of point loads. In trying to apply this information to gear tooth stressing, it becomes evident that this type of loading can be encountered only in a few extreme cases. Point loading is approximately valid for Novikov profiles; however, a line load normal to the fixed edge should be a better approximation. Helical gear teeth carry line loads, whose angle of inclination β_m is given by (see Shigley (5) for instance):

$$\tan \beta_m = \tan \psi \tan \phi_n \qquad \ldots (5.11)$$

where ψ is the helix angle

and ϕ_n is the normal pressure angle

It is possible to make a further approximation by considering the load along this line as uniformly distributed. Referring to Figure 4, the nomenclature used in this section is outlined there as follows:

η - non dimensional distance ($1 \geq \eta \geq -1$) used to indicate where the load line intersects the free edge of the plate; it is given by $\eta = y_1/a$ where y_1 is the actual value of y at which the intersection occurs

β_m - inclination angle to the free edge ($0 \leq \beta_m \leq 90^o$)

q - load intensity per unit length

The moment at the fixed edge will be nondimensionalized as $\frac{M}{P}$ where P is the applied load, i. e: $P = ql_m$ where l_m is the length of the load line. In Figure 4, for example, the length of the load line is:

$$l_m = (\eta + a) / \cos \beta_m$$

which means that

$$P = \frac{q(\eta + a)}{\cos \beta_m} \qquad \ldots \quad (5.12)$$

Equation (5.12) is not always valid, since the load line may intersect the fixed edge rather than one of the free sides for large β_m and low aspect ratio; in which case the load line would be shorter. In this case

$$l_m = \frac{b}{\sin \beta_m} \qquad \text{and} \qquad P = \frac{q\,b}{\sin \beta_m} \qquad \ldots \quad (5.13)$$

A general rule is to take the value of l_m which is the smallest from equations (5.12) or (5.13).

In order to obtain theoretical bending moments for line loadings, superposition of point loaded solutions was used. This was done by modifying the program shown in Appendix A, such that 31 points along the load line were chosen at equal intervals; the solution for each of these load points was superimposed (at 31

positions along the fixed edge) and the resulting values divided by the number of load points considered. This scheme was carried out for load lines at β_m values of 0,7,12,20,45,60 and 90 degrees, which covers the range of commonly used values as predicted by equation (5.11) using the common values of ϕ_n and Ψ.

Also to obtain experimental values, the point loading experimental values were superimposed in a fashion similar to that used for the theoretical values. The point loading bending moment values are listed in Table II. These values were used in a computer program which superimposed the moments at the gage points for loading at fixed values of α (11 in all) and the values of β determined from the values of η and β_m chosen. These values of β in general did not correspond to the values tested and interpolation of values was necessary. This means that a maximum of 11 point loads were superimposed; this happens for low values of β_m and large values of η. However, in many cases few points were considered; if the number was too low, the values were discarded.

Values of the fixed edge bending moment distribution were calculated for 7 values of β, 11 values of η and many values of aspect ratio, both theoretical and experimental by superposition. To present all of these curves would be impossible; therefore a few cases to indicate the general trends will be discussed.

In Figure 65, the fixed edge bending moments in a line loaded cantilever plate of aspect ratio 0.500, with load lines through $\eta = 1.0$, at various angles are shown. It is interesting to note that theory and experiment indicate the same shape of curve, even

though the magnitudes are significantly different. The experimental maximum moment is 11% low for β_m = 90 degrees, and 7% high for $\beta_m = 0^\circ$. For $\beta_m = 0^\circ$, it can be seen that 75% of the plate width is subjected to a uniform fixed edge bending moment, with only a slight dropping off near the ends of the plate. The distributions for 7 and 12 degrees are also quite uniform, with the moment down somewhat from the β_m = 0 curve because of the longer load line which results in a larger value of P .

In Figure 66, the same plate is shown under the action of line loads normal to the fixed edge ($\beta_m = 90^\circ$). Agreement between theory and experiment is very good for central loading, the difference being only 2% for $\eta = 0$ at the maximum value. For other values of η the comparison is poorer. It is interesting to compare these bending moment curves to those shown in Figure 45 for the same plate (aspect ratio 0.500) under point loadings along the free edge. The shape of the curves is very similar, with the results for line loadings being more localized than those for point loadings. This can be explained on the basis of the fact that for the line loading a larger percentage of the load is near the wall, which results in a more localized bending moment.

Referring to Figure 67, the theoretical and experimental fixed edge bending moments are presented for a line loaded cantilever plate of aspect ratio 0.250, with the load lines passing through $\eta = 1.0$, for various values of β_m. For $\beta_m = 0^\circ$, the theory and experiment agree within 2%. As well, for this value of β_m, 80% of the fixed edge sees a uniform bending moment, with only a slight drop off near the end of the

plate. For $\beta_m = 90^0$ the experiment predicts values which are 20% lower than the theory predicts. Similar trends exist for the intermediate values of β_m shown.

Now Figure 68 shows the fixed edge bending moments in the same plate for line loadings with $\beta_m = 90^0$ and various values of η. Agreement is excellent for $\eta = 0.0$ between theory and experiment; however for other values of η, the experiment indicates lower values than the theory does. Once again it is interesting to compare this figure to that for point loadings along the free edge (Figure 43). The curves are again quite similar with the results for line loading being more localized than those for point loading.

In the past four figures, it was obvious that agreement between theory and experiment was not as good as it had been for the point loadings. This is explainable mainly on the basis of two facts. First, superposition tends to accumulate the errors present in the initial data; in particular, if the data for loading near the wall is low, as was evidenced in the previous section 5.2.2. Also if the number of points considered is too low, a reasonable approximation of the moment at the wall will not be achieved; in some cases this condition can be violated in the data available here.

Of primary importance in gear design is the maximum bending moment in the tooth. And to that end the following 7 figures have been plotted. These give the maximum moment of a line loaded cantilever plate as a function of aspect ratio.

Figure 69 has $\beta_m = 0$ degrees and is plotted for various values of η. The curve for $\eta = -1.0$ is the same in the next 5 figures and is also the same as that shown in Figure 51 for $\alpha = 1.0$.

In all cases when $\eta = -1.0$ the load must be a corner point load which leads to the curve of Figure 51 ($\alpha = 1.0$). The nominal moment for this case was taken as the cantilever moment as given by equation (5.9) with $\beta = 1.0$. Agreement between theory and experiment is seen to be good for large aspect ratios; however, for small aspect ratios and larger values of η the two results diverge. This is due to the fact that the errors in the initial moment data are becoming large in comparison to the values of M_{max}/P which are decreasing in this region. Two experimental points of Wellauer and Seireg (4) are shown in this figure for an aspect ratio of 0.187. Their value for corner loading $\eta = -1.0$ is low as was mentioned in section 5.2.2; however, the value they predict for $\eta = 0.0$ (i. e: one half of the free edge loaded) is within 7% of the value predicted by the theory. Their value for $\eta = 1.0$ (i. e: all of free edge loaded) which is not shown in the figure, agrees within 2% of the theoretical curve. It is interesting to note that these curves do not tend to a constant value as the plate aspect ratio decreases (except for the $\eta = -1.0$ curve) as was the case with the point loaded plates of section 5.2. The curve for $\eta = 1.0$ in fact becomes identical with the cantilever curve for small aspect ratios, an effect which could have been anticipated. The curves for intermediate values of η lie between these two extremes and in the region shown in the figure (aspect ratio $\geq$ 0.02) they appear to be decreasing steadily with decreasing aspect ratio.

Figure 70 shows the variation in maximum plate bending moment as a function of aspect ratio, in line loaded cantilever plates, when $\beta_m = 7$ degrees. These curves are essentially identical

to those presented in Figure 69 for $\beta_m = 0$ degrees. With the only exception being the curve for $\eta = 1.0$. This curve now crosses the curve for $\eta = 0.8$ and will likely cross some of the other curves for lower aspect ratios. The value of nominal moment shown in this figure and the following figures is not that predicted by equation (3.28) which would be too cumbersome to use in practice. It is rather the value which would be proper for a cantilever beam with a uniformly distributed load, i. e:

$$\frac{M_{max}}{P} = \frac{1}{2}\left(\frac{b}{2a}\right) \qquad \ldots \quad (5.14)$$

this equation can be easily derived in a manner similar to that used to derive equation (5.9), with the realization that the load is $P = qb$. This value is exactly one half the value given by equation (5.9).

In Figure 71, the maximum bending moment as a function of aspect ratio is shown for $\beta_m = 12$ degrees. The curves are again quite similar to those for $\beta_m = 0$ with the exception of the curve for $\eta = 1.0$ which crosses the other curves as it did for the case of $\beta_m = 7$ degrees. However, this time it crosses at much higher values of $\frac{M_{max}}{P}$, and it appears that it will become asymptotic at some low value of maximum moment for very low aspect ratios ($\gg 0.02$). Agreement between theory and experiment is good for aspect ratios greater than 0.40, for values smaller than this with high values of η there is no comparison between theory and experiment; this is due to the fact that only a few loadings were available for superposition.

The maximum plate bending moments for $\beta_m = 20$ degrees are shown in Figure 72 as a function of aspect ratio. The curves for $\eta \leq 0.0$ are almost identical with those for lower β_m

values shown in the preceding figures. For higher η values there is a decrease in the maximum moment (as compared to the curves for lower β_m values) for aspect ratios between 1.0 and 0.1.

Figure 73 shows the maximum bending moments in line loaded cantilever plates with β_m = 45 degrees and various values of η. The curves for η = -1.0, -0.8, and -0.6 are similar to those in the previous figure for low aspect ratios. This figure indicates a definite change in shape of the curves corresponding to $-0.2 \leq \eta \leq 1.0$; these curves tend to become asymptotic to a constant value for lower aspect ratios. Again the theory and experiment agree quite well for aspect ratios greater than 0.50.

In Figure 74, the maximum plate bending moments for a line loaded cantilever plate, β_m = 60 degrees are shown as a function of aspect ratio for various values of η. Here the curves for all values of η become asymptotic to a constant value as aspect ratio decreases. The curve for η = 1.0 converges to the value $\frac{M_{max}}{P}$ = 0.242. Agreement between theory and experiment is similar to that mentioned previously.

The maximum plate bending moments as a function of aspect ratio are shown in Figure 75 for a line loaded cantilever plate with β_m = 90 degrees. The shape of these curves is very similar to those discussed in section 5.2.2 for point loading. All of the curves approach a constant value for low aspect ratios. The curve for η = 1.0 reaches the value of $\frac{M_{max}}{P}$ = 1.13 for low aspect ratios and the curves for $0.8 \geq \eta \geq 0$ reach the value of $\frac{M_{max}}{P}$ = 0.278 for low aspect ratios. For edge loading (η = 1.0) the experimental values are lower than the theoretical values and drop off severely for lower aspect ratios (36% low for 0.1). They

also tend to be somewhat high for aspect ratios greater than 1.0. Agreement is better for lower values of η, with the experimental results lower than the theory. The results of Wellauer and Seireg (4) are also shown in the figure (aspect ratio = 0.187); their value for corner loading is identical with the present experimental results, for central loading their point is significantly higher ($\frac{M_{max}}{P}$ = 0.4 vs. $\frac{M_{max}}{P}$ = 0.3).

It is interesting to compare the theoretical results for the 90 degree line load and the point loaded case where β = 0.5 (see Figure 56) for plates of low aspect ratio ($\leq$ 0.25). The values of $\frac{M_{max}}{P}$ are compared in the following table:

$M_{max}/_{P}$	Line Load	Point Load
α = 1.0	1.13	1.16
α = 0.0	0.278	0.276

The values compare within 2%; this is extremely interesting since the nominal moments given by equations (5.9) and (5.14) are identical. This means, of course, that their K_m values would be identical and shows the possibility of using the point loaded case to approximate the Novikov Line loaded case ($\beta_m = 90^\circ$).

The values of K_m (the moment distribution factor) are obtained by dividing the values of $\frac{M_{max}}{P}$ given in the preceding figures by the nominal moments also shown there. These results are presented in Figures 76 through 82.

Figure 76 presents the moment distribution factors for cantilever plates with β_m = 0.0 degrees. For high aspect ratios these curves converge to the value of 1.0 for $\frac{M_{max}}{P}$. For low aspect ratios, the curves for $\eta \geq 0.0$ assume constant values of K_m. It also appears that the curves for $0.0 \geq \eta \geq 0.8$ will also achieve

constant values for smaller values of aspect ratio. Figure 77 shows the K_m curves for β_m = 7 degrees. These curves are essentially the same as those shown in Figure 76, except that the values are twice as high since the nominal moment used was only half as large. Also, the curve for η = 1.0 curves up slightly for low aspect ratios.

The K_m curves for β_m = 12 degrees are shown in Figure 78. These curves are generally similar to those shown for β_m = 7 degrees, with the only difference being generally lower values of K_m. Figure 79 shows the K_m curves for β_m = 20 degrees. These curves no longer reach a constant value for low aspect ratios, but rather continue to increase in the region shown in the figure. Also, these curves (at least those for $\eta \geq 0.0$) dip below the value of K_m = 2.0 in the region of aspect ratios between 0.1 and 3.0

Figure 80 shows the variation of K_m with aspect ratio for β_m = 45 degrees and various values of η . These curves take on the more familiar shape noticed in section 5.2.2 for the point loaded plates considered. That is to say that the curves show a linear increase in K_m (for low aspect ratio) as a function of aspect ratio. This is not true for the η = -0.8 and -0.6 curves shown however.

The curves showing the K_m values as a function of aspect ratio for β_m = 60 degrees are shown in Figure 81. Here the curves all become parallel to the curve for η = -1.0 for low aspect ratios. They also dip below the value of K_m = 2.0 (all curves except η = -1.0 and -0.8).

Figure 82 shows the moment distribution factor K_m, as a function of aspect ratio for line loaded cantilever plates with β_m, 90 degrees. This case is of particular interest since these

curves form a reasonable approximation to Novikov gear tooth loading. These curves are quite similar to those for point loading. The values of γ for them as determined for equation (5.10) are 2.30 for η = 1.0 and 0.560 for η = 0.0. It is interesting to note that the curves seem to reach the constant value of 1.20 for aspect ratios greater than 4.0. This means that the bending moments predicted by the present theory do not correspond to the values predicted by elementary cantilever theory which were used for the nominal moment calculation. This 20% increase in moment over that predicted by the elementary theory for uniformly loaded cantilever beams should be evident if the subject were considered experimentally. It is likely that for much higher aspect ratios the curves do converge to the value of 1.0 for K_m; however, no attempt was made to check this out.

5.5 Comparison to Tests on Helical and Novikov Gears

In order to indicate the value of the moment distribution curves, it is interesting to compare the values given in the curves to some experimental results.

The first comparison will be to the results given by Hageniers (1) for a Novikov Gear Set. Figure 83 shows the experimental arrangement used to test the gear set, as well as a view of the wheel teeth with the strain gages on them. The loading is such that η must be between -0.5 and 0.5, since outside these limits double tooth contact results in the experimental system used. It was shown in the experimental work on the gears that the maximum stresses occurred for these gears approximately independent of the load position. The aspect

ratios of the gears were 0.159 for the wheel and 0.175 for the pinion. These differences come about because the shape of the teeth is different in a Novikov gear set and the pinion teeth are longer than the wheel teeth (but both are the same width). Knowing the aspect ratio, it is possible to look up the K_m values in Figure 82. A comparison of the K_m values predicted by the experiment, the present theory and the work of two other investigators is shown in the following table:

K_m	Experiment Reference (1)	Plate Expt.	Plate Theory	Wellauer & Seireg (4)	Fedyakin & Chesnokov (15)
Pinion	2.50	3.10	3.30	4.56	1.20
Wheel	3.55	3.30	3.60	5.04	1.20

The values from the present theory and Wellauer and Seireg (4) were taken for $\eta = 0.0$, since only small increases in K_m are noted for η less than 0.5. The values predicted by Fedyakin and Chesnokov are very low; however, their data is strictly emperical and presented during the early days of bending moment distribution determination. The agreement between the theory and the experimental results from reference (1) is good, being with 24% for the pinion and 2% for the wheel. The results presented by Wellauer and Seireg (4) are significantly higher, differing by 45% and 30 %. This indicates that the present method results in much better agreement with actual tests on gears.

As a second comparison, the results presented by Kugimiya (2) will be considered. He tested a helical gear set with a helix angle of 20 degrees and a normal pressure angle of 20 degrees. Using equation (5.11), β_m then is 7.5 degrees. The aspect ratio

of the gear teeth was 0.235. The gears he tested were such that no real overlap occurred; however, there was multiple tooth contact due to involute action. Since the teeth are more flexible near the ends, better tooth load sharing resulted which means that the high moments predicted by corner loading (η = -1.0) could not occur, but rather the load was shared between the two teeth in question, resulting in a lower moment. Using his experimental results and equation (2.2), values of K_m = 1.15 for the pinion and K_m = 1.41 for the wheel are obtained. His experiment also indicates that due to involute overlap, the maximum stress occurs for η = 0.7 for the pinion and η = 0.5 for the wheel. An exact explanation of the reasons for this is not possible here, nor is one given by Kugimiya (2). The corresponding values from Figure 77 must be modified since the K_m values are based on the tip loaded moment rather than the half height moment used in Figure 77. The values from Figure 77 are therefore 1.05 for the pinion and 1.38 for the wheel. These values are within 9% for the pinion and within 2% for the wheel.

The agreement between the two references quoted and the method proposed here indicates the validity of the approach outlined here. It would be desirable to compare to the results of further experiments on gear teeth, but there is a lack of suitable data in the literature that is complete enough to allow a detailed comparison.

5.6 Estimate of the Computational Error

Due to the large number of calculations required in obtaining the plate deflections and moments (even at a point) using the theory outlined in section 3.1.2, the possibility of obtaining results with poor accuracy must be considered. In order to check on the convergence of the deflections and bending moments, a modified form of the program listed in Appendix A was run which varied the number of terms used in the series from 3 to 140. A plot of the results of such a program is shown in Figure 84 for a plate with aspect ratio 0.50. The maximum deflections and moments are plotted as a function of the number of terms in the series for corner and mid point loading at the free edge. The maximum deflection for mid point loading is seen to reach an essentially constant value after 30 terms in the series. It then remains within 1% of that value for the addition of the next 100 terms after which point, it rises slightly. For corner loading an essentially constant value is also reached after 30 terms, with the value remaining within 0.5% up to 80 terms, where it rises 1% and remains constant. Beyond 110 terms, the values increase wildly and are no longer meaningful.

The maximum moment for central loading reaches an essentially constant value after 25 terms and maintains this value within 3% up to 110 terms; after this point the values drop by 16% to a new steady value. For corner loading, an essentially constant value of moment is reached after 16 terms; this value remains within 2% up to 36 terms, drops 4% and holds to 50 terms, where it drops 4% again, etc. Finally, after dropping by 28% after 110 terms, the values diverge rapidly and become meaningless. This moment

for corner loading is the least well behaved of the variables considered here. Based on the foregoing figure and similar tests on other aspect ratios, it is possible to say that the plate deflections will be within 1% of their final value if more than 30 and less than 80 terms are taken in the series. Also the plate moments will be within 5% of their final values if more than 20 terms and less than 60 terms are taken in the series. The wild fluctuations beyond 110 terms in the series indicate a loss of significance in the coefficients used to calculate the deflection series. It is also evident that the significance loss is a function of α, the load position, since it occurs only for corner loading in Figure 83 (i. e: for the number of terms less than 140).

5.7 Estimate of the Experimental Error

The determination of the deflection in holography is dependent upon two factors; first, the accuracy of fringe counting is limited to about $\pm$ 0.5, and second in live fringe work; some nulling error exists of about $\pm$ 0.5 fringe. This results in a total possible error of $\pm$ a fringe. Referring to Figures 15, 16 and 17, it can be seen that a maximum fringe order of about 30 was maintained where possible. This means that the maximum deflection is known within one part in 30 or within 3.3%. At the same time the load was known within 1% as determined in a test using a 10 pound capacity load cell, and weights which had been previously calibrated. This means that $\frac{\delta_{max}}{P}$ is known within 4.5%. The value of E and ν were obtained experimentally as outlined in Appendix B and show a variation of 2% based on the testing of four samples. The errors in the plate dimensions (a and b) are limited to a tenth of an inch

which on most plates is less than 2%. Considering all of these factors in the determination of $\frac{\delta_{max} D}{P b^2}$ results in a possible error of 9% in total.

In determination of the bending moments from the strain gage readings, several sources of error are possible. The first is due to the gages which were used in a non-temperature compensated circuit. The strain indicator can be read to $\pm$ 2 μ in/in which out of the maximum strains of 500 μ in/in represents a 0.4% error. Also, temperature variations (5° F maximum) result in a possible strain variation of $\pm$ 1 μ in/in or 0.2%. This indicates a total strain error of 0.6%. The load applied was again calibrated and a friction loss factor included in determining the load. Variations in the load were determined to be less than 2% for the maximum load used. This means that the errors in $M/_P$ are less than 3%.

Other factors which may influence the accuracy of the results, but whose effect is hard to estimate, and may be assumed to be small, are:

1) errors in strain gage alignment
2) errors in strain gage position along the plate length
3) deformations of the plate clamping jig
4) temperature changes affecting the holographic experiment
5) determination of the maximum moment from the strain gage information by plotting of the results

6. RECOMMENDATIONS

6.1 Suggestions for Experimental Improvement

The holographic part of the experiment could be improved in two ways. First, a more powerful laser would make possible more uniform illumination of test specimens and secondly, a better isolation system for the holographic table would allow the use of superior holographic arrangements. The experiment would also have been improved if a data acquisition system with more channels had been available, thus obtaining better information on M_{max}.

6.2 Suggestions for Future Work

1) An investigation to determine the effect of plate thickness on the deflections and bending moments in those cases where the thickness and plate length are comparable.

2) Tests on tooth shaped plates of various aspect ratios to determine the effect of thickness changes as a function of length on deflection and bending moment.

3) A study of the effect of degree of rigidity of the plate clamping on the plate deflections and fixed edge bending moments.

4) A theoretical study of the effect of non-uniform line loads on plates of various aspect ratios.

7. CONCLUSIONS

1) The validity of the deflection theory developed by Szmelter et. al. (3) has been shown over a large range of aspect ratio by comparison to experimental deflection contours.

2) Curves have been presented which show the variation in maximum plate deflection as a function of aspect ratio and load point. Agreement between theory and experiment in this case is very good.

3) The results of Szmelter et. al. (3) were extended to predict bending moments in cantilever plates. These results were shown to compare well with the results of other investigators.

4) Comparison of the experimental bending moments with those predicted by the theory developed here is good and curves for plates of various aspect ratios, point loaded along the free edge are presented.

5) Curves are presented which show the maximum moment as a function of aspect ratio and position of the point load. These curves were used to present moment distribution curves for point loaded cantilever plates.

6) Using superposition the theory was extended to line loaded cantilever plates and compared with experimental values obtained by superposition as well. These results showed good comparison.

7) Maximum moment curves and moment distribution curves are presented for line loaded cantilever plates, loaded at various angles and at various positions on the plate.

8) Comparison of the moment distribution factors presented here with those obtained in tests by two investigators show the value of this approach in gear design.

9) The effect of Poisson's ratio on the deflections and bending moments in cantilever plates has been shown to be quite significant.

8. BIBLIOGRAPHY

1) Hageniers, O. L., "A Study of the Bending Stresses in a Wildhaber-Novikov Gear Set", Thesis, University of Windsor, 1969.

2) Kugimiya, H., "Stresses in Helical Gear Teeth", Japan Society of Mechanical Engineers, 1966, p. 816.

3) J. Szmelter, T. Sulikowski, and J. Lipinski, "Bending of a Rectangular Plate Clamped at One Edge", Archivum Mechaniki Stoswanej, v 13 nl, 1961, pg. 63-74.

4) E. J. Wellauer and A. Seireg, "Bending Strength of Gear Teeth by Cantilever Plate Theory", Journal of ASME, Aug. 1960.

5) Shigley, J. E., "Mechanical Engineering Design" McGraw-Hill, 1963.

6) Allan, T., "Some Aspects of Design and Performance of Wildhaber-Novikov Gearing", Institution of Mechanical Engineers-Proceedings, Volume 179, n. 30, 1964-65, p. 931-54.

7) French, M. J., "Gear Conformity and Load Capacity", Institution of Mechanical Engineers-Proceedings, 1965-66, part 1, n 43, p. 1013-24.

8) Wells, C. F., and Shotter, B. A., "The Development of Circarc Gearing", AEI Engineering, Vol. 2, n. 2.

9) Davies, W. J., "Novikov Gearing" Machinery, vol. 96, January 13, 1960, p. 64-73.

10) Walker, H., "A Critical Look at the Novikov Gear", The Engineer, April 29, 1960, p. 725-729.

11) Johnson, D. C., "Gear Teeth with Circular Arc Profiles", Engineering, 1959, p. 294.

12) Wildhaber, E., "Helical Gearing", U. S. Patent 1601750, October 5, 1926.

13) Wildhaber, E., "Method of Grinding Gears", U. S. Patent 1858568, May 17, 1932.

14) Kaluzhnikov, A. N., "A New Point-Contact System for Gear Teeth", Izobretalelstov V SSSR, Nov. 11, 1957, p. 26-27, 30-31.

15) Fediankan, R. W. and Tschechnow, W. A., "Calculations for the Novikov System", Vestnik Mashin, June, 1958

16) MacGregor, C. W., "Deflections of a Long Helical Gear Tooth", Mechanical Engineering, Vol. 57, 1935, pp. 225-27.

17) Holl, D. L., "Cantilever Plate with Concentrated Edgeload", Journal of Applied Mechanics, vol. 59, 1937, pp. A-8-10.

18) Jaramillo, T. J., "Deflections and Moments Due to a Concentrated Load on a Cantilever Plate of Infinite Length", Journal of Applied Mechanics, vol. 72, 1950, pp. 67-72, pp. 342-43.

19) Vartak, G. V., "Cantilever Moments in Plates Fixed Along One of the Long Edges and Subject to Concentrated Loads at a Point on the Other Long Free Edge", Journal of the Institution of Engineers (India), vol. 37, part 1, Nov. 1956, pp. 203-12.

20) Dalley, J. W., "Experimental Values of Deflections, Stresses, and Influence Coefficients for a Thin Square Plate Fixed Along One Edge", Defense Research Laboratory Report No. 189, University of Texas, Nov. 5, 1948.

21) Timoshenko, S. and Woinowsky-Krieger, S., "Theory of Plates and Shells", McGraw-Hill Book Company, Second Edition, 1959.

22) Holand, I., and Bell, K., "Finite Element Methods in Stress Analysis", Tapir, 1969.

23) Walker, A. C., "Rayleigh-Ritz Method for Plate Flexure", Journal of the Engineering Mechanics Division, Proceedings of the ASCE, December 1967, pp. 139-151.

24) Jaeger, L. G., "Elementary Theory of Elastic Plates" Pergamon Press Ltd., 1964.

25) Stetson, K. A. and Powell, R. L., "Hologram Interferometry", Journal of the Optical Society of America, Vol. 56, No. 9, Sept., 1966, pp. 1161-1166

26) Boone, P. and Verbiest, R., "Application of Hologram Interferometry to Plate Deformation and Translation Measurements", Optica Acta, Vol. 16, No. 5, 1968, pp. 555-57.

27) Ennos, A. E., "Holography and its Applications", Contemp. Physics, 1967, vol. 8, no. 2, pp. 153-170.

28) Vander Lugt, A. and Mitchel, R. H., "Technique for Measuring Modulation Transfer Functions of Recording Media", Journal of the Optical Society of America, Vol. 57, No. 3, March, 1967, pp. 372-379.

29) Timoshenko, S., and Goodier, J. N., "Theory of Elasticity", McGraw-Hill Book Company Inc., Second Edition, 1951

30) Palmer, P. J., "The Bending Stresses in Cantilever Plates by Moire Fringes", Aircraft Engineering, December, 1957, pp. 377-380.

31) Umezawa, K., Ishikawa, J., and Hayashi, K., "Deflections due to a Concentrated Load on a Cantilever Thick Plate of Finite Length for Gears", Bulletin of the Japanese Society of Mechanical Engineers, Vol. 12, No. 53, 1969, pp. 1204-1211.

32) Smith, H. W., and Chapel, R. E., "Poisson's Ratio Determined with Strain Rosettes", Experimental Mechanics, March, 1969 pp. 140-141.

33) Dally, J. W. and Riley, W. F., "Experimental Stress Analysis", McGraw-Hill Book Company, 1965, pp. 426-429.

34) Rogers, G. L., "The Design of Experiments for Recording and Reconstructing Three-Dimensional Objects in Coherent Light (Holography)", Journal of Scientific Instruments, Vol. 43, 1966, pp. 677-684.

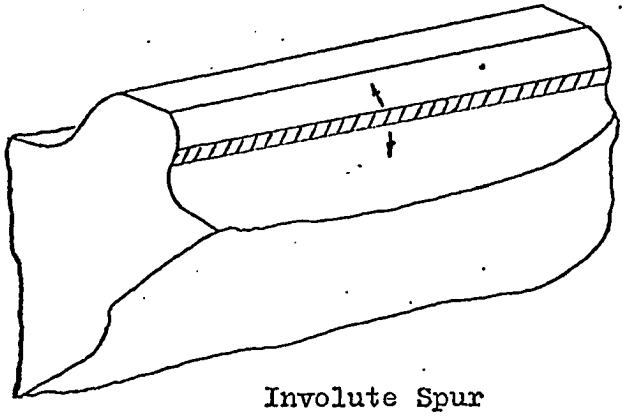

Involute Spur

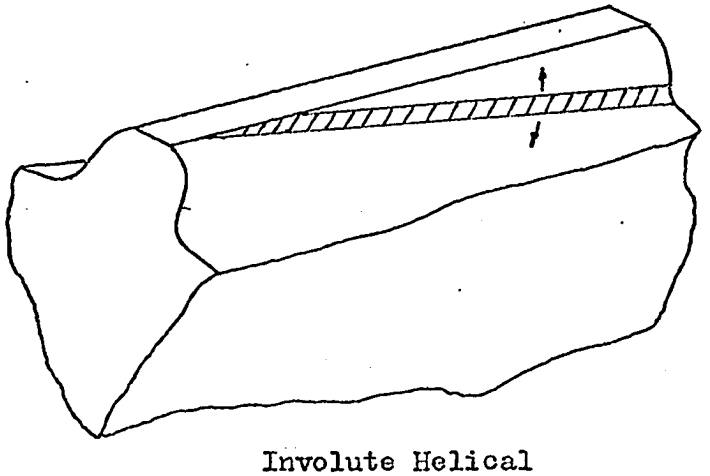

Involute Helical

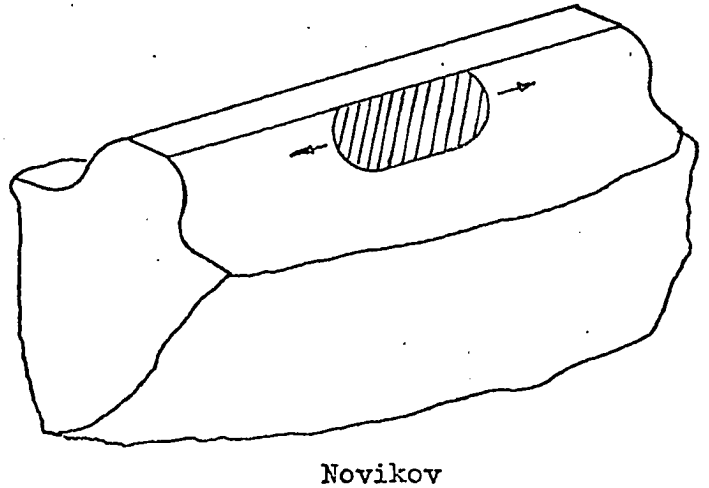

Novikov

Fig. 1 Comparison of Tooth Contact in the Novikov and Involute Systems

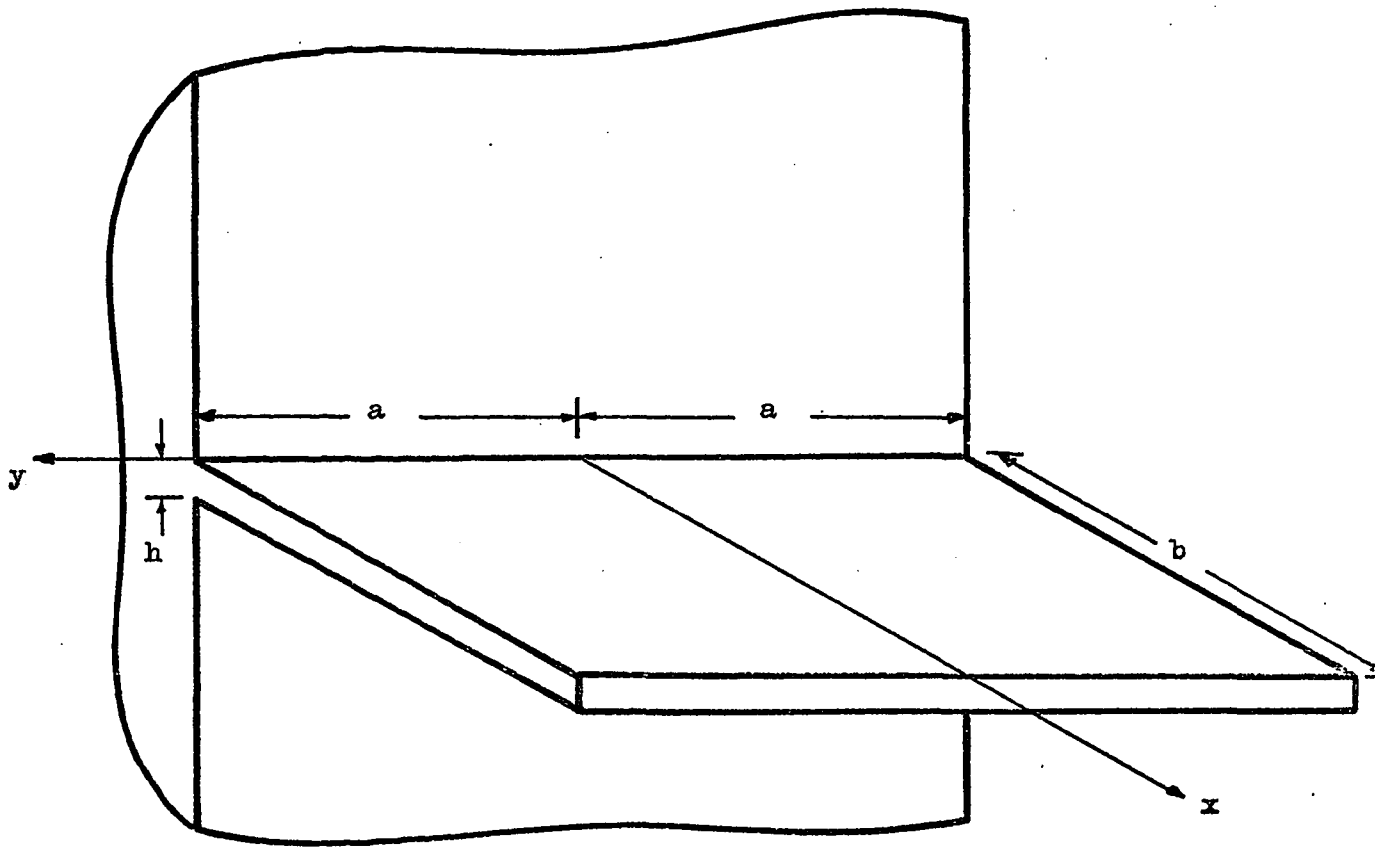

Fig. 2: Cantilever Plate Geometry

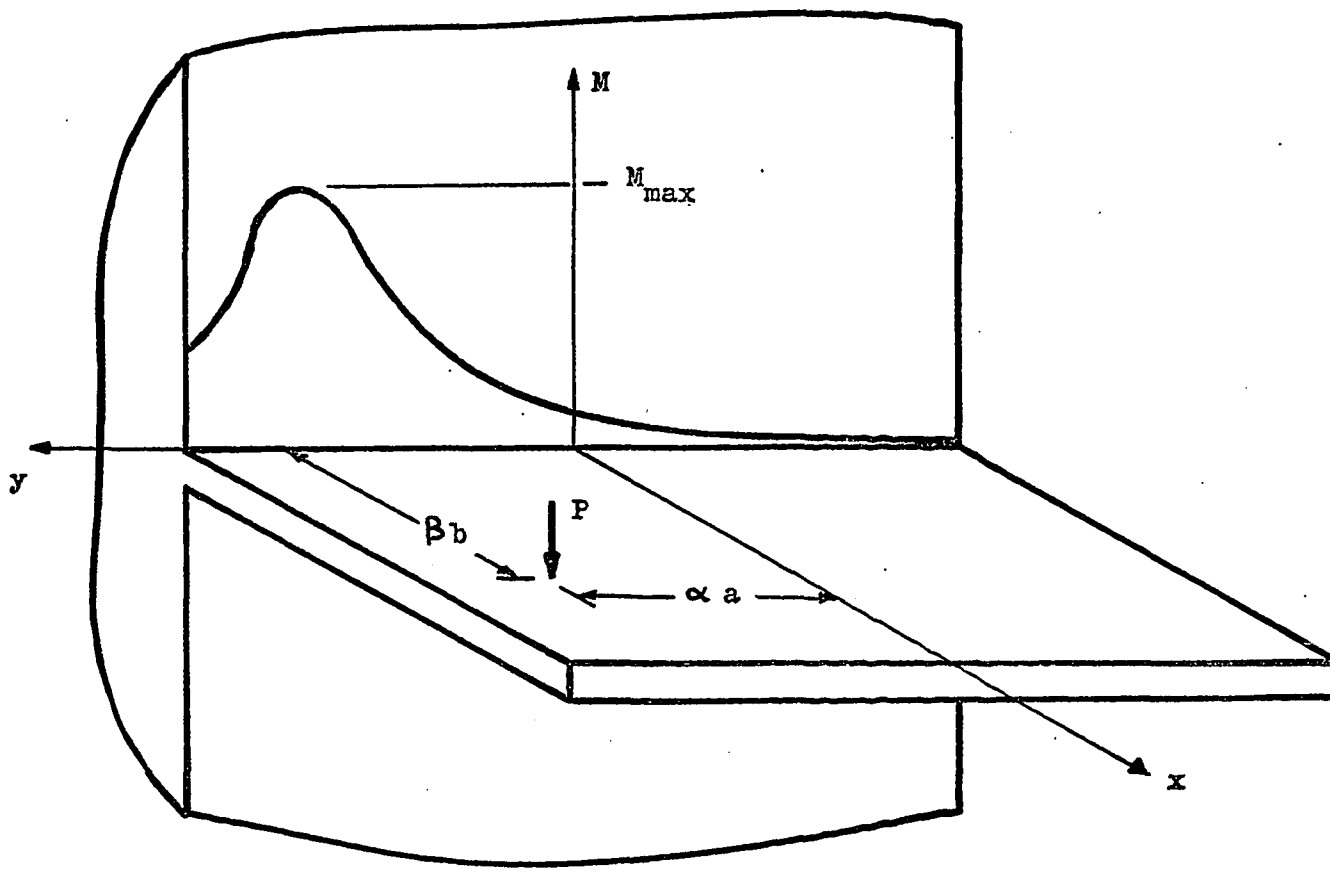

Fig. 3: Point Loaded Cantilever Plate Variables

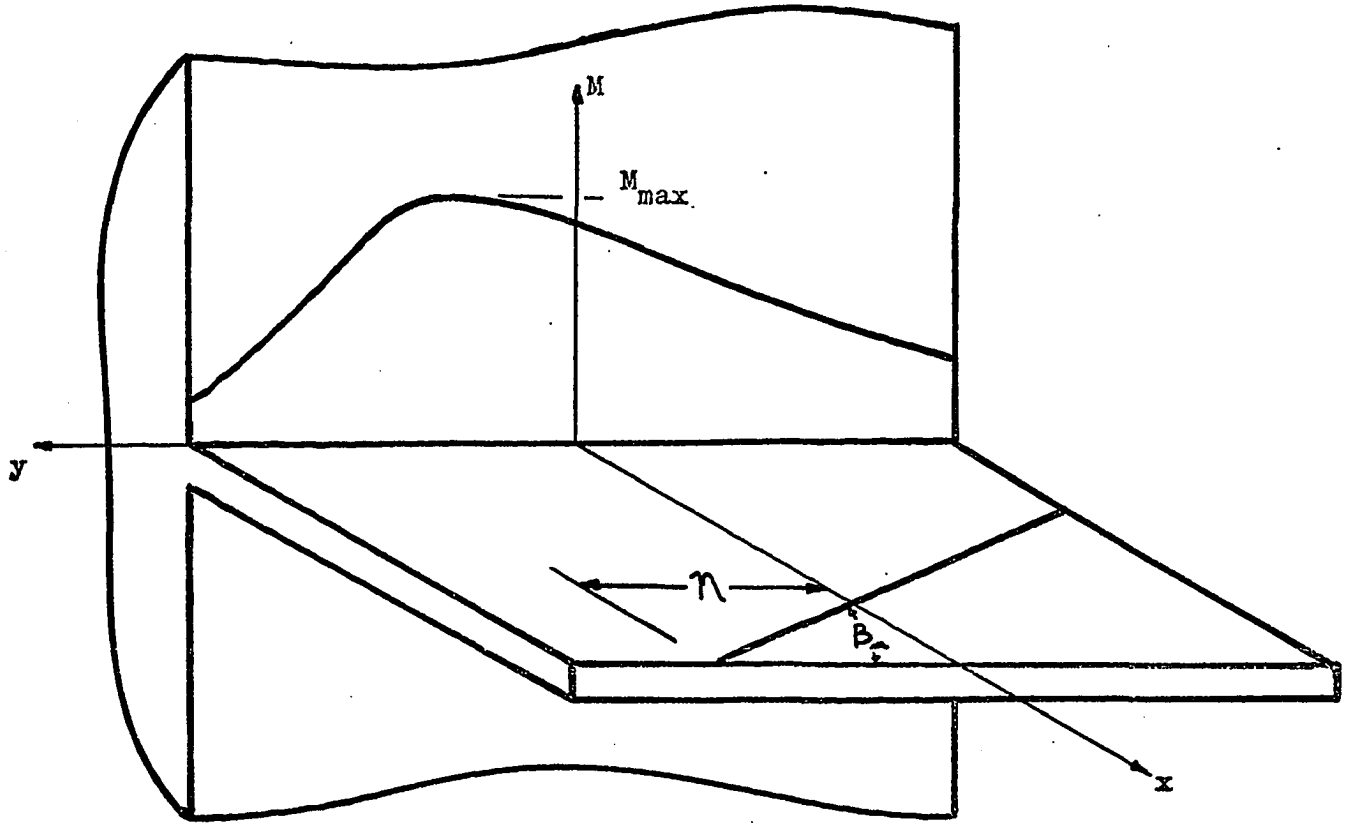

Fig. 4: Line Loaded Cantilever Plate Variables

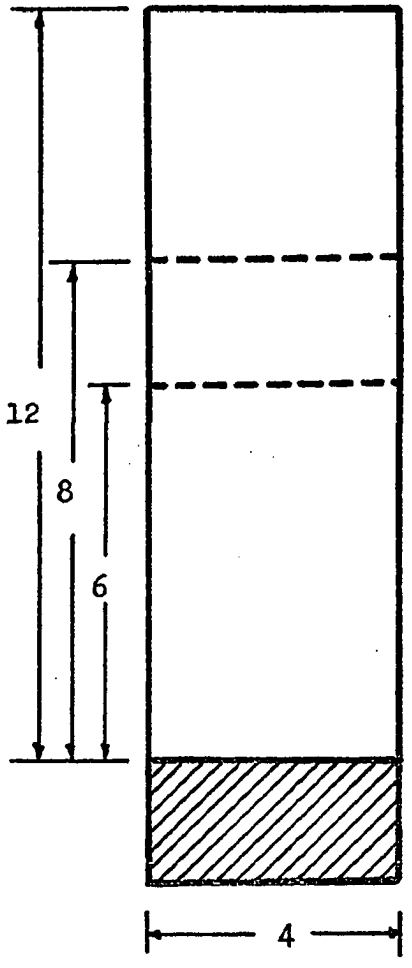

Plate I

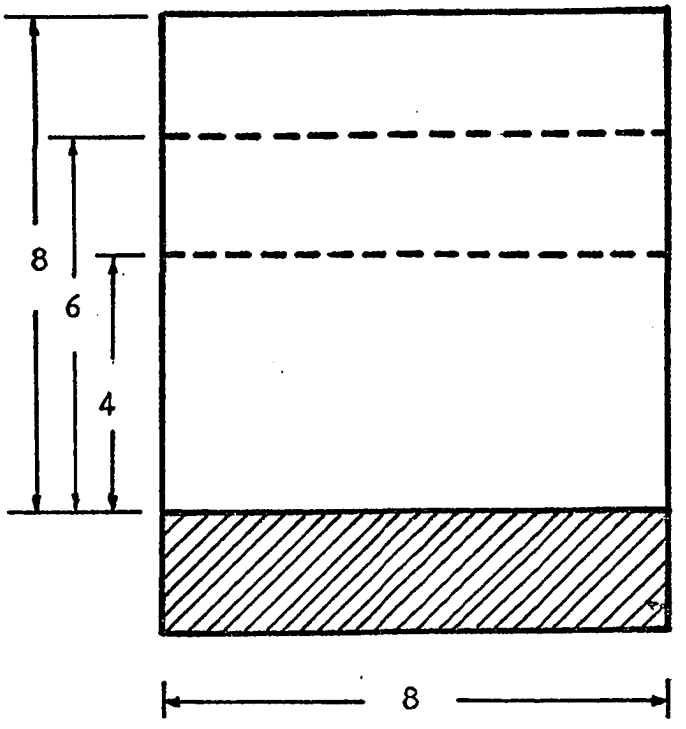

Plate II

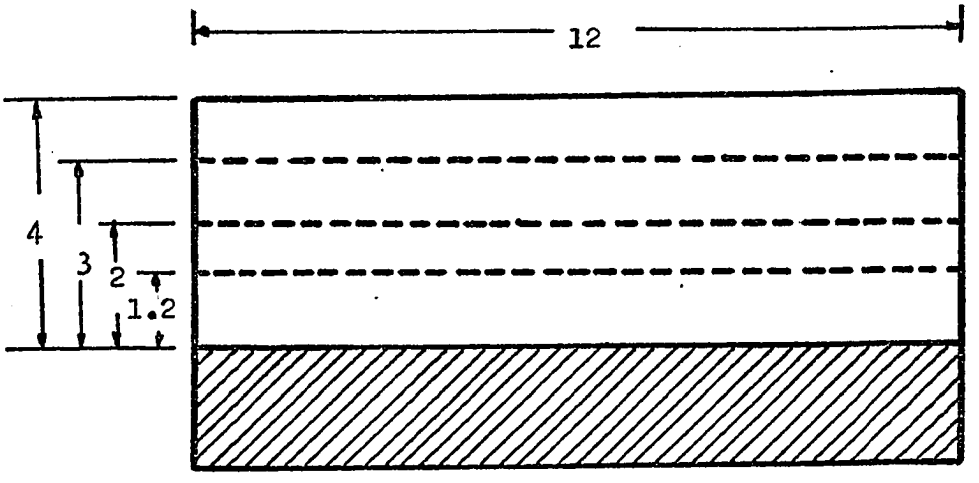

Plate III

Fig. 5: Plates Tested

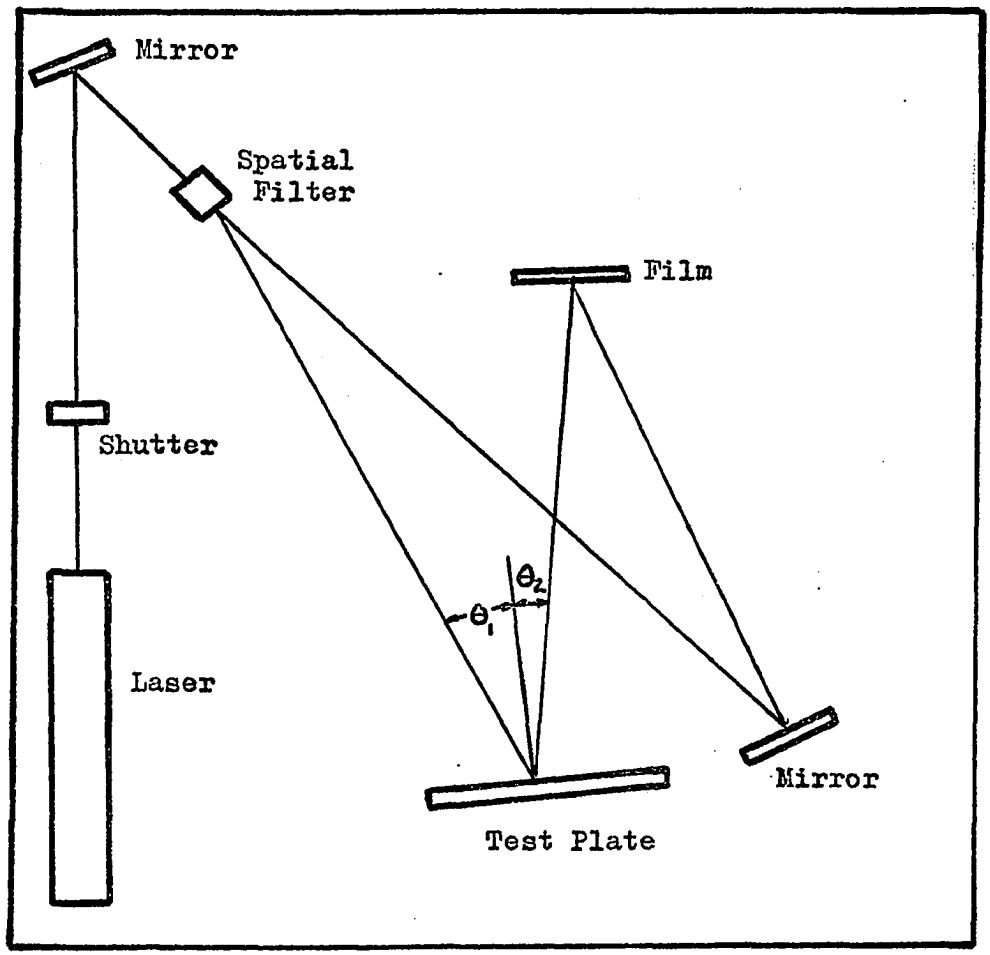

Fig. 6: Schematic of Holographic Setup

Fig 7: Experimental Arrangement Used in Making Holograms

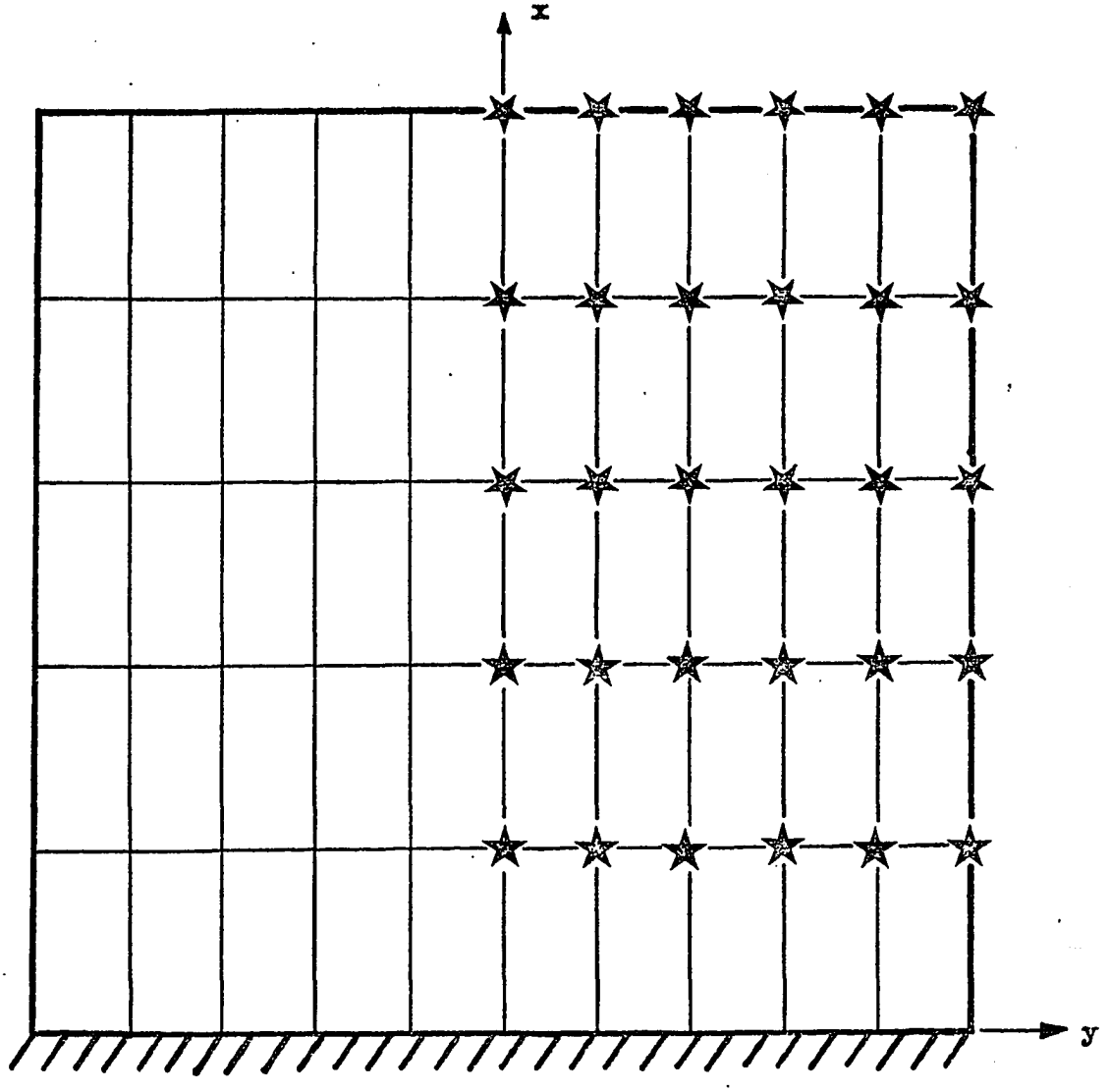

Fig. 8: Grid Marked on Plate, Showing Load Points

$$\epsilon_y = 0 \quad , \gamma_{xy} = 0$$

Then $$\sigma_x = \frac{E\epsilon_x}{(1-\nu^2)} \quad ; \quad \sigma_y = \frac{\nu E \epsilon_x}{(1-\nu^2)} \quad ; \quad \tau_{xy} = 0$$

Also $$M = \frac{\sigma h^2}{6}$$

$$\therefore \quad M_x = \frac{E h^2 \epsilon_x}{6(1-\nu^2)} \quad ; \quad M_y = \nu M_x \quad ; \quad M_{xy} = 0$$

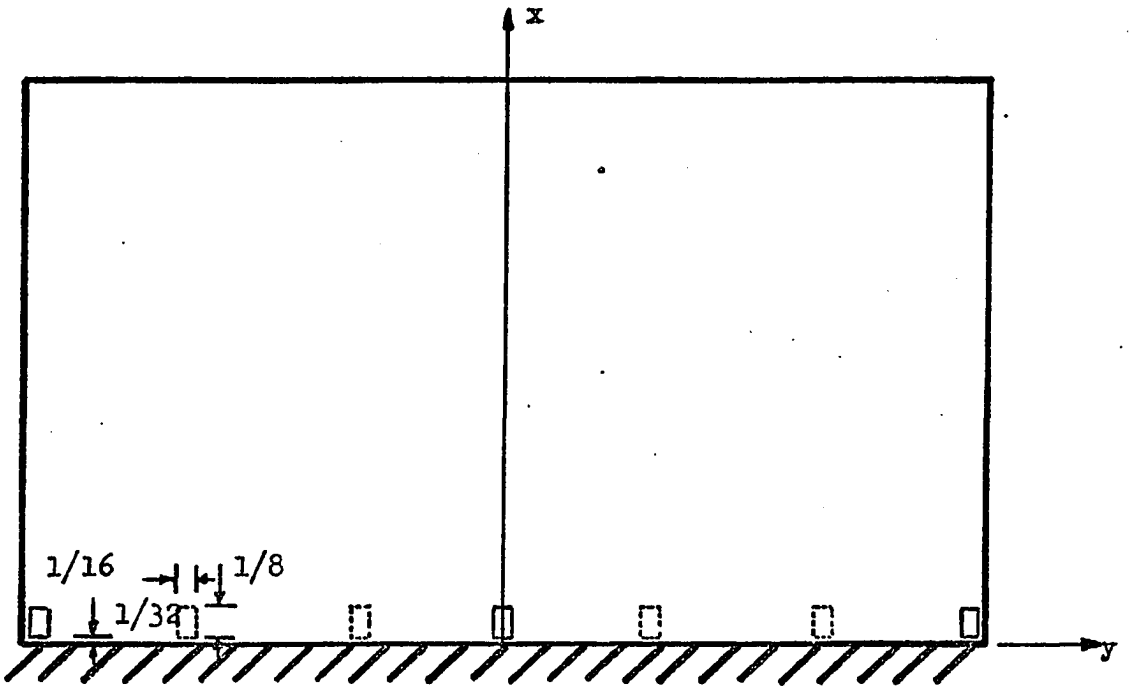

y/a	Aspect Ratio		
Gage No.	0.1,0.167,0.25,0.33	0.5,0.75,1.0	1.5,2.0,3.0
1	-0.987	-0.975	-0.95
2	-0.75	-0.66	-0.50
3	-0.50	-0.33	0
4	-0.25	0	+0.50
5	0	+0.33	+0.95
6	+0.25	+0.66	
7	+0.50	+0.975	
8	+0.75		
9	+0.987		

Fig. 9: Strain Gage Locations on Plates Tested

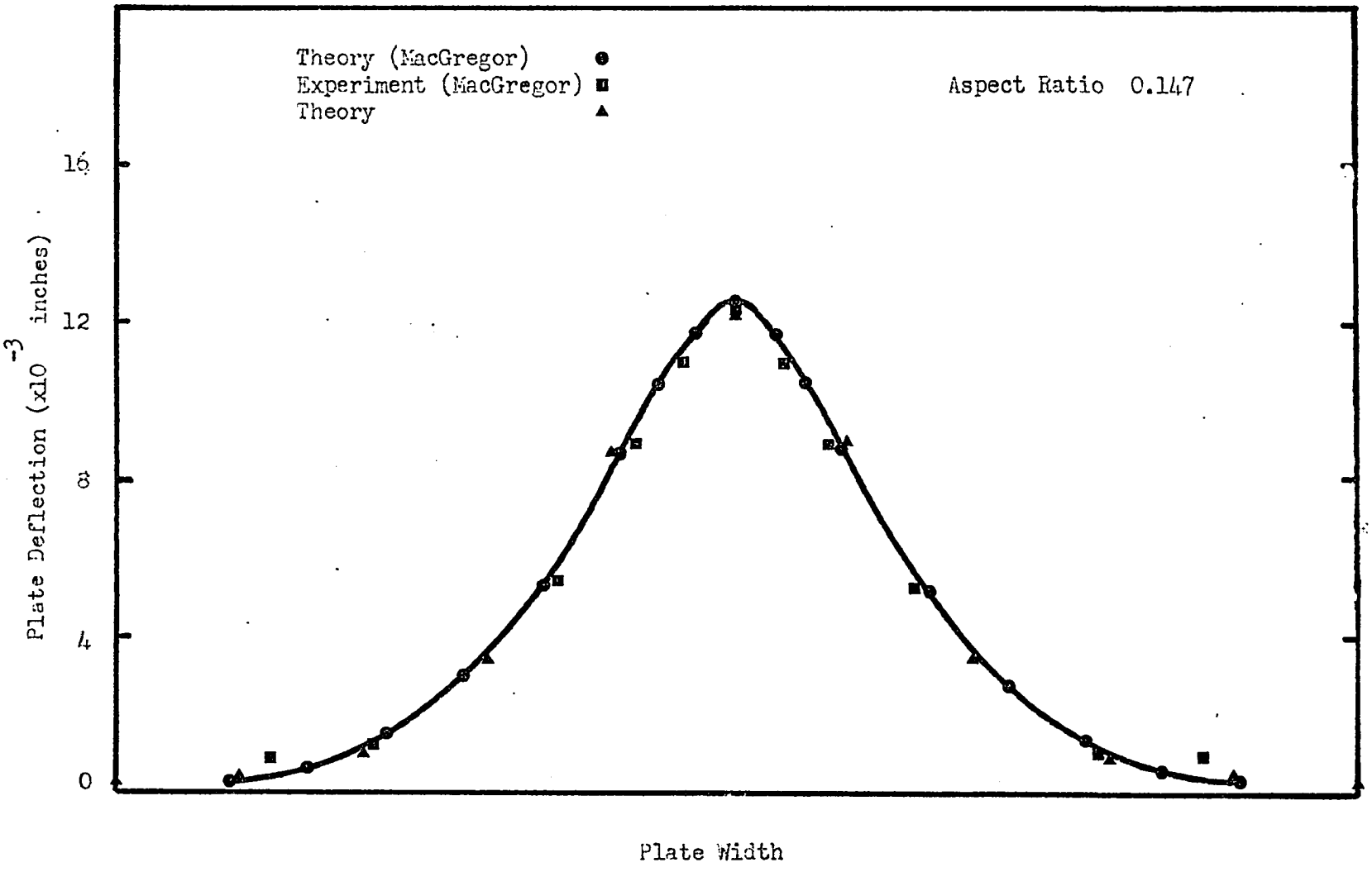

Fig. 10: Comparison of Free Edge Deflections With Those of MacGregor

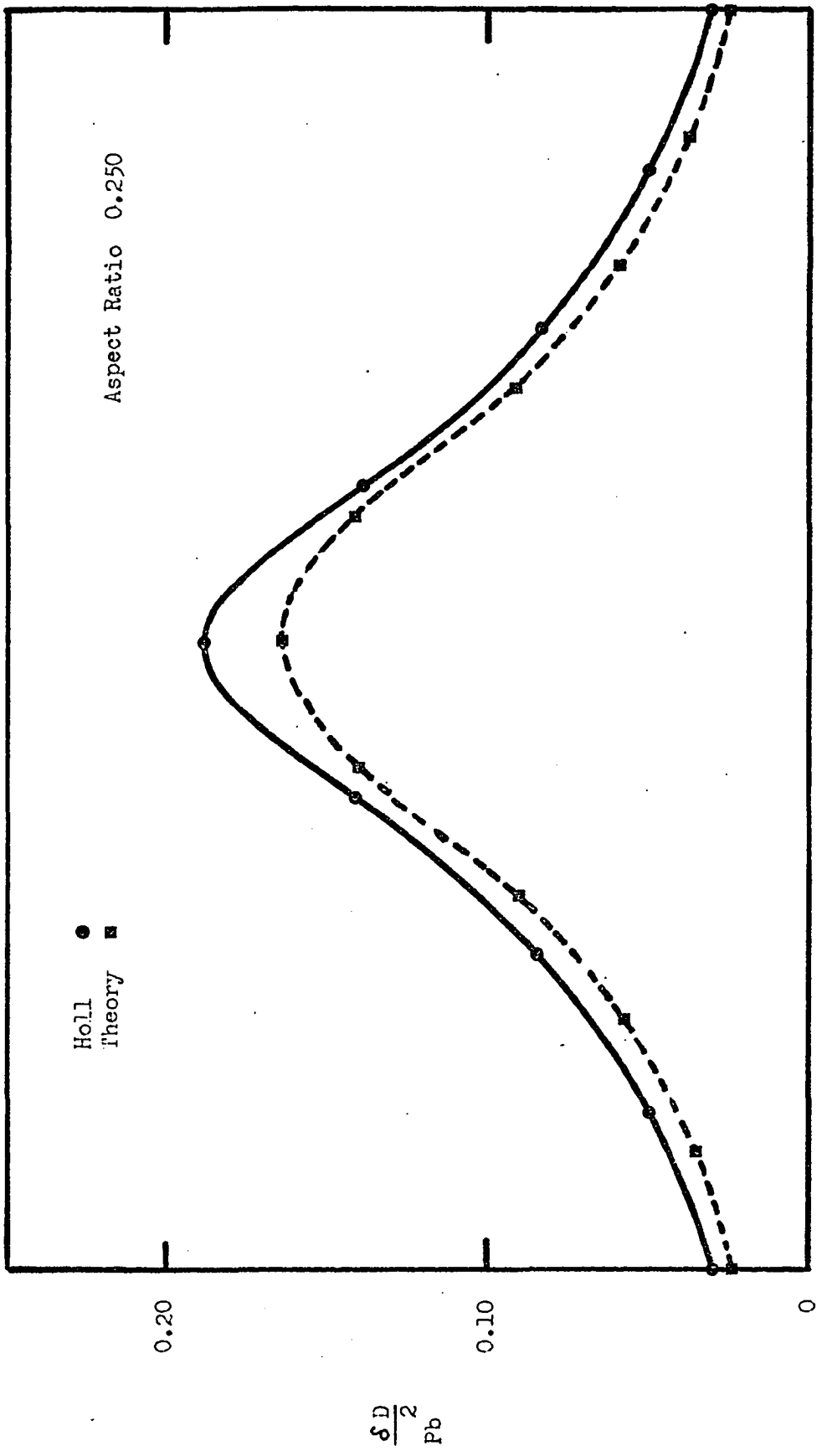

Fig. 11: Comparison of Free Edge Deflections With Holl's Results

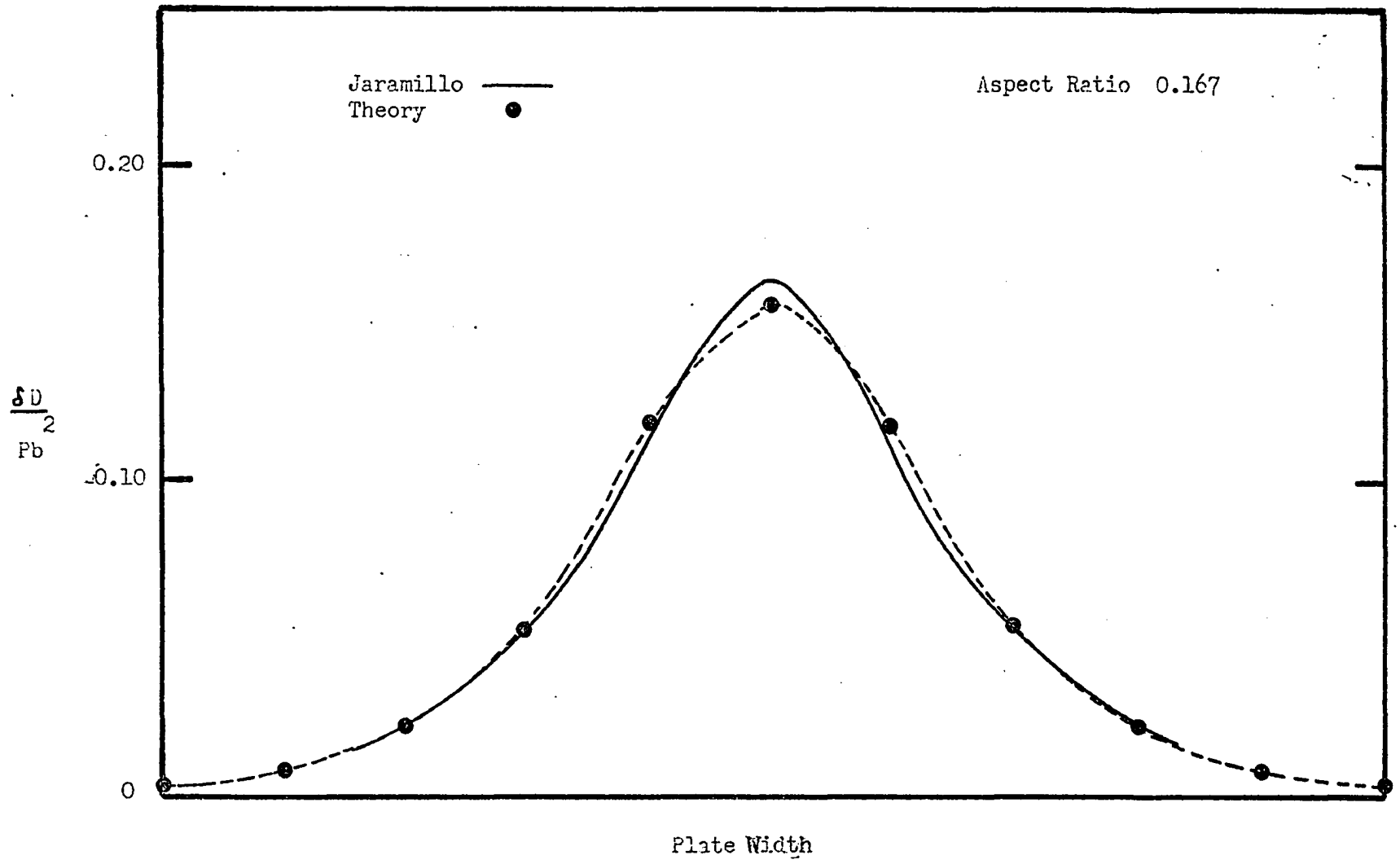

Fig. 12: comparison of Free Edge Deflections With Jaramillo's Results

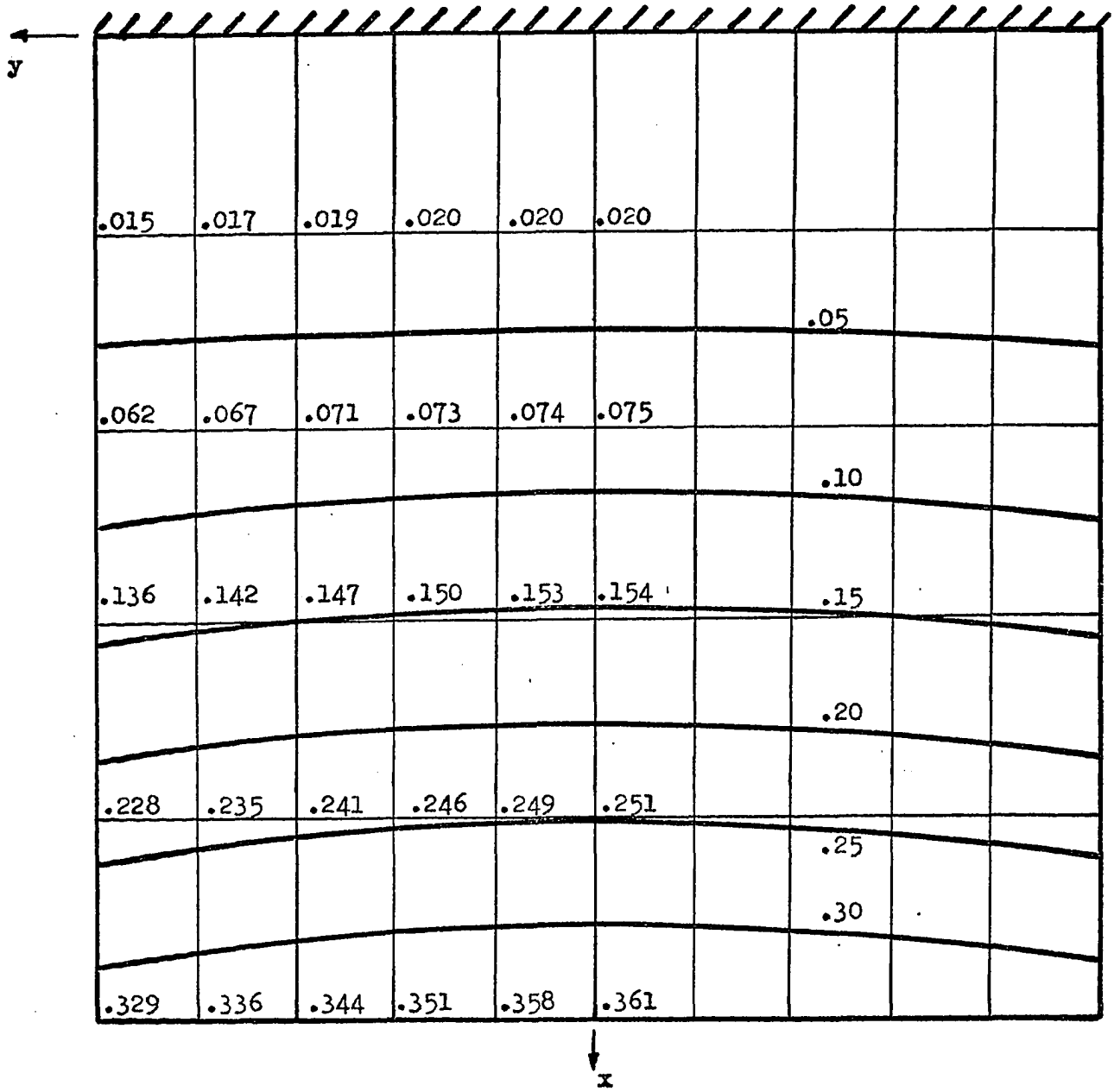

Fig. 13: Comparison of Theoretical Square Plate Deflections with those Obtained by Dalley, for a Point Load at the Center of the free Edge.

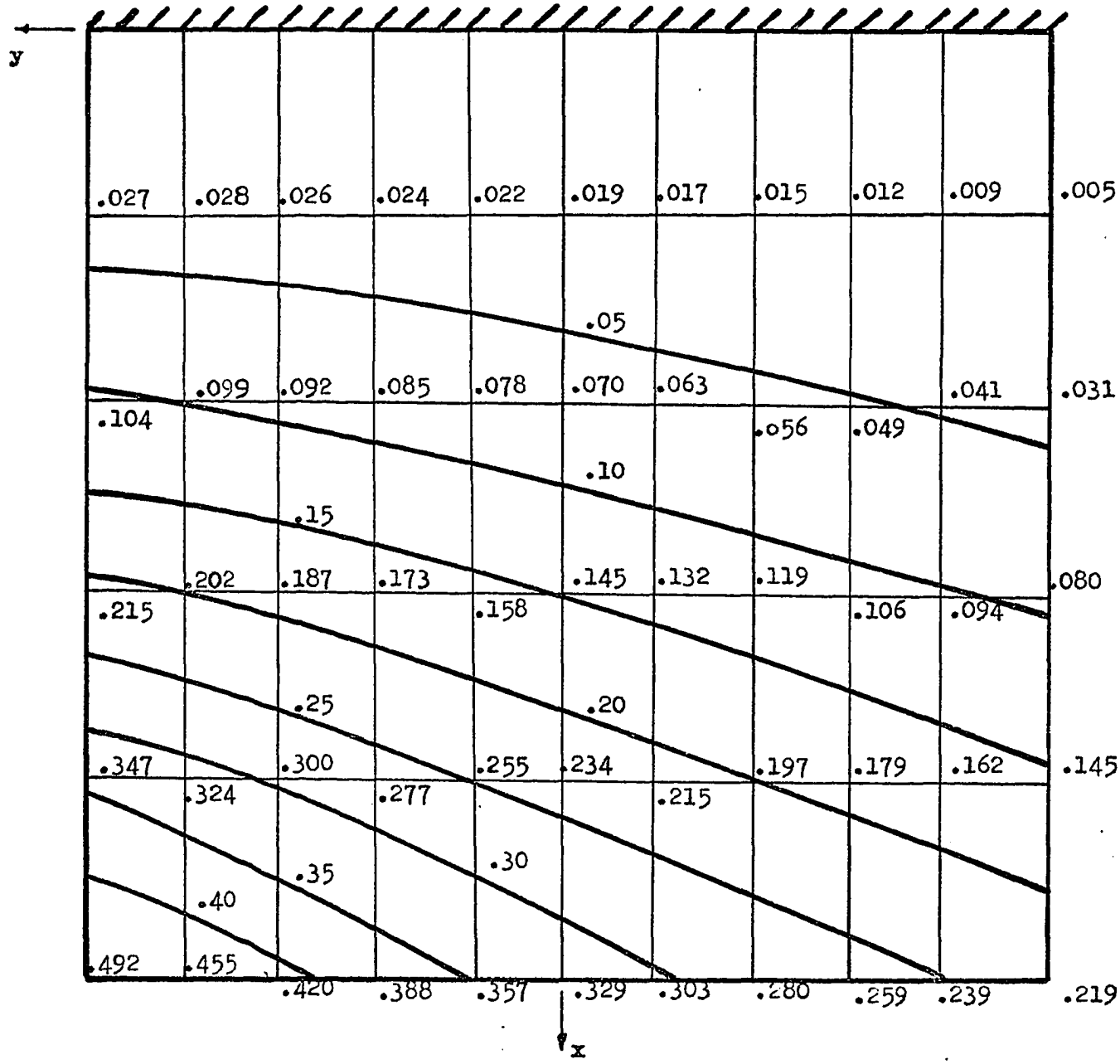

Fig 14: Comparison of Theoretical Square Plate Deflections with those Obtained by Dalley, for aPoint Load at a Free Corner of the Plate .

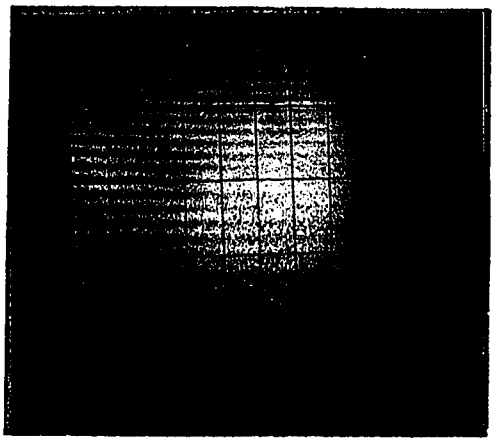

α =0.0, P=0.55 lb.

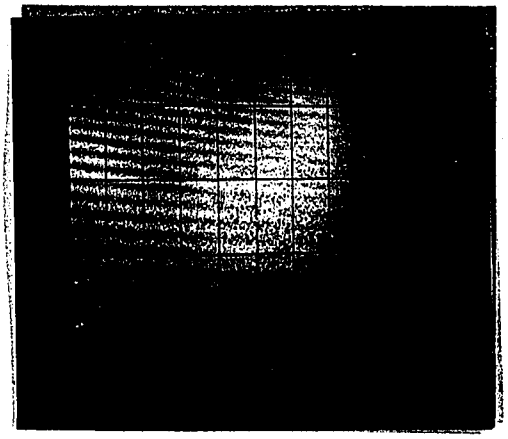

α =0.2, P=0.55 lb.

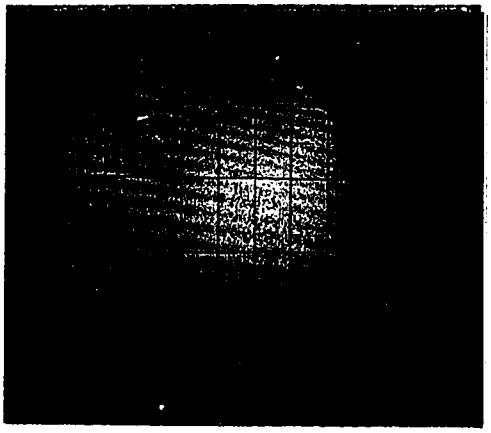

α =0.4, P=0.55 lb.

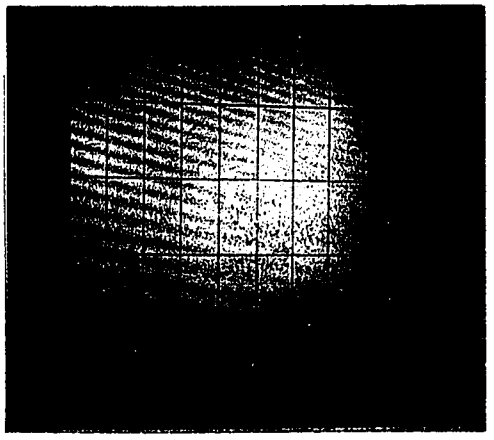

α =0.6, P=0.55 lb.

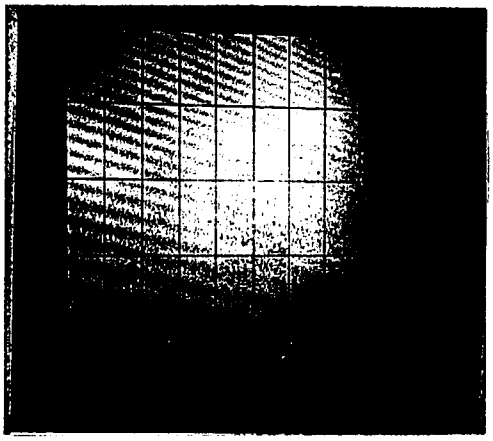

α =0.8, P=0.55 lb.

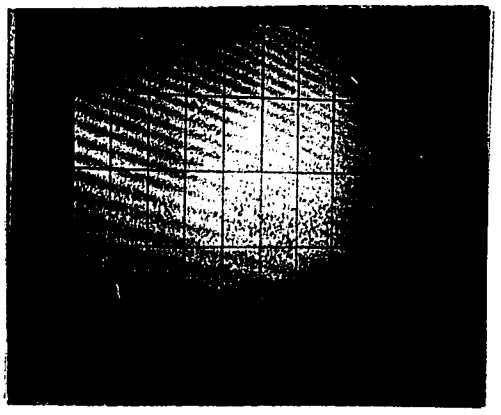

α =1.0, P=0.55 lb.

Fig. 15: Holographic Deflection Contours for a Plate with Aspect Ratio of 1.00, Loaded at Various Points Along the Free Edge (β =1).

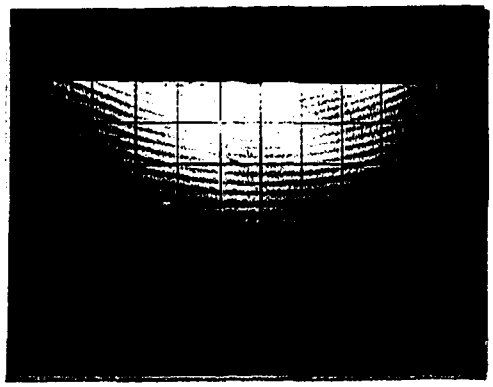

α =0.0, P=3.0 lb.

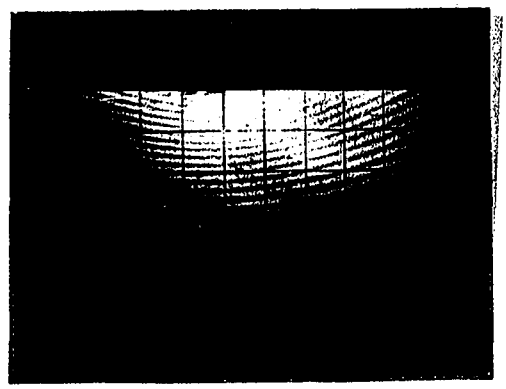

α =0.2, P=3.0 lb.

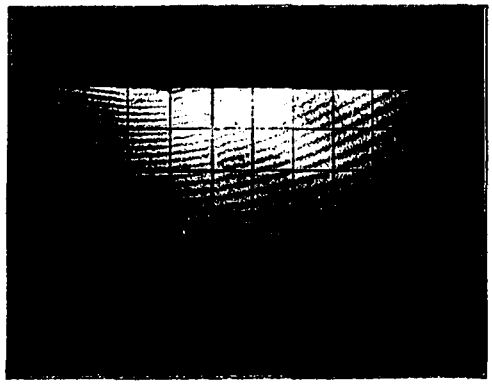

α =0.4, P=3.0 lb.

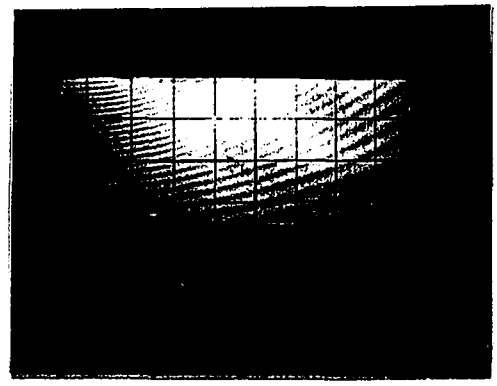

α =0.6, P=3.0 lb.

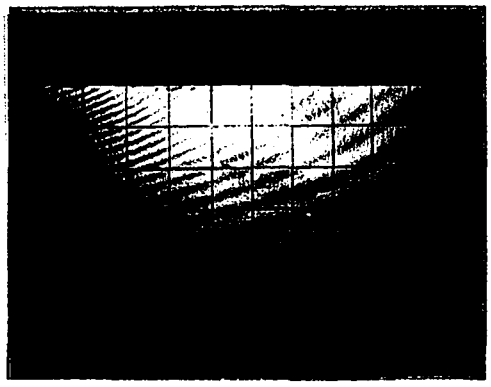

α =0.8, P=2.0 lb.

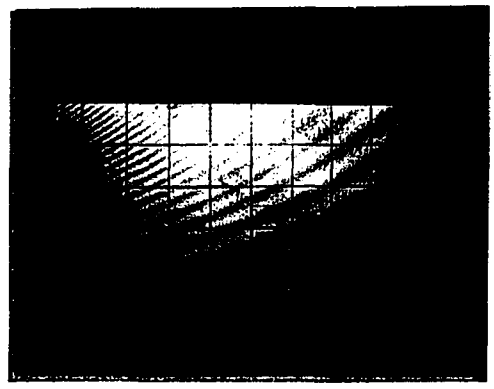

α =1.0, P=2.0 lb.

Fig. 16: Holographic Deflection Contours for a Plate with Aspect Ratio of 0.50, Loaded at Various Points Along the Free Edge (β =1).

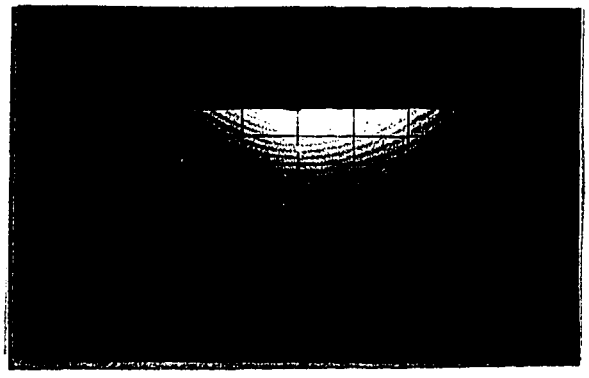

α =0.0, P=6.0 lb.

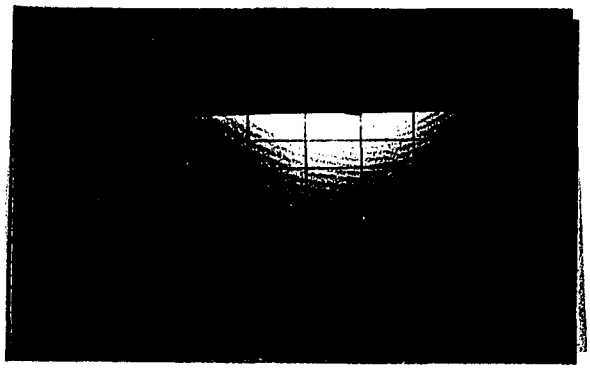

α =0.2, P=6.0 lb.

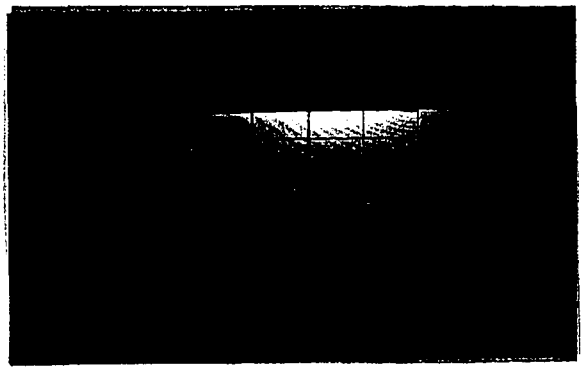

α =0.4, P=6.0 lb.

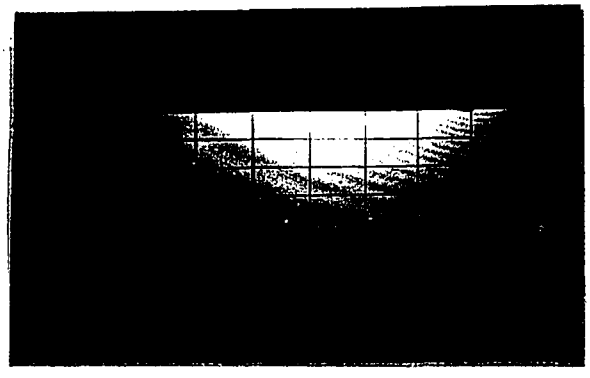

α =0.6, P=4.0 lb.

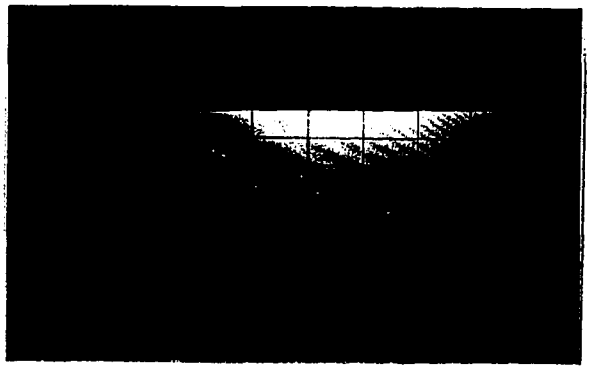

α =0.8, P=4.0 lb.

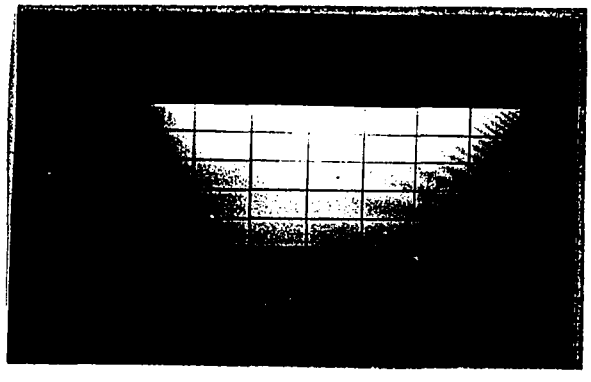

α =1.0, P=3.0 lb.

Fig. 17 : Holographic Deflection Contours for a Plate with Aspect Ratio of 0.25, Loaded at Various Positions Along the Free Edge (β =1).

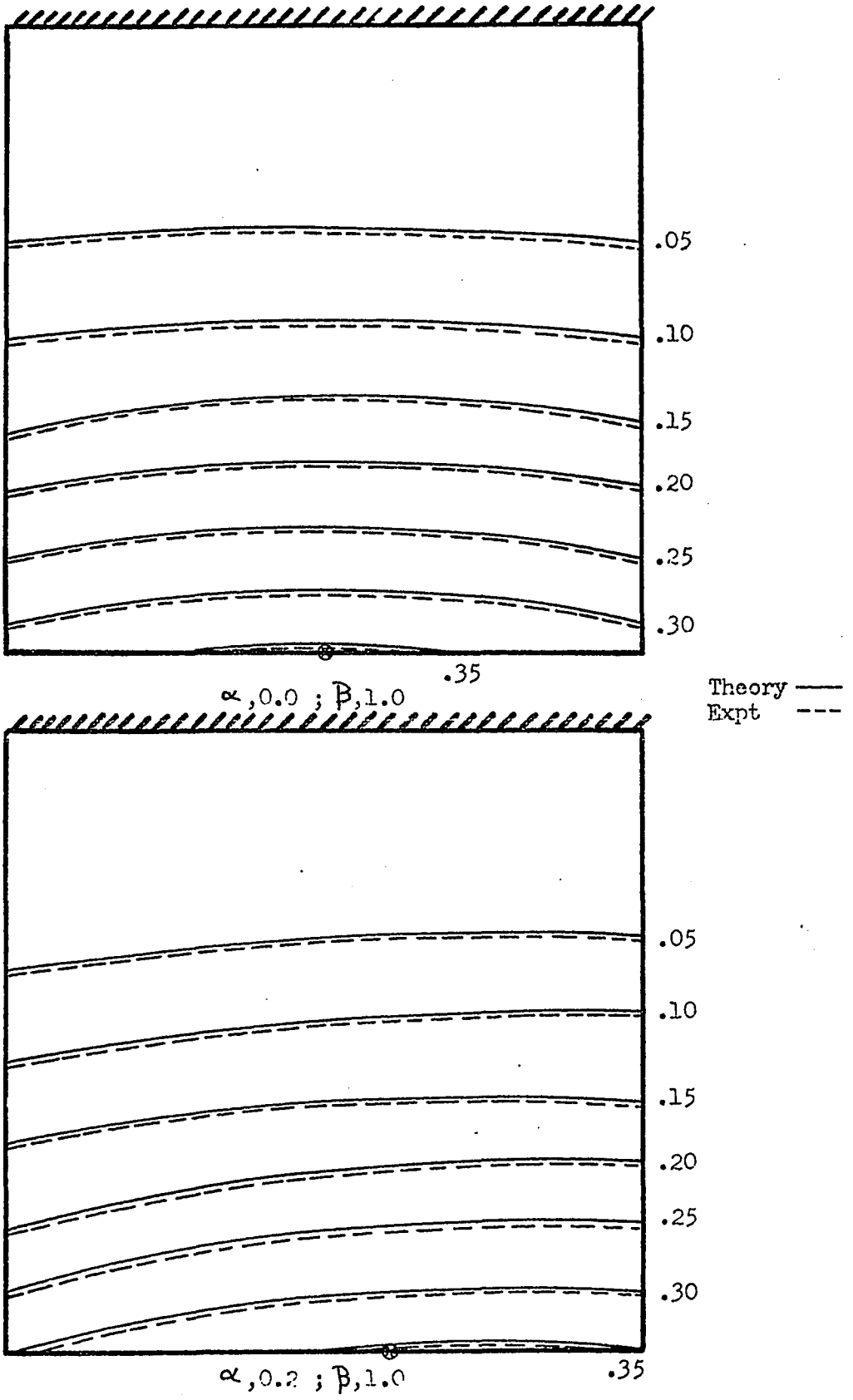

Fig. 18: Theoretical and Experimental Deflection Contours for a Plate With Aspect Ratio of 1.00 , Loaded Along the Free Edge

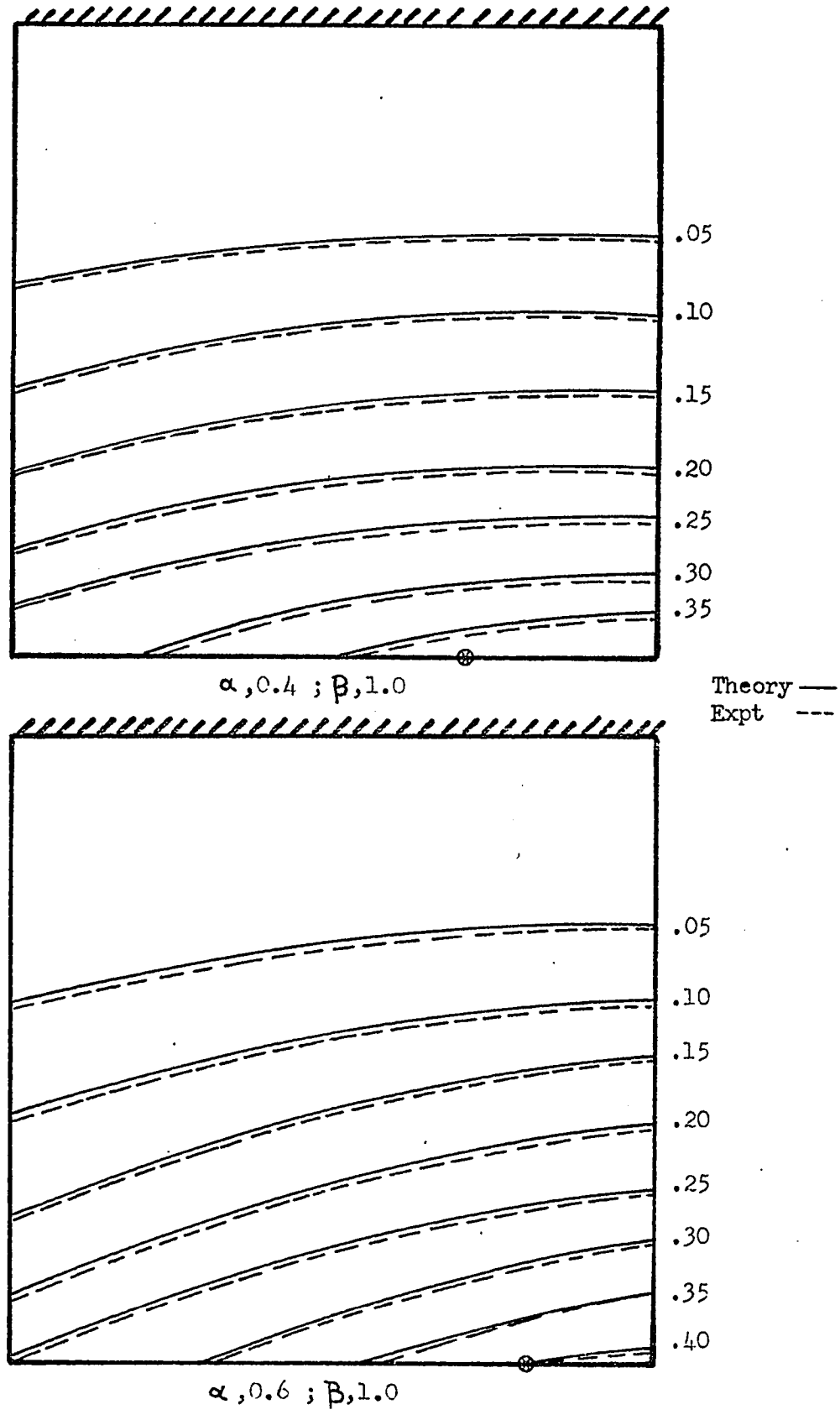

Fig. 19: Theoretical and Experimental Deflection Contours for a Plate With Aspect Ratio of 1.00, Loaded Along the Free Edge

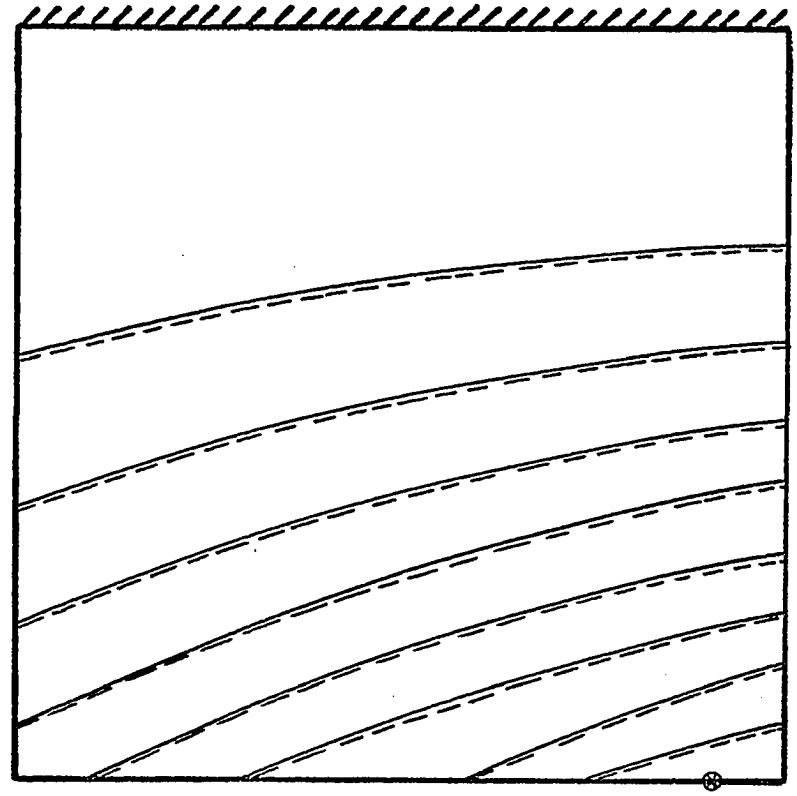

α, 0.8 ; β, 1.0

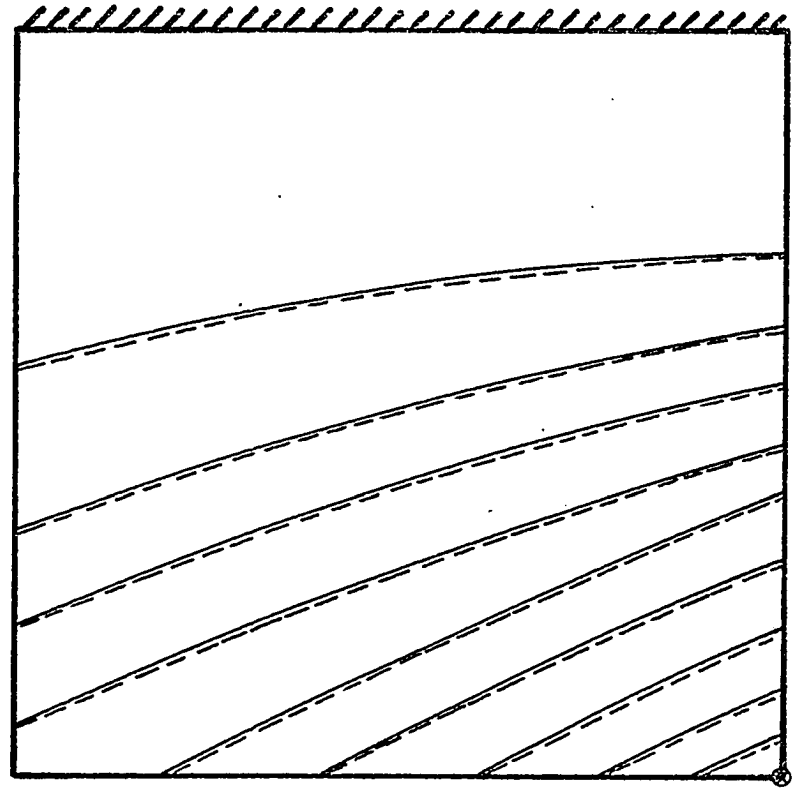

α, 1.0 ; β, 1.0

Fig. 20: Theoretical and Experimental Deflection Contours for a Plate With Aspect Ratio of 1.00, Loaded Along the Free Edge

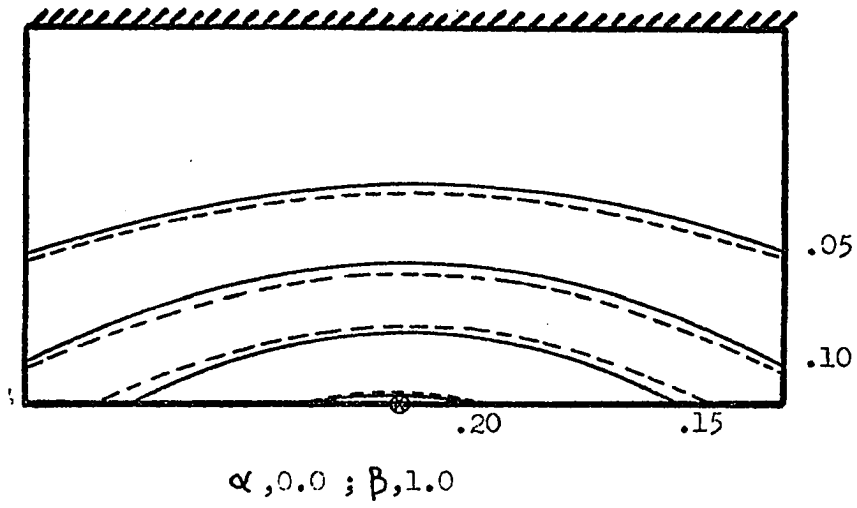

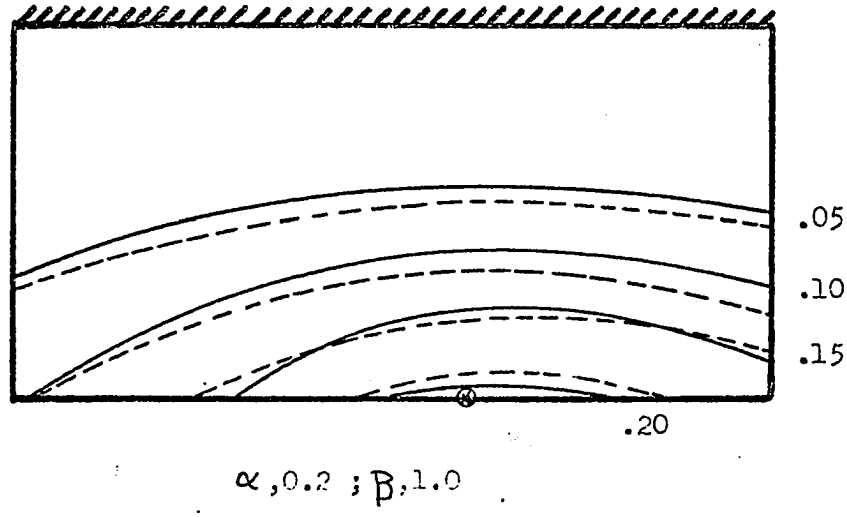

Fig. 21: Theoretical and Experimental Deflection Contours for a Plate With Aspect Ratio of 0.50, Loaded Along the Free Edge

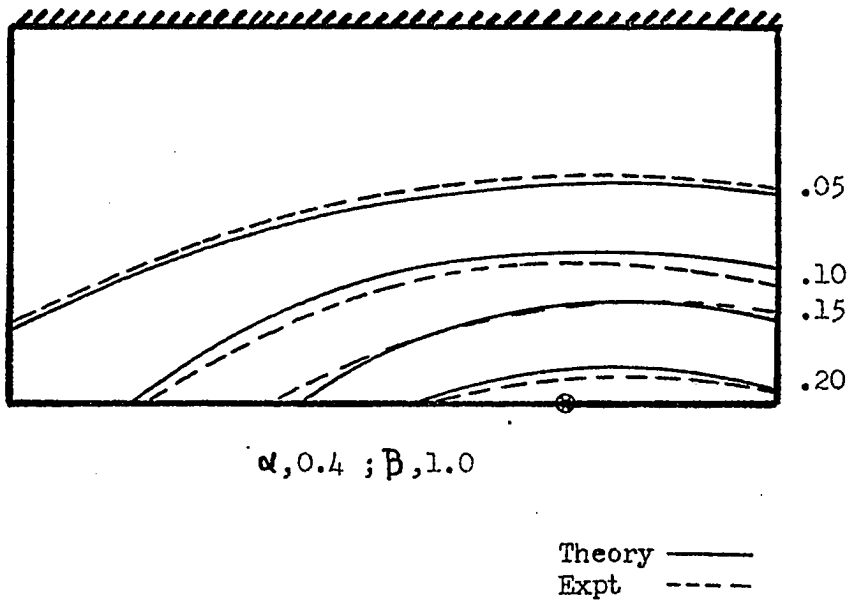

Fig. 22: Theoretical and Experimental Deflection Contours for a Plate With Aspect Ratio 0.50, Loaded Along the Free Edge

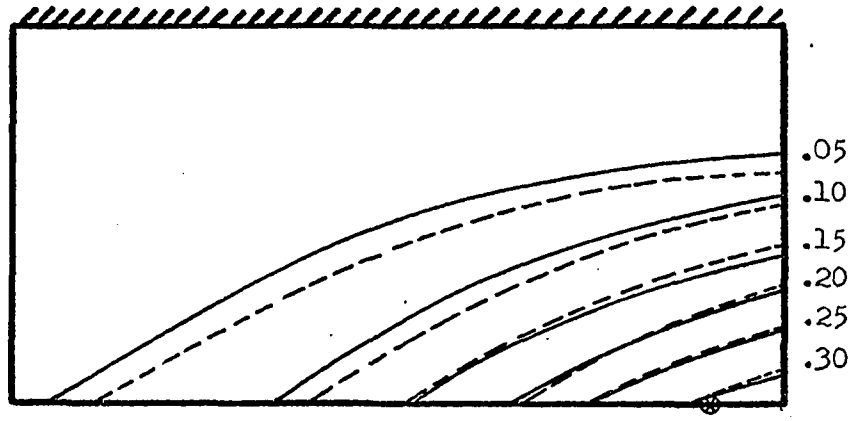

α,0.8 ; β,1.0

Theory ——
Expt ----

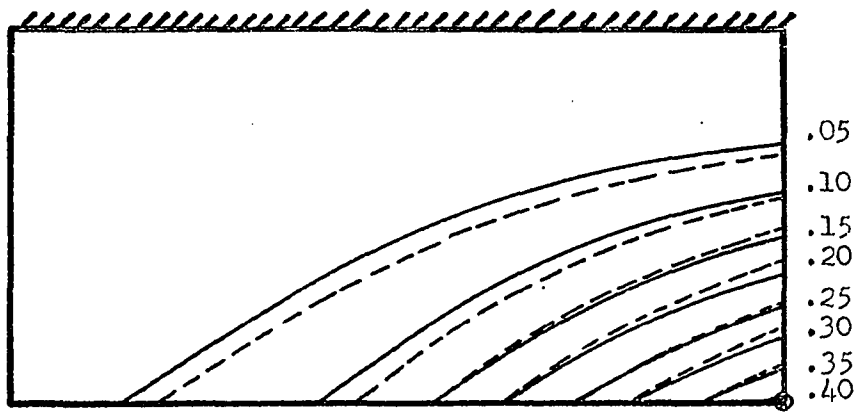

α,1.0 ; β,1.0

Fig. 23: Theoretical and Experimental Deflection Contours for a Plate With Aspect Ratio 0.50, Loaded Along the Free Edge

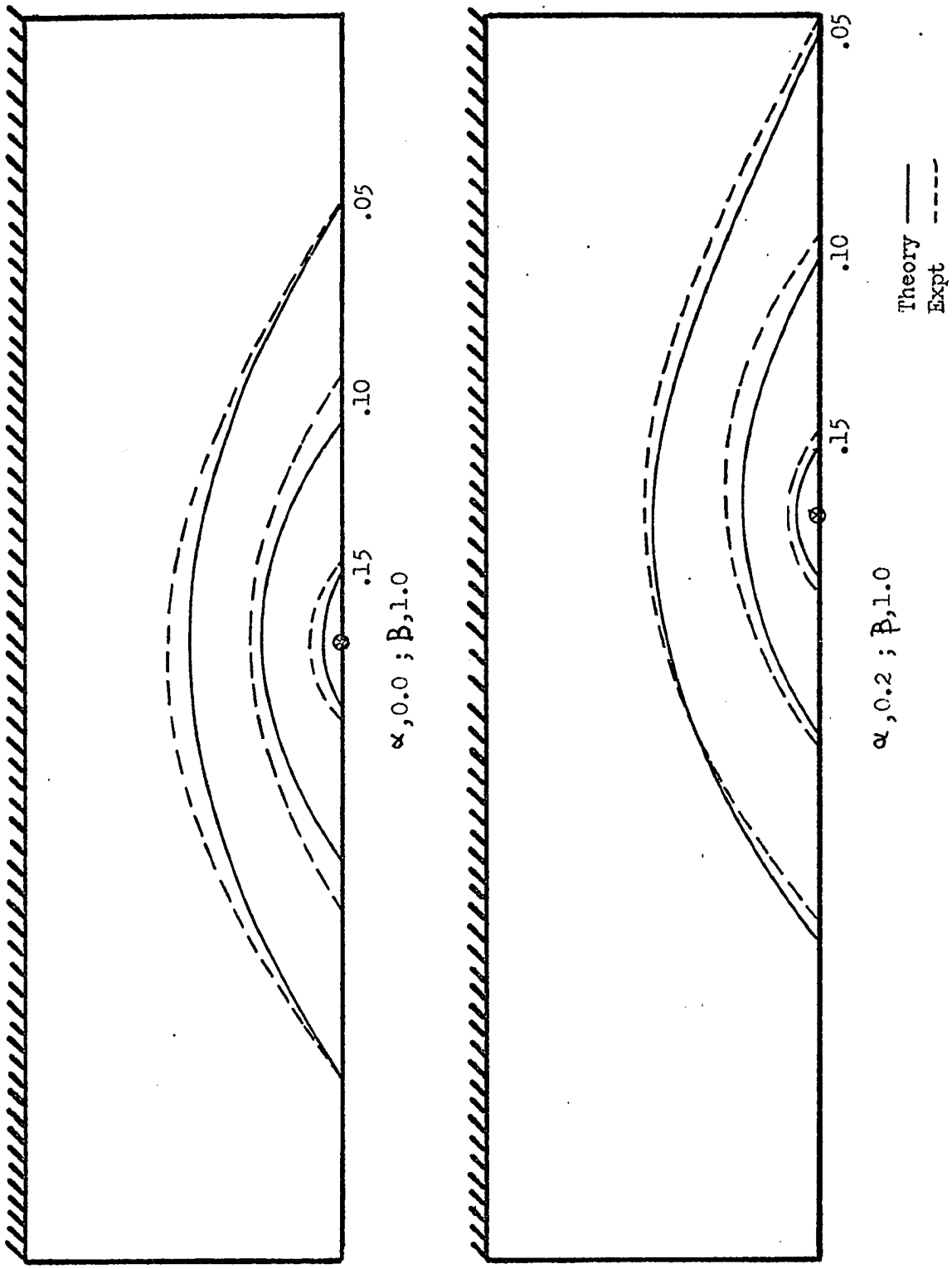

Fig. 24: Theoretical and Experimental Deflection Contours for a Plate With Aspect Ratio of 0.25, Loaded Along the Free Edge

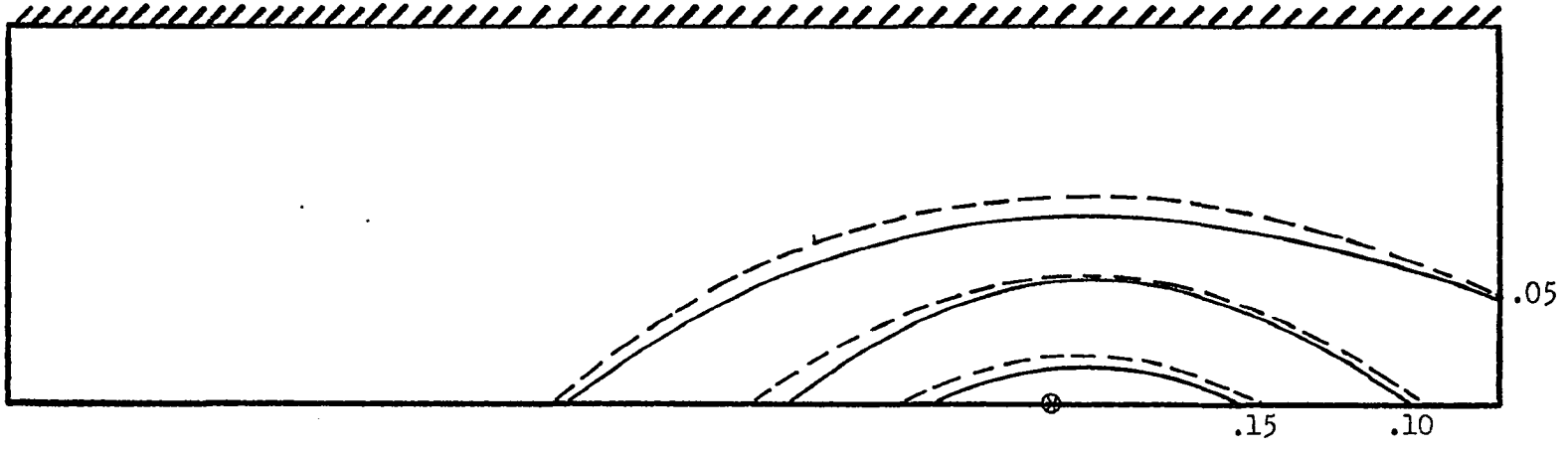

α,0.4 ; β,1.0

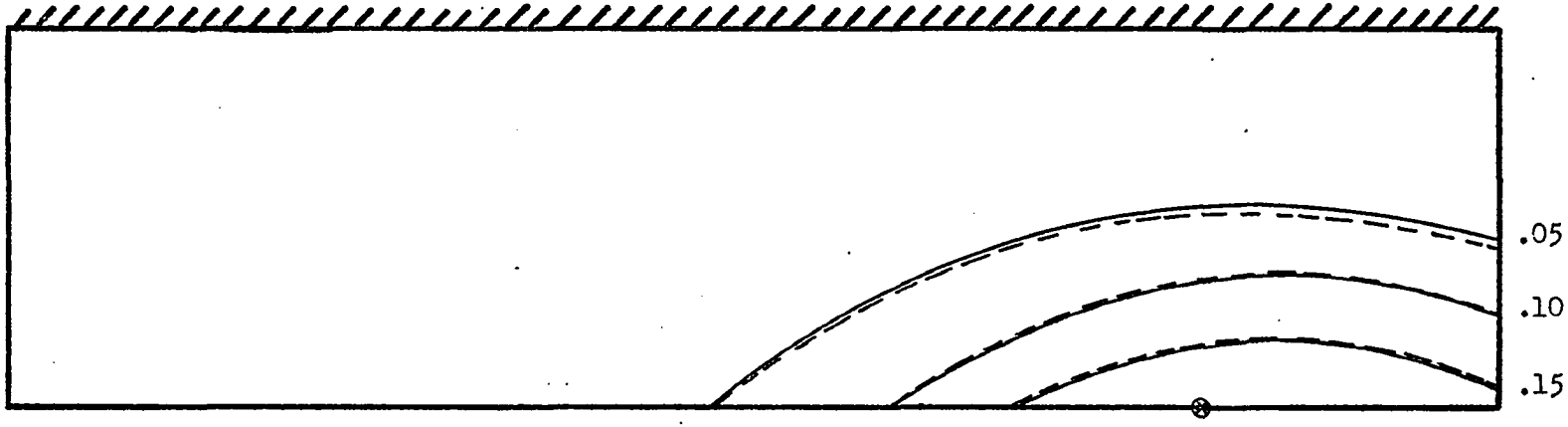

α,0.6 ; β,1.0

Theory ——
Expt ----

Fig. 25: Theoretical and Experimental Deflection Contours for a Plate With Aspect Ratio of 0.25 Loaded Along the Free Edge

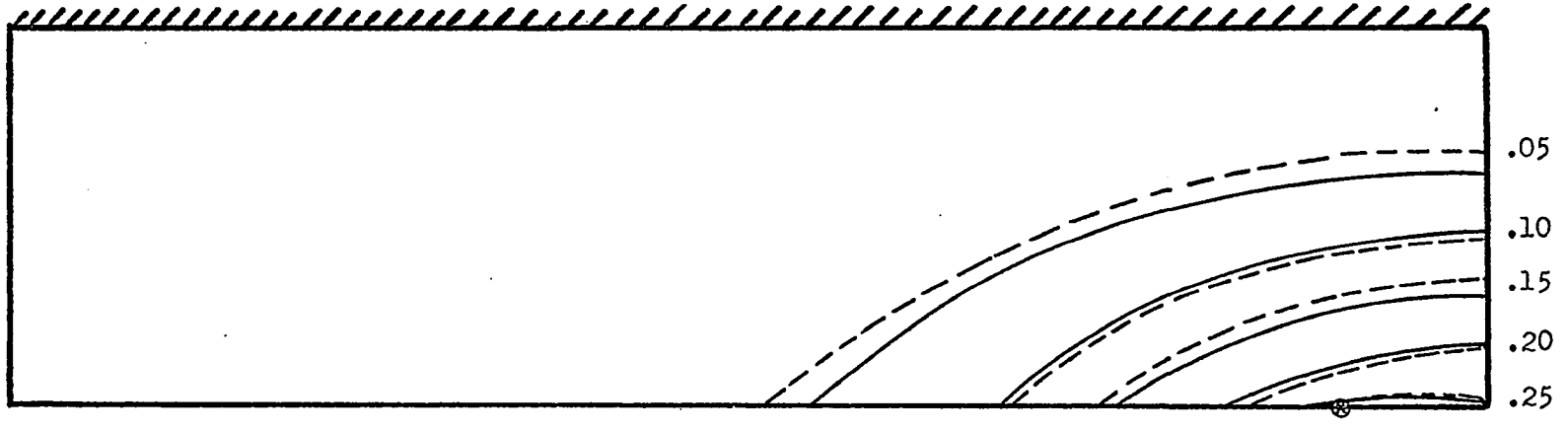

α ,0.8 ; β,1.0

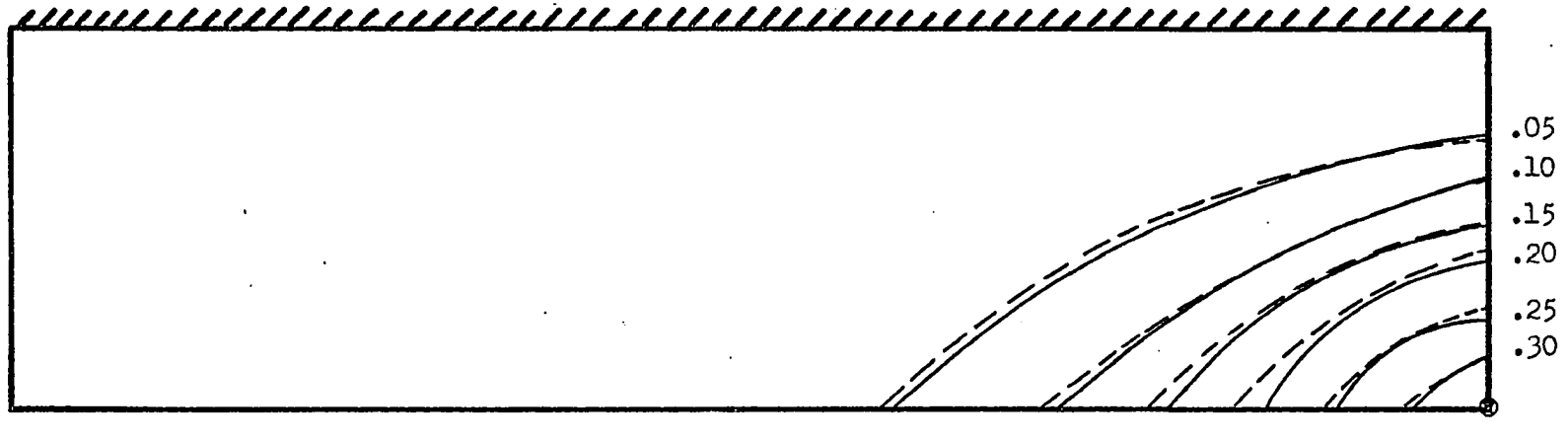

α,1.0 ; β,1.0

Theory ——
Expt ----

Fig. 26: Theoretical and Experimental Deflection Contours for a Plate With Aspect Ratio of 0.25 Loaded Along the Free Edge

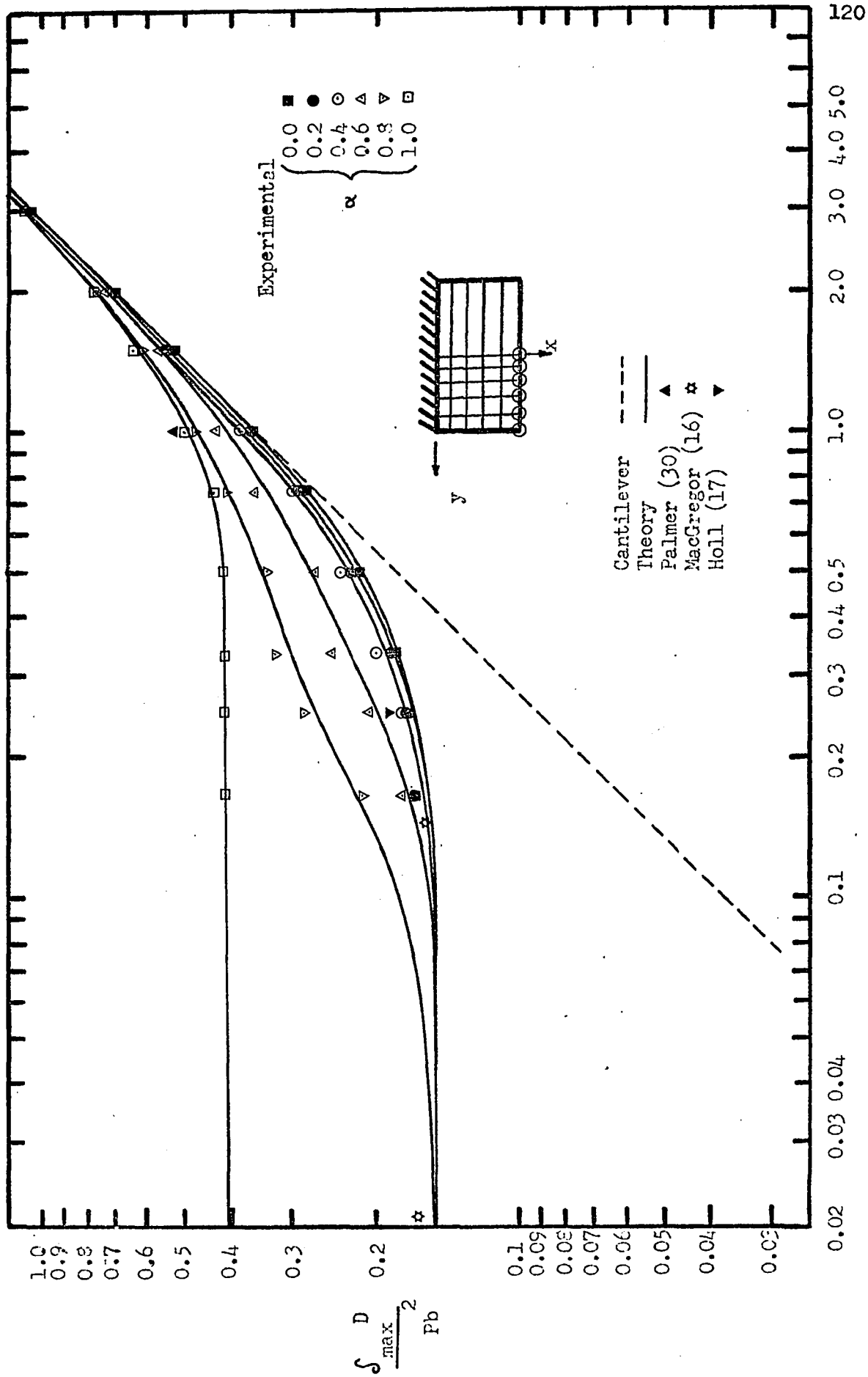

Fig. 27: Maximum Deflection vs Aspect Ratio ; β ,1.0 for Various Values of α

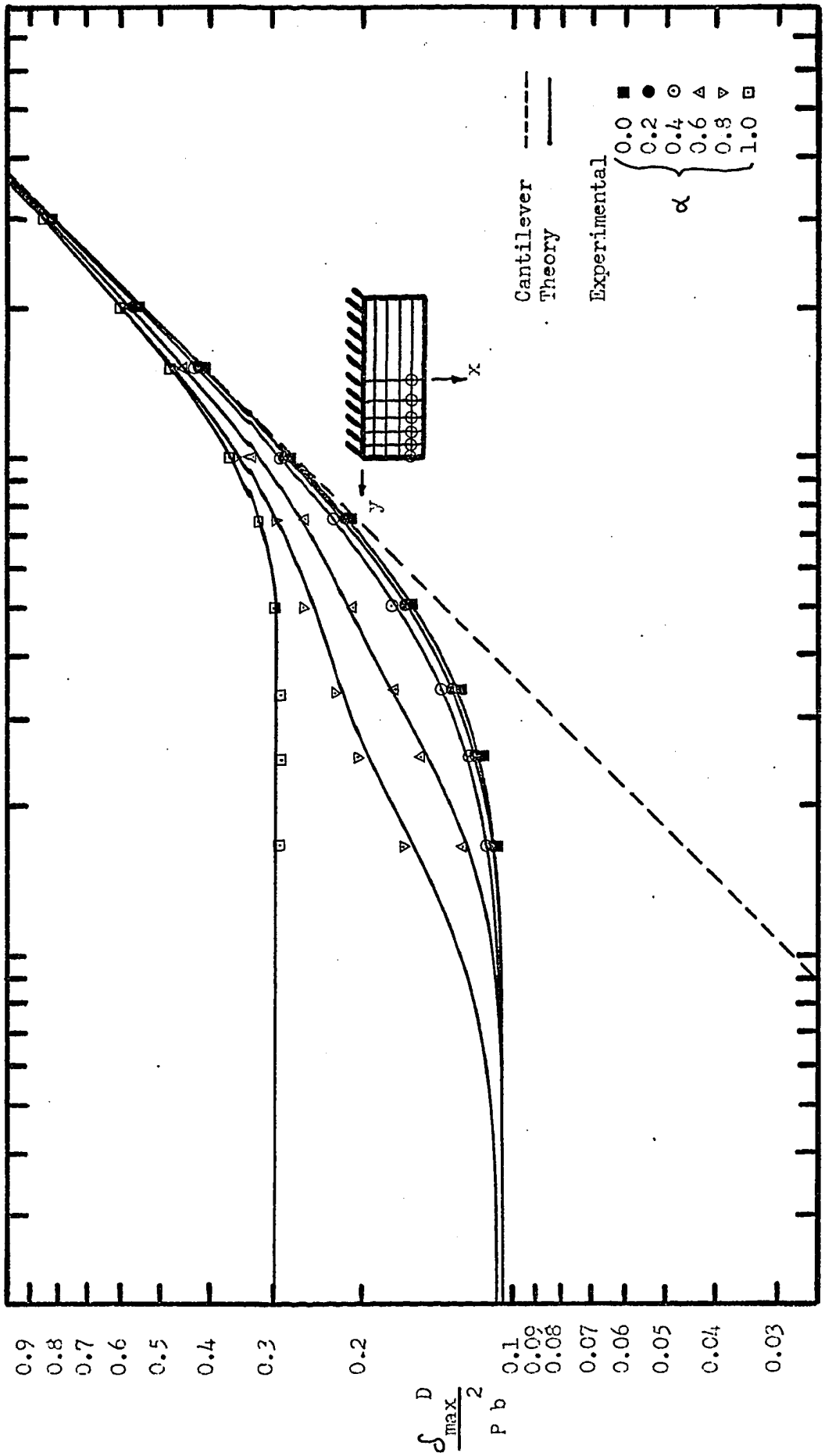

Fig. 28: Maximum Deflection vs Aspect Ratio ; β,0.8 for Various Values of α

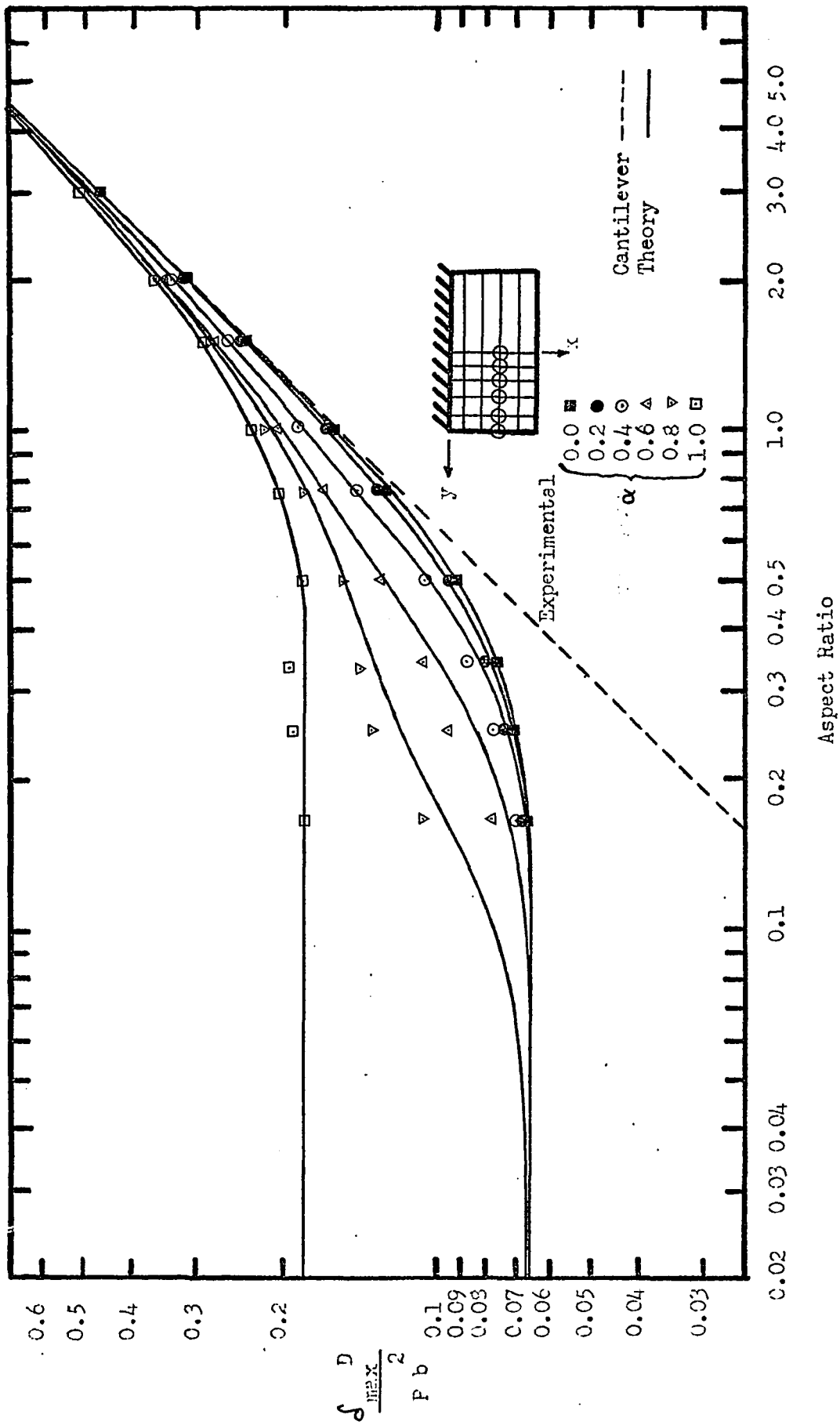

Fig. 29: Maximum Deflection vs Aspect Ratio ; β,0.6 for Various Values of α

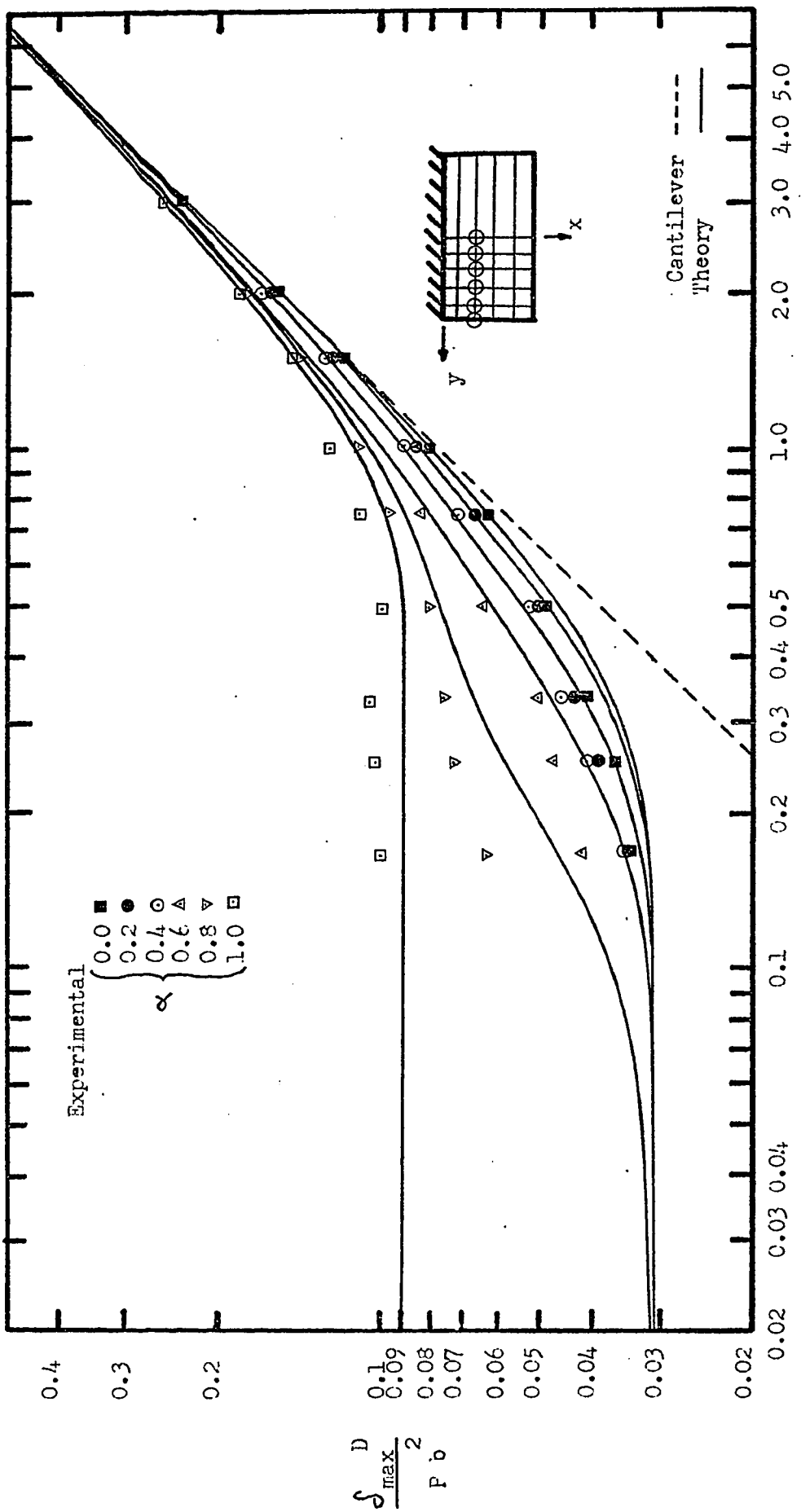

Fig. 30: Maximum Deflection vs Aspect Ratio ; β ,0.4 for Various Values of α

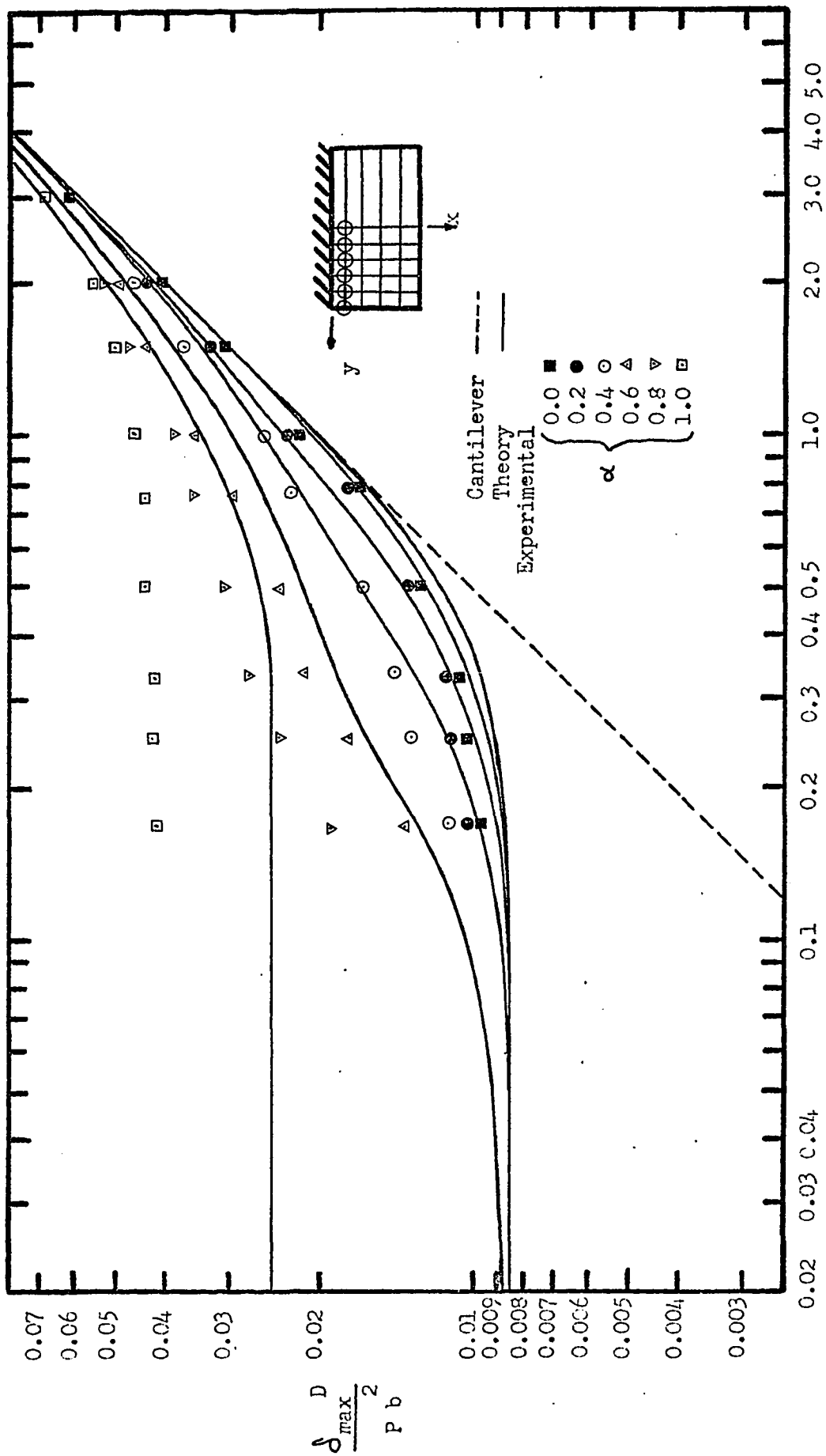

Fig. 31: maximum Deflection vs Aspect Ratio ; β,0.2 for Various Values of α

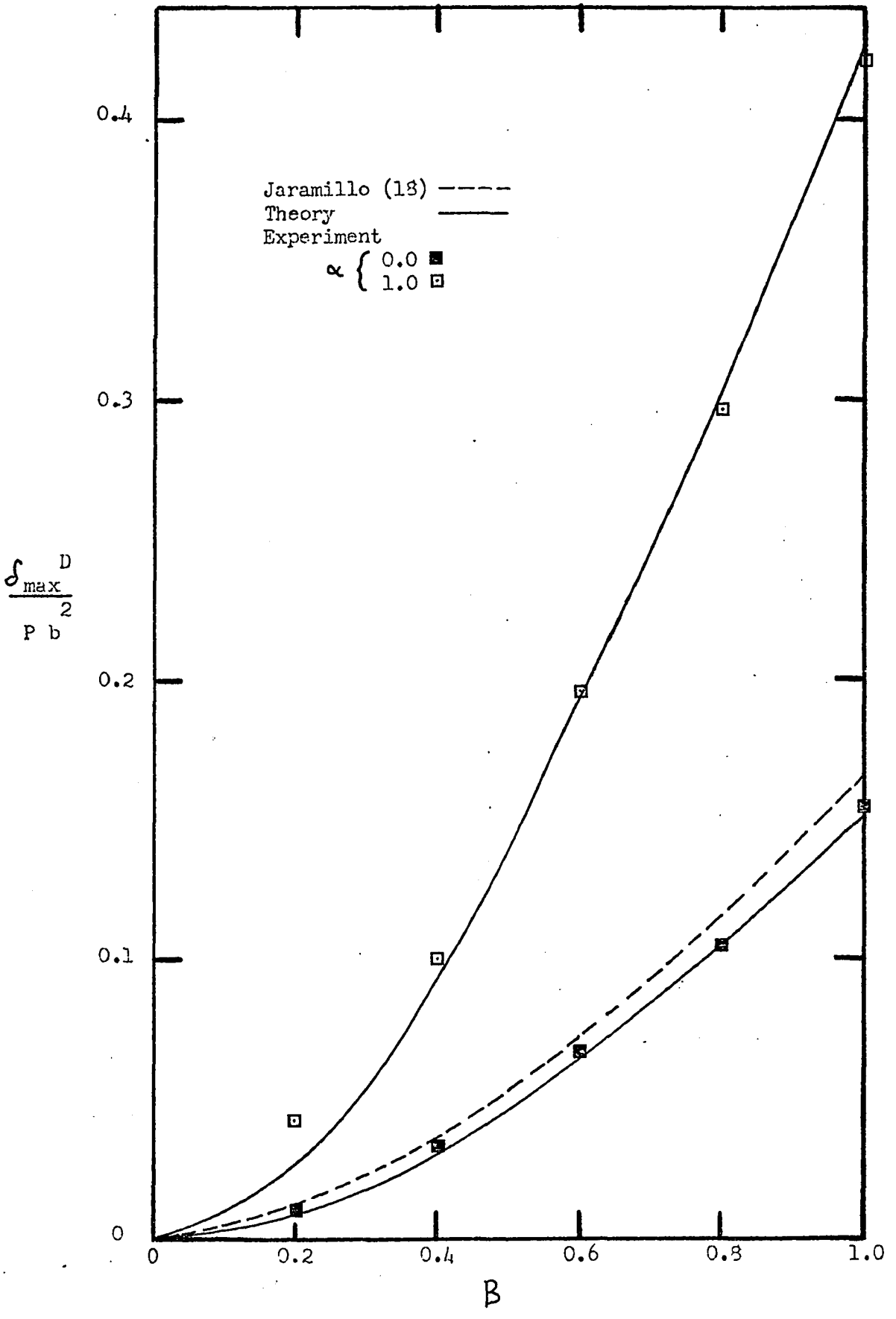

Fig. 32: Maximum Deflection of a Plate With Low Aspect Ratio (≤ 0.250) As a Function of the Load Position (β,1.0)

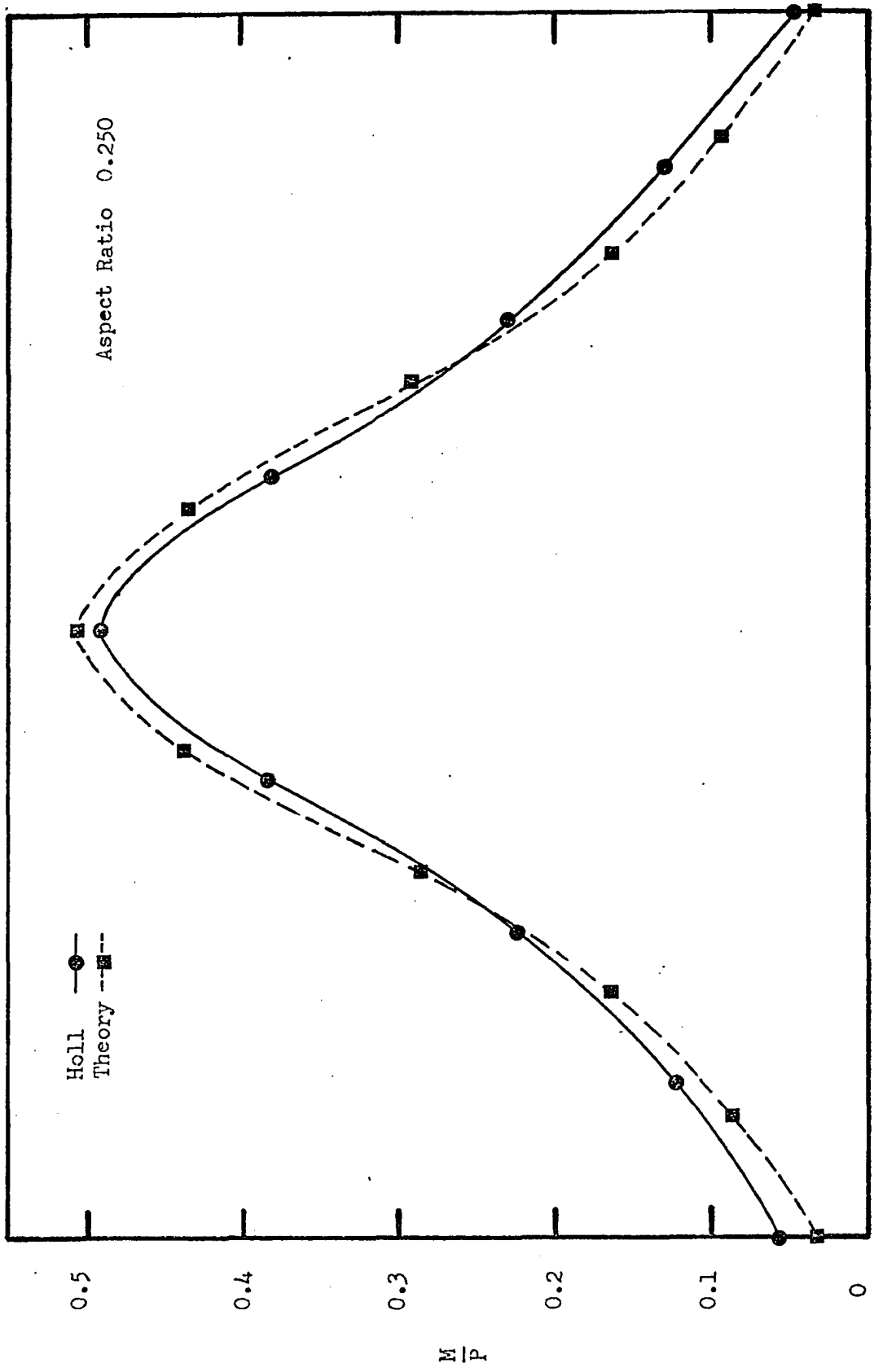

Fig. 33: Comparison of Theoretical Fixed Edge Moments With the Results of Holl (α,0.0; β,1.0)

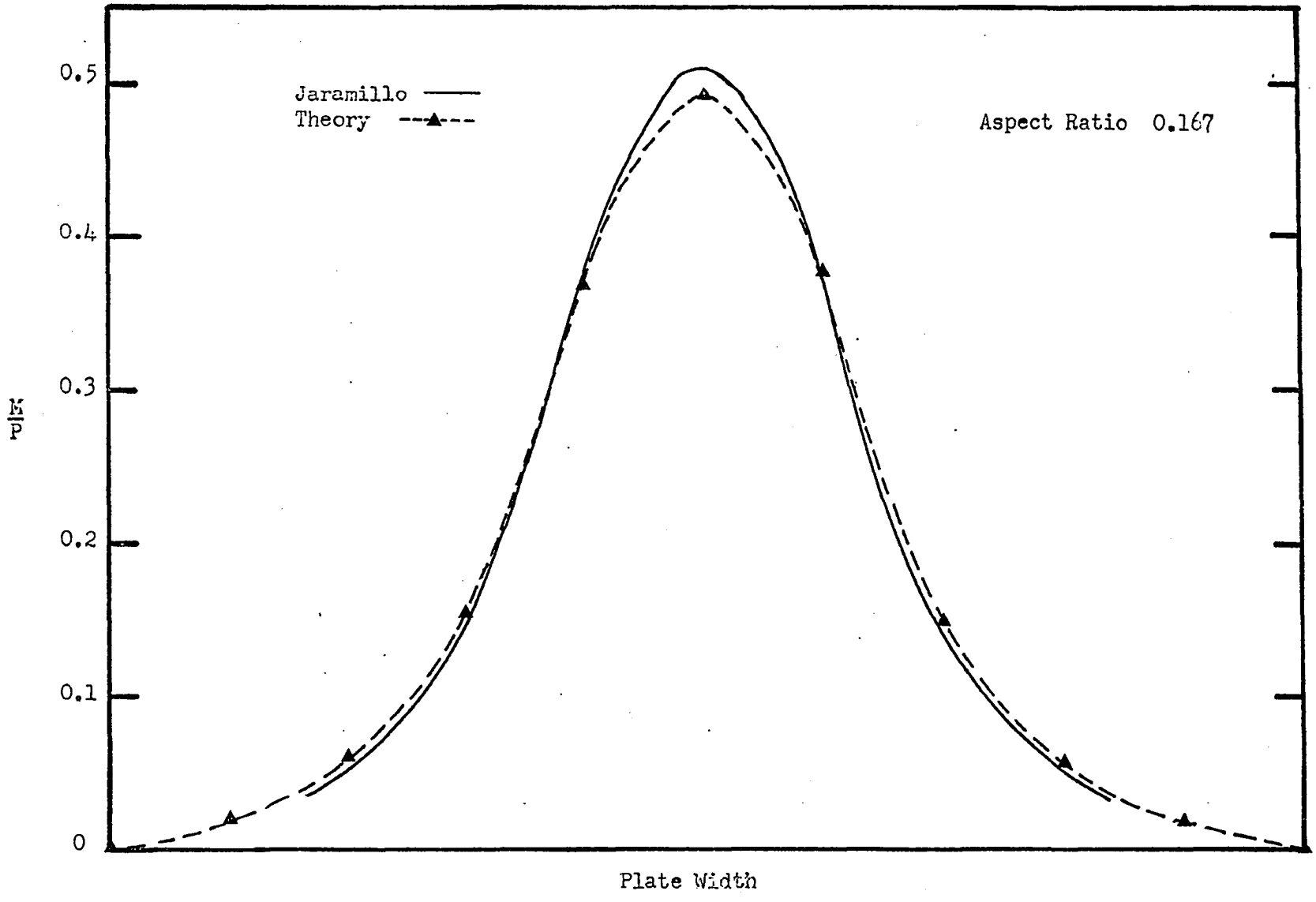

Fig. 34: Comparison ofTheoretical Fixed Edge Moments With the Results of Jaramillo (α,0.0; β,1.0)

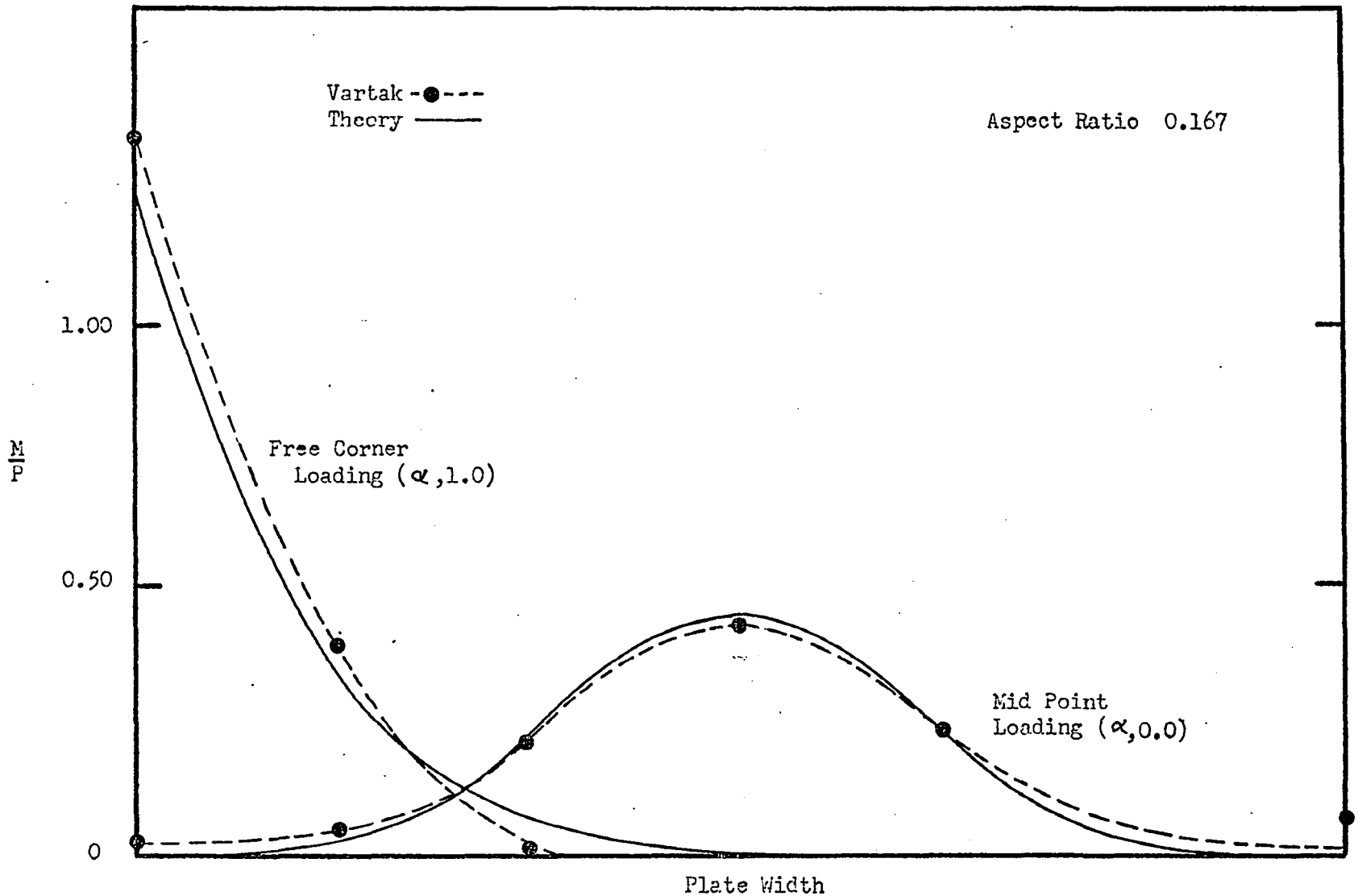

Fig. 35: Comparison of Theoretical Results With the Experimental Results of Vartak (19) for Free Edge Loading of a Cantilever Plate (β,1.0)

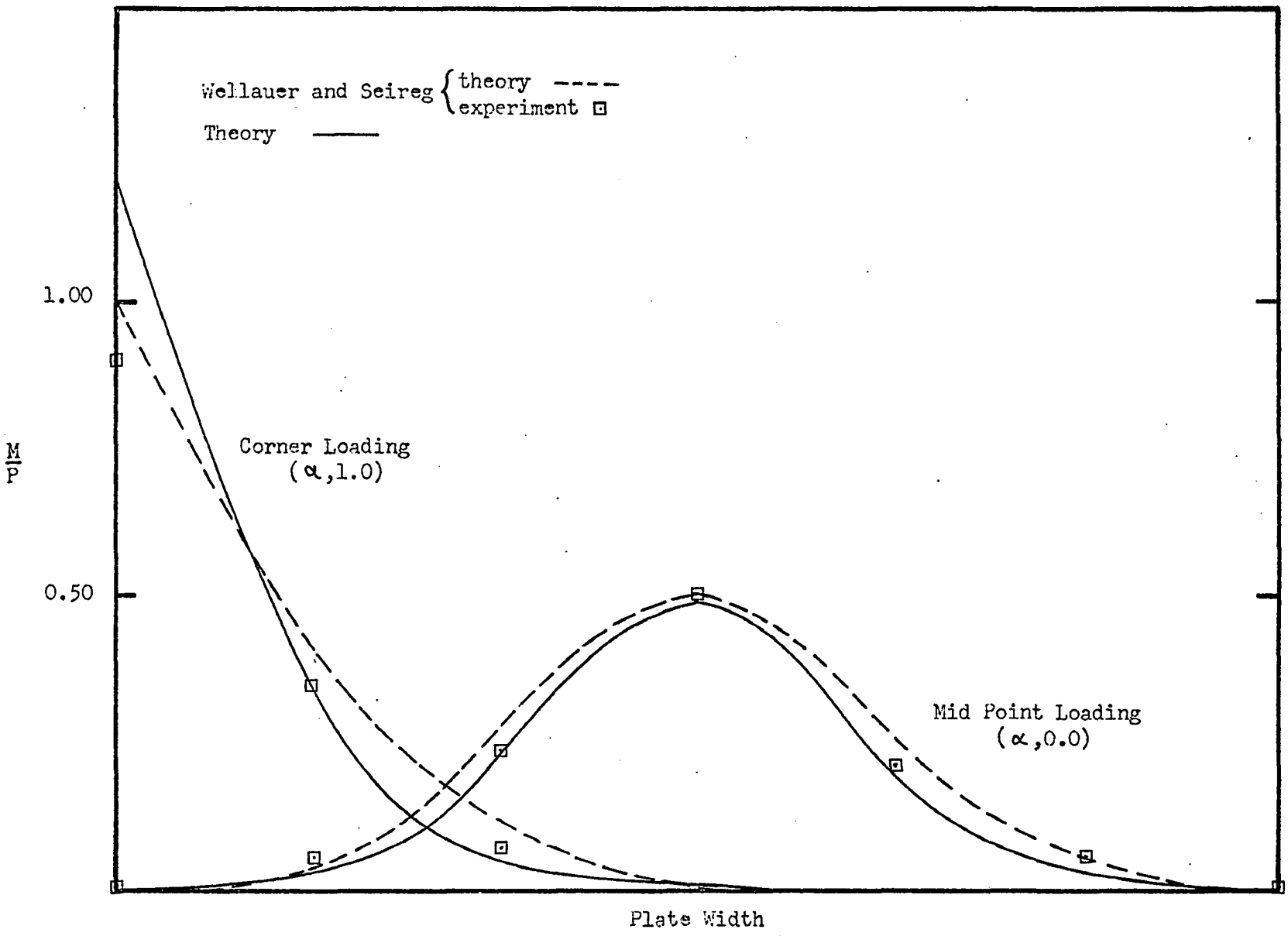

Fig. 36: Comparison of Theoretical Results With the Results of Wellauer and Seireg (4) for Loading Along the Free Edge (β,1.0)

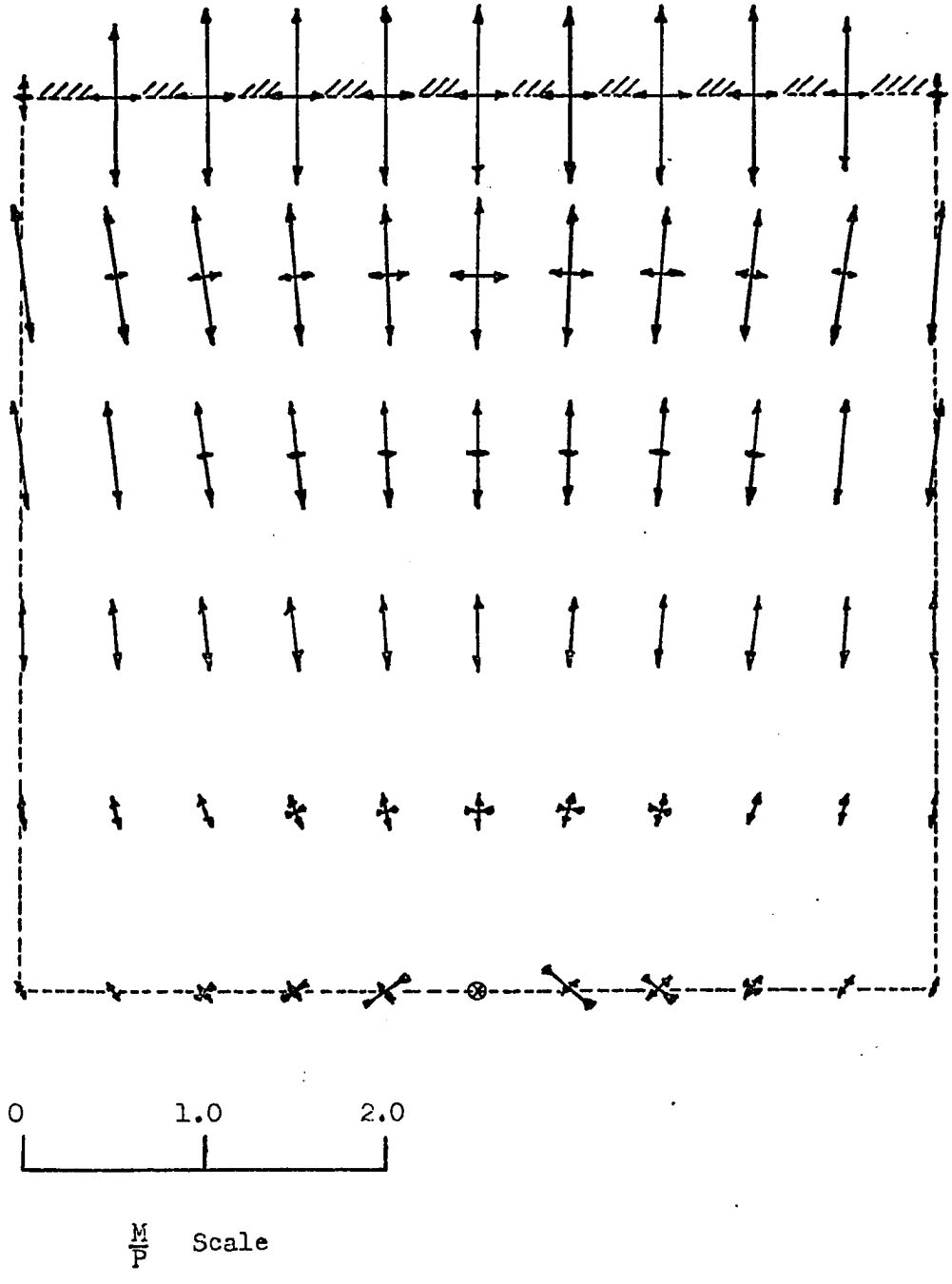

Fig. 37: Theoretical Principal Moments in a Square Plate (Aspect Ratio 1.0) Under a Point Load Applied at the Centre of the Free Edge (α,0.0; β,1.0)

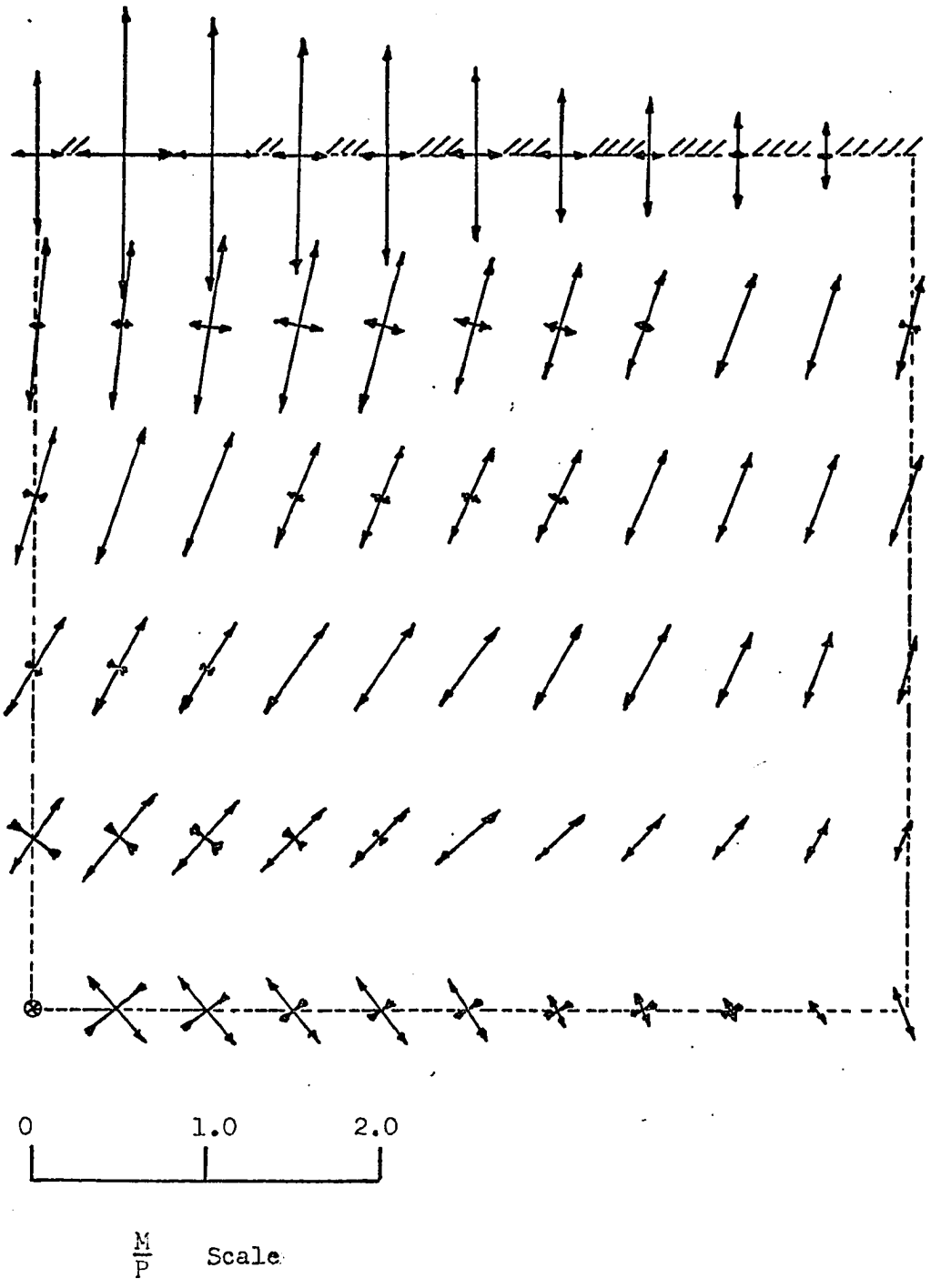

Fig 38: Theoretical Principal Moments in a Square Plate (Aspect Ratio 1.0) Under a Point Load Applied at a Free Corner (α,1.0; β,1.0)

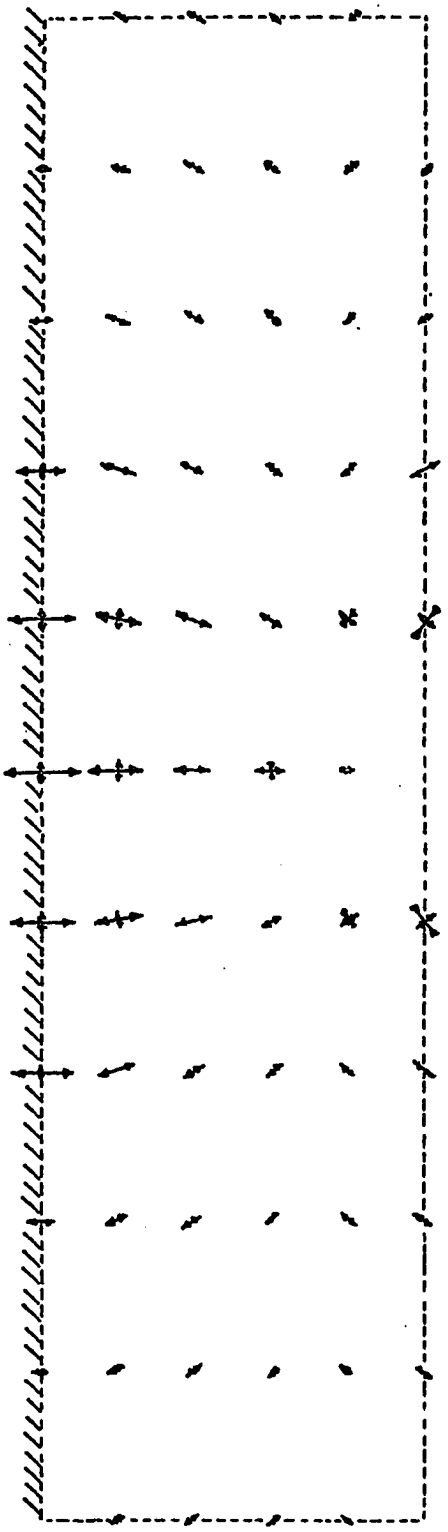

0 1.0

$\frac{M}{P}$ Scale

Fig. 39: Theoretical Principal Moments in a Rectangular Plate (Aspect Ratio 0.25) Under a Point Load Applied at the Centre of the Free Edge (α,0.0;β 1.0)

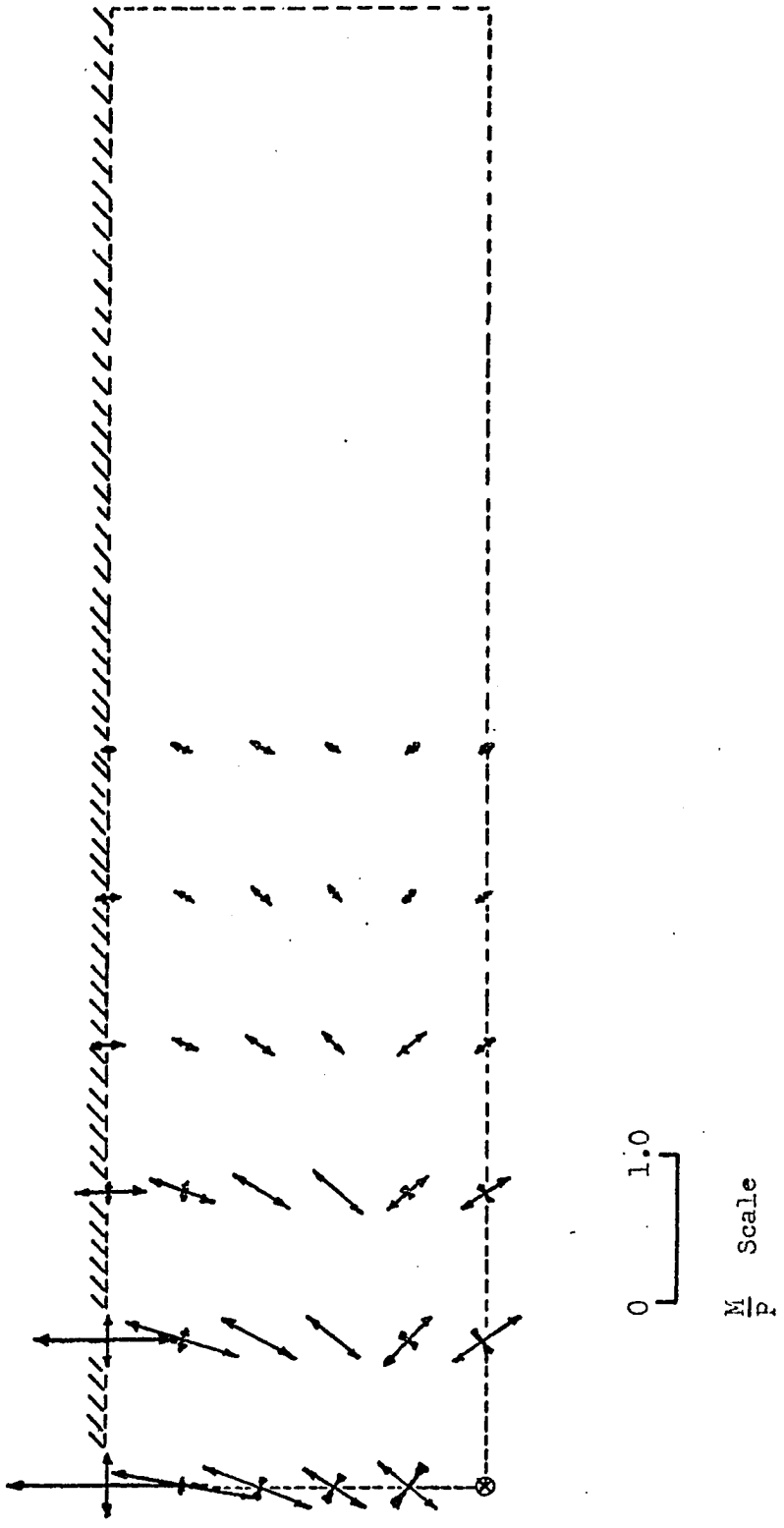

Fig. 40: Theoretical Principal Moments in a Rectangular Plate (Aspect Ratio 0.25) Under a Point Load Applied at a Free Corner (α,1.0; β,1.0)

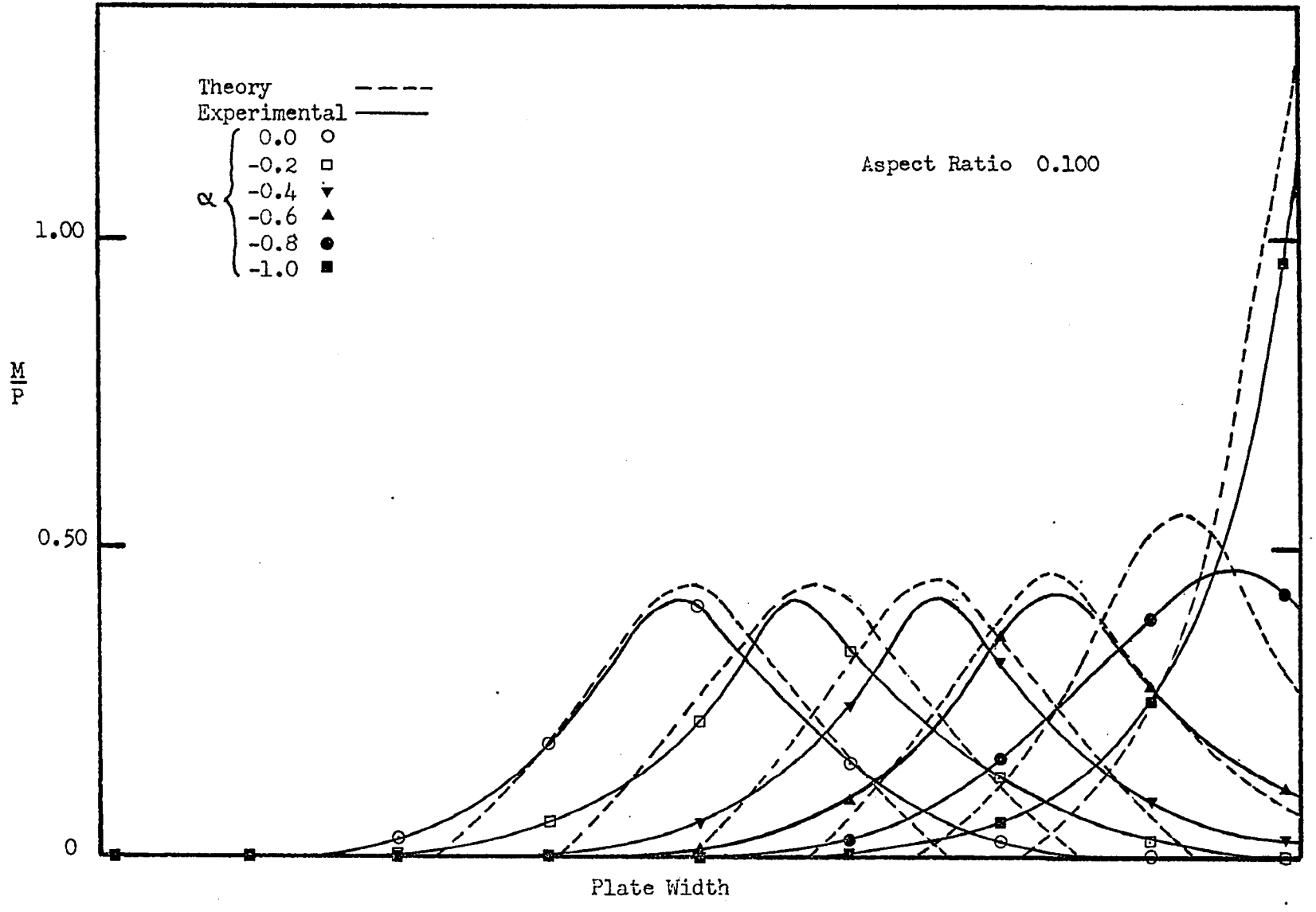

Fig. 41: Comparison of the Theoretical and Experimental Fixed Edge Bending Moments in a Tip Loaded Cantilever Plate (β,1.0)

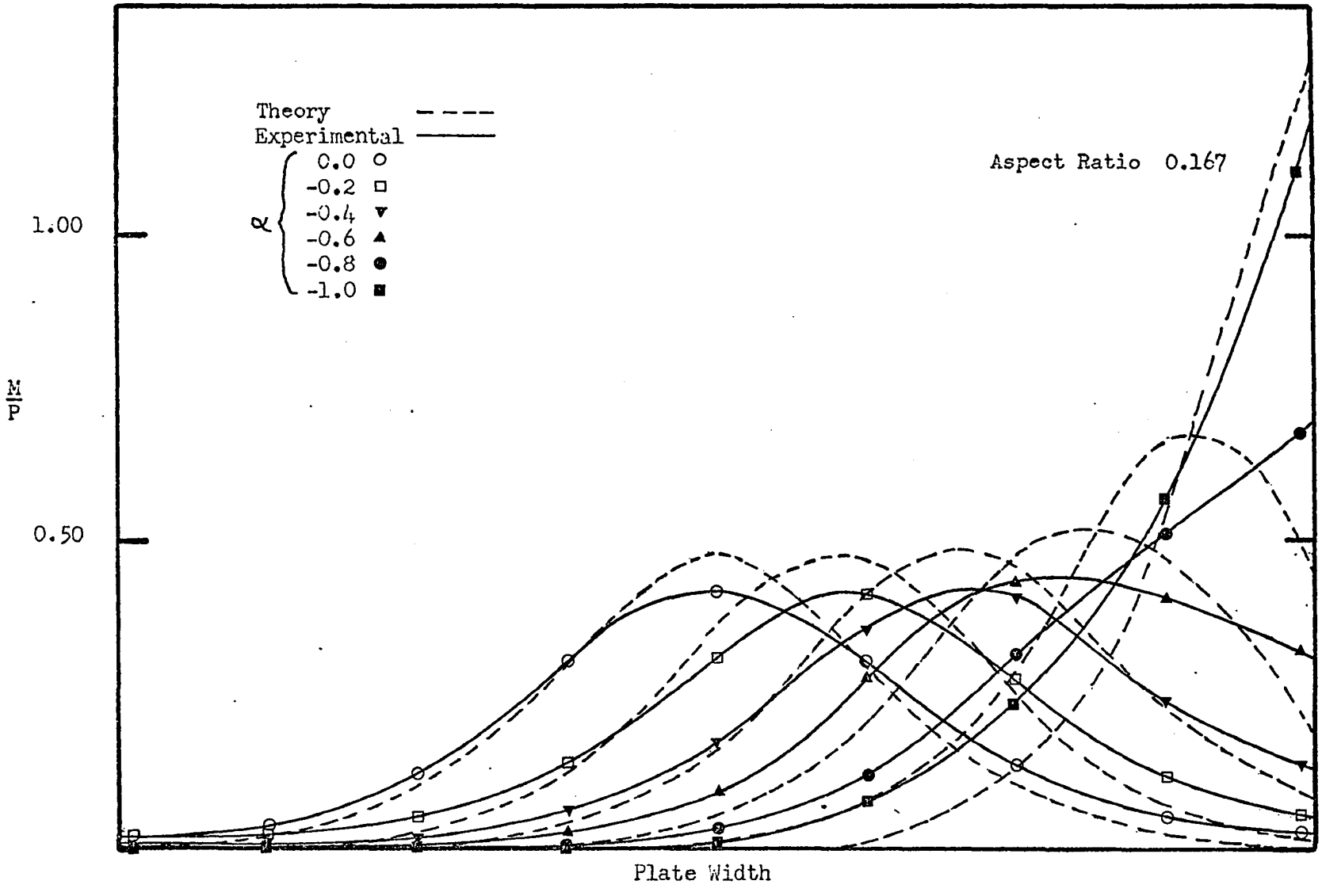

Fig. 42: Comparison of the Theoretical and Experimental Fixed Edge Bending Moments in a Tip Loaded Cantilever Plate (β,1.0)

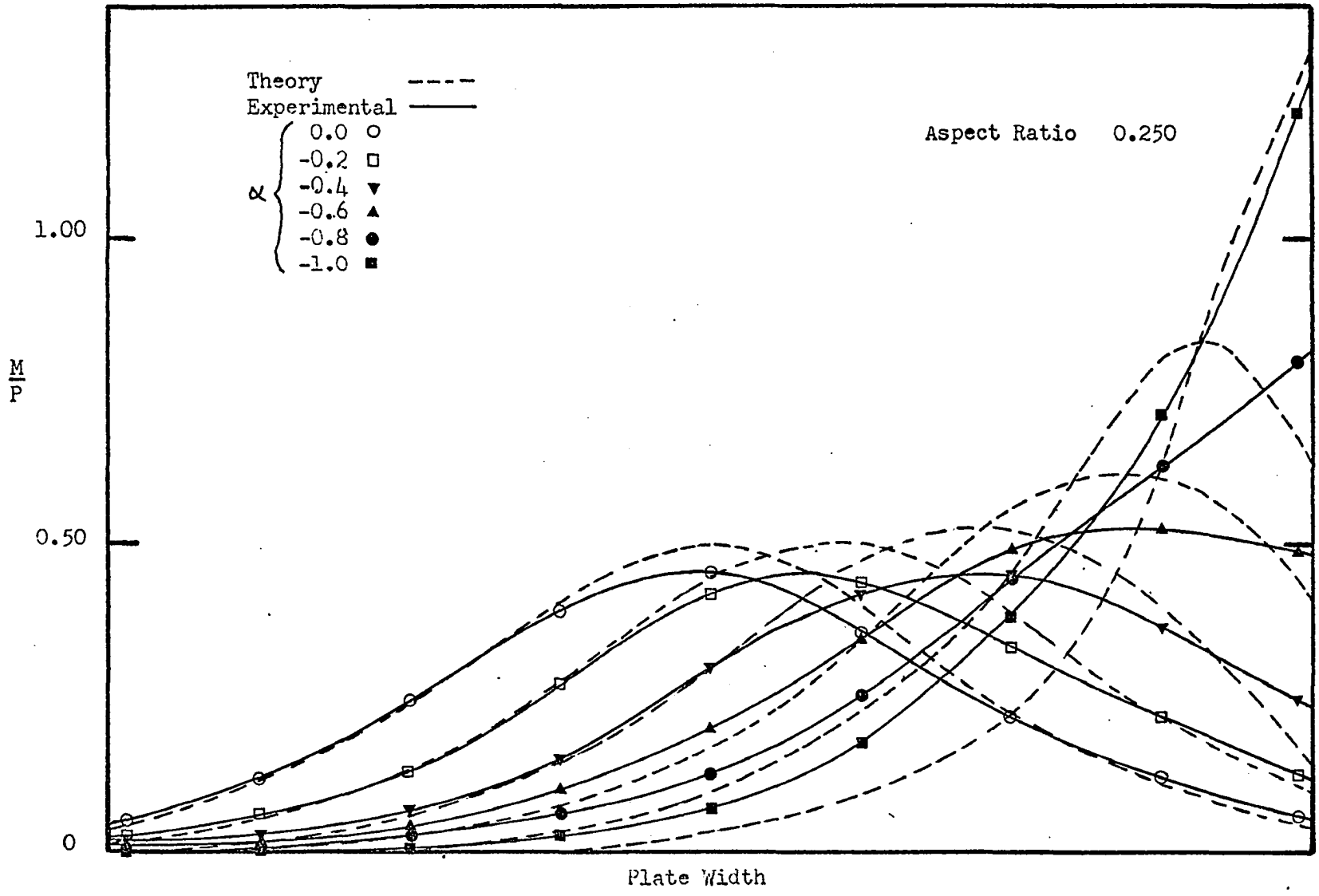

Fig. 43: Comparison of the Theoretical and Experimental Fixed Edge Bending Moments in a Tip Loaded Cantilever Plate (β,1.0)

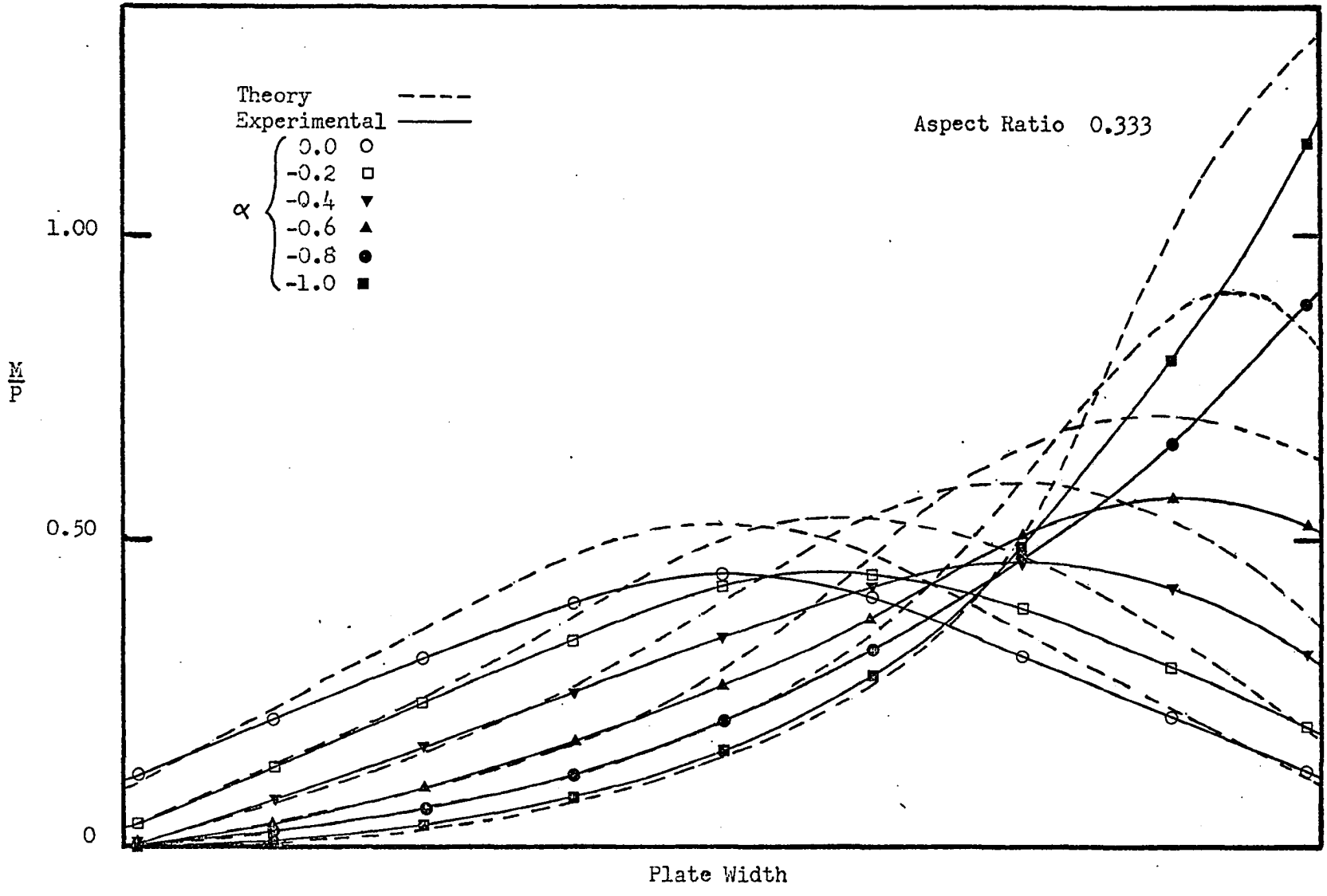

Fig. 44: Comparison of the Theoretical and Experimental Fixed Edge Bending Moments in a Tip Loaded Cantilever Plate (β,1.0)

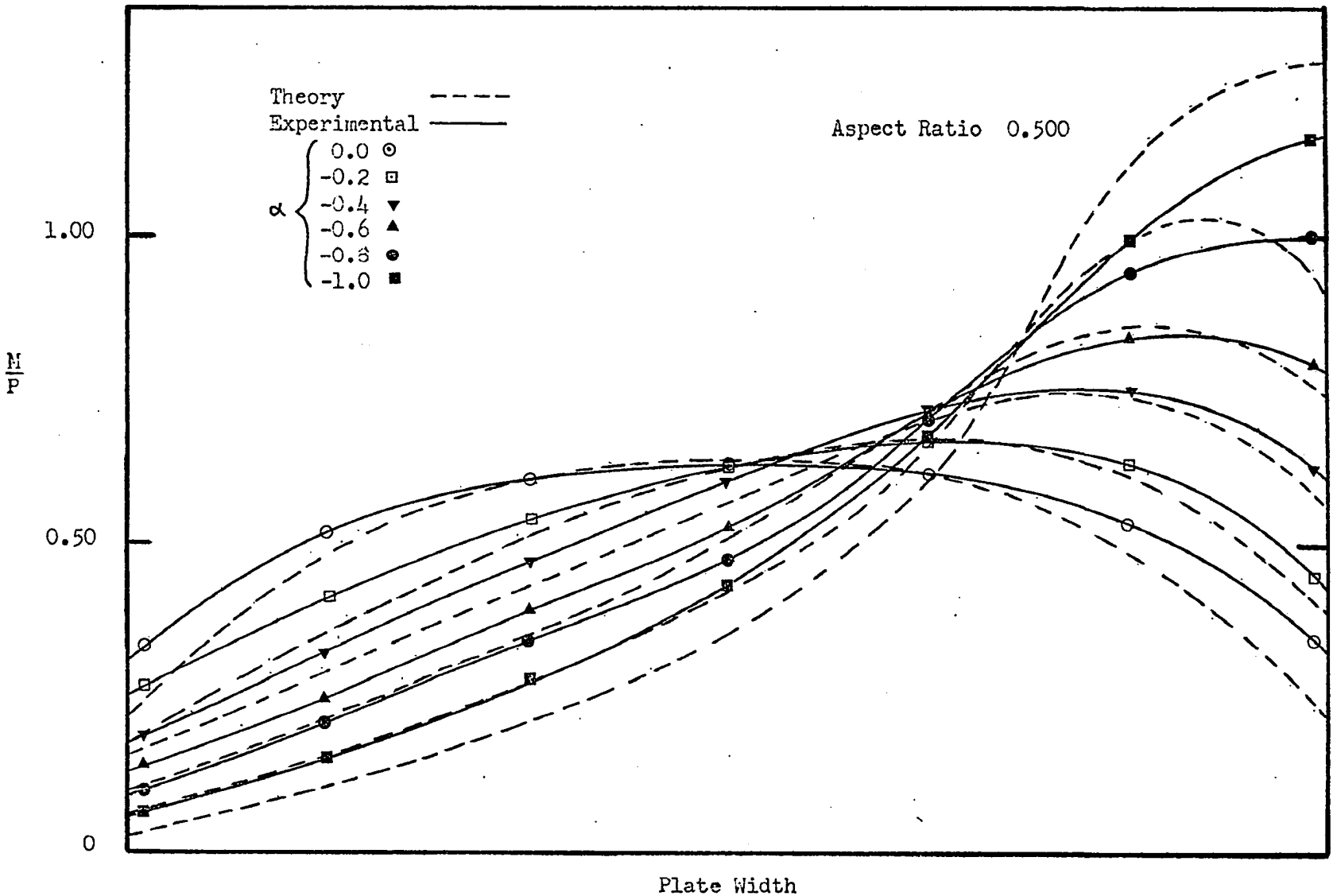

Fig. 45: Comparison of the Theoretical and Experimental Fixed Edge Bending Moments in a Tip Loaded Cantilever Plate (β,1.0)

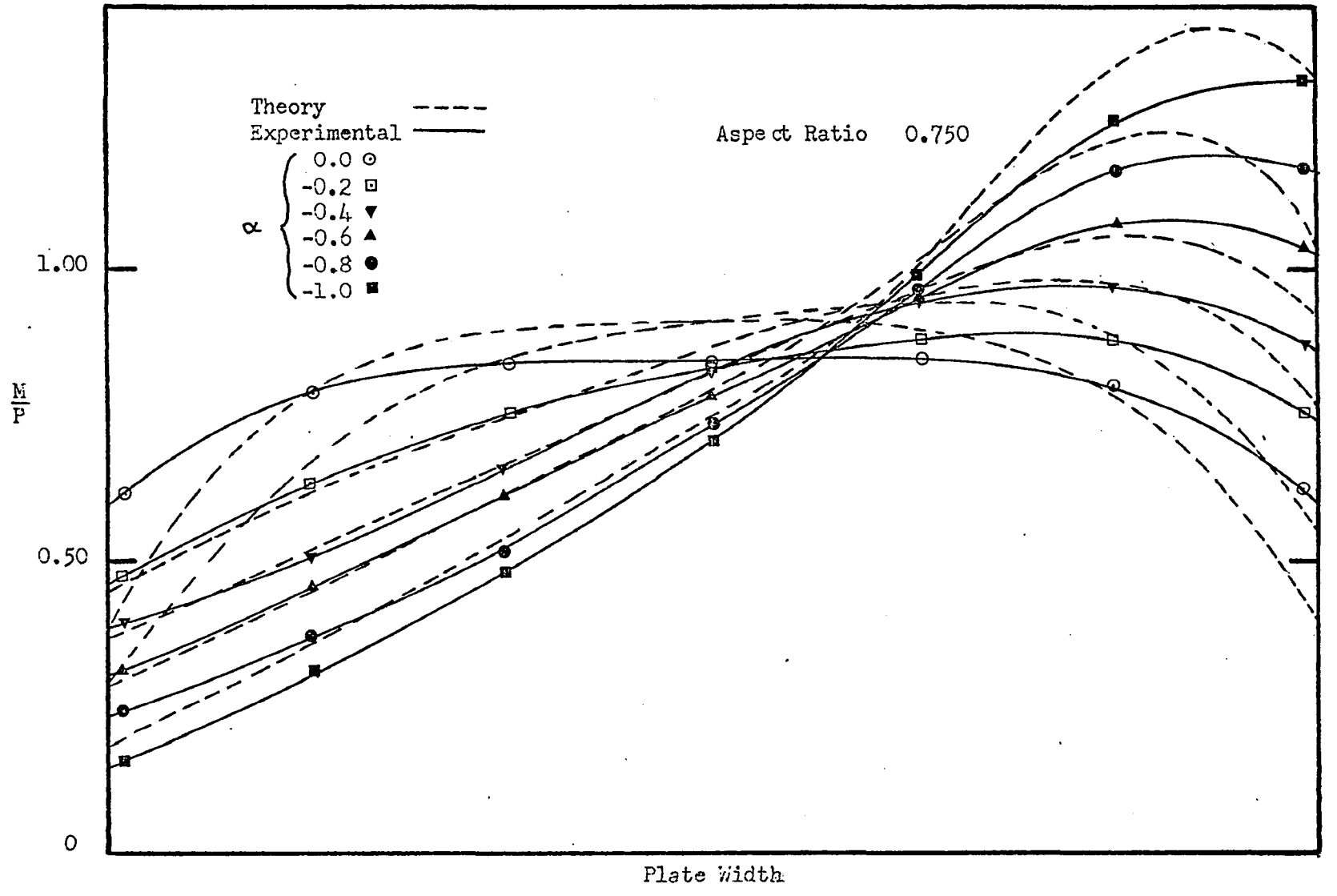

Fig. 46: Comparison of the Theoretical and Experimental Fixed Edge Bending Moments in a Tip Loaded Cantilever Plate (Þ,1.0)

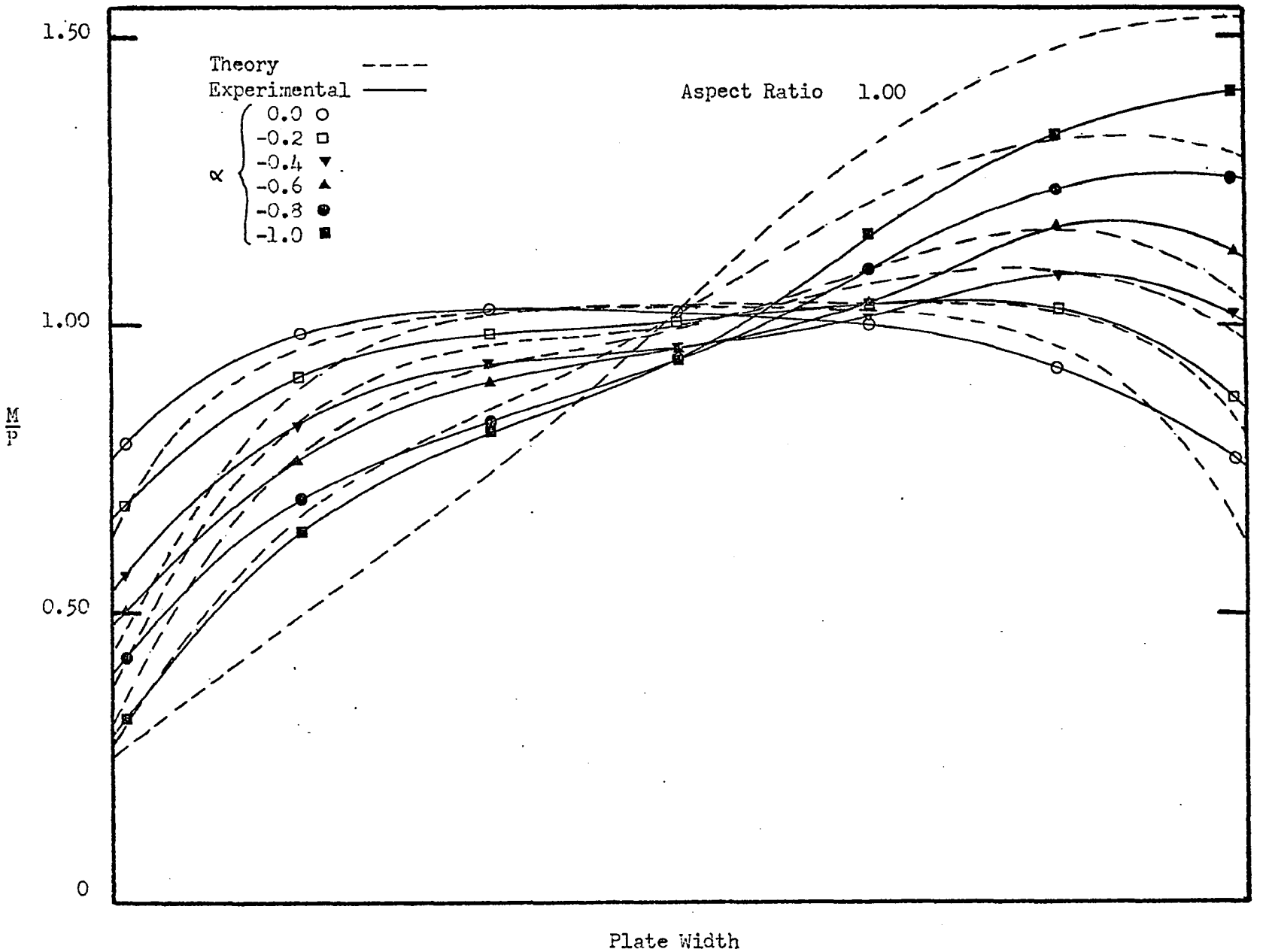

Fig. 47: Comparison of the Theoretical and Experimental Fixed Edge Bending Moments in a Tip Loaded Cantilever Plate (β,1.0)

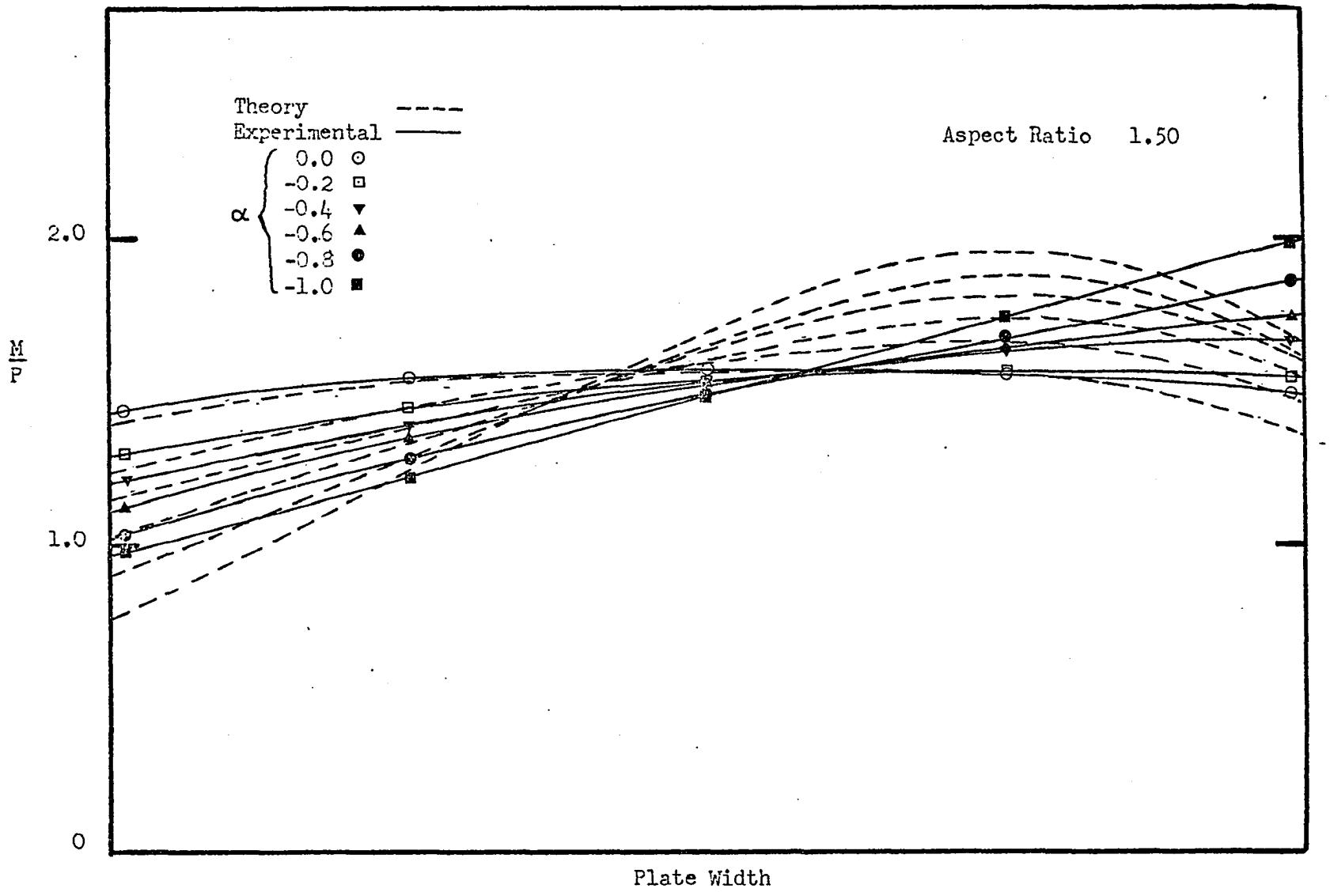

Fig. 48: Comparison of the Theoretical and Experimental Fixed Edge Bending Moments in a Tip Loaded Cantilever Plate (β,1.0)

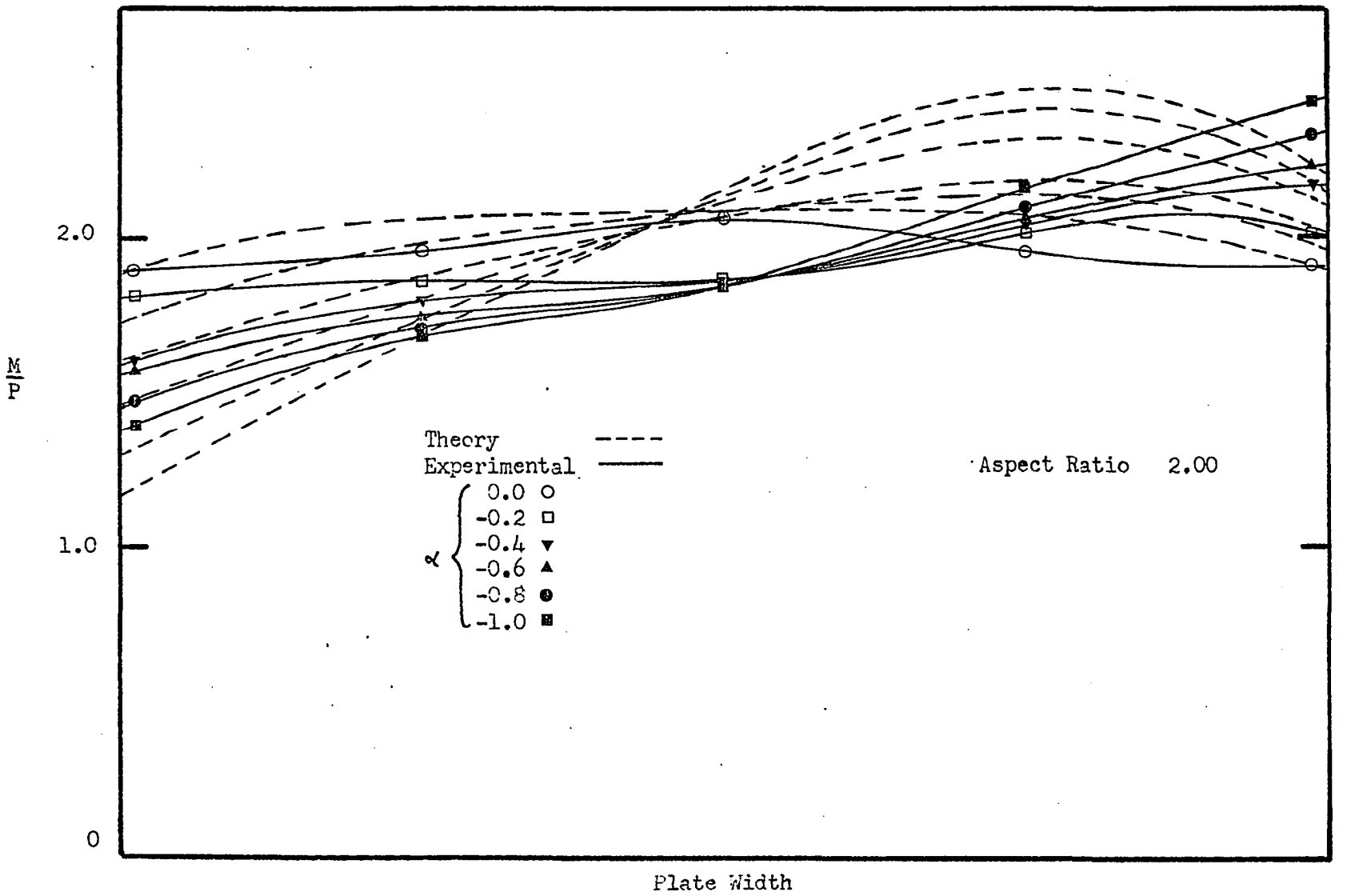

Fig. 49: Comparison of the Theoretical and Experimental Fixed Edge Bending Moments in a Tip Loaded Cantilever Plate (β,1.0)

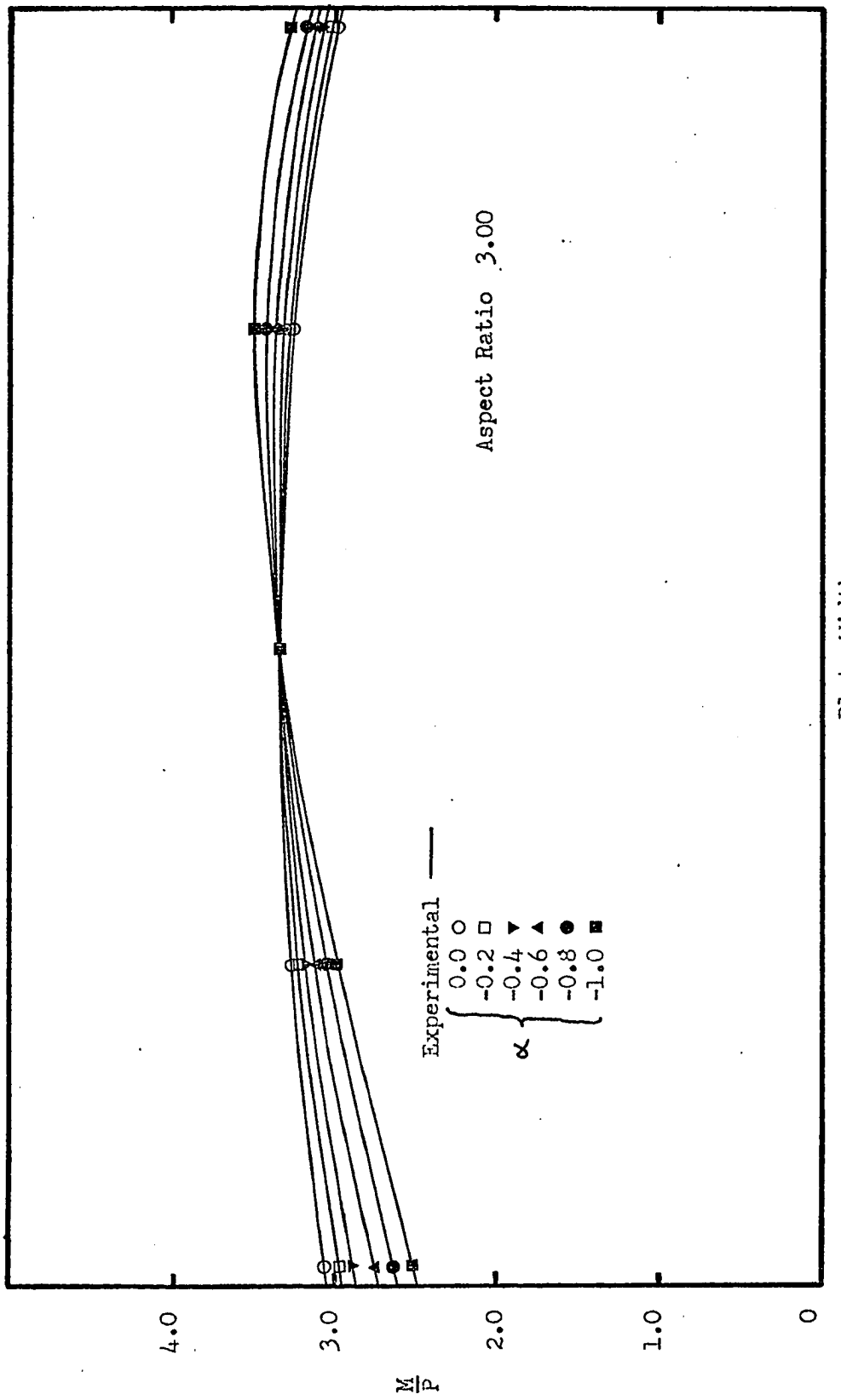

Fig. 50: Comparison of the Fixed Edge Bending Moments in a Tip Loaded Cantilever Plate (β,-1.0)

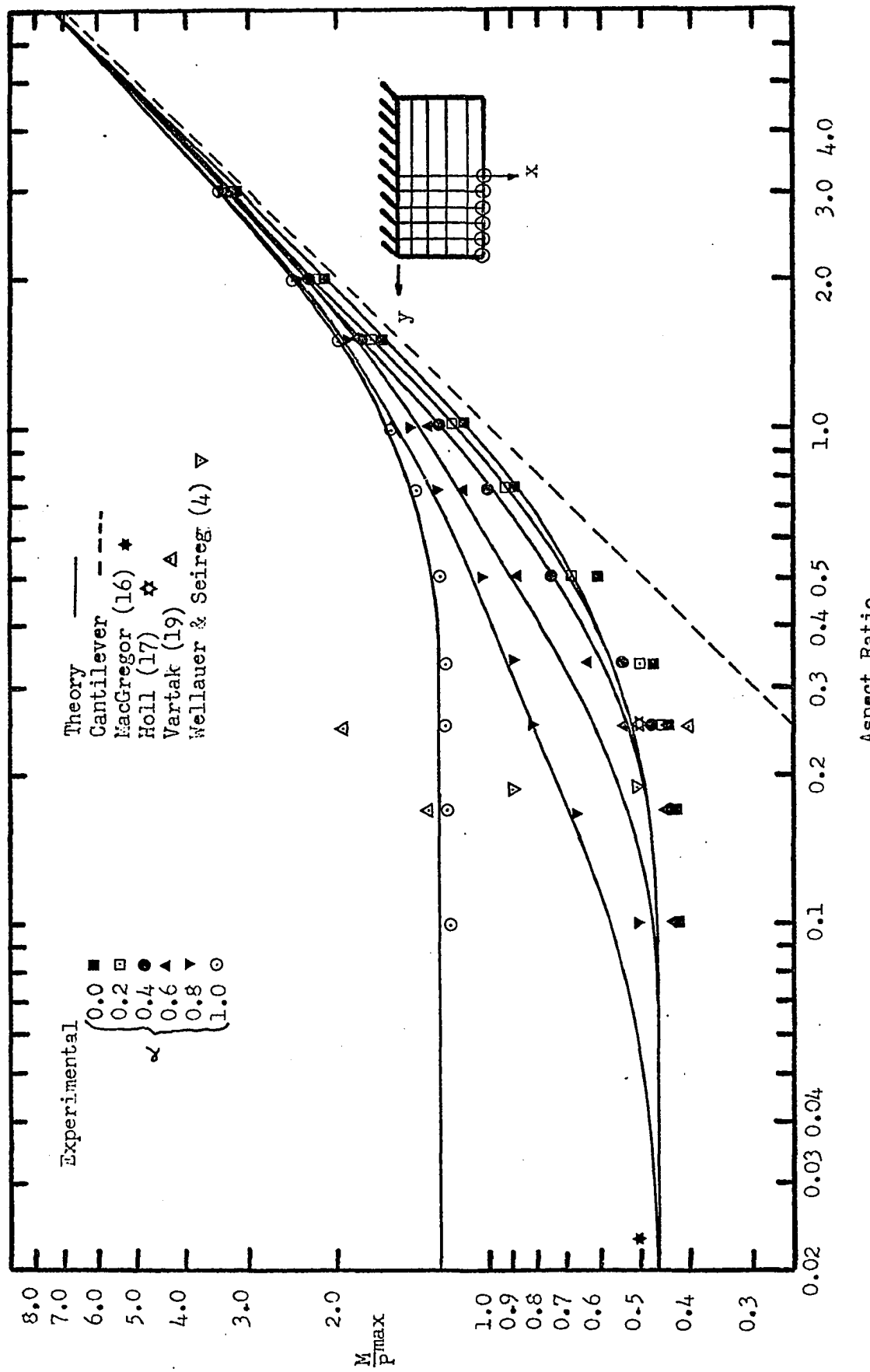

Fig. 51: Maximum Bending Moments vs Aspect Ratio, For Point Loading at β ,1.0; and Various Values of α

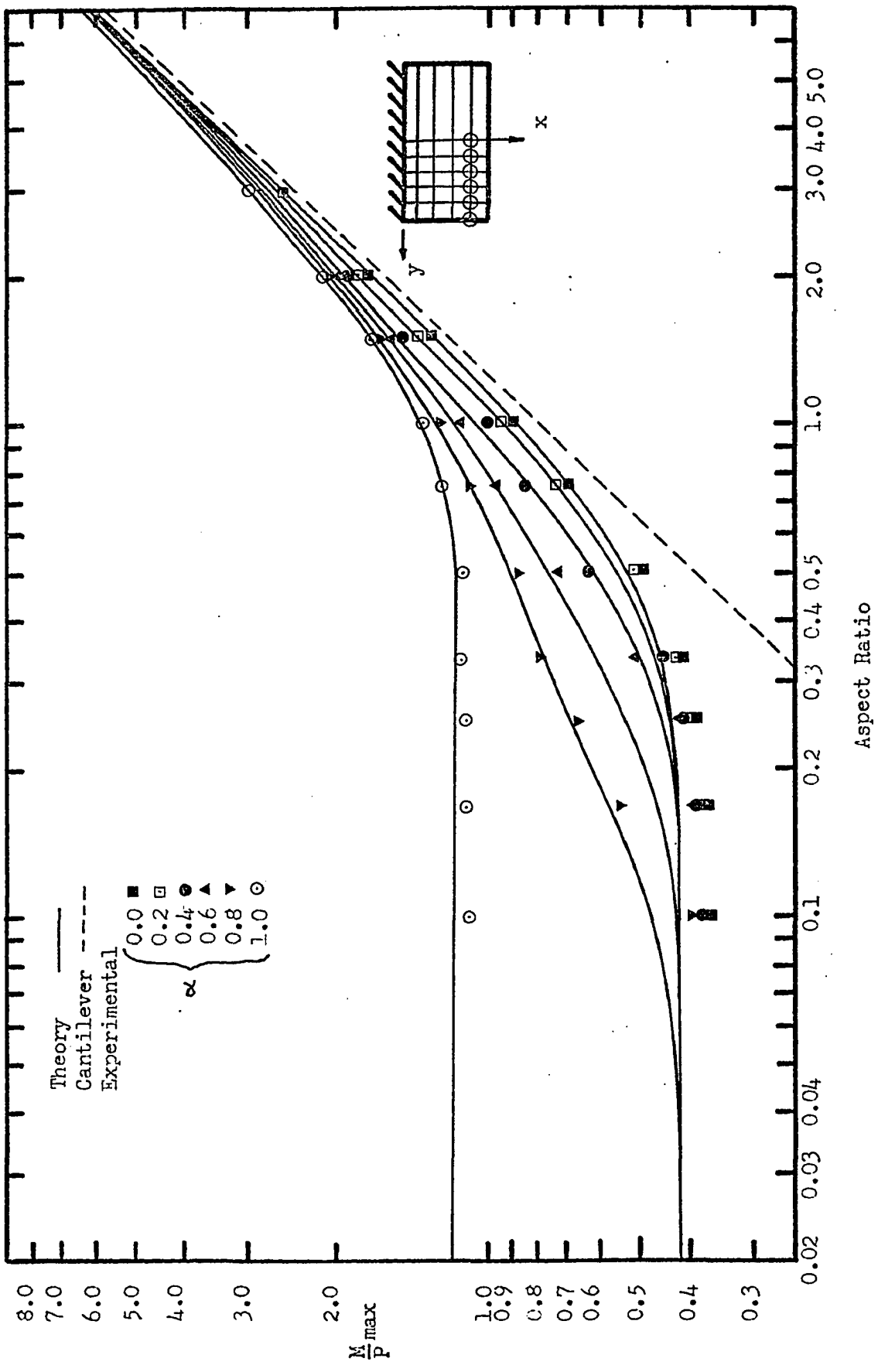

Fig. 52: Maximum Bending Moments vs Aspect Ratio, For Point Loading at β ,0.8; and Various Values of α

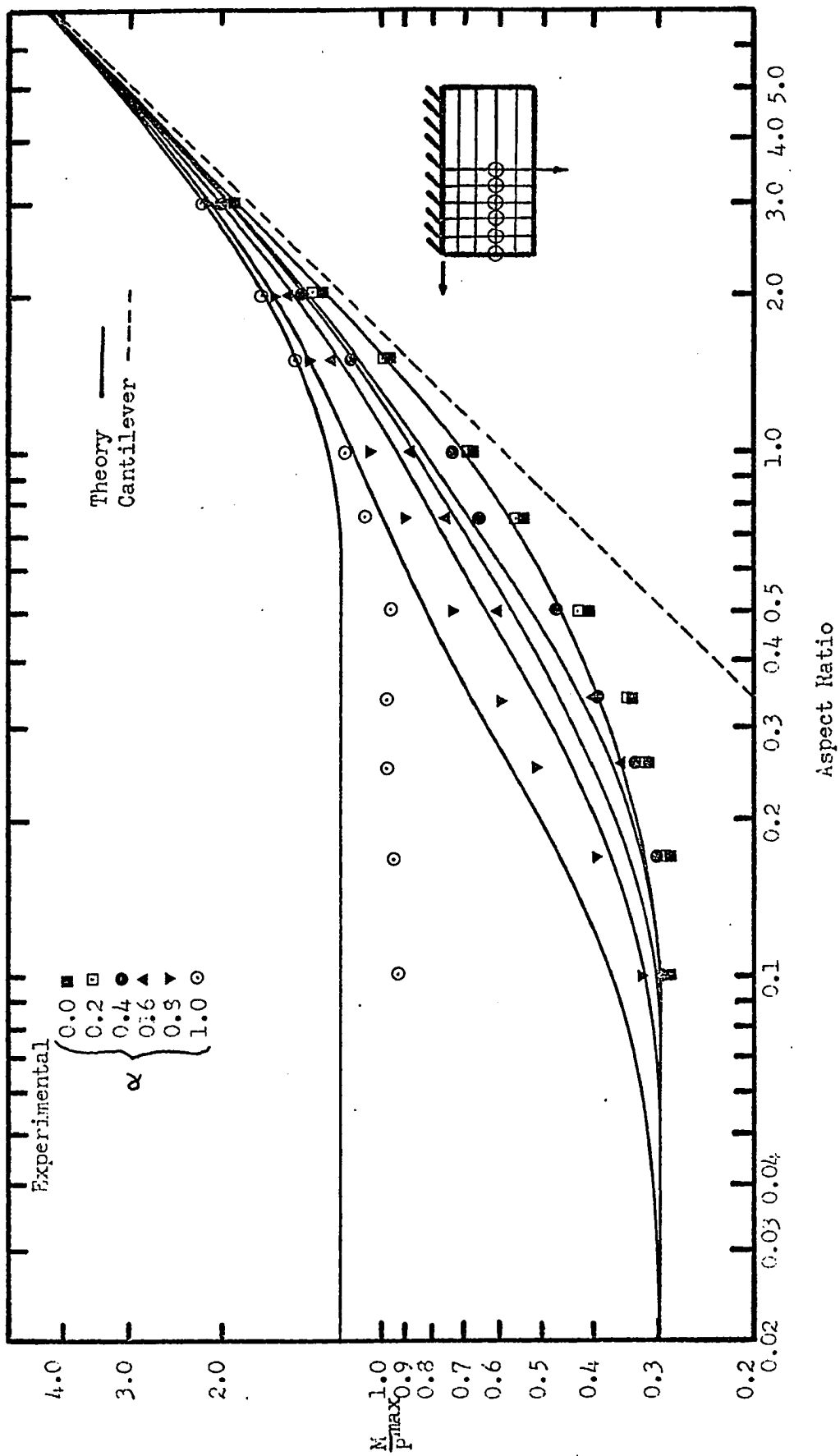

Fig. 53: Maximum Bending Moments vs Aspect Ratio, For Point Loading at β,0.6; and Various Values of α

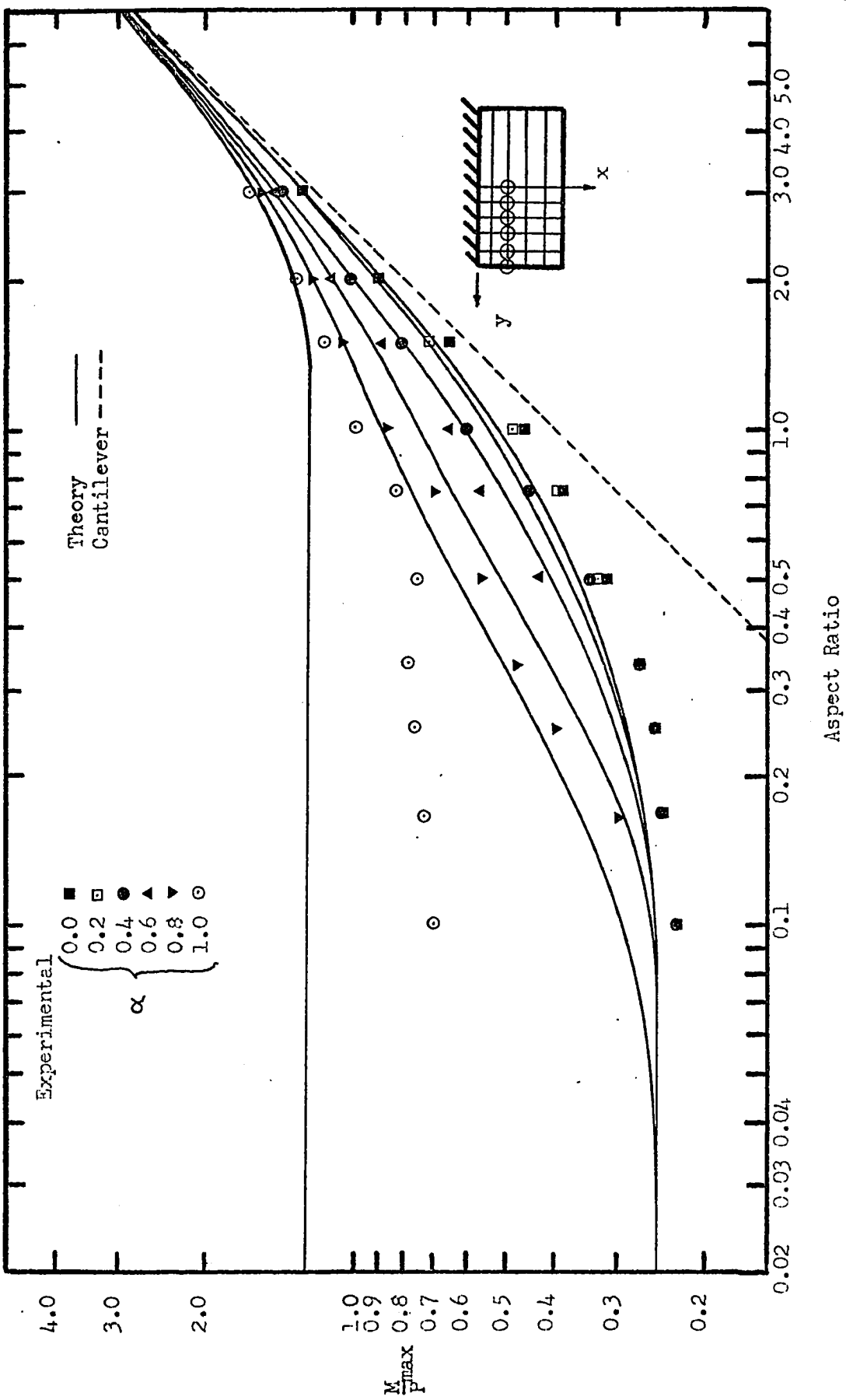

Fig. 54: Maximum Bending Moments vs Aspect Ratio, For Point Loading at β,0.4; and Various Values of α

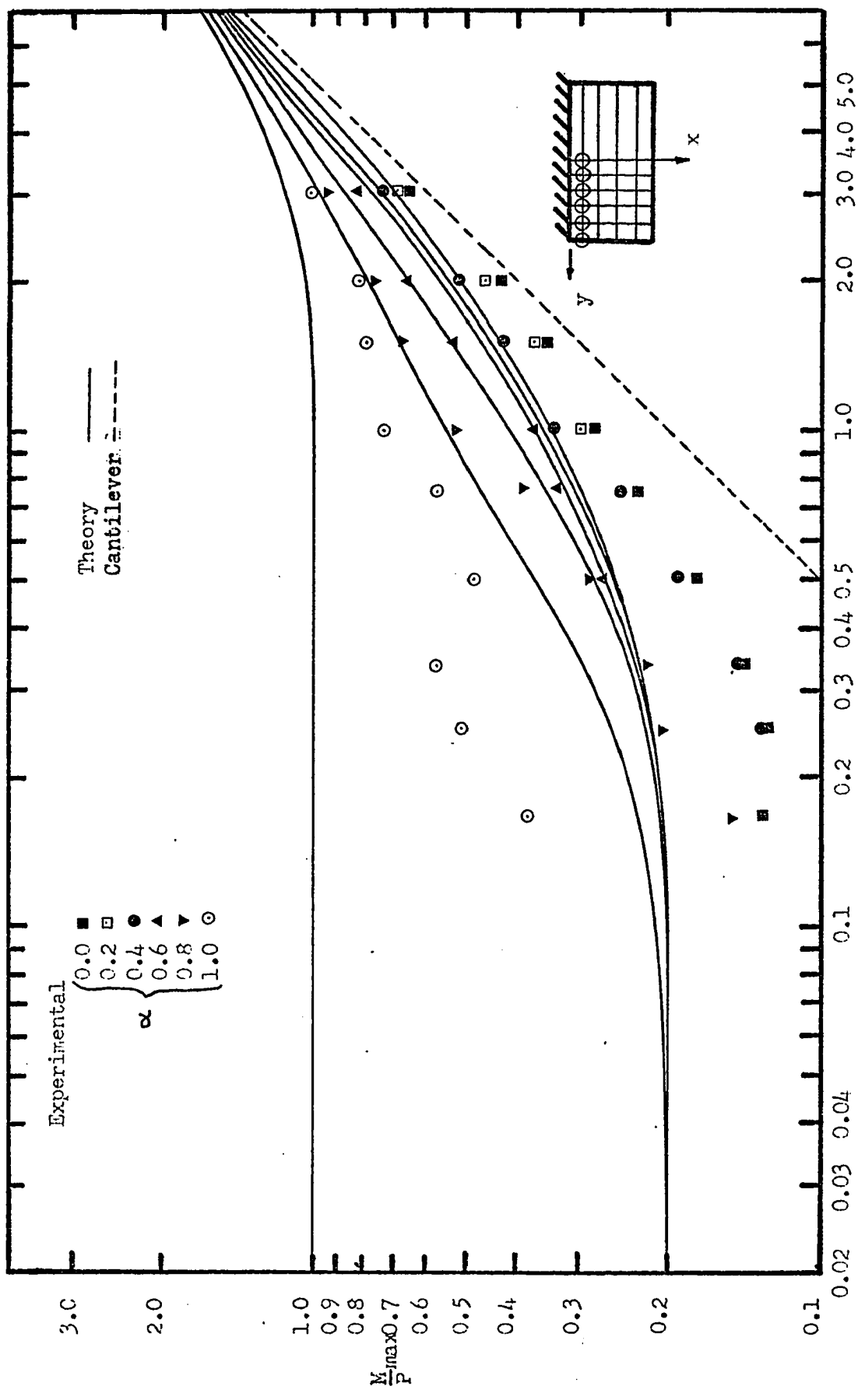

Fig. 55: Maximum Bending Moments vs Aspect Ratio, For Point Loading at β ,0.2; and Various Values of α

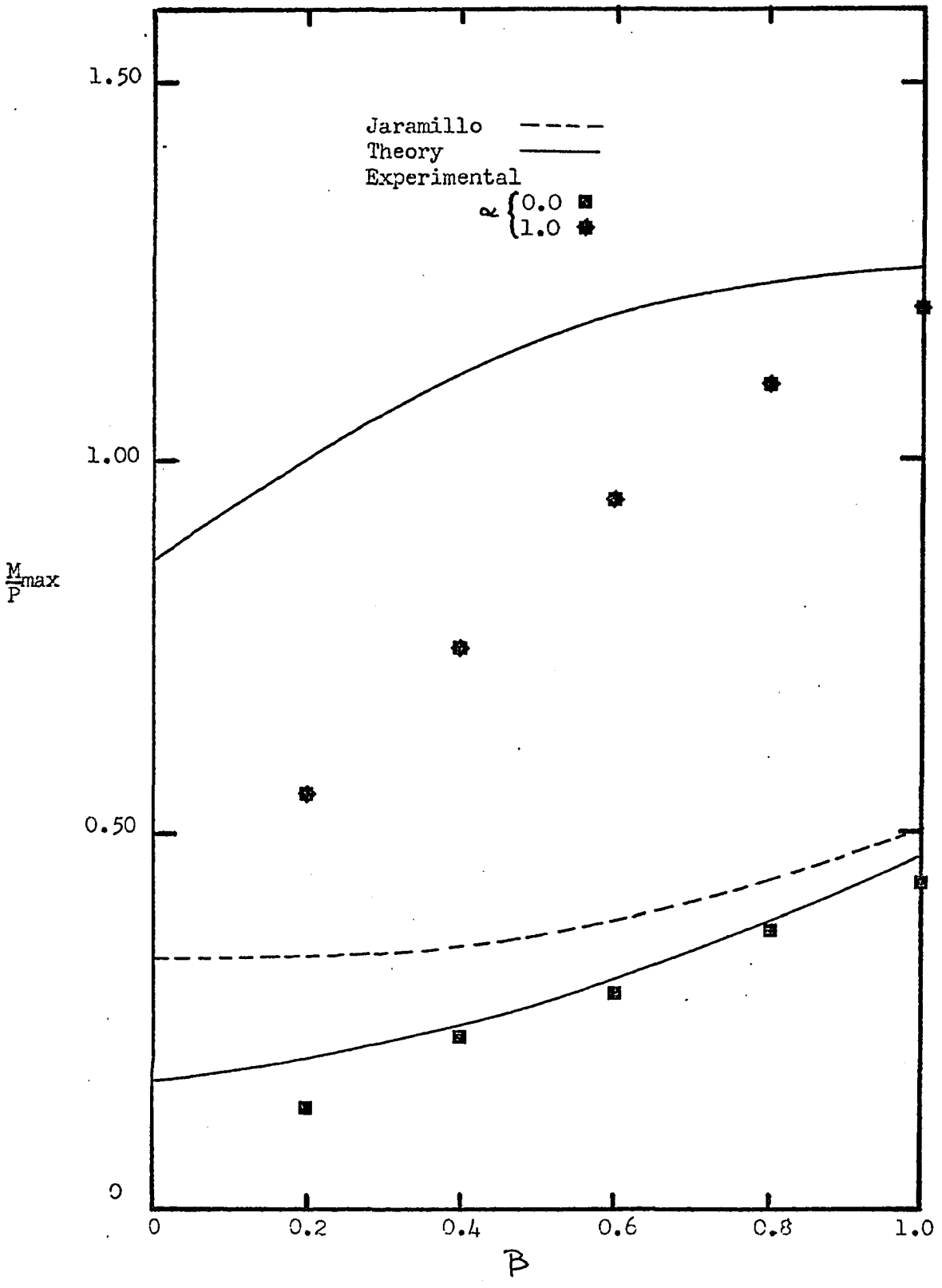

Fig. 56: Maximum Bending Moment in a Plate With Low Aspect Ratio ($\leqslant 0.25$) As a Function of Load Position

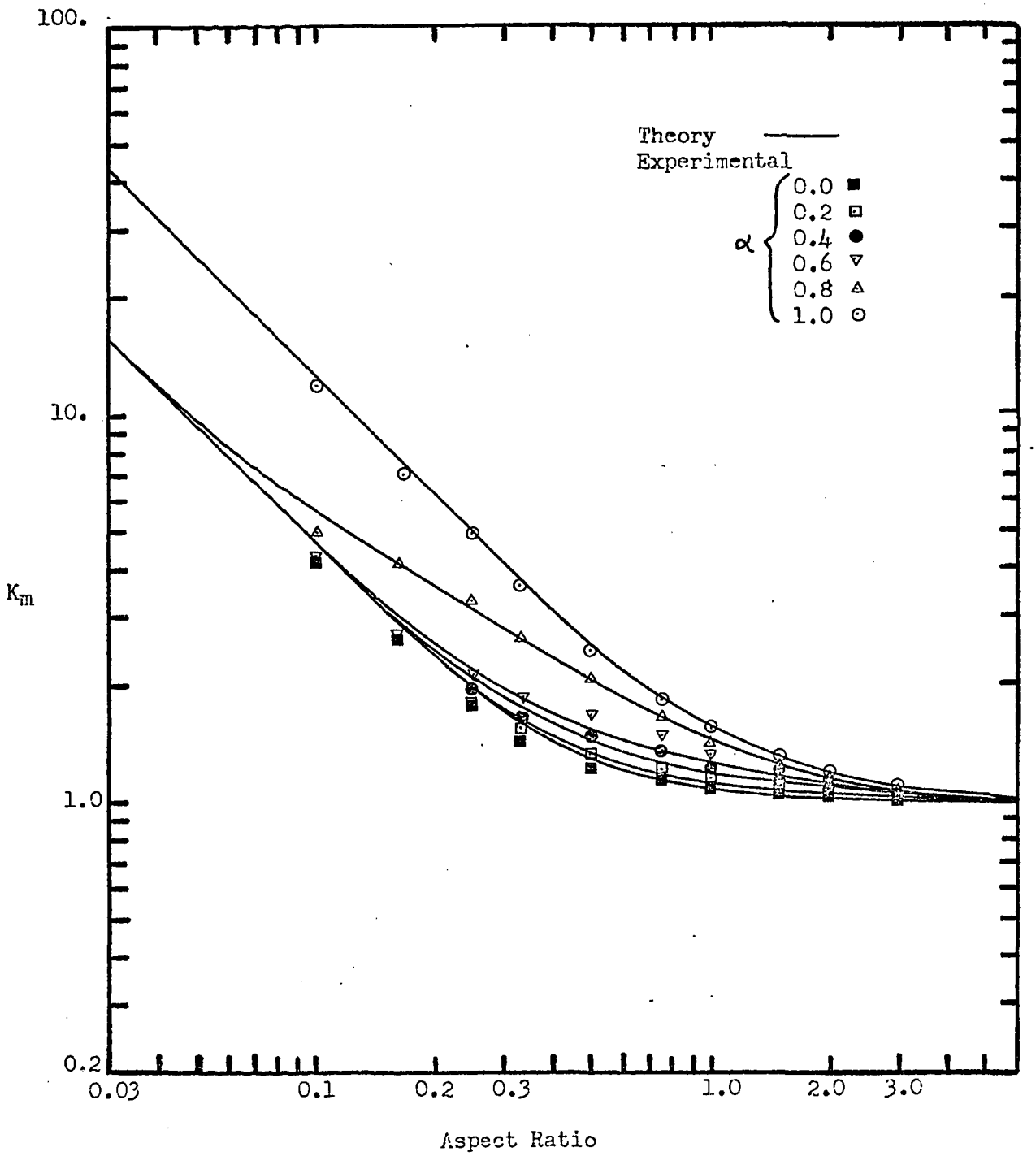

Fig. 57: Moment Distribution Factor, K_m as a Function of Aspect Ratio, For Cantilever Plates Point Loaded at β,1.0

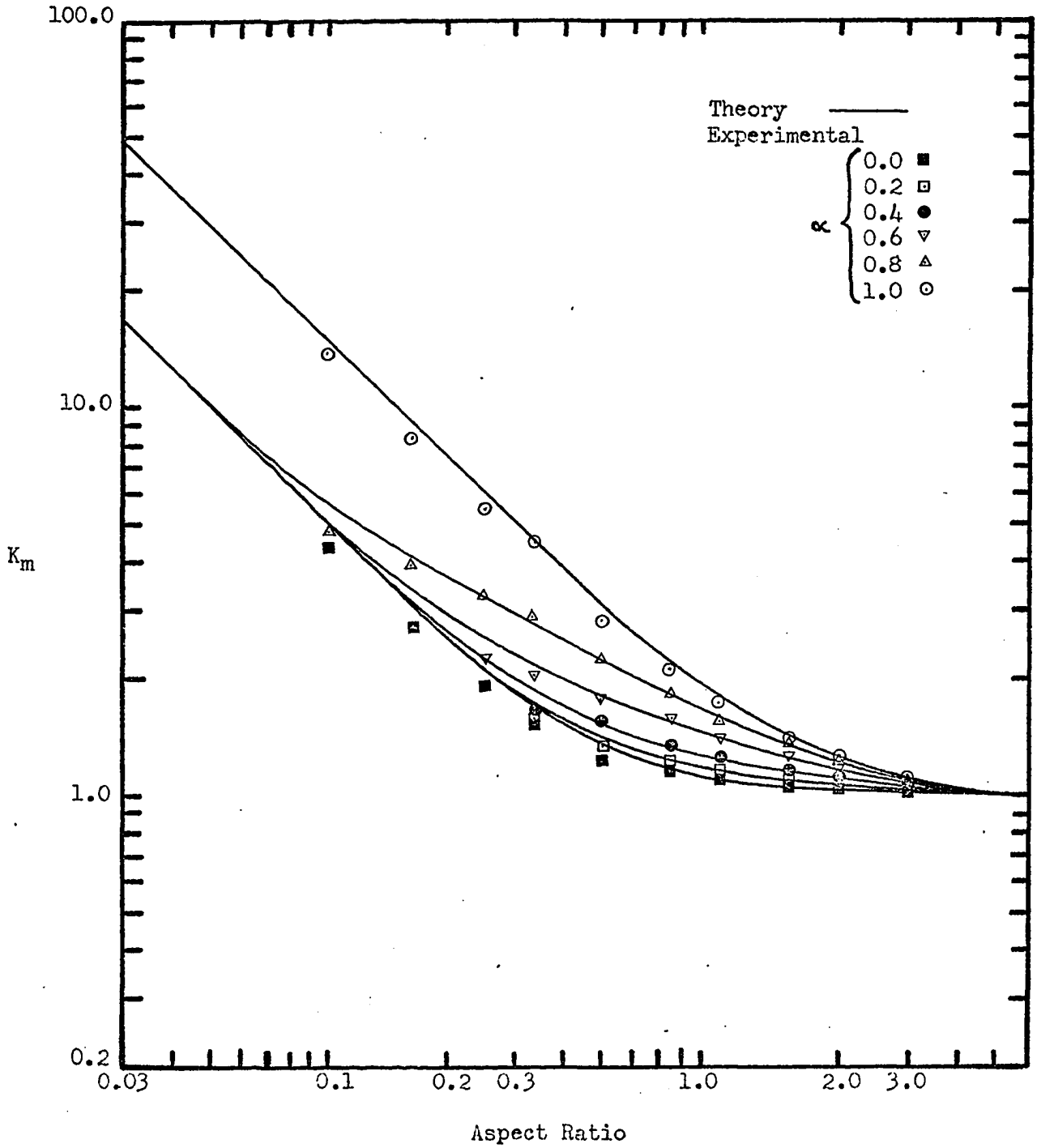

Fig. 58: Moment Distribution Factor, K_m as a Function of Aspect Ratio, For Cantilever Plates Point Loaded at β, 0.8

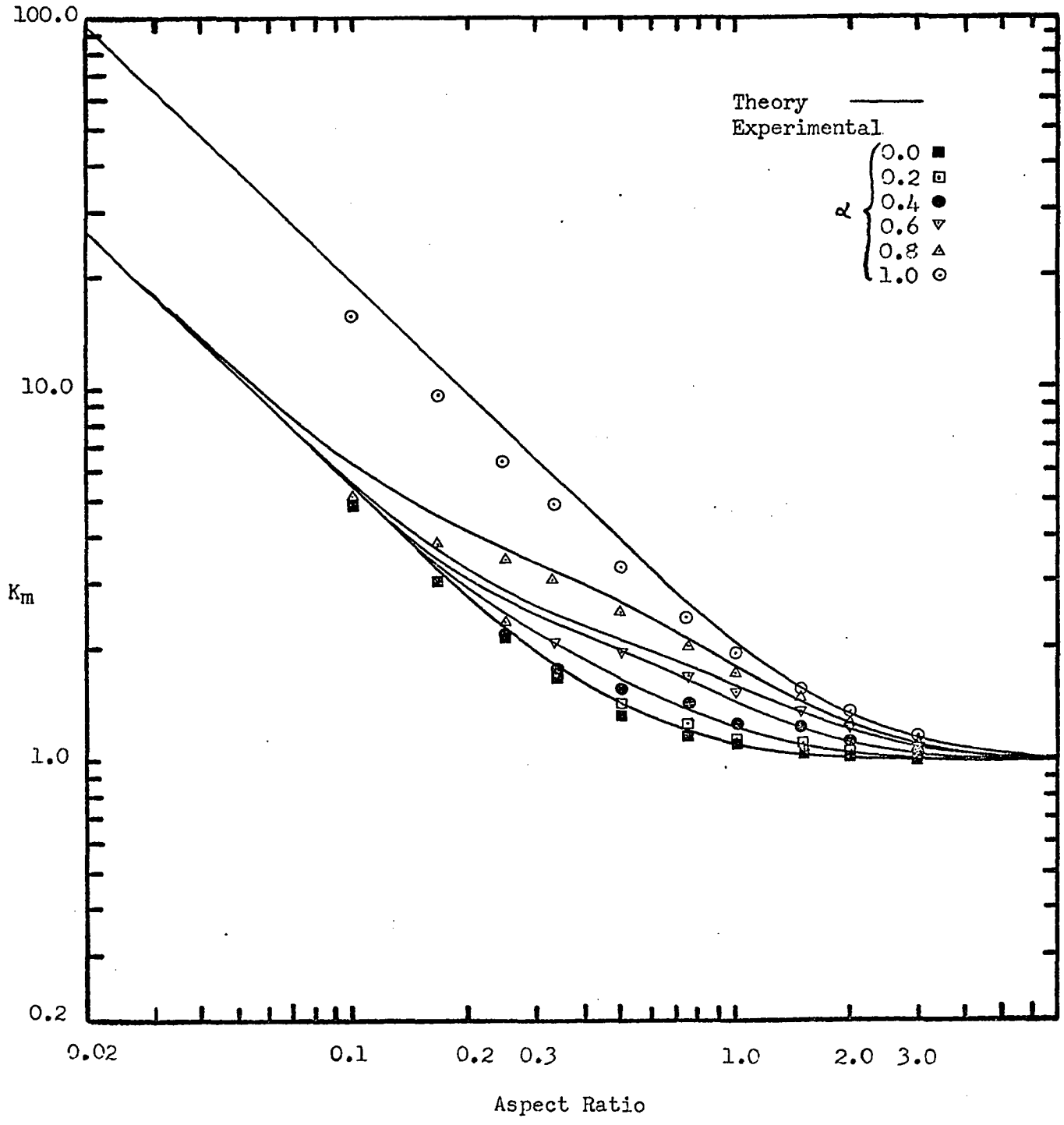

Fig. 59: Moment Distribution Factor, K_m as a Function of Aspect Ratio, For Cantilever Plates Point Loaded at β ,0.6

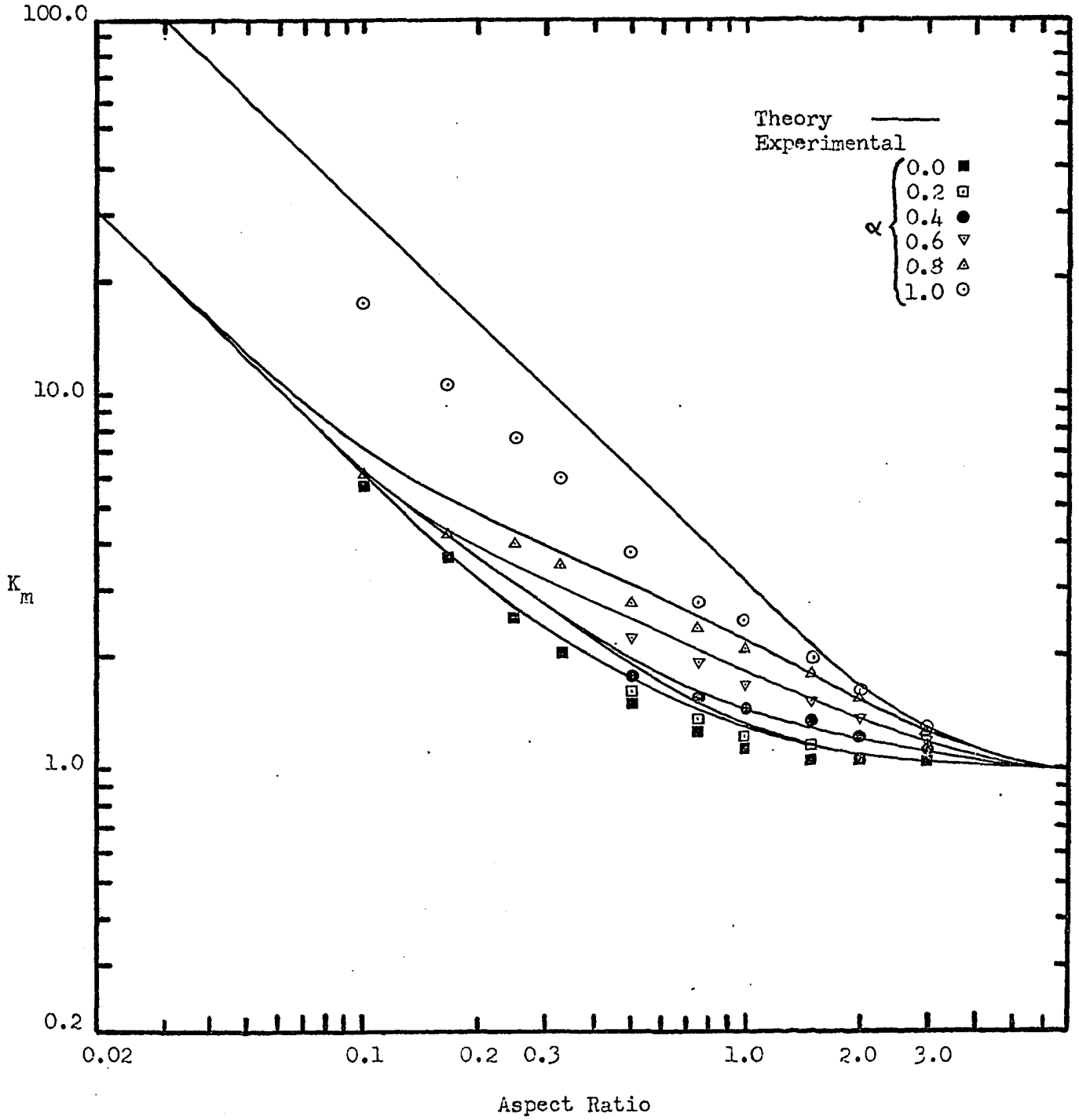

Fig. 60: Moment Distribution Factor, K_m as a Function of Aspect Ratio For Cantilever Plates Point Loaded at β, 0.4

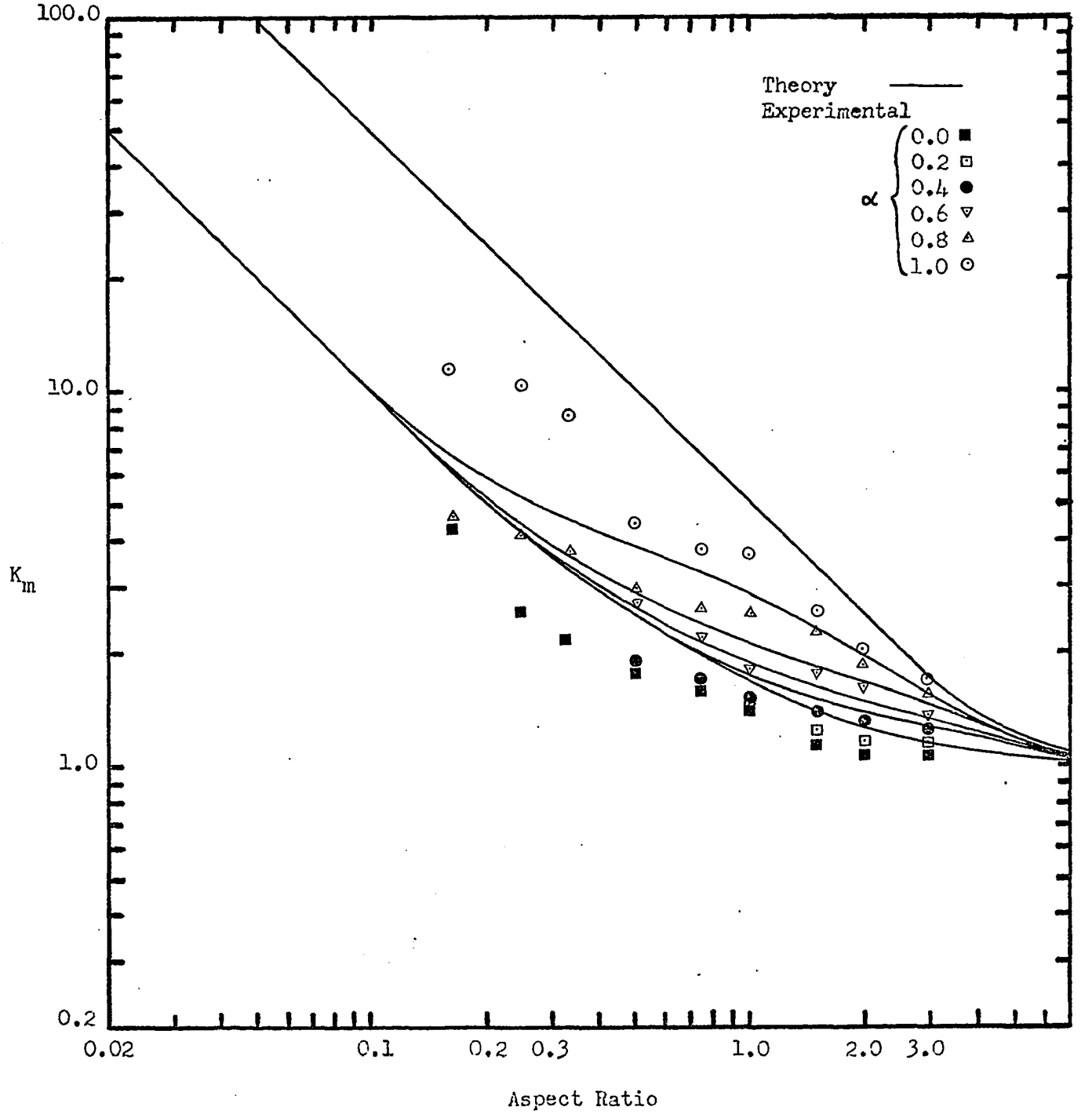

Fig. 61: Moment Distribution Factor, K_m as a Function of Aspect Ratio For Cantilever Plates Point Loaded at β ,0.2

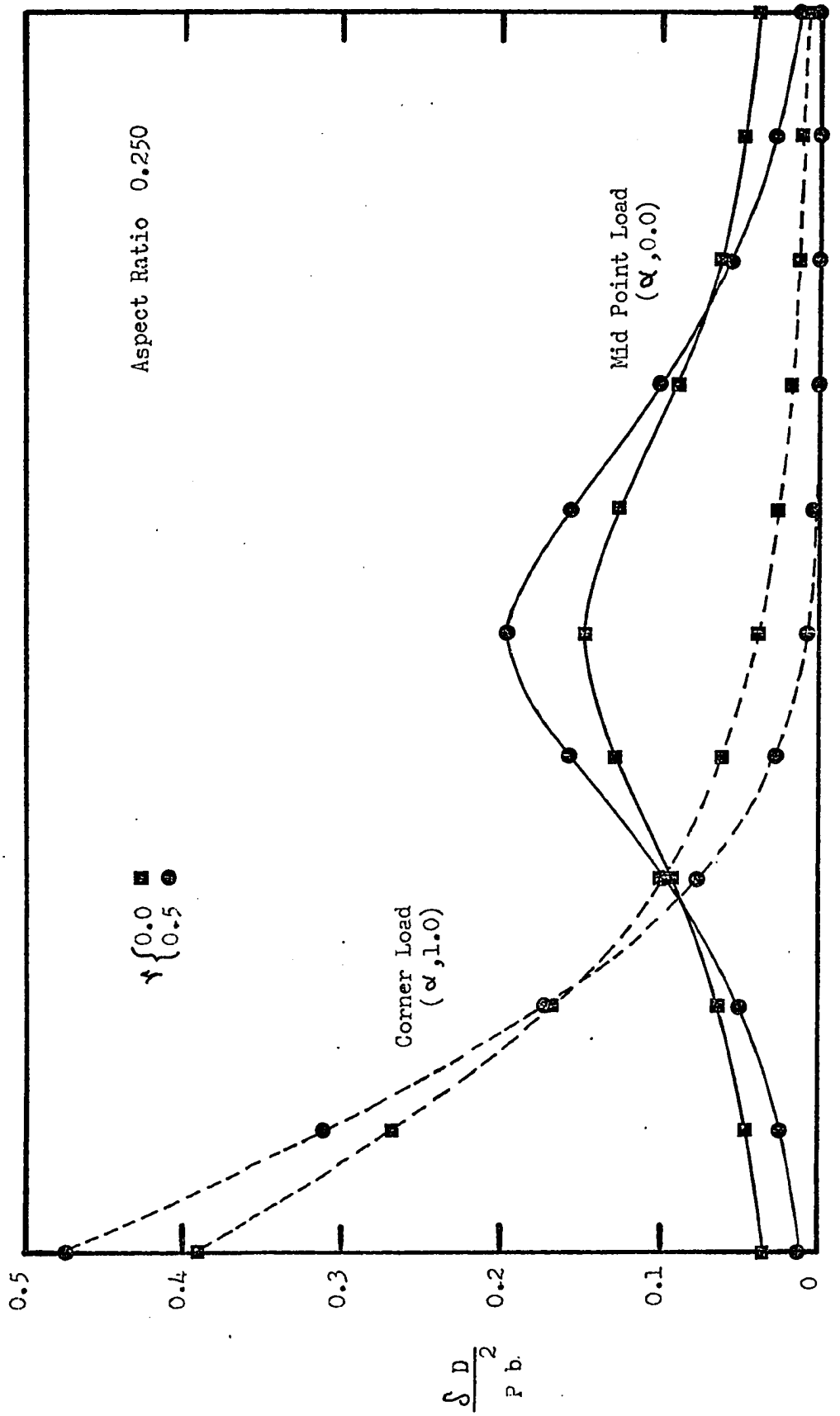

Fig. 62: Theoretical Effect of Poissons Ratio (ν) on Free Edge Deflections (β,1.0)

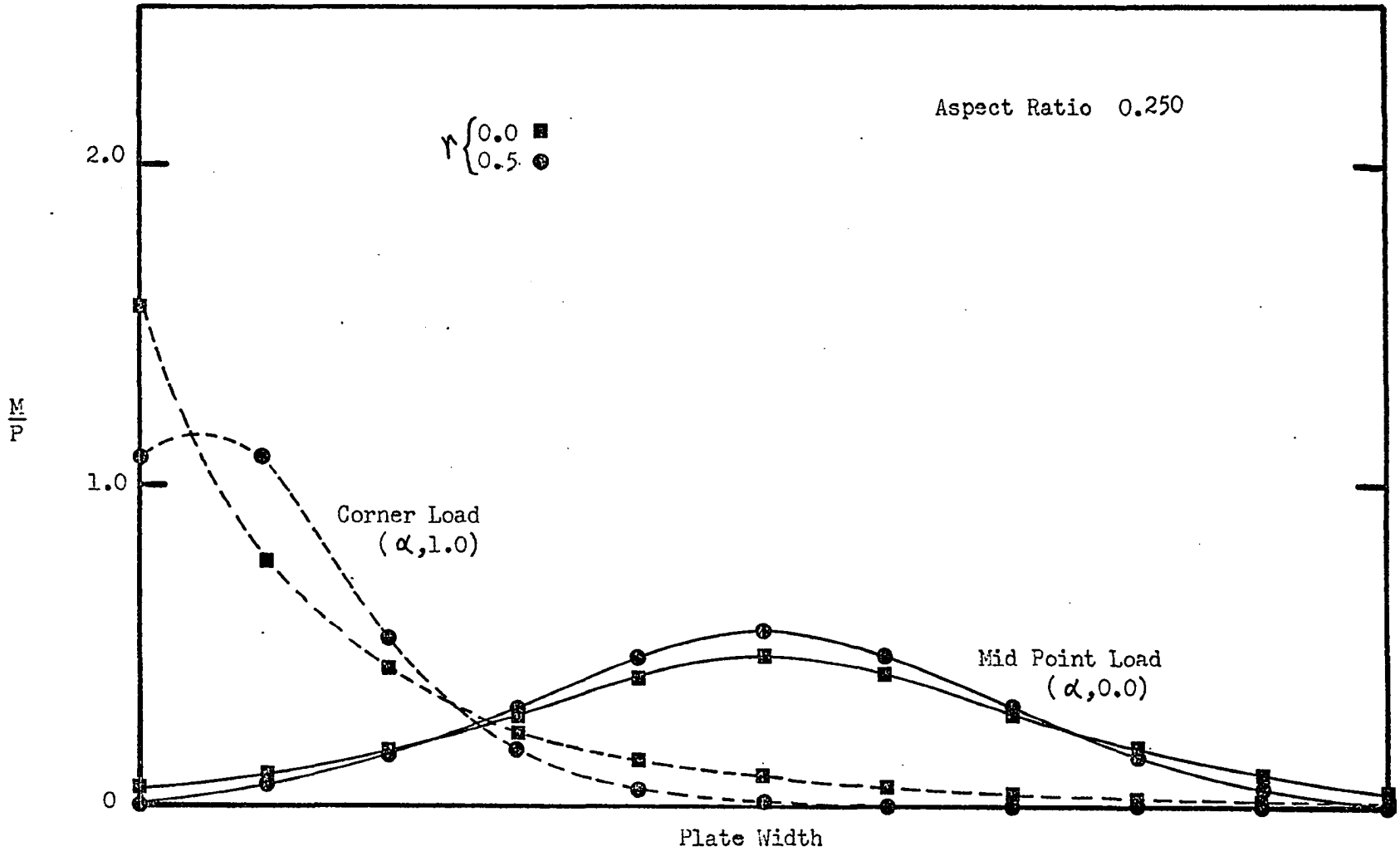

Fig. 63: Theoretical Effect of Poissons Ratio (γ) on Fixed Edge Bending Moments (β,1.0)

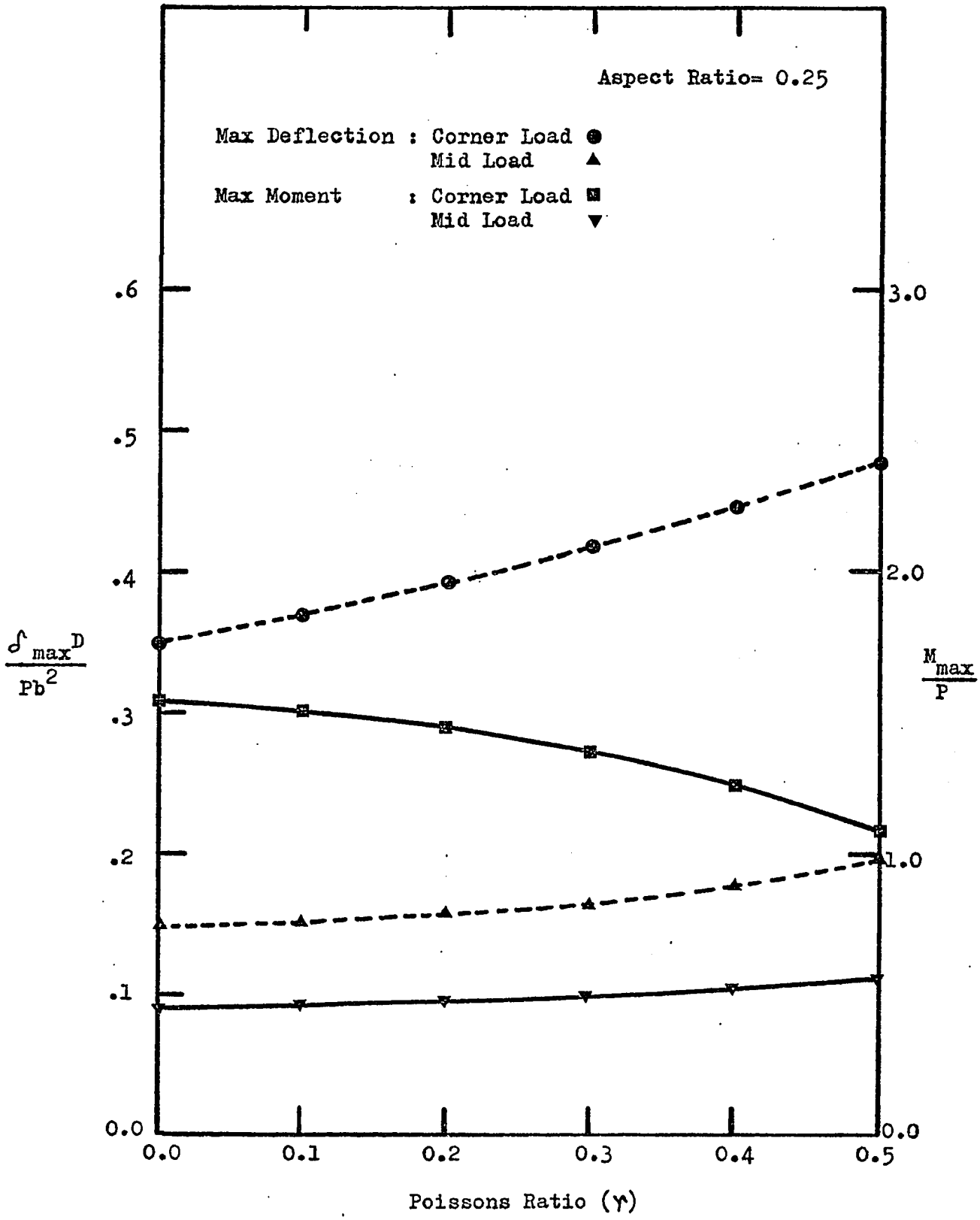

Fig. 64 : Effect of Poissons Ratio on Maximum Deflections and Moments , with Free Edge Loading

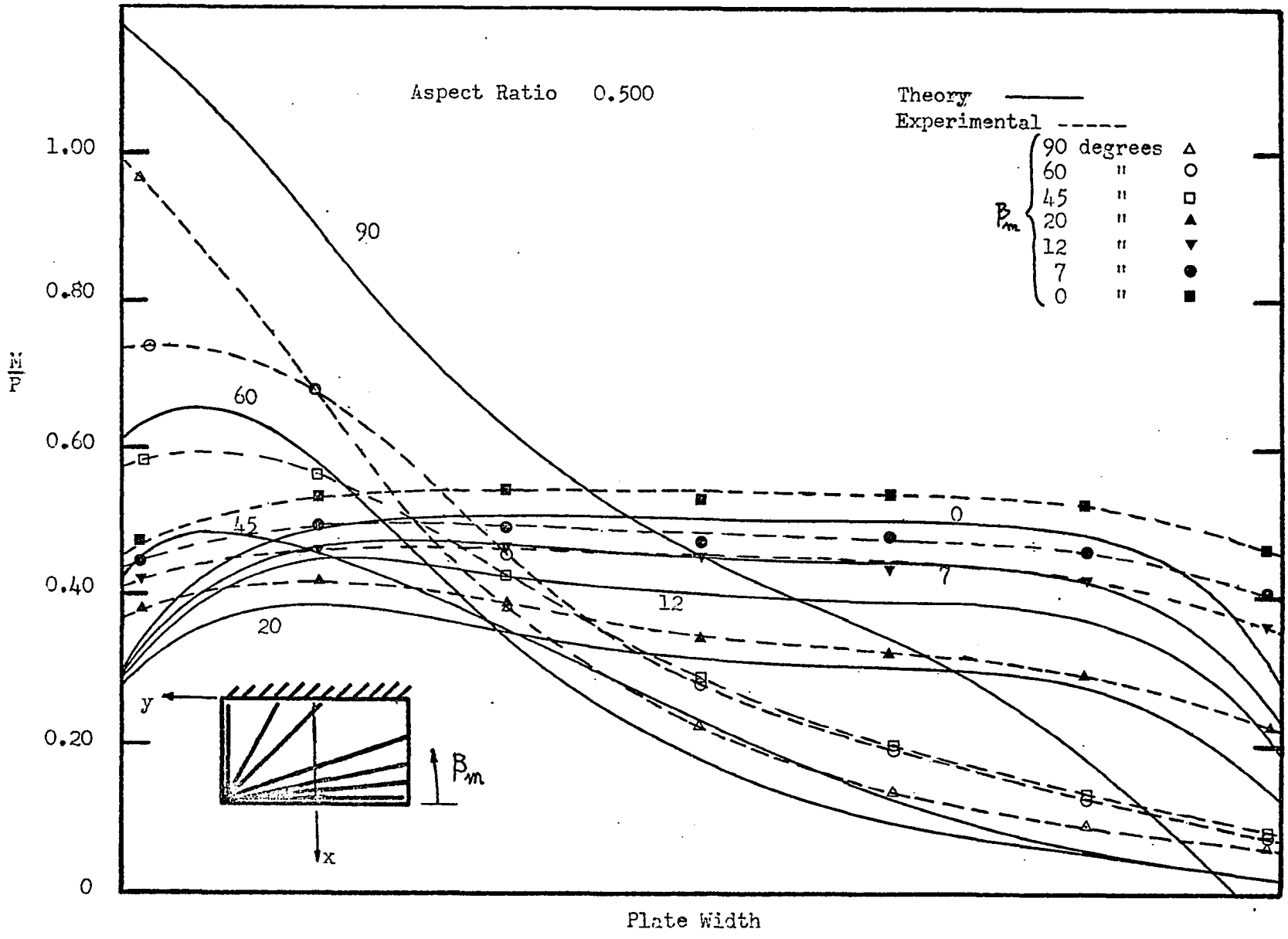

Fig. 65: Theoretical and Experimental Fixed Edge Bending Moments in a Cantilever Plate, Under Line Loadings at Various Angles Passing Through a Free Corner (η ,1.0)

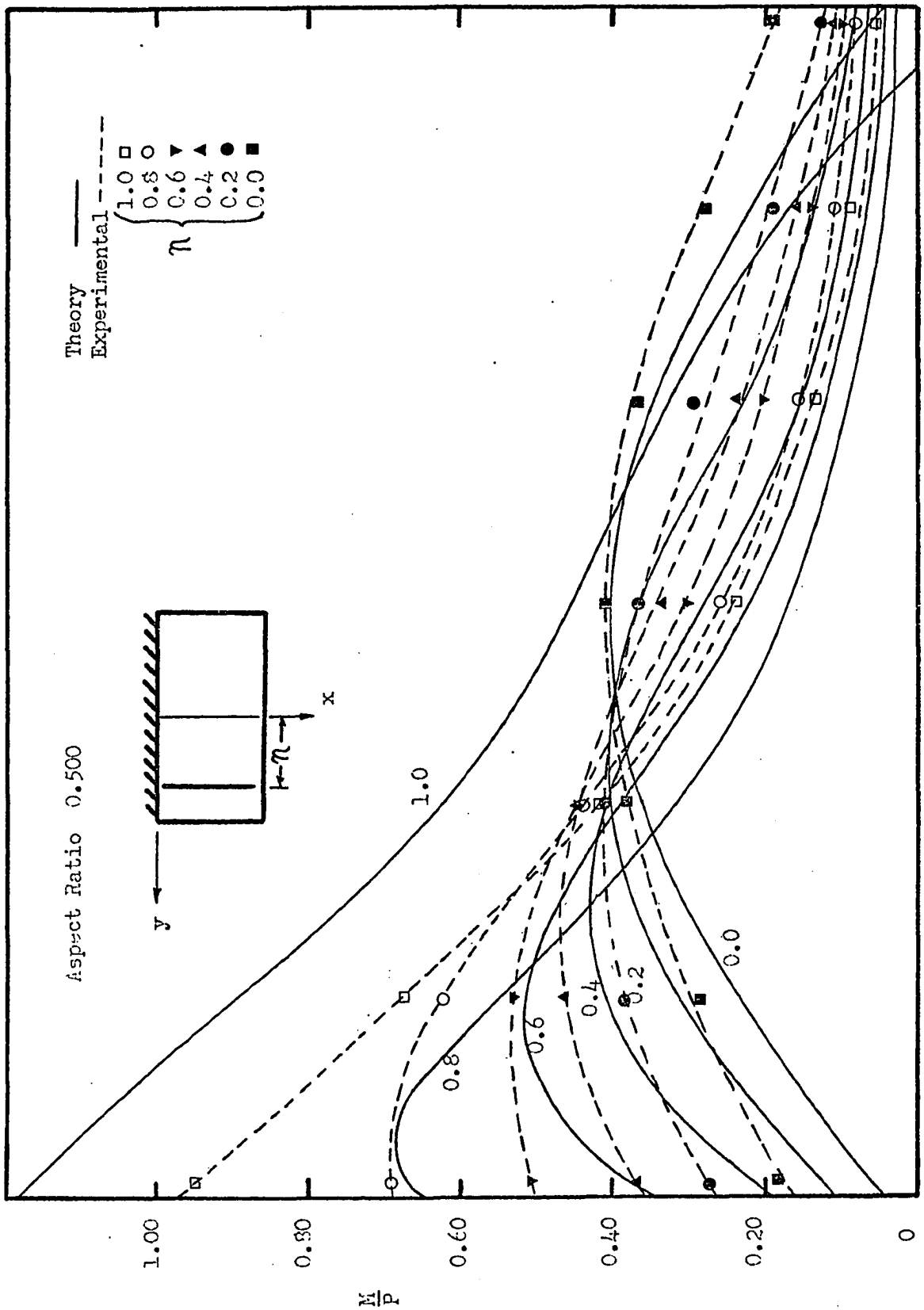

Fig. 66: Theoretical and Experimental Fixed Edge Bending Moments in a Cantilever Plate, Under Line Loadings With β_m 90 Degrees, at Various Positions Along the Plate Width (η)

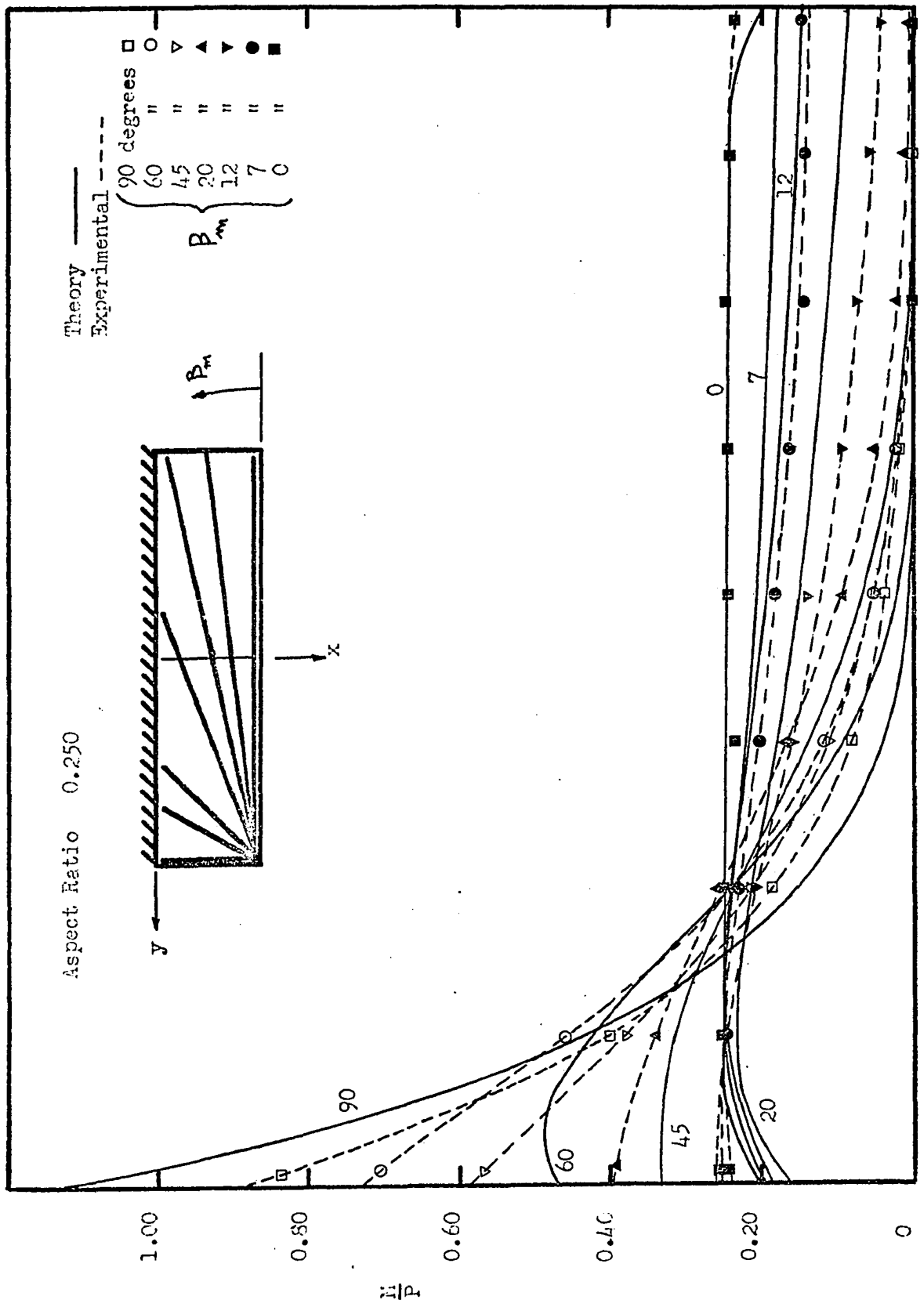

Fig. 67: Theoretical and Experimental Fixed Edge Bending Moments in a Cantilever Plate, Under Line Loadings at Various Angles Passing Through a Free Corner (η,1.0)

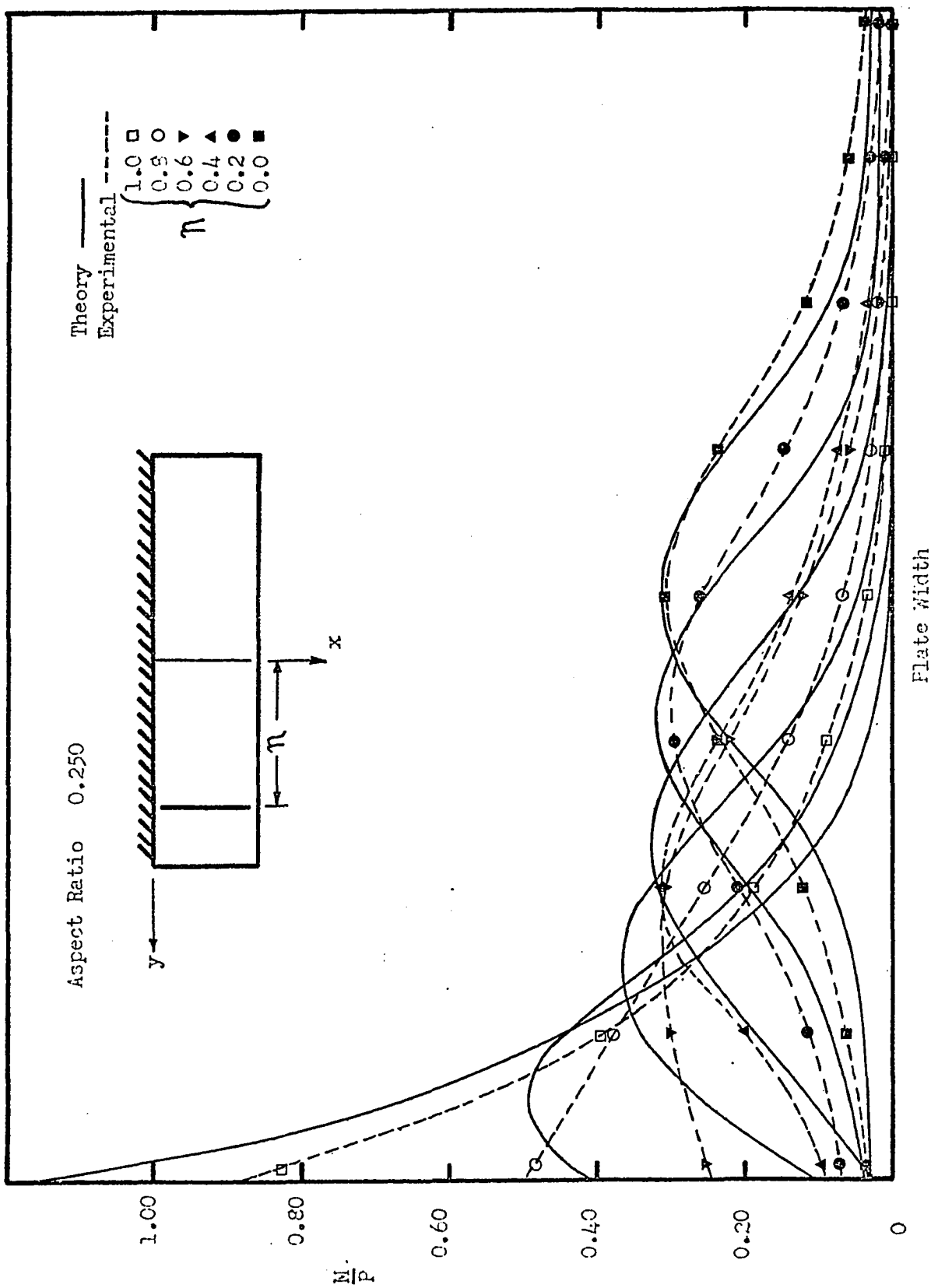

Fig. 68: Theoretical and Experimental Fixed Edge Bending Moments in a Cantilever Plate, Under Line Loadings With β_m 90 Degrees, at Various Positions Along the Plate Width (η)

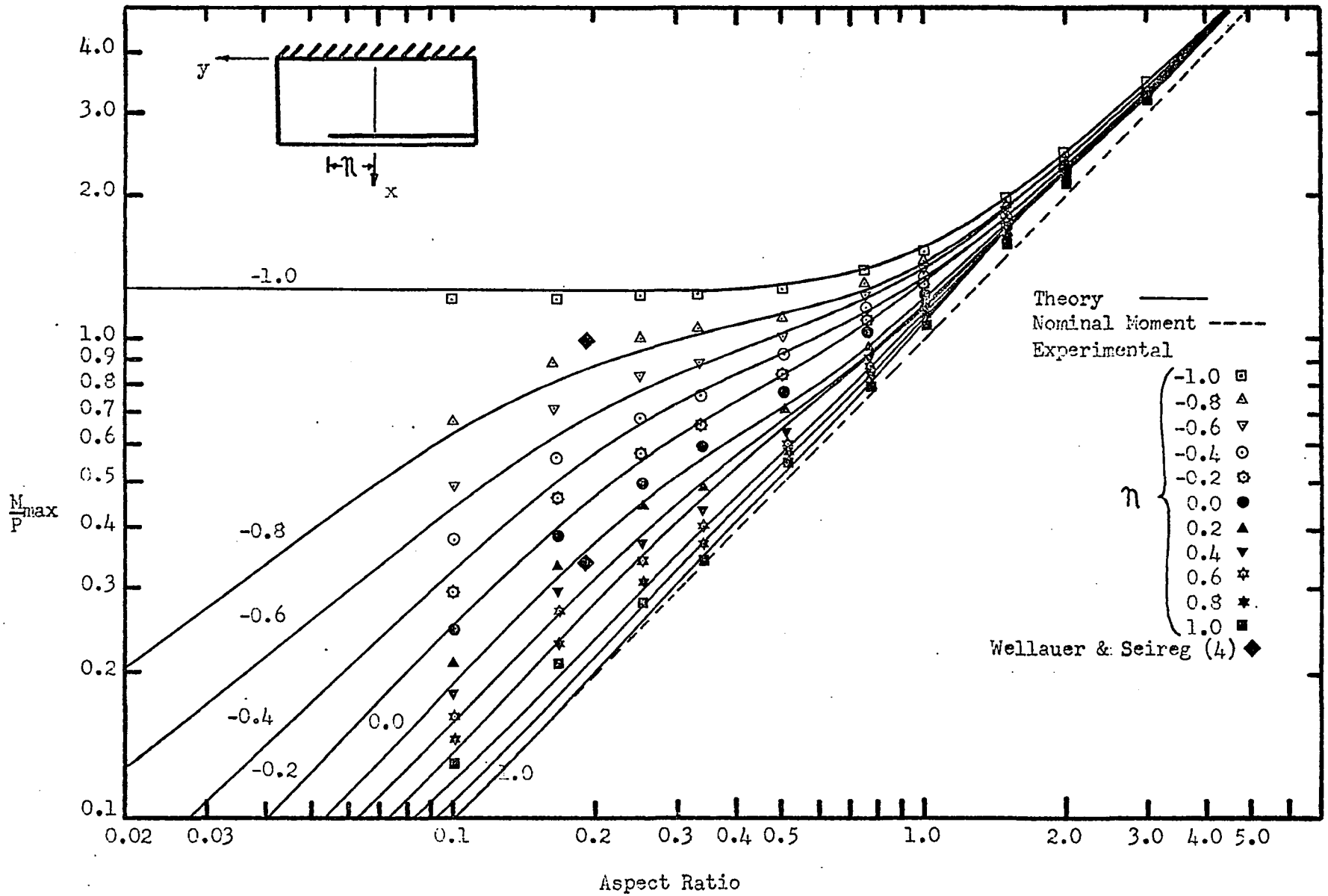

Fig. 69 : Theoretical and Experimental Maximum Bending Moments in a Line Loaded Cantilever Plate, β_m 0.0 Degrees

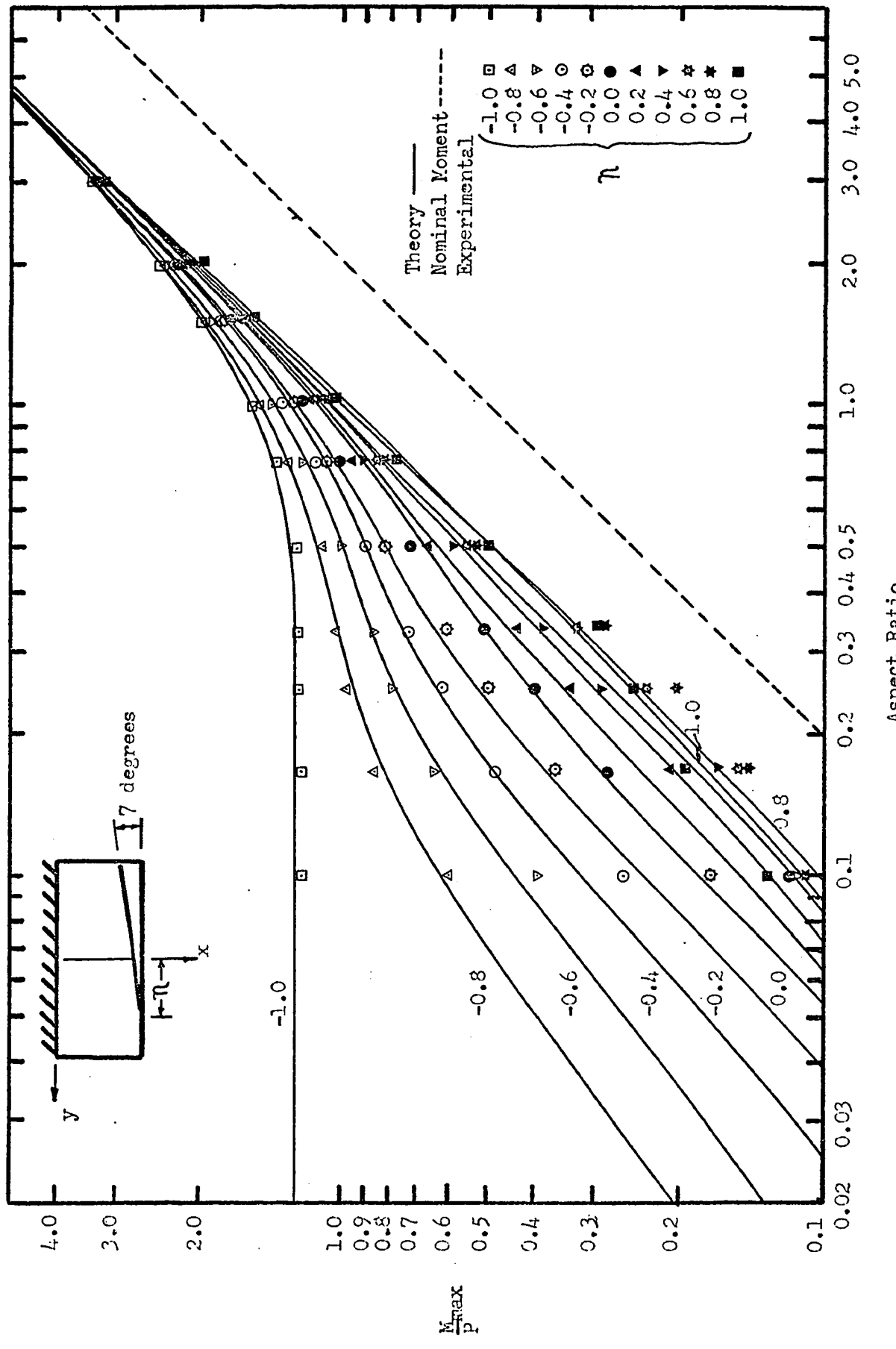

Fig. 70: Theoretical and Experimental Maximum Bending Moments in a Line Loaded Cantilever Plate, β_m, 7 Degrees

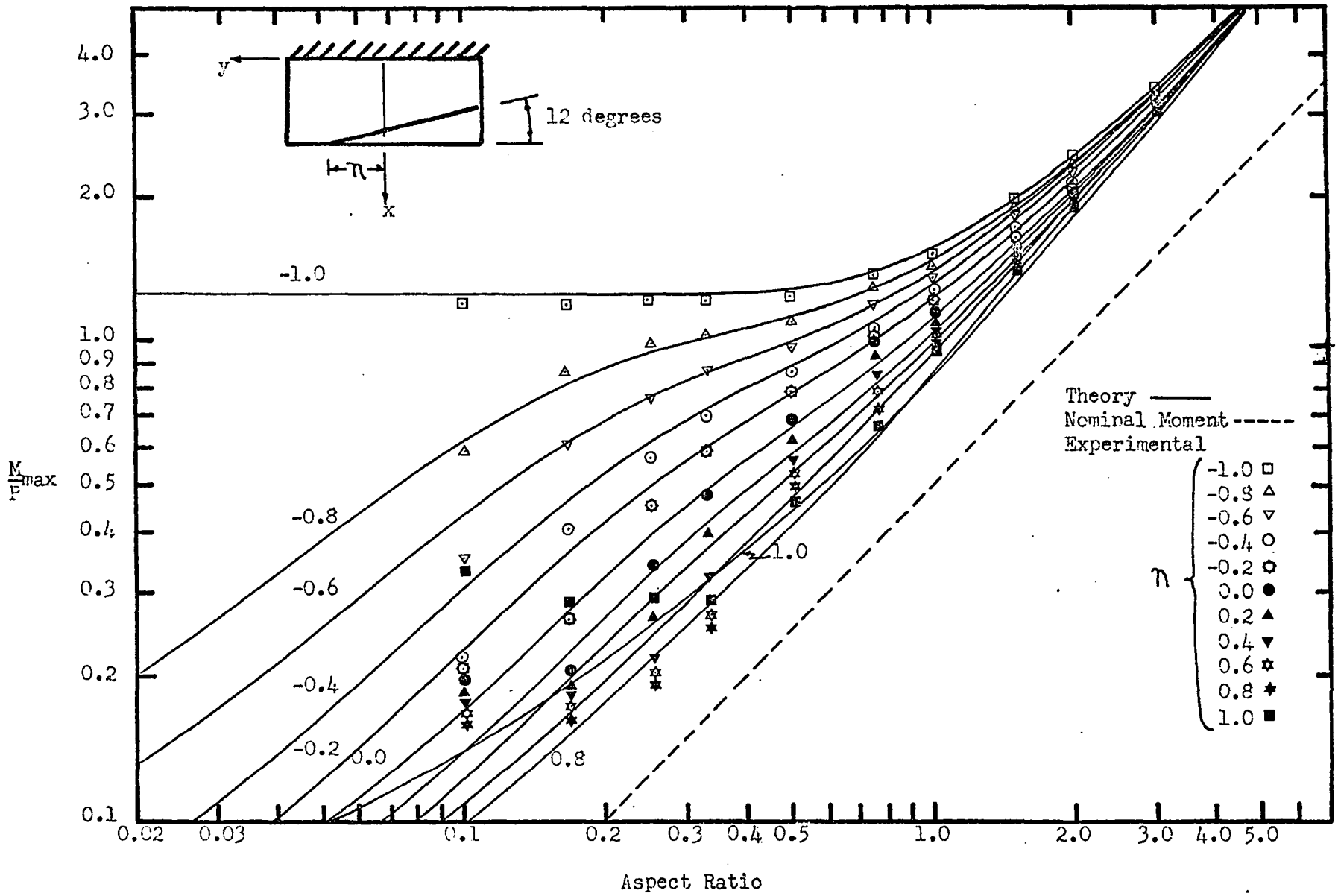

Fig. 71: Theoretical and Experimental Maximum Bending Moments in a Line Loaded Cantilever Plate, β_m, 12 Degrees

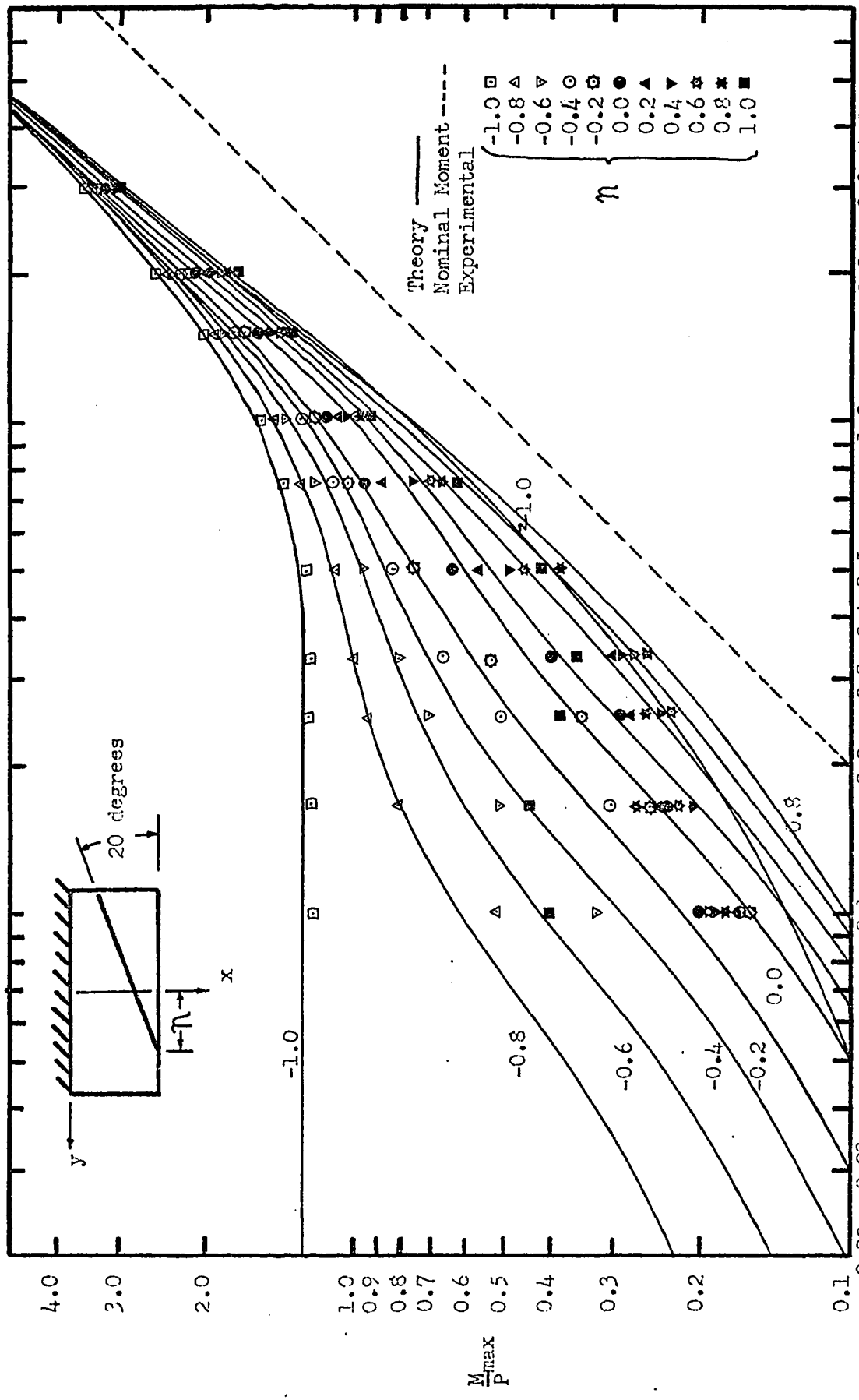

Fig. 72: Theoretical and Experimental Maximum Bending Moments in a Line Loaded Cantilever Plate, β_x, 20 Degrees

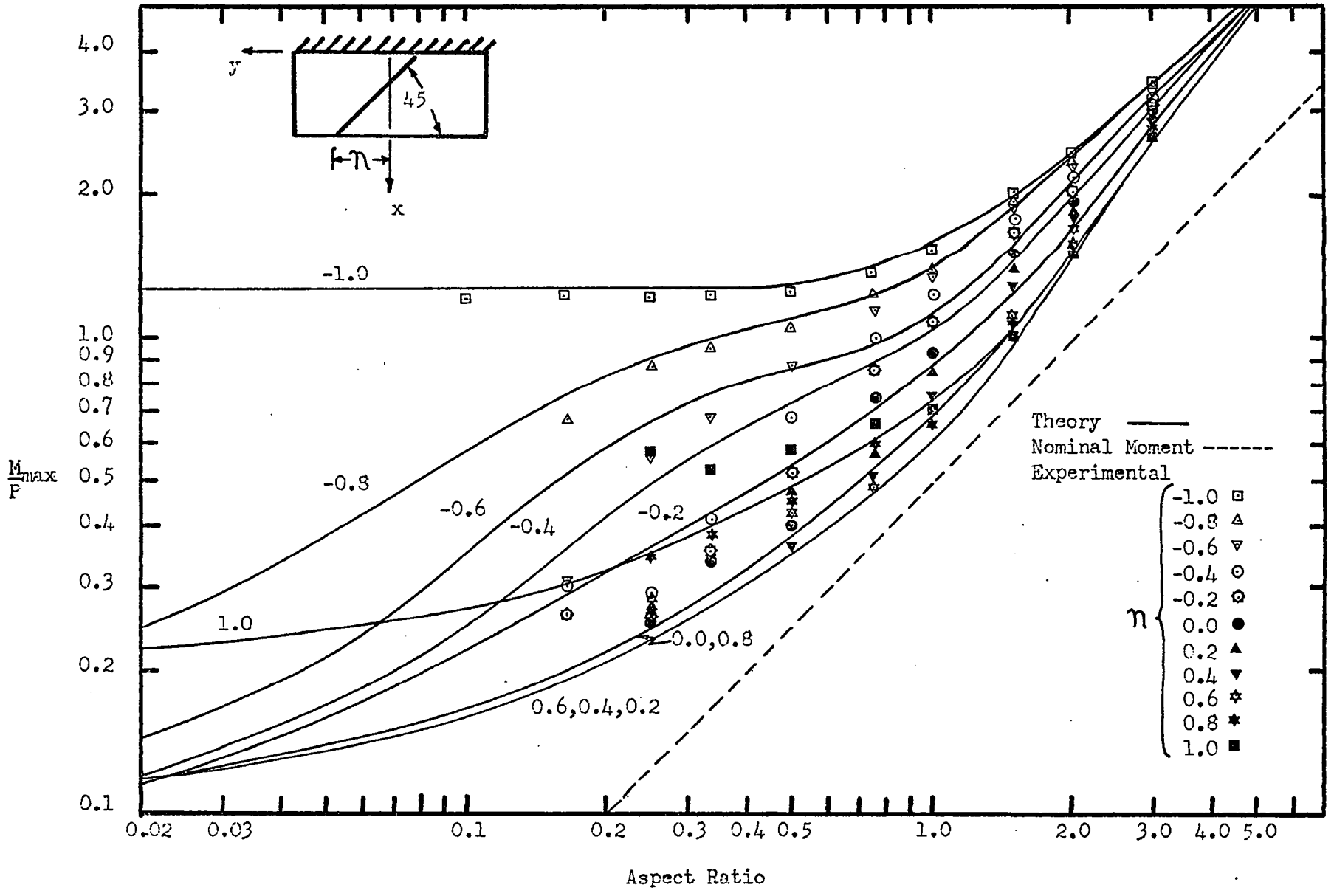

Fig. 73: Theoretical and Experimental Maximum Bending Moments in a Line Loaded Cantilever Plate, B_m, 45 Degrees

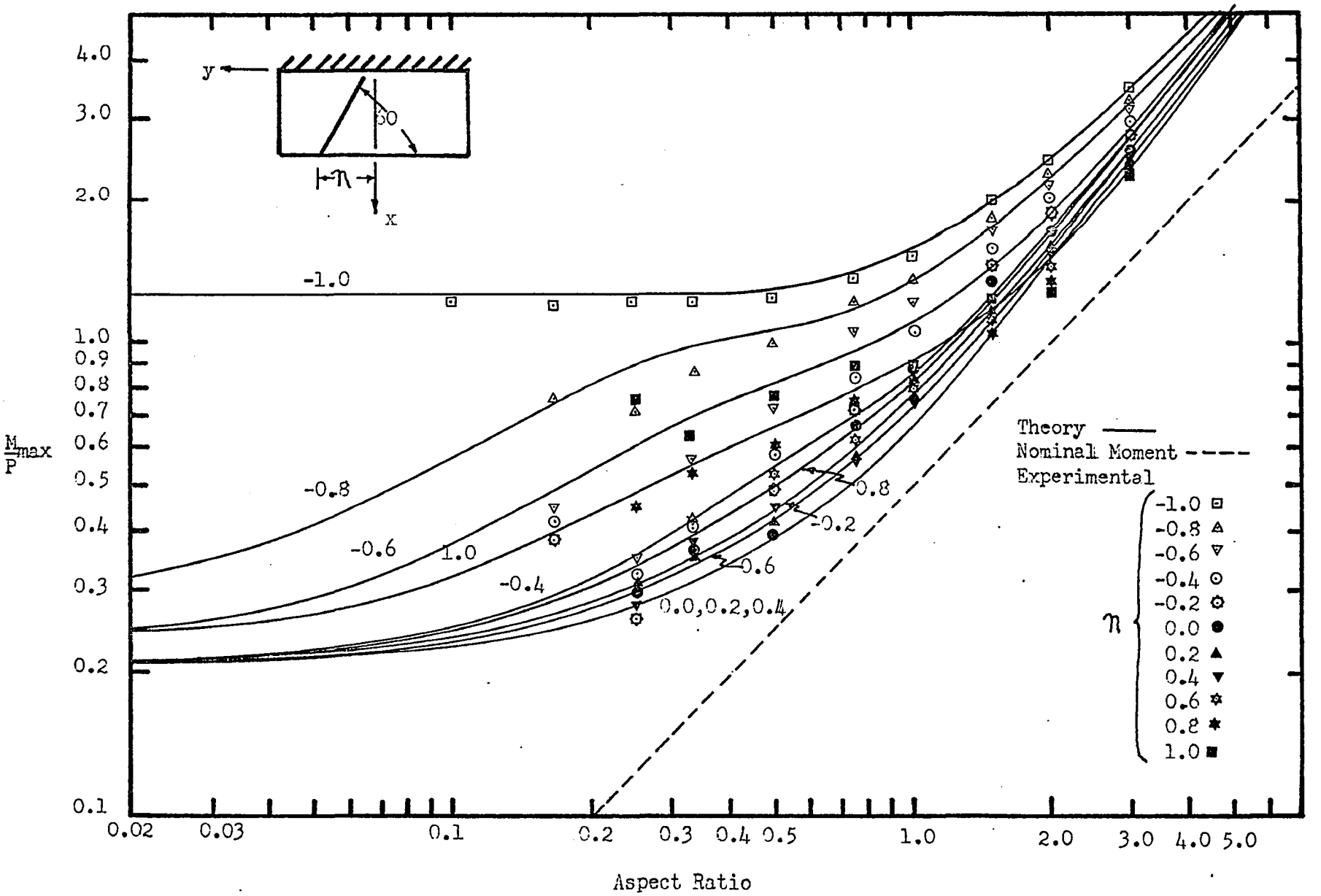

Fig. 74: Theoretical and Experimental Maximum Bending Moments in a Line Loaded Cantilever Plate, β_m, 60 Degrees

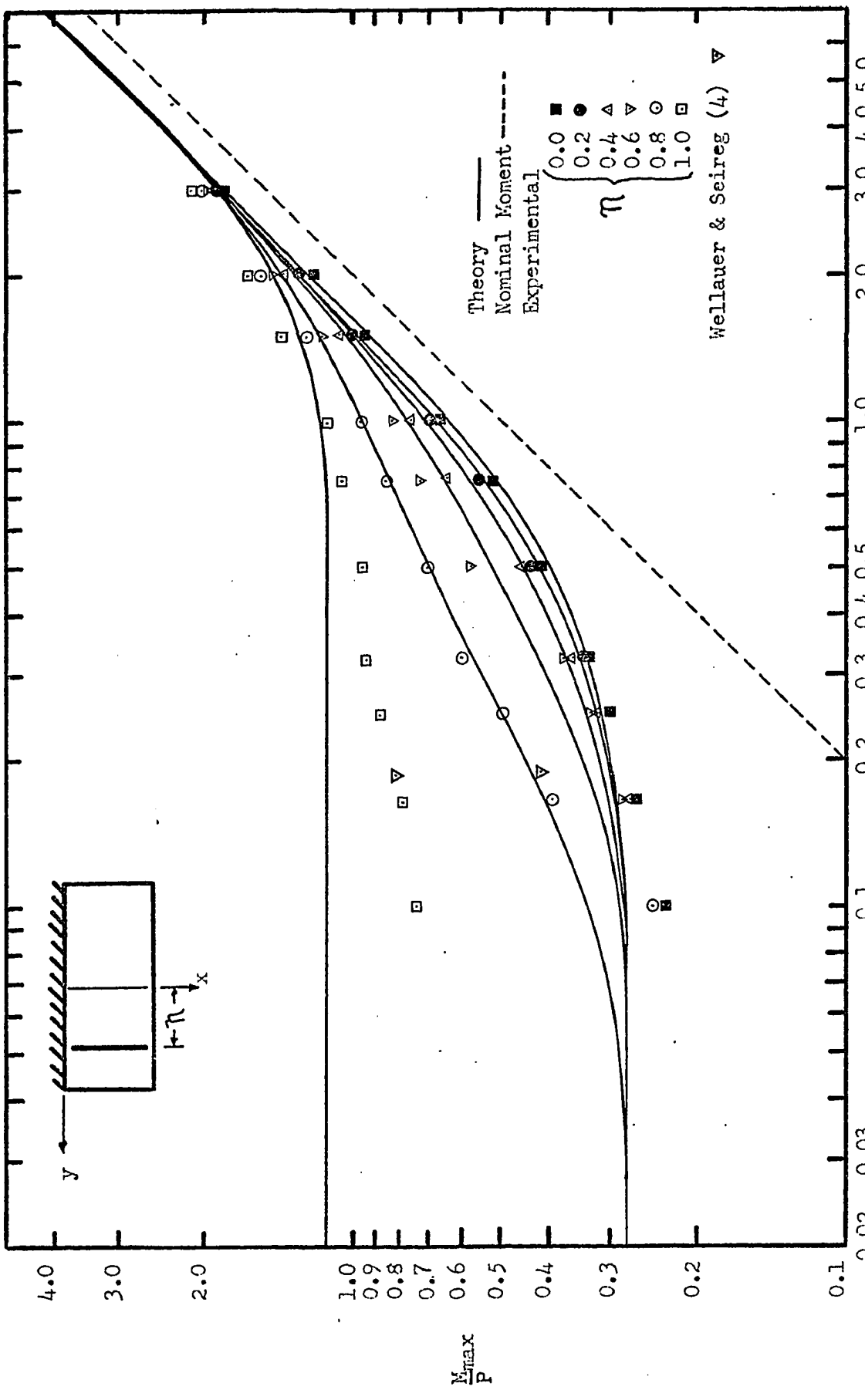

Fig. 75: Theoretical and Experimental Maximum Bending Moments in a Line Loaded Cantilever Plate, β_m, 90 degrees

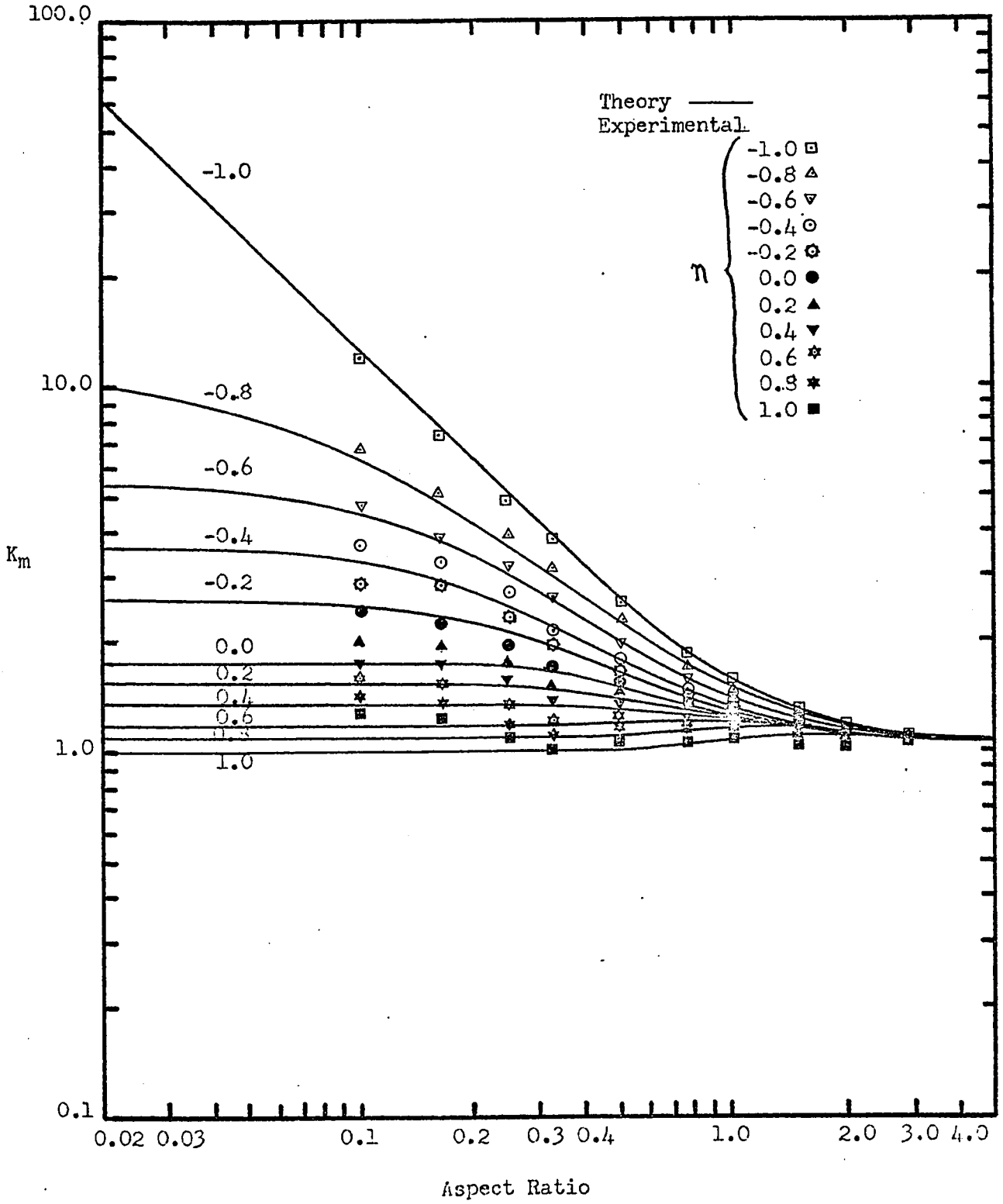

Fig. 76: Moment Distribution Factor, K_m as a Function of Aspect Ratio, For Line Loaded Cantilever Plates With β_m, 0 Degrees

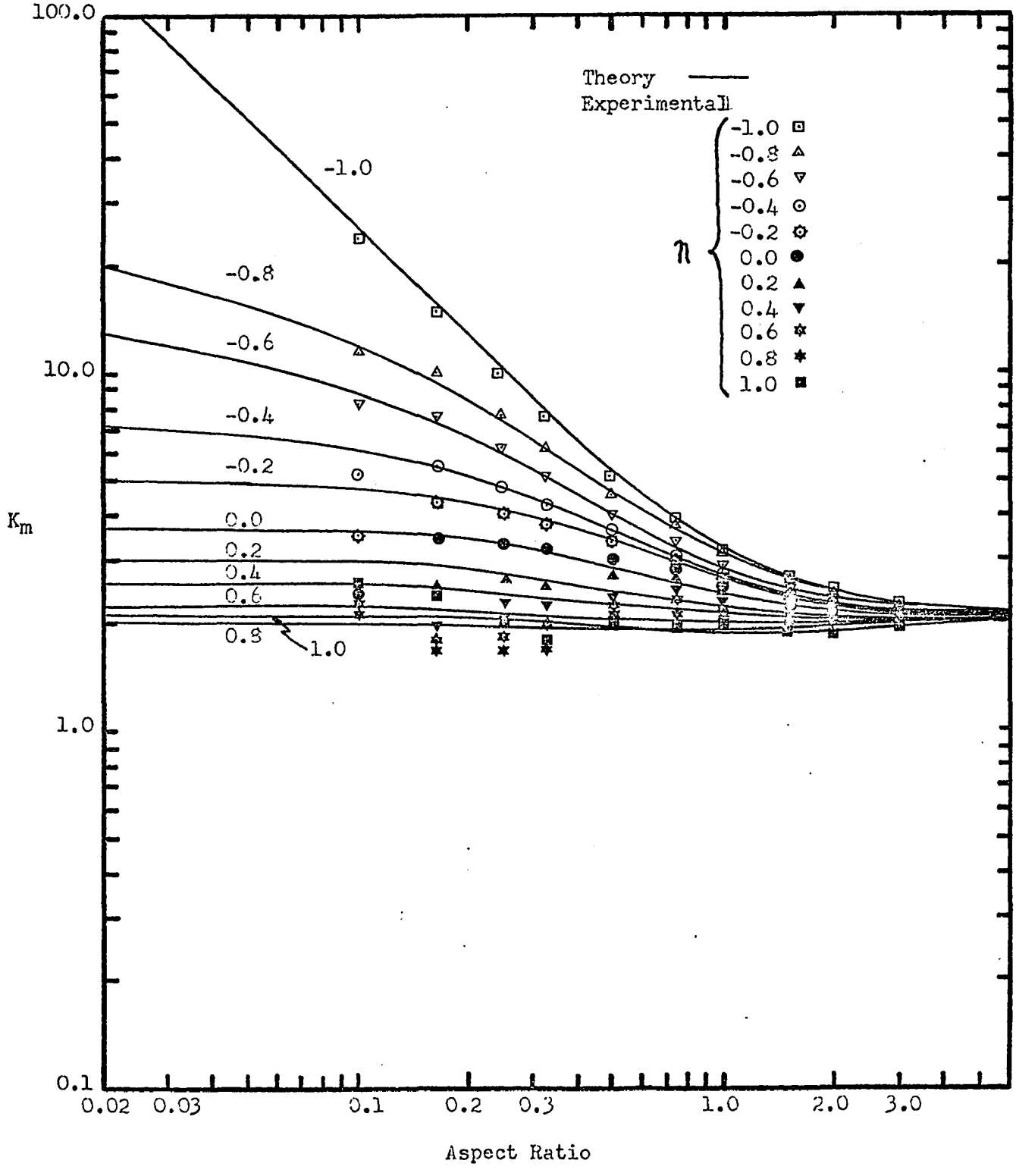

Fig. 77: Moment Distribution Factor, K_m as a Function of Aspect Ratio, For Line Loaded Cantilever Plates With β_m, 7 Degrees

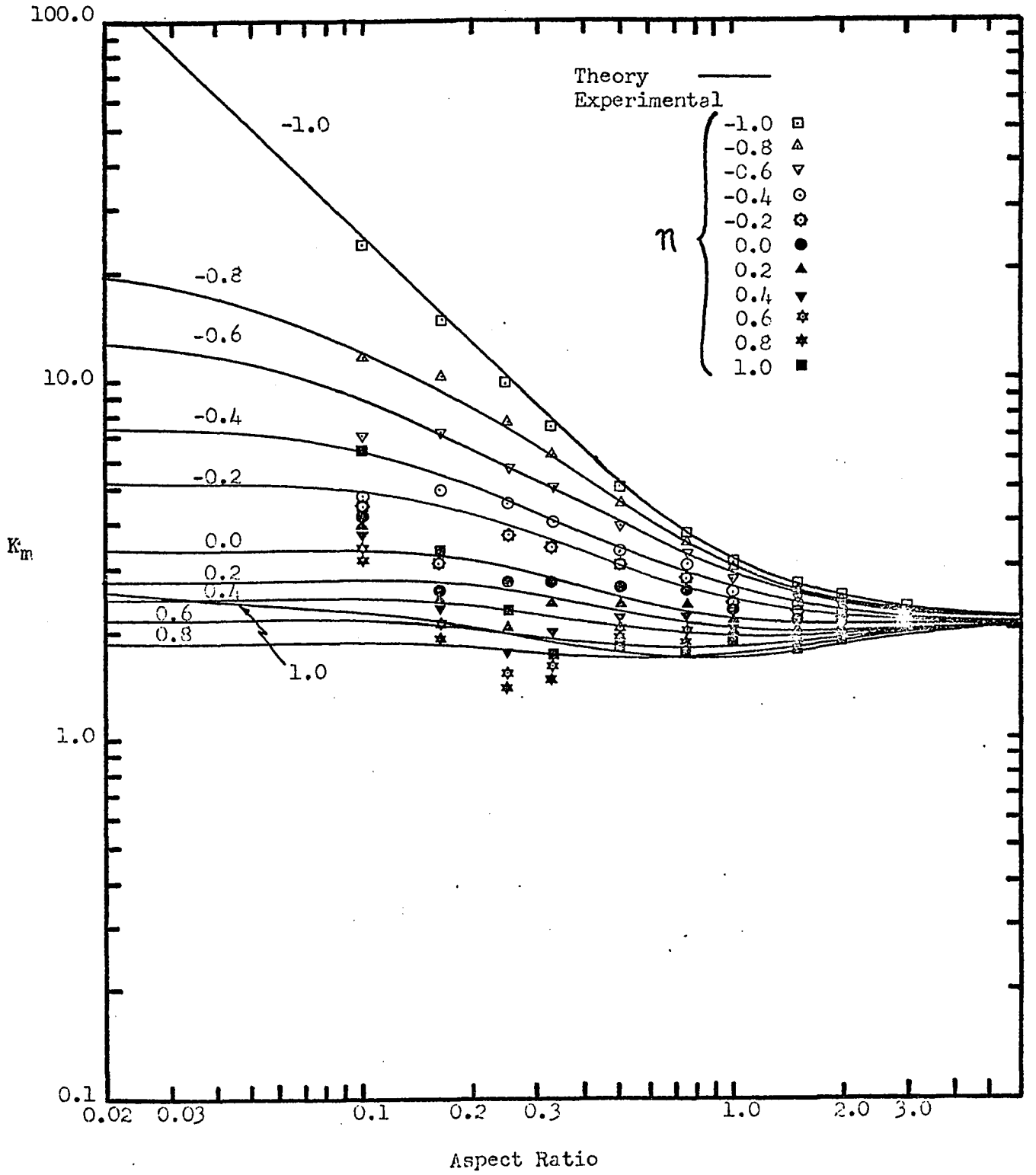

Fig. 78: Moment Distribution Factor, K_m as a Function of Aspect Ratio, For Line Loaded Cantilever Plates With β_m, 12 Degrees

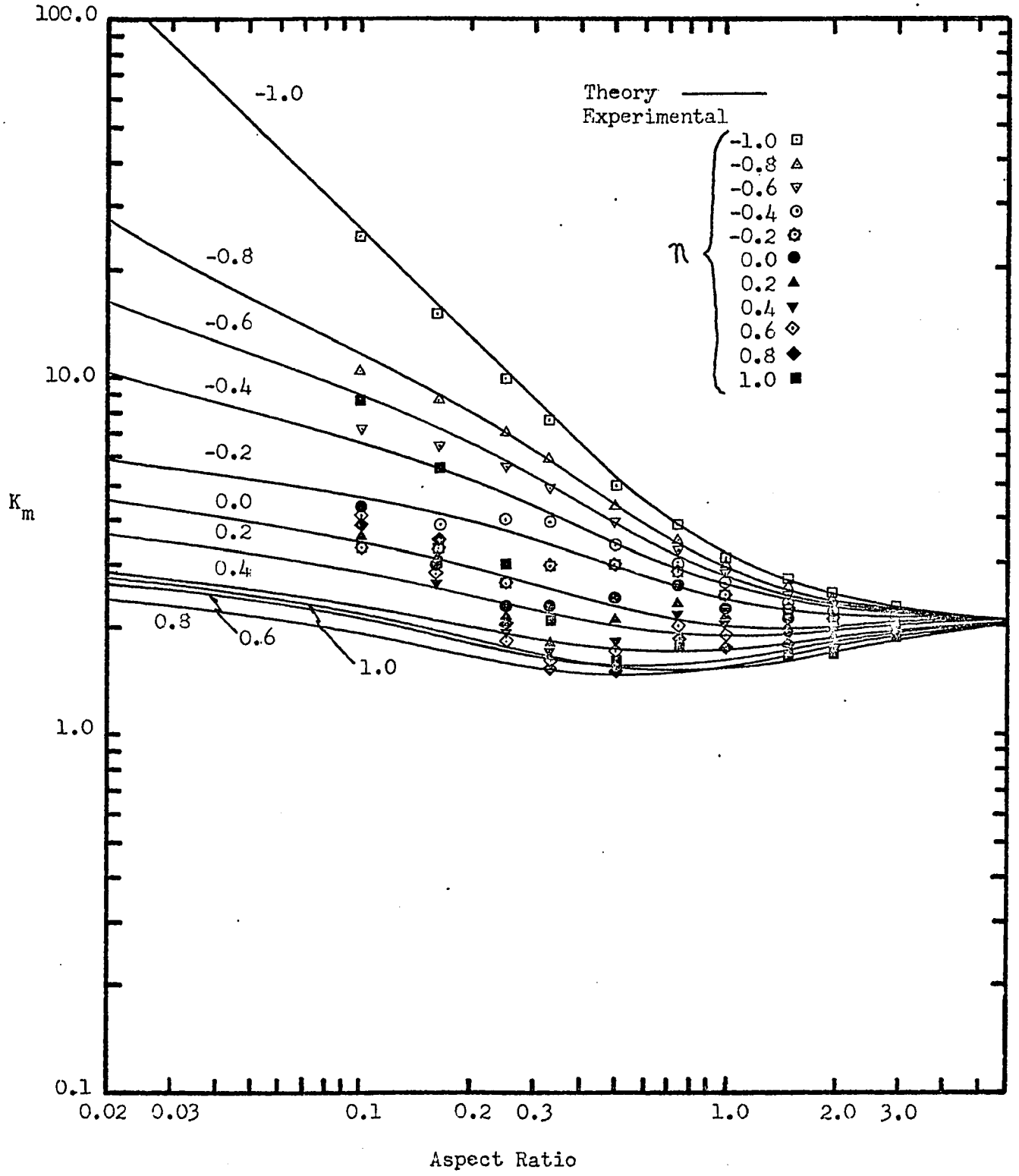

Fig. 79: Moment Distribution Factor, K_m as a Function of Aspect Ratio, For Line Loaded Cantilever Plates With β_m, 20 Degrees

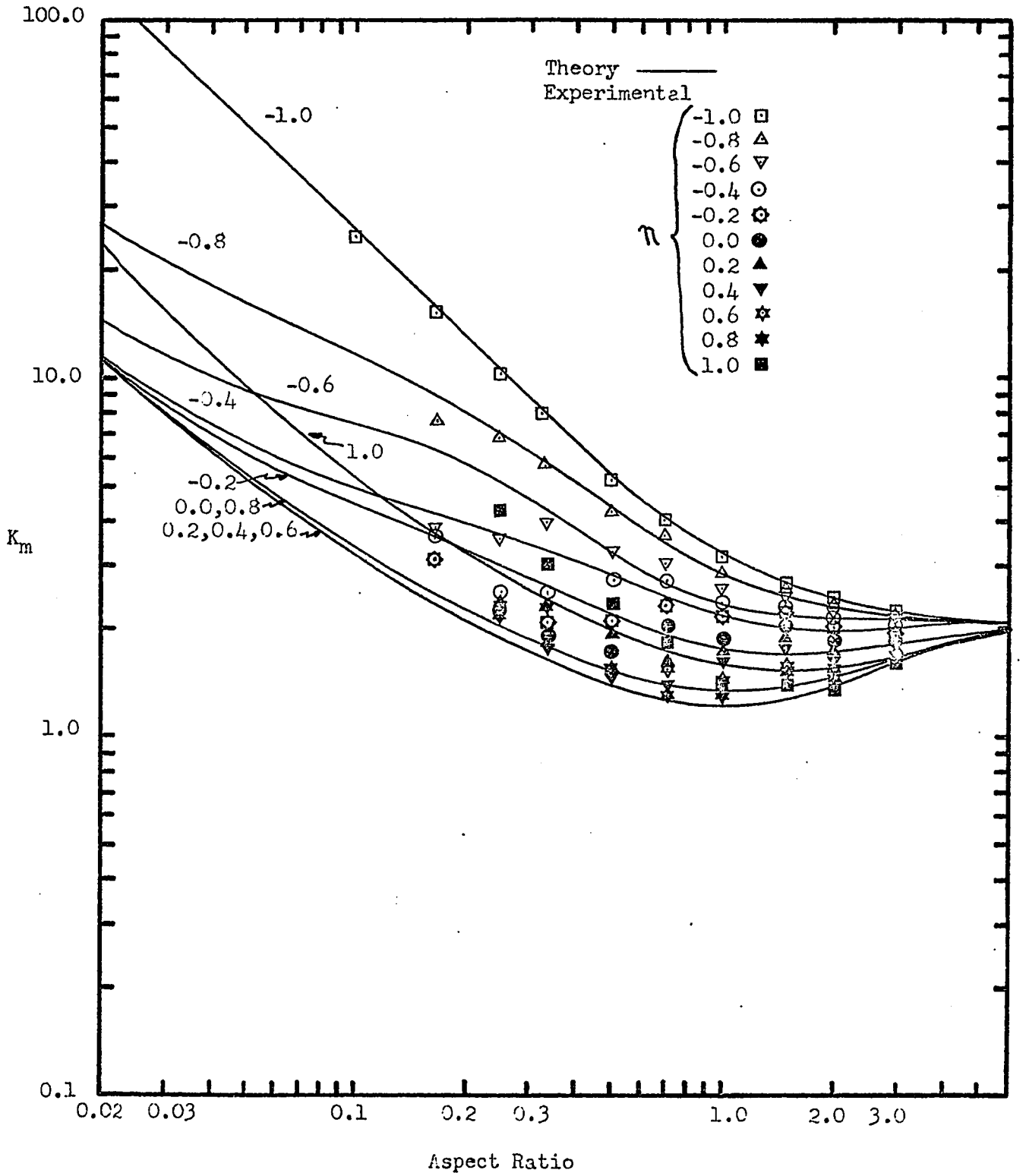

Fig. 80: Moment Distribution Factor, K_m as a Function of Aspect Ratio, For Line Loaded Cantilever Plates With β_m, 45 Degrees

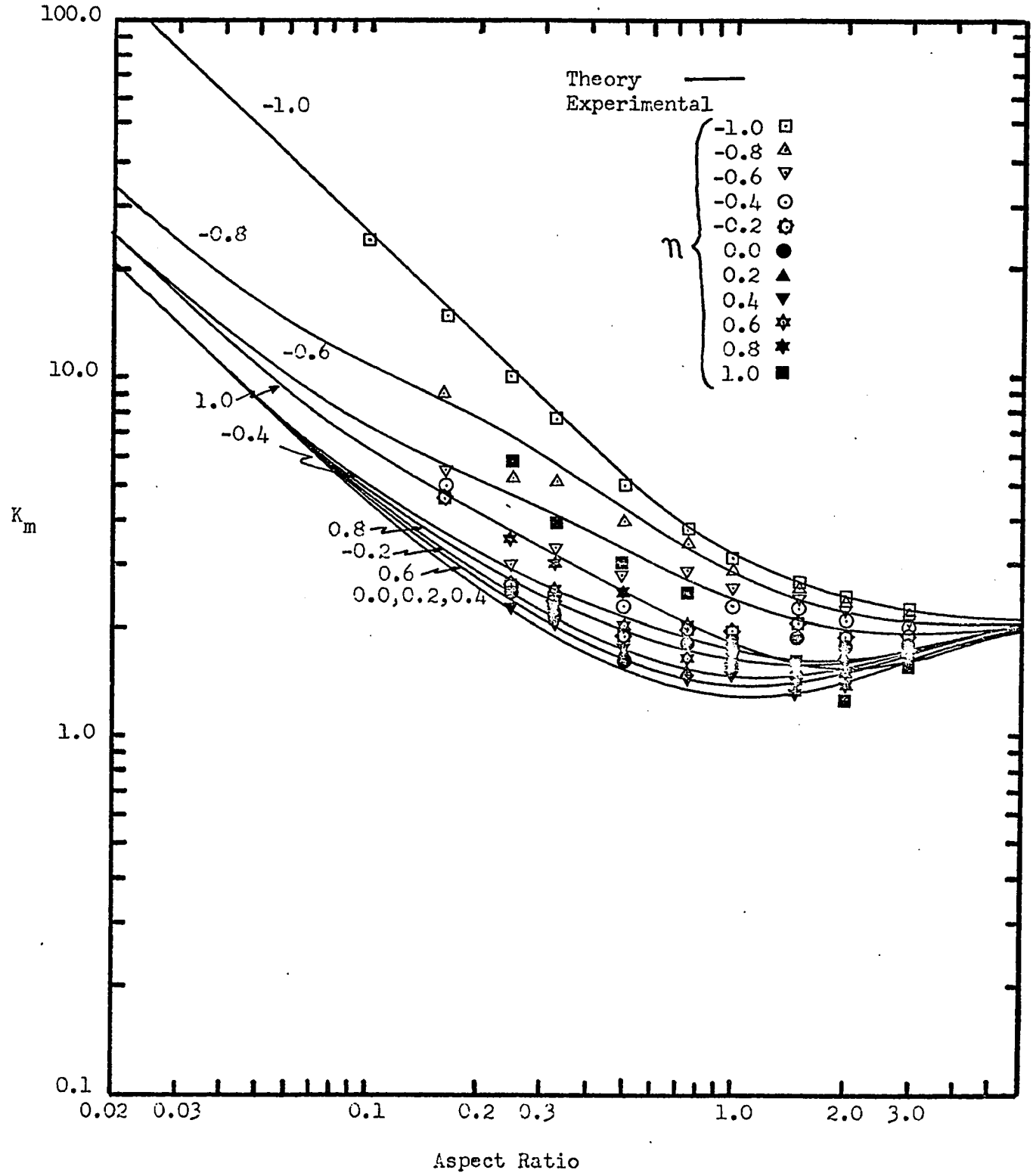

Fig. 81: Moment Distribution Factor, K_m as a Function of Aspect Ratio, For Line Loaded Cantilever Plates With β, 60 Degrees

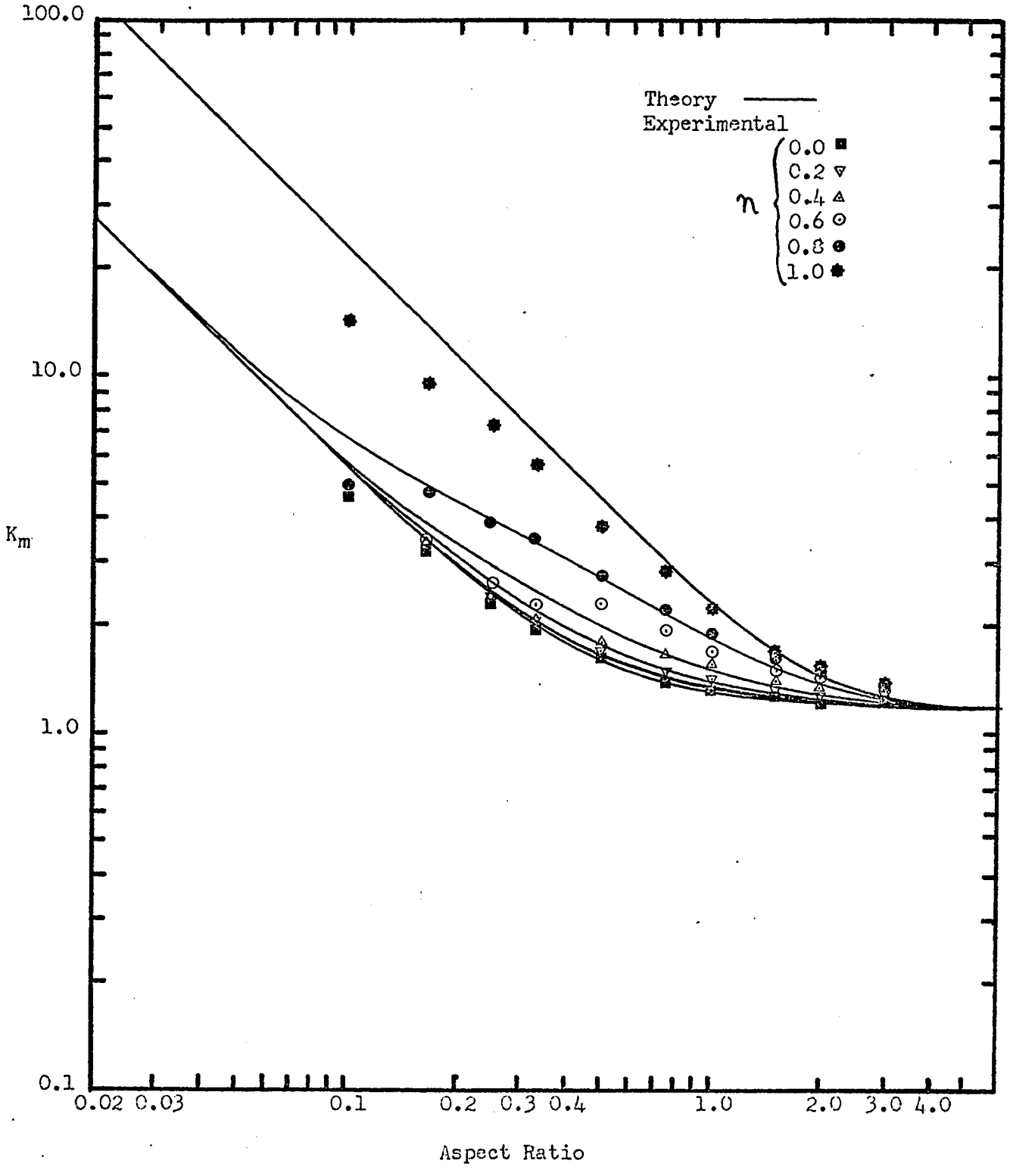

Fig. 82: Moment Distribution Factor, K_m as a Function of Aspect Ratio, For Line Loaded Cantilever Plates With β_{AM}, 90 Degrees

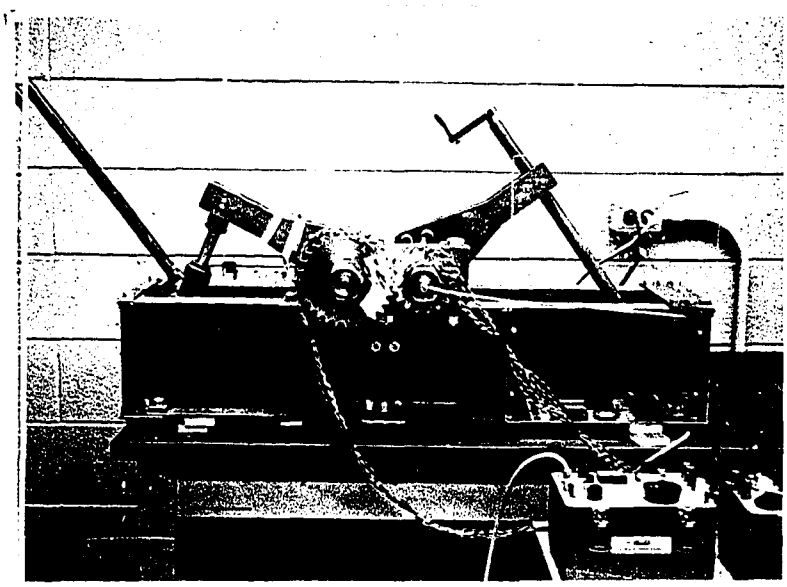

Gears Mounted on Test Rig (1)

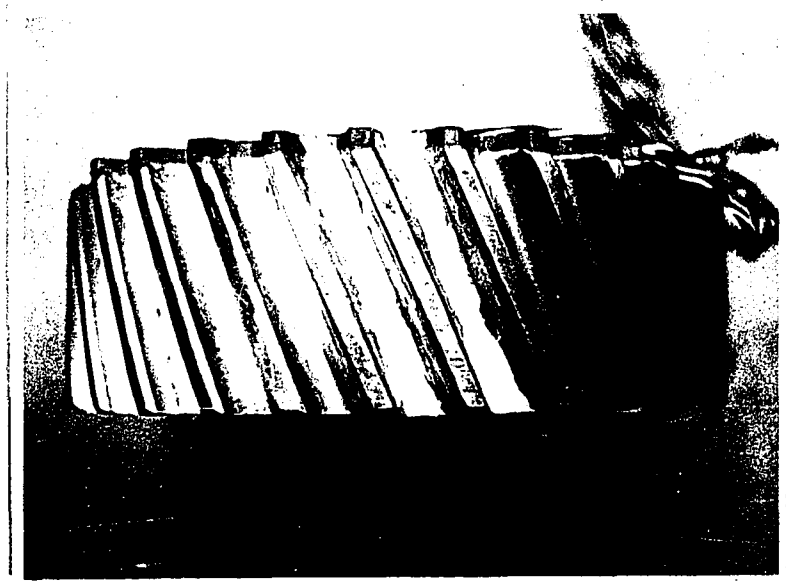

Novikov Gear

Fig. 83: Experimental Arrangement and Strain Gage Locations Used in Reference (1).

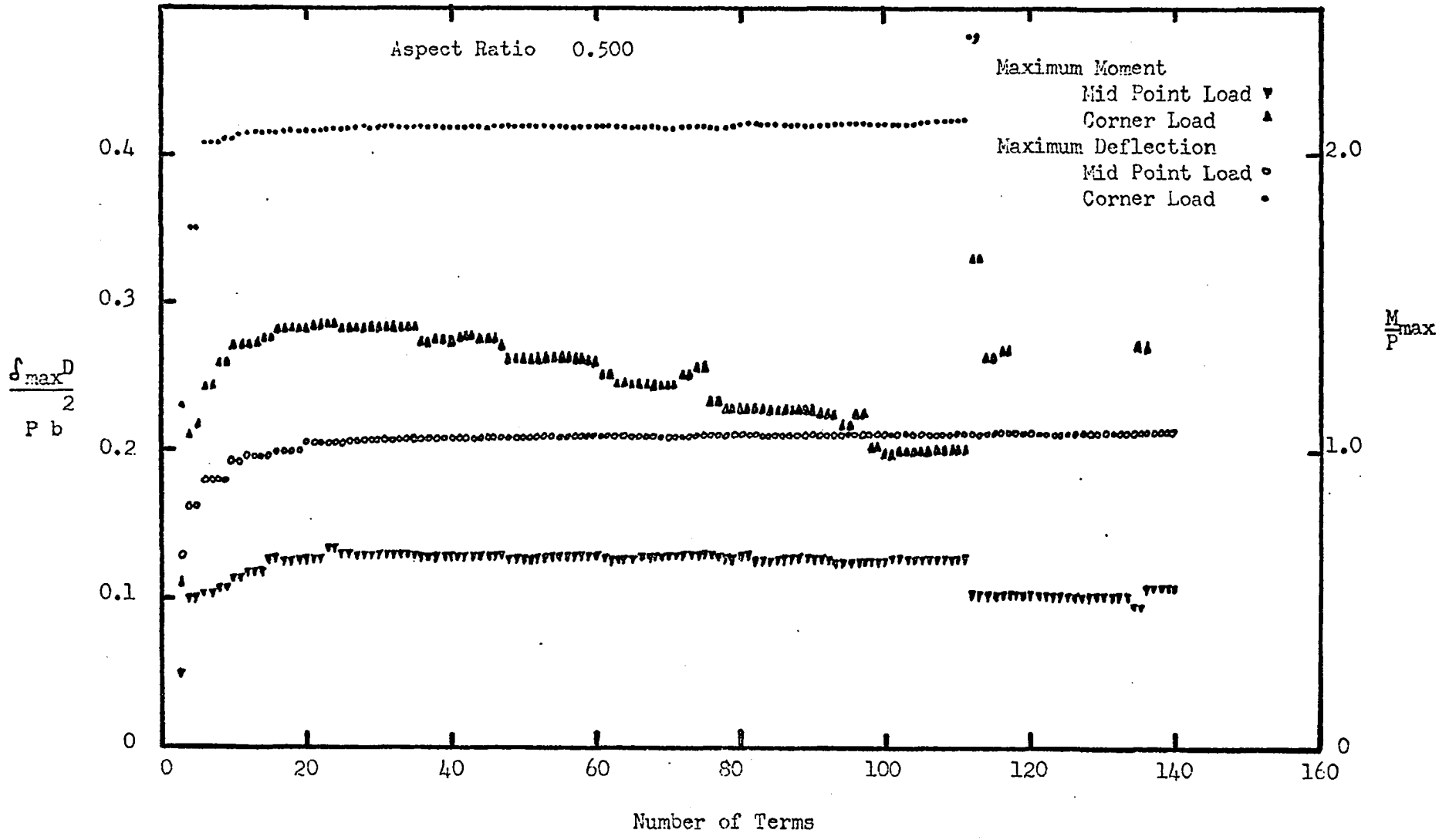

Fig. 84: Convergence of Point Loaded Cantilever Plate Deflections and Bending Moments as a Function of the Number of Terms Used in the Solution

TABLE I

Theoretical Deflection Values ($\frac{\delta D}{Pb^2}$) at grid points shown in figure 8 (for loading at the points also shown there). Aspect Ratio = 0.25

0.0	.0000	.0004	.0003	.0007	.0011	
0.0	.0001	.0004	.0008	.0013	.0019	
0.0	.0001	.0005	.0015	.0024	.0032	
0.0	.0005	.0015	.0028	.0041	.0053	$\beta = 0.2$
0.0	.0015	.0035	.0050	.0064	.0079	
0.0	.0021	.0046	.0063	.0077	.0092	$\alpha = 0.0$
0.0	.0015	.0035	.0050	.0064	.0079	
0.0	.0005	.0015	.0028	.0041	.0053	
0.0	.0001	.0005	.0015	.0024	.0032	
0.0	.0001	.0004	.0008	.0013	.0019	
0.0	.0000	.0004	.0003	.0007	.0011	

0.0	.0000	.0003	.0014	.0028	.0045	
0.0	.0005	.0016	.0032	.0052	.0075	
0.0	.0006	.0025	.0055	.0089	.0122	
0.0	.0015	.0051	.0098	.0147	.0198	$\beta = 0.4$
0.0	.0035	.0104	.0170	.0229	.0289	
0.0	.0046	.0133	.0210	.0273	.0335	$\alpha = 0.0$
0.0	.0035	.0104	.0170	.0229	.0289	
0.0	.0015	.0051	.0098	.0147	.0198	
0.0	.0006	.0025	.0055	.0089	.0122	
0.0	.0005	.0016	.0032	.0052	.0075	
0.0	.0000	.0003	.0014	.0028	.0045	

0.0	.0000	.0009	.0030	.0062	.0100	
0.0	.0009	.0033	.0064	.0112	.0159	
0.0	.0015	.0055	.0115	.0186	.0260	
0.0	.0027	.0097	.0193	.0298	.0405	$\beta = 0.6$
0.0	.0050	.0170	.0315	.0456	.0594	
0.0	.0063	.0210	.0382	.0541	.0692	$\alpha = 0.0$
0.0	.0050	.0170	.0315	.0456	.0594	
0.0	.0027	.0097	.0193	.0298	.0405	
0.0	.0015	.0055	.0115	.0186	.0260	
0.0	.0009	.0033	.0064	.0112	.0159	
0.0	.0000	.0009	.0030	.0062	.0100	

0.0	.0001	.0017	.0053	.0106	.0169	
0.0	.0013	.0050	.0111	.0184	.0263	
0.0	.0024	.0090	.0186	.0301	.0420	
0.0	.0041	.0147	.0298	.0472	.0651	$\beta = 0.8$
0.0	.0064	.0229	.0456	.0710	.0966	
0.0	.0077	.0268	.0541	.0836	.1137	$\alpha = 0.0$
0.0	.0064	.0229	.0456	.0710	.0966	
0.0	.0041	.0147	.0298	.0472	.0651	
0.0	.0024	.0090	.0186	.0301	.0420	
0.0	.0013	.0050	.0111	.0184	.0263	
0.0	.0001	.0017	.0053	.0106	.0169	

0.0	.0002	.0025	.0077	.0153	.0243	
0.0	.0019	.0073	.0156	.0260	.0373	
0.0	.0032	.0124	.0258	.0421	.0590	
0.0	.0053	.0198	.0406	.0651	.0907	$\beta = 1.0$
0.0	.0079	.0289	.0494	.0966	.1381	
0.0	.0092	.0335	.0693	.1137	.1648	$\alpha = 0.0$
0.0	.0079	.0289	.0494	.0966	.1381	
0.0	.0053	.0198	.0406	.0651	.0907	
0.0	.0032	.0124	.0258	.0421	.0590	
0.0	.0019	.0073	.0156	.0260	.0373	
0.0	.0002	.0025	.0077	.0153	.0243	

0.0	.0000	.0000	.0001	.0003	.0005	
0.0	.0000	.0001	.0003	.0007	.0009	
0.0	.0001	.0004	.0008	.0012	.0017	
0.0	.0001	.0005	.0014	.0022	.0030	$\beta = 0.2$
0.0	.0004	.0013	.0026	.0039	.0052	
0.0	.0015	.0035	.0050	.0065	.0079	$\alpha = 0.2$
0.0	.0022	.0048	.0064	.0078	.0093	
0.0	.0016	.0035	.0050	.0066	.0081	
0.0	.0004	.0016	.0029	.0043	.0057	
0.0	.0001	.0008	.0017	.0026	.0037	
0.0	.0000	.0002	.0008	.0015	.0023	

0.0	.0000	.0002	.0005	.0013	.0022	
0.0	.0001	.0006	.0015	.0026	.0038	
0.0	.0005	.0015	.0030	.0047	.0065	
0.0	.0006	.0026	.0053	.0085	.0115	$\beta = 0.4$
0.0	.0013	.0049	.0095	.0149	.0193	
0.0	.0035	.0104	.0170	.0229	.0289	$\alpha = 0.2$
0.0	.0048	.0137	.0214	.0276	.0339	
0.0	.0035	.0105	.0172	.0234	.0298	
0.0	.0014	.0053	.0103	.0158	.0212	
0.0	.0008	.0030	.0063	.0102	.0141	
0.0	.0005	.0010	.0032	.0051	.0093	

0.0	.0001	.0004	.0014	.0030	.0049	
0.0	.0003	.0014	.0034	.0058	.0085	
0.0	.0008	.0030	.0062	.0104	.0140	
0.0	.0014	.0053	.0110	.0176	.0243	$\beta = 0.6$
0.0	.0026	.0095	.0188	.0292	.0398	
0.0	.0050	.0170	.0315	.0456	.0594	$\alpha = 0.2$
0.0	.0064	.0214	.0388	.0549	.0702	
0.0	.0050	.0172	.0322	.0468	.0612	
0.0	.0029	.0103	.0207	.0321	.0487	
0.0	.0017	.0063	.0131	.0212	.0298	
0.0	.0002	.0025	.0068	.0129	.0200	

0.0	.0000	.0006	.0024	.0051	.0084	
0.0	.0006	.0026	.0058	.0098	.0142	
0.0	.0012	.0048	.0108	.0164	.0230	
0.0	.0023	.0085	.0176	.0284	.0397	$\beta = 0.8$
0.0	.0039	.0144	.0292	.0462	.0638	
0.0	.0064	.0229	.0456	.0710	.0966	$\alpha = 0.2$
0.0	.0078	.0277	.0549	.0850	.1153	
0.0	.0066	.0235	.0470	.0730	.0995	
0.0	.0044	.0158	.0320	.0509	.0703	
0.0	.0028	.0101	.0211	.0344	.0486	
0.0	.0006	.0042	.0115	.0218	.0334	

0.0	.0000	.0010	.0035	.0076	.0121	
0.0	.0009	.0038	.0083	.0149	.0200	
0.0	.0017	.0066	.0140	.0230	.0327	
0.0	.0030	.0116	.0244	.0397	.0557	$\beta = 1.0$
0.0	.0052	.0193	.0398	.0638	.0886	
0.0	.0079	.0289	.0594	.0966	.1381	$\alpha = 0.2$
0.0	.0093	.0339	.0702	.1153	.1672	
0.0	.0081	.0298	.0613	.0995	.1418	
0.0	.0058	.0213	.0488	.0703	.0982	
0.0	.0036	.0138	.0292	.0482	.0686	
0.0	.0008	.0061	.0145	.0309	.0475	

0.0	.0000	.0000	.0000	.0001	.0002	
0.0	.0000	.0001	.0002	.0003	.0004	
0.0	.0000	.0002	.0003	.0006	.0008	
0.0	.0000	.0004	.0008	.0011	.0016	$\beta = 0.2$
0.0	.0001	.0006	.0014	.0023	.0030	
0.0	.0005	.0015	.0027	.0041	.0054	$\alpha = 0.4$
0.0	.0016	.0035	.0051	.0066	.0082	
0.0	.0022	.0049	.0067	.0082	.0097	
0.0	.0016	.0036	.0054	.0070	.0088	
0.0	.0004	.0016	.0032	.0050	.0066	
0.0	.0002	.0007	.0017	.0031	.0046	

0.0	.0000	.0000	.0002	.0006	.0010
0.0	.0000	.0003	.0007	.0013	.0018
0.0	.0002	.0007	.0014	.0024	.0035
0.0	.0004	.0014	.0028	.0046	.0063
0.0	.0006	.0024	.0053	.0085	.0116
0.0	.0015	.0052	.0097	.0147	.0198
0.0	.0035	.0105	.0173	.0235	.0298
0.0	.0049	.0141	.0222	.0290	.0357
0.0	.0039	.0111	.0184	.0253	.0324
0.0	.0016	.0059	.0118	.0184	.0249
0.0	.0006	.0029	.0070	.0124	.0182

$\beta = 0.4$

$\alpha = 0.4$

0.0	.0000	.0001	.0006	.0014	.0024
0.0	.0002	.0008	.0017	.0029	.0041
0.0	.0004	.0015	.0032	.0053	.0076
0.0	.0008	.0028	.0059	.0097	.0134
0.0	.0014	.0053	.0110	.0177	.0244
0.0	.0027	.0098	.0194	.0298	.0406
0.0	.0050	.0172	.0322	.0469	.0613
0.0	.0067	.0222	.0406	.0576	.0738
0.0	.0055	.0185	.0347	.0507	.0668
0.0	.0033	.0118	.0239	.0376	.0518
0.0	.0011	.0062	.0150	.0263	.0388

$\beta = 0.6$

$\alpha = 0.4$

0.0	.0000	.0003	.0011	.0024	.0041
0.0	.0003	.0013	.0029	.0049	.0071
0.0	.0006	.0025	.0053	.0089	.0126
0.0	.0011	.0046	.0097	.0158	.0222
0.0	.0023	.0085	.0176	.0285	.0397
0.0	.0040	.0147	.0298	.0473	.0652
0.0	.0066	.0235	.0468	.0730	.0995
0.0	.0082	.0290	.0576	.0894	.1213
0.0	.0072	.0254	.0508	.0793	.1084
0.0	.0050	.0183	.0373	.0598	.0836
0.0	.0018	.0099	.0243	.0428	.0635

$\beta = 0.8$

$\alpha = 0.4$

0.0	.0000	.0004	.0016	.0035	.0059
0.0	.0004	.0018	.0040	.0069	.0102
0.0	.0009	.0036	.0076	.0126	.0178
0.0	.0016	.0063	.0135	.0222	.0313
0.0	.0030	.0116	.0243	.0397	.0558
0.0	.0054	.0198	.0406	.0651	.0907
0.0	.0082	.0298	.0612	.0995	.1418
0.0	.0097	.0357	.0738	.1213	.1758
0.0	.0090	.0325	.0668	.1083	.1542
0.0	.0067	.0246	.0511	.0829	.1168
0.0	.0026	.0138	.0338	.0600	.0895

$\beta = 1.0$

$\alpha = 0.4$

0.0	.0000	.0000	.0001	.0001	.0001	
0.0	.0000	.0000	.0001	.0002	.0003	
0.0	.0000	.0000	.0002	.0003	.0004	
0.0	.0001	.0002	.0004	.0006	.0009	$\beta = 0.2$
0.0	.0001	.0005	.0008	.0012	.0017	
0.0	.0001	.0006	.0015	.0024	.0033	$\alpha = 0.6$
0.0	.0004	.0014	.0029	.0044	.0058	
0.0	.0016	.0037	.0055	.0072	.0086	
0.0	.0025	.0053	.0073	.0091	.0111	
0.0	.0017	.0039	.0061	.0084	.0107	
0.0	.0003	.0019	.0042	.0065	.0089	

0.0	.0000	.0000	.0001	.0003	.0005	
0.0	.0000	.0002	.0004	.0006	.0010	
0.0	.0000	.0002	.0007	.0013	.0017	
0.0	.0002	.0007	.0015	.0025	.0036	$\beta = 0.4$
0.0	.0005	.0016	.0031	.0048	.0066	
0.0	.0006	.0025	.0055	.0090	.0123	$\alpha = 0.6$
0.0	.0014	.0053	.0103	.0159	.0213	
0.0	.0036	.0111	.0185	.0254	.0325	
0.0	.0053	.0153	.0244	.0323	.0403	
0.0	.0040	.0124	.0214	.0302	.0393	
0.0	.0018	.0073	.0154	.0247	.0340	

0.0	.0000	.0000	.0002	.0006	.0011	
0.0	.0001	.0004	.0008	.0014	.0022	
0.0	.0002	.0007	.0016	.0028	.0039	
0.0	.0003	.0014	.0032	.0053	.0076	$\beta = 0.6$
0.0	.0008	.0030	.0063	.0100	.0140	
0.0	.0015	.0055	.0116	.0186	.0259	$\alpha = 0.6$
0.0	.0029	.0104	.0207	.0321	.0438	
0.0	.0054	.0184	.0347	.0508	.0668	
0.0	.0073	.0244	.0450	.0645	.0834	
0.0	.0063	.0215	.0409	.0684	.0812	
0.0	.0035	.0145	.0314	.0508	.0710	

0.0	.0000	.0001	.0004	.0011	.0020	
0.0	.0002	.0006	.0015	.0025	.0037	
0.0	.0003	.0013	.0028	.0047	.0067	
0.0	.0006	.0024	.0053	.0089	.0126	$\beta = 0.8$
0.0	.0012	.0047	.0100	.0164	.0231	
0.0	.0024	.0090	.0186	.0301	.04208	$\alpha = 0.6$
0.0	.0044	.0158	.0321	.0509	.0735	
0.0	.0070	.0253	.0507	.0793	.1083	
0.0	.0091	.0323	.0645	.1001	.1370	
0.0	.0086	.0303	.0607	.0956	.1315	
0.0	.0050	.0221	.0487	.0806	.1149	

0.0	.0000	.0001	.0006	.0017	.0029
0.0	.0002	.0010	.0021	.0036	.0054
0.0	.0004	.0017	.0039	.0067	.0096
0.0	.0009	.0035	.0076	.0126	.0178
0.0	.0017	.0066	.0140	.0231	.0327
0.0	.0032	.0122	.0258	.0420	.0591
0.0	.0057	.0212	.0437	.0703	.0982
0.0	.0090	.0324	.0668	.1084	.1542
0.0	.0111	.0403	.0834	.1370	.1980
0.0	.0108	.0391	.0804	.1301	.1861
0.0	.0065	.0289	.0654	.1109	.1606

$\beta = 1.0$

$\alpha = 0.6$

0.0	.0000	.0000	.0000	.0001	.0001
0.0	.0000	.0000	.0000	.0001	.0001
0.0	.0000	.0001	.0001	.0002	.0002
0.0	.0000	.0001	.0002	.0003	.0004
0.0	.0001	.0001	.0003	.0006	.0010
0.0	.0001	.0005	.0009	.0013	.0019
0.0	.0001	.0008	.0017	.0027	.0037
0.0	.0004	.0016	.0033	.0050	.0067
0.0	.0017	.0040	.0063	.0086	.0108
0.0	.0030	.0066	.0093	.0119	.0146
0.0	.0020	.0060	.0102	.0135	.0167

$\beta = 0.2$

$\alpha = 0.8$

0.0	.0000	.0000	.0001	.0001	.0003
0.0	.0000	.0000	.0002	.0003	.0005
0.0	.0001	.0002	.0004	.0006	.0010
0.0	.0001	.0003	.0008	.0013	.0018
0.0	.0001	.0006	.0015	.0026	.0038
0.0	.0005	.0016	.0033	.0052	.0073
0.0	.0008	.0031	.0063	.0101	.0139
0.0	.0016	.01059	.0118	.0183	.0246
0.0	.0039	.0124	.0215	.0303	.0391
0.0	.0066	.0195	.0314	.0420	.0527
0.0	.0056	.0191	.0340	.0475	.0599

$\beta = 0.4$

$\alpha = 0.8$

0.0	.0000	.0000	.0001	.0003	.0005
0.0	.0000	.0001	.0004	.0007	.0011
0.0	.0001	.0004	.0009	.0015	.0021
0.0	.0002	.0008	.0017	.0029	.0040
0.0	.0003	.0015	.0038	.0058	.0083
0.0	.0009	.0032	.0068	.0112	.0156
0.0	.0017	.0063	.0131	.0211	.0293
0.0	.0032	.0118	.0239	.0373	.0511
0.0	.0061	.0214	.0486	.0607	.0804
0.0	.0093	.0314	.0579	.0834	.1082
0.0	.0092	.0327	.0631	.0931	.1215

$\beta = 0.6$

$\alpha = 0.8$

0.0	.0000	.0000	.0001	.0005	.0009	
0.0	.0001	.0003	.0007	.0012	.0019	
0.0	.0001	.0006	.0014	.0025	.0036	
0.0	.0003	.0013	.0029	.0049	.0070	$\beta = 0.8$
0.0	.0007	.0027	.0059	.0098	.0140	
0.0	.0013	.0052	.0112	.0185	.0261	$\alpha = 0.8$
0.0	.0026	.0102	.0212	.0344	.0482	
0.0	.0050	.0184	.0376	.0598	.0829	
0.0	.0084	.0302	.0608	.0956	.1308	
0.0	.0119	.0420	.0834	.1300	.1766	
0.0	.0119	.0448	.0912	.1428	.1940	

0.0	.0000	.0000	.0003	.0009	.0015	
0.0	.0001	.0005	.0011	.0019	.0028	
0.0	.0003	.0010	.0022	.0037	.0054	
0.0	.0004	.0018	.0041	.0071	.0103	$\beta = 1.0$
0.0	.0009	.0039	.0085	.0142	.0200	
0.0	.0019	.0075	.0160	.0264	.0374	$\alpha = 0.8$
0.0	.0037	.0142	.0298	.0486	.0686	
0.0	.0066	.0249	.0518	.0836	.1168	
0.0	.0107	.0393	.0812	.1315	.1861	
0.0	.0146	.0527	.1082	.1766	.2537	
0.0	.0140	.0551	.1170	.1912	.2703	

0.0	.0000	.0000	.0000	.0000	.0000	
0.0	.0000	.0000	.0000	.0000	.0000	
0.0	.0000	.0000	.0000	.0000	.0000	
0.0	.0000	.0000	.0000	.0000	.0000	$\beta = 0.2$
0.0	.0000	.0000	.0000	.0000	.0000	
0.0	.0000	.0000	.0000	.0002	.0002	$\alpha = 1.0$
0.0	.0001	.0001	.0003	.0006	.0009	
0.0	.0002	.0006	.0011	.0018	.0026	
0.0	.0003	.0018	.0035	.0049	.0065	
0.0	.0020	.0056	.0092	.0119	.0140	
0.0	.0135	.0180	.0202	.0226	.0248	

0.0	.0000	.0000	.0000	.0000	.0000	
0.0	.0000	.0000	.0000	.0000	.0000	
0.0	.0000	.0000	.0000	.0001	.0001	
0.0	.0000	.0001	.0001	.0003	.0004	$\beta = 0.4$
0.0	.0000	.0002	.0004	.0007	.0010	
0.0	.0000	.0003	.0010	.0017	.0025	$\alpha = 1.0$
0.0	.0002	.0010	.0025	.0042	.0061	
0.0	.0007	.0029	.0062	.0099	.0138	
0.0	.0019	.0073	.0145	.0221	.0289	
0.0	.0060	.0192	.0327	.0448	.0551	
0.0	.0180	.0478	.0673	.0790	.0902	

0.0	.0000	.0000	.0000	.0000	.0002	
0.0	.0000	.0001	.0001	.0001	.0003	
0.0	.0000	.0001	.0002	.0004	.0006	
0.0	.0000	.0002	.0006	.0011	.0016	β = 0.6
0.0	.0001	.0006	.0014	.0025	.0036	
0.0	.0003	.0014	.0031	.0053	.0078	α = 1.0
0.0	.0008	.0032	.0069	.0116	.0165	
0.0	.0017	.0070	.0150	.0243	.0338	
0.0	.0042	.0154	.0314	.0487	.0654	
0.0	.0102	.0340	.0631	.0912	.1170	
0.0	.0202	.0673	.1178	.1550	.1839	

0.0	.0000	.0000	.0000	.0001	.0003	
0.0	.0001	.0001	.0003	.0005	.0009	
0.0	.0001	.0003	.0006	.0011	.0017	
0.0	.0001	.0006	.0014	.0024	.0035	β = 0.8
0.0	.0003	.0013	.0030	.0051	.0075	
0.0	.0007	.0028	.0062	.0107	.0153	α = 1.0
0.0	.0015	.0060	.0130	.0218	.0309	
0.0	.0031	.0124	.0263	.0428	.0600	
0.0	.0065	.0247	.0508	.0807	.1109	
0.0	.0135	.0475	.0931	.1428	.1912	
0.0	.0226	.0790	.1550	.2320	.2952	

0.0	.0000	.0000	.0000	.0003	.0006	
0.0	.0000	.0003	.0005	.0009	.0015	
0.0	.0001	.0005	.0011	.0020	.0029	
0.0	.0002	.0010	.0024	.0041	.0059	β = 1.0
0.0	.0005	.0022	.0050	.0084	.0121	
0.0	.0011	.0045	.0100	.0169	.0243	α = 1.0
0.0	.0023	.0093	.0200	.0334	.0475	
0.0	.0046	.0182	.0388	.0635	.0895	
0.0	.0090	.0340	.0710	.1149	.1606	
0.0	.0167	.0599	.1215	.1940	.2703	
0.0	.0248	.0902	.1839	.2952	.4152	

TABLE II : EXPERIMENTAL VALUES OF PLATE BENDING MOMENTS

ASPECT RATIO = 3.000

GAGE NO.		1	2	3	4	5
α	β					
1.00	1.00	2.561	2.393	3.254	3.446	3.297
0.80	1.00	2.678	2.473	3.254	3.425	3.212
0.60	1.00	2.764	3.115	3.265	3.372	3.137
0.40	1.00	2.892	3.169	3.296	3.329	3.021
0.20	1.00	2.909	3.222	3.286	3.307	3.027
0.00	1.00	2.115	3.297	3.297	3.222	2.892
1.00	0.80	2.006	2.401	2.614	2.838	2.742
0.80	0.80	2.134	2.445	2.667	2.833	2.680
0.60	0.80	2.219	2.625	2.657	2.838	2.603
0.40	0.80	2.305	2.539	2.646	2.721	2.497
0.20	0.80	2.422	2.593	2.614	2.657	2.491
0.00	0.80	2.539	2.582	2.603	2.582	2.293
1.00	0.60	1.430	1.782	1.995	2.231	2.209
0.80	0.60	1.526	1.825	1.995	2.197	2.134
0.60	0.60	1.611	1.857	1.963	2.113	2.017
0.40	0.60	1.729	1.921	1.985	2.112	2.017
0.20	0.60	1.846	1.953	1.985	2.017	1.935
0.00	0.60	1.899	1.942	1.953	1.942	1.718
1.00	0.40	0.813	1.142	1.323	1.558	1.642
0.80	0.40	0.898	1.163	1.323	1.536	1.568
0.60	0.40	1.004	1.195	1.322	1.483	1.462
0.40	0.40	1.110	1.249	1.302	1.408	1.344
0.20	0.40	1.216	1.291	1.312	1.355	1.270
0.00	0.40	1.270	1.312	1.312	1.332	1.184
1.00	0.20	0.241	0.432	0.599	0.869	1.008
0.80	0.20	0.360	0.445	0.615	0.838	0.925
0.60	0.20	0.395	0.509	0.623	0.796	0.811
0.40	0.20	0.476	0.559	0.635	0.732	0.722
0.20	0.20	0.566	0.615	0.635	0.686	0.635
0.00	0.20	0.635	0.635	0.641	0.635	0.641

TABLE II : EXPERIMENTAL VALUES OF PLATE BENDING MOMENTS

ASPECT RATIO = 2.000

GAGE NO.		1	2	3	4	5
α	β					
1.0	1.0	1.410	1.689	1.839	2.159	2.449
0.8	1.0	1.428	1.719	1.916	2.138	2.339
0.6	1.0	1.583	1.772	1.829	2.074	2.241
0.4	1.0	1.636	1.838	1.843	2.050	2.170
0.2	1.0	1.821	1.876	1.843	1.980	2.011
0.0	1.0	1.918	1.949	2.080	1.956	1.918
1.0	0.8	1.950	1.298	1.438	1.769	2.089
0.8	0.8	1.120	1.348	1.458	1.610	1.980
0.6	0.8	1.240	1.388	1.478	1.699	1.888
0.4	0.8	1.348	1.458	1.498	1.678	1.850
0.2	0.8	1.429	1.518	1.489	1.638	1.718
0.0	0.8	1.486	1.528	1.478	1.558	1.588
1.0	0.6	0.694	0.912	1.168	1.368	1.608
0.8	0.6	0.766	0.945	1.178	1.338	1.588
0.6	0.6	0.861	0.984	1.088	1.298	1.498
0.4	0.6	0.962	1.048	1.098	1.278	1.408
0.2	0.6	1.050	1.138	1.128	1.248	1.328
0.0	0.6	1.110	1.128	1.118	1.178	1.188
1.0	0.4	0.335	0.407	0.683	0.945	1.288
0.8	0.4	0.407	0.542	0.689	0.923	1.198
0.6	0.4	0.493	0.594	0.716	0.895	1.188
0.4	0.4	0.559	0.637	0.721	0.844	0.984
0.2	0.4	0.669	0.698	0.727	0.911	0.866
0.0	0.4	0.727	0.721	0.727	0.771	0.783
1.0	0.2	0.093	0.151	0.279	0.403	0.796
0.8	0.2	0.124	0.179	0.307	0.481	0.727
0.6	0.2	0.185	0.229	0.352	0.475	0.637
0.4	0.2	0.213	0.257	0.246	0.447	0.519
0.2	0.2	0.263	0.295	0.269	0.391	0.408
0.0	0.2	0.313	0.324	0.269	0.358	0.346

TABLE II : EXPERIMENTAL VALUES OF PLATE BENDING MOMENTS

ASPECT RATIO = 1.500

GAGE NO.		1	2	3	4	5
α	β					
1.0	1.0	[illegible]	1.240	1.400	1.730	1.970
0.8	1.0	1.040	1.280	1.500	1.490	1.860
0.6	1.0	1.130	1.330	1.510	1.640	1.760
0.4	1.0	1.220	1.390	1.520	1.560	1.670
0.2	1.0	1.310	1.450	1.520	1.550	1.550
0.0	1.0	1.410	1.520	1.540	1.530	1.470
1.0	0.8	0.690	0.954	1.210	1.440	1.680
0.8	0.8	0.773	1.020	1.230	1.440	1.650
0.6	0.8	0.841	1.060	1.210	1.360	1.490
0.4	0.8	0.921	1.110	1.240	1.320	1.390
0.2	0.8	1.010	1.130	1.210	1.240	1.260
0.0	0.8	1.120	1.190	1.230	1.220	1.180
1.0	0.6	0.437	0.657	0.888	1.150	1.430
0.8	0.6	0.496	0.707	0.911	1.110	1.340
0.6	0.6	0.576	0.767	0.922	1.090	1.290
0.4	0.6	0.657	0.826	0.934	1.030	1.110
0.2	0.6	0.749	0.941	0.919	0.954	0.991
0.0	0.6	0.853	0.984	0.939	0.933	0.918
1.0	0.4	0.307	0.358	0.565	0.896	1.140
0.8	0.4	0.348	0.403	0.582	0.796	1.030
0.6	0.4	0.392	0.461	0.611	0.749	0.987
0.4	0.4	0.398	0.502	0.622	0.714	0.789
0.2	0.4	0.449	0.518	0.611	0.657	0.681
0.0	0.4	0.541	0.582	0.622	0.611	0.574
1.0	0.2	0.035	0.121	0.242	0.432	0.772
0.8	0.2	0.063	0.150	0.276	0.437	0.657
0.6	0.2	0.092	0.184	0.294	0.426	0.524
0.4	0.2	0.150	0.219	0.311	0.392	0.423
0.2	0.2	0.196	0.248	0.334	0.357	0.345
0.0	0.2	0.190	0.276	0.346	0.305	0.265

TABLE II : EXPERIMENTAL VALUES OF PLATE BENDING MOMENTS

ASPECT RATIO = 1.000

GAGE NO.		1	2	3	4	5	6	7
α	β							
1.0	1.0	0.342	0.668	0.848	0.998	1.091	1.098	1.072
0.8	1.0	0.440	0.736	0.915	1.024	1.071	1.112	1.034
0.6	1.0	0.524	0.801	0.954	1.031	1.069	1.027	1.016
0.4	1.0	0.601	0.866	0.992	1.038	1.096	1.052	1.018
0.2	1.0	0.726	0.982	1.041	1.049	1.105	1.078	0.934
0.0	1.0	0.833	1.057	1.078	1.057	1.142	0.982	0.911
1.0	0.8	0.228	0.447	0.638	0.860	1.035	1.163	1.202
0.8	0.8	0.314	0.552	0.696	0.858	1.022	1.059	1.174
0.6	0.8	0.405	0.630	0.744	0.824	0.983	1.029	1.140
0.4	0.8	0.444	0.711	0.801	0.825	0.973	0.965	0.925
0.2	0.8	0.514	0.783	0.825	0.840	0.944	0.858	0.786
0.0	0.8	0.638	0.887	0.887	0.839	0.819	0.829	0.676
1.0	0.6	0.120	0.286	0.433	0.599	0.782	0.959	1.142
0.8	0.6	0.204	0.357	0.482	0.626	0.763	0.887	1.001
0.6	0.6	0.309	0.419	0.529	0.636	0.749	0.819	0.853
0.4	0.6	0.276	0.402	0.561	0.664	0.726	0.737	0.724
0.2	0.6	0.353	0.593	0.611	0.633	0.695	0.644	0.601
0.0	0.6	0.448	0.648	0.657	0.620	0.629	0.627	0.487
1.0	0.4	0.038	0.129	0.228	0.305	0.506	0.724	0.972
0.8	0.4	0.095	0.176	0.267	0.334	0.456	0.654	0.811
0.6	0.4	0.142	0.176	0.223	0.367	0.506	0.595	0.648
0.4	0.4	0.133	0.282	0.357	0.420	0.587	0.521	0.519
0.2	0.4	0.186	0.344	0.410	0.419	0.476	0.439	0.396
0.0	0.4	0.258	0.405	0.448	0.443	0.457	0.448	0.314
1.0	0.2	0.010	0.019	0.058	0.095	0.180	0.306	0.697
0.8	0.2	0.029	0.052	0.085	0.124	0.214	0.371	0.606
0.6	0.2	0.067	0.077	0.114	0.157	0.249	0.344	0.369
0.4	0.2	0.019	0.095	0.133	0.191	0.282	0.257	0.238
0.2	0.2	0.049	0.133	0.181	0.230	0.305	0.257	0.166
0.0	0.2	0.071	0.172	0.229	0.267	0.224	0.241	0.148

TABLE II : EXPERIMENTAL VALUES OF PLATE BENDING MOMENTS

ASPECT RATIO = 0.750

GAGE NO.		1	2	3	4	5	6	7
α	β							
1.0	1.0	0.178	0.332	0.535	0.714	0.956	1.285	1.372
0.8	1.0	0.248	0.369	0.479	0.752	0.949	1.190	1.231
0.6	1.0	0.216	0.447	0.654	0.784	0.936	1.107	1.076
0.4	1.0	0.401	0.493	0.741	0.912	0.903	1.008	0.993
0.2	1.0	0.484	0.558	0.771	0.929	0.973	0.918	0.778
0.0	1.0	0.631	0.828	0.979	0.965	0.957	0.828	0.631
1.0	0.8	0.114	0.235	0.376	0.548	0.967	1.112	1.229
0.8	0.8	0.172	0.268	0.484	0.631	0.765	1.028	1.081
0.6	0.8	0.242	0.306	0.555	0.623	0.765	0.974	0.974
0.4	0.8	0.310	0.357	0.585	0.650	0.752	0.941	0.793
0.2	0.8	0.401	0.414	0.637	0.667	0.713	0.732	0.573
0.0	0.8	0.484	0.490	0.698	0.676	0.676	0.651	0.471
1.0	0.6	0.044	0.140	0.217	0.392	0.554	0.892	1.064
0.8	0.6	0.093	0.159	0.223	0.423	0.570	0.828	0.993
0.6	0.6	0.141	0.191	0.263	0.465	0.586	0.746	0.739
0.4	0.6	0.204	0.248	0.407	0.483	0.573	0.659	0.572
0.2	0.6	0.255	0.274	0.459	0.497	0.529	0.553	0.515
0.0	0.6	0.345	0.338	0.519	0.529	0.515	0.479	0.338
1.0	0.4	0.021	0.051	0.109	0.203	0.337	0.644	0.829
0.8	0.4	0.032	0.077	0.153	0.242	0.369	0.503	0.698
0.6	0.4	0.064	0.102	0.193	0.285	0.395	0.523	0.549
0.4	0.4	0.108	0.121	0.235	0.319	0.471	0.446	0.429
0.2	0.4	0.134	0.152	0.281	0.343	0.369	0.350	0.255
0.0	0.4	0.191	0.204	0.243	0.292	0.362	0.292	0.172
1.0	0.2	0.0	0.013	0.019	0.044	0.114	0.310	0.554
0.8	0.2	0.006	0.026	0.051	0.102	0.141	0.330	0.382
0.6	0.2	0.013	0.032	0.064	0.121	0.191	0.299	0.268
0.4	0.2	0.024	0.038	0.093	0.150	0.217	0.224	0.195
0.2	0.2	0.044	0.051	0.121	0.204	0.211	0.159	0.083
0.0	0.2	0.064	0.070	0.121	0.235	0.127	0.114	0.077

TABLE II : EXPERIMENTAL VALUES OF PLATE BENDING MOMENTS

ASPECT RATIO = 0.500

GAGE NO.		1	2	3	4	5	6	7
α	β							
1.0	1.0	0.079	0.144	0.208	0.427	0.674	1.030	1.172
0.8	1.0	0.107	0.177	0.253	0.472	0.697	0.964	1.011
0.6	1.0	0.140	0.219	0.410	0.516	0.712	0.961	0.835
0.4	1.0	0.200	0.261	0.478	0.567	0.697	0.757	0.633
0.2	1.0	0.251	0.321	0.548	0.596	0.660	0.632	0.465
0.0	1.0	0.354	0.386	0.610	0.610	0.630	0.530	0.358
1.0	0.8	0.047	0.103	0.218	0.316	0.535	0.884	1.058
0.8	0.8	0.084	0.139	0.271	0.372	0.567	0.813	0.865
0.6	0.8	0.121	0.172	0.226	0.418	0.582	0.731	0.679
0.4	0.8	0.167	0.223	0.384	0.465	0.577	0.623	0.512
0.2	0.8	0.196	0.246	0.433	0.494	0.526	0.497	0.400
0.0	0.8	0.270	0.298	0.488	0.493	0.474	0.396	0.317
1.0	0.6	0.023	0.065	0.139	0.214	0.395	0.706	0.897
0.8	0.6	0.056	0.093	0.186	0.263	0.428	0.654	0.725
0.6	0.6	0.079	0.121	0.233	0.316	0.465	0.586	0.531
0.4	0.6	0.098	0.121	0.242	0.326	0.433	0.451	0.362
0.2	0.6	0.131	0.193	0.316	0.372	0.418	0.367	0.297
0.0	0.6	0.195	0.223	0.376	0.400	0.367	0.284	0.186
1.0	0.4	0.010	0.042	0.079	0.126	0.246	0.512	0.721
0.8	0.4	0.037	0.067	0.112	0.169	0.270	0.493	0.540
0.6	0.4	0.051	0.079	0.139	0.195	0.312	0.428	0.368
0.4	0.4	0.047	0.065	0.149	0.239	0.312	0.306	0.223
0.2	0.4	0.074	0.098	0.205	0.271	0.312	0.237	0.191
0.0	0.4	0.112	0.139	0.261	0.298	0.251	0.177	0.182
1.0	0.2	0.014	0.033	0.042	0.056	0.102	0.307	0.433
0.8	0.2	0.028	0.037	0.061	0.074	0.130	0.274	0.279
0.6	0.2	0.028	0.047	0.075	0.121	0.181	0.271	0.186
0.4	0.2	0.023	0.028	0.065	0.093	0.186	0.144	0.102
0.2	0.2	0.037	0.037	0.088	0.130	0.167	0.093	0.084
0.0	0.2	0.047	0.075	0.149	0.177	0.149	0.075	0.047

TABLE II : EXPERIMENTAL VALUES OF PLATE BENDING MOMENTS

ASPECT RATIO = 0.333

GAGE NO.		1	2	3	4	5	6	7	8	9
α	β									
1.0	1.0	0.0	0.028	0.046	0.080	0.168	0.295	0.493	0.704	1.101
0.8	1.0	0.004	0.029	0.071	0.131	0.224	0.344	0.534	0.717	0.872
0.6	1.0	0.011	0.057	0.099	0.179	0.292	0.434	0.614	0.604	0.670
0.4	1.0	0.025	0.096	0.150	0.256	0.371	0.442	0.495	0.456	0.356
0.2	1.0	0.043	0.146	0.266	0.356	0.440	0.445	0.414	0.331	0.207
0.0	1.0	0.121	0.235	0.313	0.418	0.484	0.476	0.313	0.228	0.114
1.0	0.8	0.0	0.018	0.035	0.053	0.123	0.206	0.335	0.672	1.101
0.8	0.8	0.0	0.028	0.050	0.092	0.164	0.263	0.417	0.502	0.765
0.6	0.8	0.007	0.046	0.078	0.143	0.231	0.331	0.449	0.402	0.484
0.4	0.8	0.021	0.071	0.124	0.224	0.302	0.381	0.427	0.371	0.263
0.2	0.8	0.043	0.114	0.175	0.287	0.371	0.414	0.383	0.267	0.157
0.0	0.8	0.079	0.175	0.246	0.378	0.414	0.360	0.242	0.171	0.064
1.0	0.6	0.0	0.011	0.019	0.032	0.067	0.131	0.269	0.506	0.934
0.8	0.6	0.0	0.018	0.032	0.057	0.107	0.185	0.317	0.474	0.630
0.6	0.6	0.004	0.032	0.054	0.092	0.164	0.249	0.364	0.384	0.350
0.4	0.6	0.018	0.043	0.071	0.125	0.224	0.302	0.335	0.267	0.200
0.2	0.6	0.032	0.071	0.118	0.207	0.303	0.317	0.256	0.185	0.099
0.0	0.6	0.050	0.118	0.178	0.310	0.346	0.291	0.171	0.114	0.039
1.0	0.4	0.0	0.004	0.007	0.011	0.035	0.064	0.143	0.334	0.769
0.8	0.4	0.0	0.011	0.018	0.028	0.060	0.113	0.199	0.342	0.645
0.6	0.4	0.0	0.019	0.028	0.046	0.092	0.161	0.241	0.253	0.210
0.4	0.4	0.011	0.025	0.035	0.067	0.132	0.214	0.245	0.157	0.114
0.2	0.4	0.014	0.039	0.067	0.125	0.217	0.242	0.143	0.104	0.043
0.0	0.4	0.021	0.060	0.100	0.196	0.274	0.178	0.093	0.057	0.014
1.0	0.2	0.0	0.0	0.0	0.0	0.007	0.021	0.046	0.143	0.513
0.8	0.2	0.0	0.0	0.0	0.007	0.025	0.039	0.093	0.183	0.221
0.6	0.2	0.0	0.007	0.014	0.035	0.064	0.138	0.117	0.093	0.050
0.4	0.2	0.007	0.007	0.014	0.021	0.053	0.110	0.129	0.071	0.043
0.2	0.2	0.0	0.014	0.021	0.050	0.107	0.143	0.064	0.025	0.0
0.0	0.2	0.011	0.021	0.043	0.089	0.143	0.175	0.035	0.018	0.011

TABLE II : EXPERIMENTAL VALUES OF PLATE BENDING MOMENTS

ASPECT RATIO = 0.250

GAGE NO.	1	2	3	4	5	6	7	8	9
α	β								
1.0	1.0	0.115	0.115	0.115	0.033	0.085	0.185	0.296	0.684	1.100
0.8	1.0	0.011	0.014	0.026	0.048	0.133	0.247	0.454	0.617	0.813
0.6	1.0	0.115	0.022	0.144	0.093	0.213	0.328	0.408	0.503	0.481
0.4	1.0	0.022	0.041	0.074	0.162	0.306	0.403	0.466	0.354	0.241
0.2	1.0	0.133	0.079	0.133	0.266	0.413	0.419	0.354	0.219	0.122
0.0	1.0	0.163	0.129	0.221	0.305	0.454	0.243	0.220	0.132	0.055
1.0	0.8	0.011	0.011	0.015	0.015	0.052	0.126	0.224	0.521	1.130
0.8	0.8	0.007	0.007	0.019	0.037	0.101	0.192	0.349	0.499	0.641
0.6	0.8	0.011	0.015	0.030	0.066	0.162	0.266	0.419	0.359	0.354
0.4	0.8	0.011	0.026	0.052	0.114	0.232	0.325	0.365	0.251	0.151
0.2	0.8	0.022	0.052	0.092	0.207	0.320	0.347	0.284	0.191	0.100
0.0	0.8	0.044	0.096	0.166	0.318	0.301	0.266	0.177	0.096	0.044
1.0	0.6	0.0	0.004	0.007	0.037	0.033	0.081	0.100	0.300	0.893
0.8	0.6	0.004	0.014	0.011	0.026	0.063	0.137	0.262	0.297	0.409
0.6	0.6	0.007	0.011	0.019	0.046	0.111	0.206	0.325	0.303	0.266
0.4	0.6	0.007	0.015	0.030	0.078	0.170	0.249	0.295	0.174	0.100
0.2	0.6	0.115	0.133	0.063	0.148	0.262	0.273	0.203	0.114	0.066
0.0	0.6	0.037	0.059	0.114	0.199	0.325	0.199	0.122	0.066	0.033
1.0	0.4	0.0	0.0	0.0	0.0	0.015	0.127	0.163	0.244	0.452
0.8	0.4	0.0	0.004	0.007	0.007	0.033	0.074	0.150	0.262	0.319
0.6	0.4	0.004	0.007	0.011	0.018	0.055	0.118	0.225	0.195	0.126
0.4	0.4	0.004	0.007	0.022	0.037	0.100	0.113	0.191	0.107	0.070
0.2	0.4	0.011	0.022	0.033	0.081	0.185	0.199	0.133	0.063	0.041
0.0	0.4	0.022	0.037	0.059	0.151	0.251	0.118	0.070	0.037	0.019
1.0	0.2	0.0	0.0	0.0	0.0	0.0	0.011	0.037	0.085	0.260
0.8	0.2	0.0	0.0	0.0	0.007	0.015	0.033	0.070	0.122	0.124
0.6	0.2	0.0	0.0	0.0	0.0	0.026	0.044	0.096	0.055	0.037
0.4	0.2	0.0	0.0	0.004	0.015	0.044	0.081	0.089	0.033	0.0
0.2	0.2	0.007	0.011	0.011	0.022	0.089	0.126	0.059	0.026	0.011
0.0	0.2	0.007	0.011	0.019	0.066	0.163	0.059	0.026	0.015	0.007

TABLE II : EXPERIMENTAL VALUES OF PLATE BENDING MOMENTS

ASPECT RATIO = 0.167

GAGE NO.	1	2	3	4	5	6	7	8	9
α / β									
1.0 / 1.0	0.0	0.0	0.0	0.033	0.017	0.064	0.231	0.523	1.111
0.8 / 1.0	0.0	0.0	0.003	0.011	0.024	0.129	0.329	0.558	0.672
0.6 / 1.0	0.0	0.003	0.010	0.027	0.085	0.227	0.441	0.455	0.322
0.4 / 1.0	0.007	0.007	0.020	0.061	0.176	0.350	0.414	0.234	0.132
0.2 / 1.0	0.110	0.117	0.051	0.140	0.325	0.380	0.264	0.108	0.048
0.0 / 1.0	0.020	0.048	0.115	0.208	0.424	0.264	0.120	0.046	0.017
1.0 / 0.8	0.0	0.0	0.0	0.0	0.010	0.044	0.173	0.414	0.676
0.8 / 0.8	0.0	0.0	0.0	0.007	0.027	0.092	0.268	0.434	0.510
0.6 / 0.8	0.0	0.0	0.003	0.020	0.061	0.169	0.372	0.325	0.214
0.4 / 0.8	0.0	0.003	0.014	0.048	0.146	0.281	0.342	0.179	0.085
0.2 / 0.8	0.010	0.014	0.034	0.115	0.264	0.312	0.196	0.070	0.034
0.0 / 0.8	0.014	0.034	0.085	0.237	0.370	0.211	0.102	0.024	0.014
1.0 / 0.6	0.0	0.0	0.0	0.0	0.003	0.020	0.108	0.295	0.767
0.8 / 0.6	0.0	0.0	0.0	0.003	0.017	0.061	0.190	0.332	0.383
0.6 / 0.6	0.0	0.0	0.0	0.014	0.044	0.113	0.278	0.241	0.126
0.4 / 0.6	0.0	0.003	0.010	0.031	0.102	0.210	0.268	0.125	0.068
0.2 / 0.6	0.010	0.010	0.024	0.075	0.197	0.271	0.143	0.054	0.027
0.0 / 0.6	0.010	0.027	0.058	0.176	0.296	0.149	0.061	0.024	0.007
1.0 / 0.4	0.0	0.0	0.0	0.0	0.0	0.014	0.061	0.179	0.583
0.8 / 0.4	0.0	0.0	0.0	0.0	0.010	0.024	0.125	0.227	0.237
0.6 / 0.4	0.0	0.0	0.0	0.010	0.024	0.075	0.200	0.156	0.068
0.4 / 0.4	0.0	0.0	0.003	0.024	0.061	0.149	0.190	0.075	0.037
0.2 / 0.4	0.003	0.003	0.014	0.048	0.132	0.214	0.095	0.034	0.017
0.0 / 0.4	0.007	0.014	0.034	0.109	0.244	0.092	0.034	0.014	0.003
1.0 / 0.2	0.0	0.0	0.0	0.0	0.0	0.0	0.020	0.071	0.251
0.8 / 0.2	0.0	0.0	0.0	0.0	0.0	0.017	0.041	0.085	0.095
0.6 / 0.2	0.0	0.0	0.0	0.0	0.014	0.037	0.098	0.068	0.034
0.4 / 0.2	0.0	0.0	0.0	0.010	0.027	0.068	0.095	0.034	0.020
0.2 / 0.2	0.0	0.003	0.007	0.024	0.054	0.132	0.044	0.014	0.010
0.0 / 0.2	0.003	0.007	0.014	0.051	0.129	0.048	0.014	0.007	0.0

TABLE II : EXPERIMENTAL VALUES OF PLATE BENDING MOMENTS

ASPECT RATIO = [illegible]

GAGE NO.	1	2	3	4	5	6	7	8	9
α	β								
1.0	1.0	0.0[illegible]	0.0[illegible]	0.0[illegible]	0.0[illegible]	0.0[illegible]	0.010	0.062	0.265	0.915
0.8	1.0	0.0[illegible]	0.0[illegible]	0.0[illegible]	0.0[illegible]	0.004	0.021	0.155	0.389	0.427
0.6	1.0	0.0[illegible]	0.0[illegible]	0.0[illegible]	0.0[illegible]	0.017	0.096	0.242	0.265	0.117
0.4	1.0	0.0[illegible]	0.0[illegible]	0.0[illegible]	0.014	0.062	0.242	0.324	0.103	0.021
0.2	1.0	0.0[illegible]	0.0[illegible]	0.0[illegible]	0.048	0.221	0.324	0.131	0.021	0.004
0.0	1.0	0.0[illegible]	0.104	0.035	0.170	0.301	0.152	0.025	0.004	0.0[illegible]
1.0	0.8	0.0[illegible]	0.0[illegible]	0.0[illegible]	0.0[illegible]	0.0[illegible]	0.004	0.041	0.103	0.734
0.8	0.8	0.0[illegible]	0.0[illegible]	0.0[illegible]	0.0[illegible]	0.0[illegible]	0.021	0.128	0.311	0.321
0.6	0.8	0.0[illegible]	0.0[illegible]	0.0[illegible]	0.0[illegible]	0.014	0.070	0.276	0.2[illegible]	0.097
0.4	0.8	0.0[illegible]	0.0[illegible]	0.004	0.027	0.055	0.197	0.269	0.062	0.021
0.2	0.8	0.0[illegible]	0.0[illegible]	0.007	0.035	0.173	0.247	0.097	0.017	0.007
0.0	0.8	0.0[illegible]	0.004	0.024	0.135	0.318	0.111	0.024	0.035	0.0[illegible]
1.0	0.6	0.0[illegible]	0.0[illegible]	0.0[illegible]	0.0[illegible]	0.0[illegible]	0.0[illegible]	0.028	0.135	0.507
0.8	0.6	0.0[illegible]	0.0[illegible]	0.0[illegible]	0.0[illegible]	0.0[illegible]	0.014	0.083	0.217	0.228
0.6	0.6	0.0[illegible]	0.0[illegible]	0.0[illegible]	0.0[illegible]	0.010	0.052	0.2[illegible]	0.138	0.[illegible]
0.4	0.6	0.0[illegible]	0.0[illegible]	0.004	0.004	0.035	0.135	0.183	0.045	0.0[illegible]
0.2	0.6	0.0[illegible]	0.0[illegible]	0.0[illegible]	0.021	0.127	0.176	0.[illegible]	0.[illegible]	0.0[illegible]
0.0	0.6	0.0[illegible]	0.0[illegible]	0.0[illegible]	0.[illegible]	0.252	0.076	0.021	0.0[illegible]	0.0[illegible]
1.0	0.4	0.0[illegible]	0.0[illegible]	0.0[illegible]	0.0[illegible]	0.0[illegible]	0.0[illegible]	0.014	0.073	0.352
0.8	0.4	0.0[illegible]	0.0[illegible]	0.0[illegible]	0.0[illegible]	0.0[illegible]	0.0[illegible]	0.010	0.114	0.125
0.6	0.4	0.0[illegible]	0.0[illegible]	0.0[illegible]	0.0[illegible]	0.007	0.035	0.124	0.0[illegible]	0.0[illegible]
0.4	0.4	0.0[illegible]	0.0[illegible]	0.0[illegible]	0.004	0.021	0.07[illegible]	0.[illegible]	0.[illegible]	0.0[illegible]
0.2	0.4	0.0[illegible]	0.0[illegible]	0.004	0.010	0.076	0.0[illegible]	0.041	0.0[illegible]	0.0[illegible]
0.0	0.4	0.0[illegible]	0.0[illegible]	0.007	0.055	0.166	0.045	0.[illegible]	0.0[illegible]	0.0[illegible]
1.0	0.2	0.0[illegible]	0.0[illegible]	0.0[illegible]	0.0[illegible]	0.0[illegible]	0.0[illegible]	0.0[illegible]	0.0[illegible]	0.0[illegible]
0.8	0.2	0.0[illegible]	0.0[illegible]	0.0[illegible]	0.0[illegible]	0.0[illegible]	0.0[illegible]	0.0[illegible]	0.0[illegible]	0.0[illegible]
0.6	0.2	0.0[illegible]	0.0[illegible]	0.0[illegible]	0.0[illegible]	0.0[illegible]	0.0[illegible]	0.0[illegible]	0.0[illegible]	0.0[illegible]
0.4	0.2	0.0[illegible]	0.0[illegible]	0.0[illegible]	0.0[illegible]	0.0[illegible]	0.0[illegible]	0.0[illegible]	0.0[illegible]	0.0[illegible]
0.2	0.2	0.0[illegible]	0.0[illegible]	0.0[illegible]	0.0[illegible]	0.0[illegible]	0.0[illegible]	0.0[illegible]	0.0[illegible]	0.0[illegible]
0.0	0.2	0.0[illegible]	0.0[illegible]	0.0[illegible]	0.0[illegible]	0.0[illegible]	0.0[illegible]	0.0[illegible]	0.0[illegible]	0.0[illegible]

APPENDIX A

COMPUTER LISTING

The following listing was generated on January 20, 1970 at the University of Windsor Computer Centre on their IBM System 360/Model 40 (256K). Running time for deflection and moment information (based on a 60 term series) at 66 points, for loadings at 30 different points was about 30 minutes. This is quite a bit of time, however the number of calculations required is large, as is the total amount of information given by the program. The program consists of 12 subroutines which are called into an overlay area sequentially as they are required.

```
C IN THIS PROGRAM THE NUMBER OF TERMS USED IS SET AT 140
C THE GRID SIZE IS ALSO SET AT 6 BY 12                          A2
C TO OBTAIN MORE ACCURACY THIS PROGRAM USES DOUBLE PRECISION
C CORE AREAS ARE OVERLAYED TO MAKE ROOM FOR MORE TERMS
      DIMENSION ISP(24,24),W(140,140),A(140),MO(70),NO(70),ME(70),NE(70)
     1,BL(140).
      DOUBLE PRECISION A,W
      COMMON ISP,W,A,MO,ME,NO,NE
      P=0.3
      AB=4
      MN=60
      CALL ESTISR (ISP)
      CALL SETW (AB,P,MN)
      CALL SETM (MN)
      CALL SETA (MN)
      CALL SHIFT (MN)
      CALL SORT (MN)
      CALL ESTW (AB,MN)
      CALL ESTMXY (AB,P,MN)
      DO 1 I=1,6
      DO 1 J=2,6
      CALL SETL (I,J,BL,MN)
      CALL DETW(I,J,BL,MN)
      CALL DETM (I,J,BL,MN)
      CALL MMAX
    1 CONTINUE
      CALL EXIT
      END
```

```
      SUBROUTINE ESTISR (MSR)                                          A3
C SUBROUTINE TO ESTABLISH INTERRELATION OF INDICES
C THE NUMBER OF TERMS USED IN ISR IS ADEQUATE FOR ANY SIZE OF MATRIX CONSIDERED
      DIMENSION MSR(24,24),MD(12,24),N(24)
      DO 1 J=1,24
    1 MD(1,J)=J*(J-1)
      DO 2 I=2,12
      DO 2 J=1,24
    2 MD(I,J)=MD(I-1,J)+2*(I+J-1)
      DO 3 I=1,12
      DO 3 J=1,24
      II=2*I-1
      MSR(II,J)=MD(I,J)
    3 MSR(II+1,J)=MSR(II,J)+1
      PRINT 4
    4 FORMAT (13H1S,R TABLE IS//)
      DO 7 I=1,24
    7 N(I)=I-1
      PRINT 6,(N(I),I=1,24)
    6 FORMAT (8H M OR Q=,24I4/)
      DO 5 I=1,24
    5 N(I)=I+1
      PRINT 10
   10 FORMAT (8H N OR P=/)
      DO 8 I=1,24
    8 PRINT 9,N(I),(MSR(J,I),J=1,24)
    9 FORMAT (4X,I4,24I4)
      RETURN
      END
```

```
      SUBROUTINE SETW (S,T,MN)
C THE SIZE OF THE W MATRIX IS FIXED AT 80 SQUARE IN THIS ROUTINE
C SET UP THE INTERMEDIATE W MATRIX
      DIMENSION ISR(24,24),W(140,140)
      DOUBLE PRECISION W,R,P,T1,T2,T3,T4,T5,T6,T7,T8
      COMMON ISR,W
      R=S
      P=T
      DO 1 I=1,MN
      DO 1 J=1,I
      IS=I-1
      JS=J-1
   13 DO 2 K=1,24
      DO 2 L=1,24
      IF(ISR(K,L)-IS)2,3,2
    3 M=K-1
      N=L+1
      GO TO 4
    2 CONTINUE
    4 DO 5 K=1,24
      DO 5 L=1,24
      IF(ISR(K,L)-JS)5,6,5
    6 IQ=K-1
      IP=L+1
      GO TO 7
    5 CONTINUE
    7 IT=M+IQ
      IF(IT)15,8,15
   15 IC=IT-1
      IT=IT/2
      IC=IC/2
      IF(IT-IC)8,9,8
    9 W(I,J)=0
      GO TO 1
    8 T1=N*(N-1)*IP*(IP-1)
      T2=(N+IP-3)*(M+IQ+1)
      T3=M*(M-1)*IQ*(IQ-1)
      T4=(M+IQ-3)*(N+IP+1)
      T5=N*M*IP*IQ
      T6=(N+IP-1)*(M+IQ-1)
      T7=N*(N-1)*IQ*(IQ-1)
      T8=M*(M-1)*IP*(IP-1)
      W(I,J)=T1/T2+(R**4.)*(T3/T4)+P*P*(P*(T7+T8)+2.*(1.-P)*T5)/T6
    1 CONTINUE
      RETURN
      END
```

A4

A5

```
      SUBROUTINE SETM (MN)
C SET UP THE M MATRIX
C THE M MATRIX IS COMPUTED AND STORED IN THE W MATRIX TO CONSERVE SPACE
C THE A MATRIX IS USED AS TEMPORARY STORAGE TO SAVE SPACE
      DIMENSION ISR(24,24),W(140,140),A(140)
      DOUBLE PRECISION W,A,TOT,SQ
      COMMON ISR,W,A
      DO 20 I=1,MN
   20 A(I)=W(I,I)
      DO 1 I=1,MN
      DO 1 J=I,MN
    1 W(I,J)=0
      DO 2 I=1,MN
      IK=I-1
      DO 2 J=I,MN
      TOT=0
      DO 3 K=1,IK
    3 TOT=TOT+W(K,J)*W(K,I)
      IF(I-J)4,5,4
    5 SQ=A(I)-TOT
      IF(SQ)10,11,11
   10 M1=I-1
      M2=M1-1
      M1=M1/2
      M2=M2/2
      IF(M1-M2)14,15,14
   15 MN=I-2
      GO TO 16
   14 MN=I-1
   16 PRINT 12,MN
   12 FORMAT (23HOTHE NUMBER OF TERMS IS,I4)
      GO TO 13
   11 W(I,J)=DSQRT(SQ)
      GO TO 2
    4 W(I,J)=(W(J,I)-TOT)/W(I,I)
    2 CONTINUE
   13 PRINT 8
    8 FORMAT (16H1THE M MATRIX IS//)
      PRINT 9,((W(I,J),I=1,MN),J=1,MN)
    9 FORMAT (1X,10D13.6)
      RETURN
      END
```

A6

```
      SUBROUTINE SETA (MN)
C SET UP PRELIMINARY A MATRIX (IN R FORMAT )
C THE FORMAT OF THE A MATRIX IS FIXED BY THAT OF THE N MATRIX
      DIMENSION ISR(24,24),W(140,140),A(140)
      DOUBLE PRECISION W,A,C,TOT
      COMMON ISR,W,A
      DO 8 I=1,MN
      A(I)=W(I,I)
      DO 8 J=1,I
    8 W(I,J)=0
      DO 1 I=1,MN
      DO 1 J=1,I
      IF(I-J)2,3,2
    3 C=1
      GO TO 4
    2 C=0
    4 TOT=0
      IK=I-1
      JK=J-1
      DO 5 K=1,IK
      IF(JK-K)20,20,5
   20 TOT=TOT+W(K,J)*W(K,I)
    5 CONTINUE
      W(I,J)=(C-TOT)/A(I)
    1 CONTINUE
      DO 11 I=1,MN
      DO 11 J=I,MN
      W(I,J)=W(J,I)
      IF(I-J)12,11,12
   12 W(J,I)=0
   11 CONTINUE
      PRINT 9
    9 FORMAT (21H1A MATRIX IN R FORMAT//)
      PRINT 10,((W(I,J),I=1,MN),J=1,MN)
   10 FORMAT (1X,10D13.6)
      RETURN
      END
```

A7

```
      SUBROUTINE SHIFT (MN)
      DIMENSION ISP(24,24),W(140,140),A(140)
      DOUBLE PRECISION W,A
      COMMON ISP,W,A
      NN=MN/2+1
      MM=MN-1
      DO 1 I=2,NN
      DO 2 J=1,MN
    2 A(J)=W(J,I)
      DO 3 K=I,MM
      DO 3 J=1,MN
    3 W(J,K)=W(J,K+1)
      DO 4 J=1,MN
    4 W(J,MN)=A(J)
    1 CONTINUE
      RETURN
      END
```

A8

```
      SUBROUTINE SORT (MN)
C THIS SUBROUTINE DIVIDES THE A MATRIX AS IN THE PAPER
C THE A MATRIX IS SORTED INTO ITS ODD AND EVEN COMPONENTS
      DIMENSION ISR(24,24),W(140,140),A(140),MO(70),NO(70),ME(70),NE(70)
     1,AE(70,70),AO(70,70)
      DOUBLE PRECISION A,W
      COMMON ISR,W,A,MO,ME,NO,NE
      EQUIVALENCE (AE(1),W(1)),(AO(1),W(2451))
      MM=MN/2
      NN=MN-1
      DO 2 J=1,MM
      DO 2 I=1,NN,2
      II=I/2+1
      JJ=J
    2 AE(II,JJ)=W(I,J)
      MS=MM+1
      DO 3 I=2,MN,2
      DO 3 J=MS,MN
      II=I/2
      JJ=J-MM
    3 AO(II,JJ)=W(I,J)
      DO 4 I=1,MN
      IS=I-1
      KK=IS/2+1
      NI=MM-1
      DO 5 K=1,NI
      DO 5 L=1,NI
      IF(ISR(K,L)-IS)5,6,5
    6 IK=K-1
      IJ=L+1
      GO TO 7
    5 CONTINUE
    7 IF(IS)8,9,8
    8 IT=IS-1
      IC=IS/2
      IT=IT/2
      IF(IC-IT)9,10,9
    9 ME(KK)=IK
      NE(KK)=IJ
      GO TO 4
   10 MO(KK)=IK
      NO(KK)=IJ
    4 CONTINUE
      PRINT 11
   11 FORMAT (32H1THE EVEN AND ODD A MATRICES ARE//)
      PRINT 12,(ME(I),I=1,MM)
   12 FORMAT (4H ME=,2514/)
      PRINT 13,(NE(I),I=1,MM)
   13 FORMAT (4H NE=,2514//)
      PRINT 14
   14 FORMAT (12H EVEN MATRIX/)
      DO 30 I=1,MM
   30 PRINT 15,(AE(J,I),J=1,MM)
   15 FORMAT (1X,10E13.6)
      PRINT 16
   16 FORMAT (//)
      PRINT 17,(MO(I),I=1,MM)
   17 FORMAT (4H MO=,2514/)
```

```
      PRINT 18,(NO(I),I=1,MM)                                    A9
   18 FORMAT (4H NO=,2514//)
      PRINT 19
   19 FORMAT (11H ODD MATRIX/)
      DO 31 I=1,MM
   31 PRINT 15,(AO(J,I),J=1,MM)
      RETURN
      END
```

```
      SUBROUTINE ESTW(R,MN)
C SET UP DEFLECTION SUB MATRICES
C THE NUMBER OF GRID POINTS DETERMINE THE NUMBER OF TERMS IN THE MATRICES
      DIMENSION ISR(24,24),W(140,140),A(140),MO(70),NO(70),ME(70),NE(70)
     1,AE(70,70),AO(70,70),RE(6,6,70),RO(6,6,70),X(6),Y(6)
      DOUBLE PRECISION A,W
      COMMON ISR,W,A,MO,ME,NO,NE
      EQUIVALENCE (AE(1),W(1)),(AO(1),W(2451)),(RE(1),W(490)),(RO(1),W(
     16161)),(X(1),ISR(1)),(Y(1),ISR(7))
      MM=MN/2
      DO 1 I=1,6
      P=I-1
      X(I)=P*0.2
    1 Y(I)=P*0.2
      DO 2 I=1,MM
      DO 2 J=1,6
      DO 2 K=1,6
      TOTE=0
      TOTO=0
      DO 3 L=1,I
      IF(NO(L))20,21,20
   21 P=1
      GO TO 24
   20 IF(X(J))22,23,22
   23 P=0
      GO TO 24
   22 P=X(J)**NO(L)
   24 IF(MO(L))25,26,25
   26 Q=1
      GO TO 27
   25 IF(Y(K))28,29,28
   29 Q=0
      GO TO 27
   28 Q=Y(K)**MO(L)
   27 TOTO=TOTO+AO(L,I)*P*Q
      IF(NE(L))30,31,30
   31 P=1
      GO TO 34
   30 IF(X(J))32,33,32
   33 P=0
      GO TO 34
   32 P=X(J)**NE(L)
   34 IF(ME(L))35,36,35
   36 Q=1
      GO TO 3
   35 IF(Y(K))38,39,38
   39 Q=0
      GO TO 3
   38 Q=Y(K)**ME(L)
    3 TOTE=TOTE+AE(L,I)*P*Q
      RE(J,K,I)=TOTE*10000
    2 RO(J,K,I)=TOTO*10000
      PRINT 4,R
    4 FORMAT (38H1THE DEFLECTION SUB MATRICES FOR B/A= ,F7.2,4H ARE//)
      PRINT 5
    5 FORMAT (25H VALUES OF W,I(X,Y).10**4//)
      PRINT 6,(X(I),I=1,6),(X(I),I=1,6)
    6 FORMAT (5X,4HX/B=,6F10.1,4X,6F10.1/)
```

```
      PRINT 7                                                          All
    7 FORMAT (5H Y/A=/)
      DO 8 I=1,MM
      DO 8 J=1,6
      IF(J-1)9,10,9
   10 I1=(I-1)*2
      I2=I1+1
      PRINT 11,Y(J),I1,(PE(K,J,I),K=1,6),I2,(RO(K,J,I),K=1,6)
   11 FORMAT (1H0,F4.1,2HW,,I2,6F10.3,2HW,,I2,6F10.3)
      GO TO 8
    9 PRINT 12,Y(J),(PE(K,J,I),K=1,6),(RO(K,J,I),K=1,6)
   12 FORMAT (1X,F4.1,4X,6F10.3,4X,6F10.3)
    8 CONTINUE
      RETURN
      END
```

```
      SUBROUTINE ESTMXY (R,S,MN)                                        A12
C CALCULATE X,Y,AND XY MOMENT SUB MATRICIES
C SUB MATRICES ARE CALCULATED FOR THE GRID POINTS CHOSEN
      DIMENSION ISR(24,24),W(140,140),A(140),MO(70),NO(70),ME(70),NE(70)
     1,AE(70,70),AO(70,70),RE(6,6,70),RO(6,6,70),X(6),Y(6),ROX(6,6,70),R
     2EX(6,6,70),ROY(6,6,70),REY(6,6,70),ROXY(6,6,70),REXY(6,6,70)
      DOUBLE PRECISION A,W
      COMMON ISR,W,A,MO,ME,NO,NE
      EQUIVALENCE (AE(1),W(1)),(AO(1),W(2451)),(RE(1),W(4901)),(RO(1),W(
     16161)),(X(1),ISR(1)),(Y(1),ISR(7)),(ROX(1),W(7421)),(REX(1),W(8881
     2)),(ROY(1),W(9941)),(REY(1),W(11201)),(ROXY(1),W(12461)),(REXY(1),
     3W(13721))
      MM=MN/2
      DO 2 I=1,MM
      DO 2 J=1,6
      DO 2 K=1,6
      TOTOX=0
      TOTEX=0
      TOTOY=0
      TOTEY=0
      TOTOXY=0
      TOTEXY=0
      DO 3 L=1,I
      IF(NO(L))5,5,4
    5 P=1
      GO TO 100
    4 IF(X(J))6,7,6
    7 P=0
      GO TO 100
    6 P=X(J)**NO(L)
  100 IF(MO(L))8,8,9
    8 Q=1
      GO TO 200
    9 IF(Y(K))10,11,10
   11 Q=0
      GO TO 200
   10 Q=Y(K)**MO(L)
  200 IF(NO(L)-1)12,12,13
   12 P1=1
      GO TO 300
   13 IF(X(J))14,15,14
   15 P1=0
      GO TO 300
   14 P1=X(J)**(NO(L)-1)
  300 IF(MO(L)-1)16,16,17
   16 Q1=1
      GO TO 400
   17 IF(Y(K))18,19,18
   19 Q1=0
      GO TO 400
   18 Q1=Y(K)**(MO(L)-1)
  400 IF(NO(L)-2)20,20,21
   20 P2=1
      GO TO 500
   21 IF(X(J))22,23,22
   23 P2=0
      GO TO 500
   22 P2=X(J)**(NO(L)-2)
```

A13

```
  500 IF(MO(L)-2)24,24,25
   24 Q2=1
      GO TO 600
   25 IF(Y(K))26,27,26
   27 Q2=0
      GO TO 600
   26 Q2=Y(K)**(MO(L)-2)
  600 T1=NO(L)
      T2=NO(L)-1
      T3=MO(L)
      T4=MO(L)-1
      TOTOX=TOTOX+AO(L,I)*(T1*T2*P2*Q+S*R**P*T3*T4*P*Q2)
      TOTOY=TOTOY+AO(L,I)*(R*R*T3*T4*P*Q2+S*T1*T2*P2*Q)
      TOTOXY=TOTOXY+AO(L,I)*R*(1.-S)*T1*T3*P1*Q1
      IF(NE(L))35,35,34
   35 P=1
      GO TO 700
   34 IF(X(J))36,37,36
   37 P=0
      GO TO 700
   36 P=X(J)**NE(L)
  700 IF(ME(L))38,38,39
   38 Q=1
      GO TO 800
   39 IF(Y(K))40,41,40
   41 Q=0
      GO TO 800
   40 Q=Y(K)**ME(L)
  800 IF(NE(L)-1)42,42,43
   42 P1=1
      GO TO 900
   43 IF(X(J))44,45,44
   45 P1=0
      GO TO 900
   44 P1=X(J)**(NE(L)-1)
  900 IF(ME(L)-1)46,46,47
   46 Q1=1
      GO TO 1000
   47 IF(Y(K))48,49,48
   49 Q1=0
      GO TO 1000
   48 Q1=Y(K)**(ME(L)-1)
 1000 IF(NE(L)-2)50,50,51
   50 P2=1
      GO TO 1100
   51 IF(X(J))52,53,52
   53 P2=0
      GO TO 1100
   52 P2=X(J)**(NE(L)-2)
 1100 IF(ME(L)-2)54,54,55
   54 Q2=1
      GO TO 1200
   55 IF(Y(K))56,57,56
   57 Q2=0
      GO TO 1200
   56 Q2=Y(K)**(ME(L)-2)
 1200 T1=NE(L)
      T2=NE(L)-1
```

A14

```
      T3=ME(L)
      T4=ME(L)-1
      TOTEX=TOTEX+AE(L,I)*(T1*T2*P2*Q+S*P*P*T3*T4*P*Q2)
      TOTEY=TOTEY+AE(L,I)*(R*R*T3*T4*P*Q2+S*T1*T2*P2*Q)
      TOTEXY=TOTEXY+AE(L,I)*R*(1.-S)*T1*T3*P1*Q1
    3 CONTINUE
      ROX(J,K,I)=TOTOX
      REX(J,K,I)=TOTEX
      ROY(J,K,I)=TOTOY
      REY(J,K,I)=TOTEY
      ROXY(J,K,I)=TOTOXY
    2 REXY(J,K,I)=TOTEXY
      RETURN
      END
```

A15

```
      SUBROUTINE SETL(M,N,C,MN)
C SET UP THE WORK VECTOR
      DIMENSION ISR(24,24),W(140,140),A(140),MO(70),NO(70),ME(70),NE(70)
     1,AE(70,70),AO(70,70),RE(6,6,70),RO(6,6,70),X(6),Y(6),C(140),ERROR(
     2140)
      DOUBLE PRECISION A,W
      COMMON ISR,W,A,MO,ME,NO,NE
      EQUIVALENCE (AE(1),W(1)),(AO(1),W(2451)),(RE(1),W(490)),(RO(1),W(
     16161)),(X(1),ISR(1)),(Y(1),ISR(7))
      MM=MN/2
      DO 1 I=1,MM
      II=2*(I-1)+1
      III=II+1
      C(II)=RE(N,M,I)/10000
    1 C(III)=RO(N,M,I)/10000
C CALCULATE RELATIVE CONTRIBUTION TO SUM
      SOM=0
      DO 2 I=1,MN
      SOM=SOM+C(I)*C(I)
    2 ERROR(I)=(C(I)*C(I))/SOM
      RETURN
      END
```

```
      SUBROUTINE DETW (M,N,C,MN)
C DEFLECTIONS ARE DETERMINED AT THE POINTS SHOWN FOR THE LOADING INDICATED
C CALCULATE THE DEFLECTION MATRIX
      DIMENSION ISR(24,24),W(140,140),A(140),NO(70),NO(70),NE(70),NE(70)
     1,AE(70,70),AO(70,70),RE(6,6,70),RO(6,6,70),X(6),Y(6),C(140),D(6,11
     2),YR(11)
      DOUBLE PRECISION A,W
      COMMON ISR,W,A,MO,ME,NO,NE
      EQUIVALENCE (AE(1),W(1)),(AO(1),W(2451)),(RE(1),W(4901)),(RO(1),W(
     16161)),(X(1),ISR(1)),(Y(1),ISR(7))
      MM=MN/2
      DO 1 I=1,6
      DO 1 J=1,11
    1 D(I,J)=0
      DO 2 I=1,MM
      II=2*(I-1)+1
      DO 3 J=1,6
      DO 3 L=1,6
      K=L+5
    3 D(J,K)=D(J,K)+C(II)*RE(J,L,I)
      DO 4 J=1,6
      DO 4 L=2,6
      K=2-L
    4 D(J,K+5)=D(J,K+5)+C(II)*RE(J,L,I)
      II=II+1
      DO 5 J=1,6
      DO 5 K=1,6
      L=K+5
      MI=2-K
      D(J,L)=D(J,L)+C(II)*RO(J,K,I)
    5 D(J,MI+5)=D(J,MI+5)-C(II)*RO(J,K,I)
    2 CONTINUE
      PRINT 6,X(M),Y(M)
    6 FORMAT (27H1DEFLECTION MATRIX FOR X/B=,F4.1,8HAND Y/A=,F4.1//)
      PRINT 9,(X(I),I=1,6)
    9 FORMAT (1X,4HX/B=,6F15.1//)
      DO 10 I=1,6
      Q=I
      YR(I)=-0.2*(6.-Q)
   10 YR(I+5)=Y(I)
      PRINT 11
   11 FORMAT (5H Y/A=//)
      DO 7 I=1,11
    7 PRINT 8,YR(I),(D(J,I),J=1,6)
    8 FORMAT (1X,F4.1,6F15.8)
      RETURN
      END
```

```
      SUBROUTINE DETM (M,N,C,MN)                                        A17
C CALCULATE THE MOMENT ARRAYS
C THE MOMENTS ARE CALCULATED FOR THE LOADING CHOSEN
      DIMENSION ISR(24,24),W(140,140),A(140),MO(70),NO(70),ME(70),NE(70)
     1,AE(70,70),AO(70,70),RE(6,6,70),RO(6,6,70),X(6),Y(6),RDX(6,6,70),R
     2EX(6,6,70),RDY(6,6,70),REY(6,6,70),RDXY(6,6,70),REXY(6,6,70),C(140
     3),DX(6,11),DY(6,11),DXY(6,11),YR(11)
      DOUBLE PRECISION A,W
      COMMON ISR,W,A,MO,ME,NO,NE
      EQUIVALENCE (AE(1),W(1)),(AO(1),W(2451)),(RE(1),W(4901)),(RO(1),W(
     16161)),(X(1),ISR(1)),(Y(1),ISR(7)),(RDX(1),W(7421)),(REX(1),W(8681
     2)),(RDY(1),W(9941)),(REY(1),W(11201)),(RDXY(1),W(12461)),(REXY(1),
     3W(13721)),(DX(1),W(14981)),(DY(1),W(15014)),(DXY(1),W(15047)),(YR(
     41),W(15080))
      MM=MN/2
      DO 1 I=1,6
      DO 1 J=1,11
      DX(I,J)=0
      DY(I,J)=0
    1 DXY(I,J)=0
      DO 2 I=1,MM
      II=2*(I-1)+1
      IJ=II+1
      DO 3 J=1,6
      DO 3 L=1,6
      K=L+5
      DX(J,K)=DX(J,K)+C(II)*REX(J,L,I)
      DY(J,K)=DY(J,K)+C(II)*REY(J,L,I)
    3 DXY(J,K)=DXY(J,K)+C(IJ)*RDXY(J,L,I)
      DO 4 J=1,6
      DO 4 L=2,6
      K=2-L
      DX(J,K+5)=DX(J,K+5)+C(II)*REX(J,L,I)
      DY(J,K+5)=DY(J,K+5)+C(II)*REY(J,L,I)
    4 DXY(J,K+5)=DXY(J,K+5)+C(IJ)*RDXY(J,L,I)
      DO 5 J=1,6
      DO 5 K=1,6
      L=K+5
      MI=2-K
      DX(J,L)=DX(J,L)+C(IJ)*RDX(J,K,I)
      DX(J,MI+5)=DX(J,MI+5)-C(IJ)*RDX(J,K,I)
      DY(J,L)=DY(J,L)+C(IJ)*RDY(J,K,I)
      DY(J,MI+5)=DY(J,MI+5)-C(IJ)*RDY(J,K,I)
      DXY(J,L)=DXY(J,L)+C(II)*REXY(J,K,I)
    5 DXY(J,MI+5)=DXY(J,MI+5)-C(II)*REXY(J,K,I)
    2 CONTINUE
      PRINT 6
    6 FORMAT (29HOTHE MOMENT DISTRIBUTIONS ARE//)
      DO 8 I=1,6
      Q=I
      YR(I)=-0.2*(6.-Q)
    8 YR(I+5)=Y(I)
      PRINT 7
    7 FORMAT (10H X MOMENTS/)
      PRINT 9,(Y(I),I=1,6)
    9 FORMAT (1X,4HX/B=,6F15.1//)
      PRINT 10
   10 FORMAT(5H Y/A=//)
```

A18

```
      DO 11 I=1,11
   11 PRINT 12,YR(I),(DX(J,I),J=1,6)
   12 FORMAT(1X,F4.1,6E15.8)
      PRINT 13
   13 FORMAT (10H Y MOMENTS/)
      PRINT 9,(X(I),I=1,6)
      PRINT 10
      DO 14 I=1,11
   14 PRINT 12,YR(I),(DY(J,I),J=1,6)
      PRINT 15
   15 FORMAT (11H XY MOMENTS/)
      PRINT 9,(X(I),I=1,6)
      PRINT 10
      DO 16 I=1,11
   16 PRINT 12,YR(I),(DXY(J,I),J=1,6)
      RETURN
      END
```

```
      SUBROUTINE MMAX
      DIMENSION ISR(24,24),W(140,140),A(140),MC(70),MD(70),ME(70),MF(70)
     1,AE(70,70),AO(70,70),BE(6,6,70),BO(6,6,70),X(6),Y(6),BOX(6,6,70),B
     2EX(6,6,70),BOY(6,6,70),BEY(6,6,70),BOXY(6,6,70),BEXY(6,6,70),C(140
     3),DX(6,11),DY(6,11),DXY(6,11),YR(11),DM1(6,11),DM2(6,11),DM3(6,11)
     4,TH(6,11)
      DOUBLE PRECISION A,W
      COMMON ISR,W,A,MD,ME,MC,MF
      EQUIVALENCE (AE(1),W(1)),(AO(1),W(2451)),(BE(1),W(4901)),(BO(1),W(
     16161)),(X(1),ISR(1)),(Y(1),ISR(7)),(BOX(1),W(7421)),(BEX(1),W(8681
     2)),(BOY(1),W(9941)),(BEY(1),W(11201)),(BOXY(1),W(12461)),(BEXY(1),
     3W(13721)),(DX(1),W(14981)),(DY(1),W(15014)),(DXY(1),W(15047)),(YR(
     41),W(15080))
      DO 1 I=1,6
      DO 1 J=1,11
      T1=(DX(I,J)+DY(I,J))/2.
      XX=(DX(I,J)-DY(I,J))/2.
      T2=SQRT(XX*XX+DXY(I,J)*DXY(I,J))
      DM1(I,J)=T1+T2
      DM2(I,J)=T1-T2
      DM3(I,J)=T2
      TH(I,J)=(ATAN(DXY(I,J)/(DX(I,J)-T1))/2.)*180./3.14159
    1 CONTINUE
      PRINT 2
    2 FORMAT (22H PRINCIPAL MOMENTS ARE//)
      PRINT 3
    3 FORMAT (6H M MAX/)
      PRINT 4,(X(I),I=1,6)
    4 FORMAT (1X,4HX/B=,6F15.1//)
      PRINT 8
    8 FORMAT (5H Y/A=//)
      DO 5 I=1,11
    5 PRINT 6,YR(I),(DM1(J,I),J=1,6)
      PRINT 7
    6 FORMAT (1X,F4.1,6E15.8)
    7 FORMAT (6H M MIN//)
      PRINT 4,(X(I),I=1,6)
      PRINT 8
      DO 9 I=1,11
    9 PRINT 6,YR(I),(DM2(J,I),J=1,6)
      PRINT 10
   10 FORMAT (6H T MAX//)
      PRINT 4,(X(I),I=1,6)
      PRINT 8
      DO 11 I=1,11
   11 PRINT 6,YR(I),(DM3(J,I),J=1,6)
      PRINT 12
   12 FORMAT (16H ANGLE TO X AXIS//)
      PRINT 4,(X(I),I=1,6)
      PRINT 8
      DO 13 I=1,11
   13 PRINT 14,YR(I),(TH(J,I),J=1,6)
   14 FORMAT (1X,F4.1,6F15.3)
      RETURN
      END
```

APPENDIX B

MATERIAL PROPERTIES

In order to determine the material properties, it was decided to test four tension specimens cut from the plate from which the test plates were cut. Figure 85 shows how these were cut; the tension samples being cut from material surrounding the test plates. The specimens meet the standard ASTM E8-61T for tension specimens; this means they are 18 inches long and approximately $1\frac{1}{2}$ inches wide. To insure that the material is isotropic (or to determine if it is anisotropic) two samples were cut in the rolling direction of the plate (numbers 1 and 2) and two were cut at right angles to this (numbers 3 and 4). The rolling direction was determined from visible markings in the scale on the plate.

In order to determine both modulus (E) and Poisson's ratio (ν) it is necessary to have a two element gage; as well to eliminate any error due to gage alignment it was decided to use a three element rectangular rosette. The three element rosette will allow the accurate determination of the principal strains, from which the modulus and Poisson's ratio can be determined. Also, since the specimens may not be perfectly straight, gages were mounted on both sides of the specimens to nullify any bending effects due to specimen curvatures. This procedure and the need for it is outlined in a paper by Smith and Chapel (32). The specimens were tension tested on a Tinius Olsen, 120,000 pound capacity

Universal Testing Machine. Strain readings were taken at 2,000 pound intervals after the specimen had been cycled 5 times to 7,500 pounds, to remove any gage hysterises effects. The maximum load reached was 12,000 pounds since all specimens showed signs of yield before this point was reached. The gages were connected to a Budd P-350 strain indicator through a Model SB-1 switch and balance unit. This allowed the six gages on any specimen to be read out sequentially at any load held on the testing machine.

Once the rosette strains were available, the principal strains were calculated using the method outlined by Dally and Riley (33). The principal strains were then averaged across the two sides of the test specimen - this has the effect of cancelling bending moments. The largest principal strain was then plotted against stress (calculated from load and cross sectional area) for the four specimens. This plot is shown in Figure 86 , and it can be seen that the last set of readings show signs of yielding. These readings were then discarded while the remaining values were used to calculate the line of best fit for each specimen to determine its modulus. Also, the line of best fit was calculated for the minimum principal strain; this value was used to calculate Poisson's Ratio for each specimen. The resulting values of E, and are listed in the following table:

Specimen No.	Dir'n	Modulus (psi)	ν
1	‖	30.4×10^6	0.277
2	‖	30.3×10^6	0.274
3	=	29.7×10^6	0.274
4	=	30.2×10^6	0.280

The variation in modulus shown is a maximum of 2% with three of the values within $\frac{1}{2}$%, while the Poisson's ratio variations are all within 2%. These variations can be expected since the gage factor on the gages is only $\pm$ 1% and reading errors could easily account for a 1% error as well. It seems, therefore, that the samples cut from the two directions are equivalent and the material is isotropic (at least in the plane of the plate which contains the directions of interest). The modulus and Poisson's ratio used were then the average values of the 4 specimens tested; these were: $E = 30.1 \times 10^6$ psi and $\nu = 0.276$. When these values are used with the plate thickness of 0.257 inches, we obtain the plate stiffness (D) as

$$D = \frac{E h^3}{12 (1 - \nu^2)} = 4.62 \times 10^4 \text{ lb - in.}$$

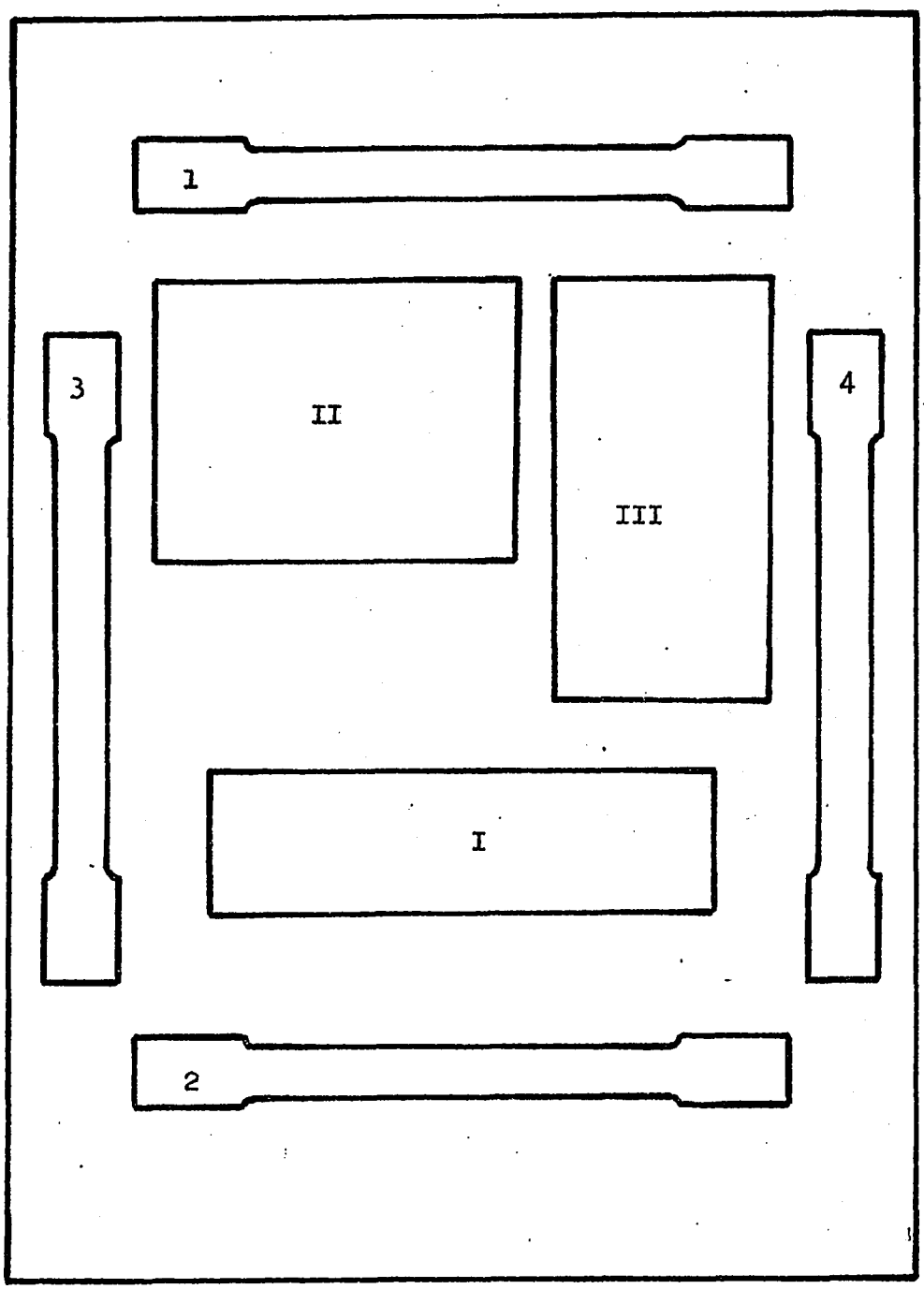

Fig.85 : Specimen Cutting Scheme

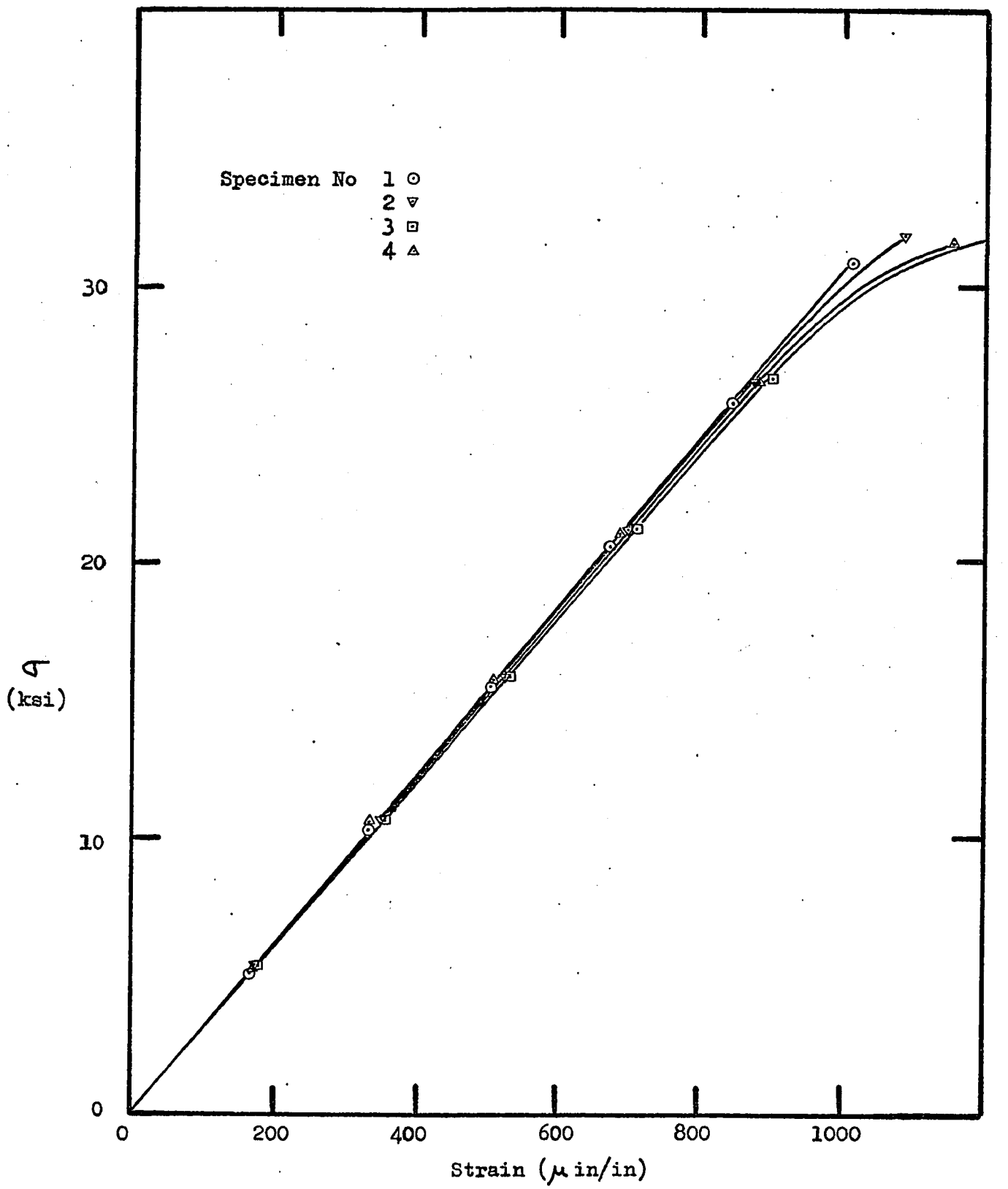

Fig. 86 : Stress vs Strain, Tension Tests

C. Holographic Table and Equipment

The holographic table is shown in Figure 7 with all of the elements in the position that they were used. The table itself was originally a cast iron machine base which was donated to the University of Windsor by Ford Motor Company of Canada when they closed out their testing facility in Windsor. It weighs approximately 3200 lbs. and has slots machined in its surface which are suitable for the clamping of components. The large mass of the table is important in providing isolation from vibration. The machine base also has the advantage that its working surface is relatively large; being approximately 5 feet square, allowing a great deal of versatility in experimental arrangement.

The need for special concern in building a hologram table arises due to the extreme amount of stability required in making holograms. During the exposure of a hologram, all of the elements must remain in the same relation within a fraction of a wavelength of light (24.9×10^{-6} inches for the present experiment). Rogers (34) states that the maximum vibration allowed within the plate exposure time is 1/8 of a wavelength which corresponds to about 3 micro inches. This limitation is for a high quality reconstruction, while some degradation is allowable in most experiments. Stability of this type is difficult to attain since building floors usually vibrate and therefore act as a forcing function on the table. The floor in the lab where our table is located is vibrating at approximately 30 cycles per second. This frequency is probably excited by electrical machinery in the building. There are, however, transient vibrations of lower frequency whose origin is unknown.

When the table was first set up in the lab, it was placed on four legs consisting of three layers of concrete blocks and 8 inches of styrofoam (16" by 16" square). The styrofoam was topped by a $\frac{1}{2}$ inch thick steel plate of the same size which was bolted to the bottom of the table. This plate distributed the load on the styrofoam so that the maximum pressure was about 4 psi, which is well below the yield point or creep limit of styrofoam. The static deflection under load of the styrofoam was about 0.10 inches, which results in about 60% isolation from the 30 cps floor vibration. In the summer of 1969, low angle transmission holograms were made on this table but their quality was poor. The support system finally employed is shown in Figure 87; the main change being the insertion of "AEON" hollow rubber springs. These springs were obtained from Go Tract Systems Limited, Quebec, Canada, and are Model No. 535/65. Under the load of the table (800 pounds per leg), the springs deflect approximately 1.0 inches which results in about 97% isolation from the floor excitation. These springs have a further advantage in that they have considerable hysterisis losses, resulting in significant damping of vibrations. Holograms made on this table, after the installation of these springs, showed that acceptable reflection holograms could be made of a quality suitable for multiple exposure or live fringe hologram interferometry.

Another element which required a considerable amount of special attention is the plate holder (shown in Figure 7) which is designed so that the plate can be repositioned to within 1/8 wave length in all three directions (as well as all three possible rotations).

This was done by positioning the glass plate back and edges against steel pins and holding it in place with powerful springs during the exposure. When the film is developed and replaced in the holder, it is possible to rposition it within the specified tolerance. This technique was suggested to us by T. Allan when he visited the University in the spring of 1969.

Another element requiring special concern is the holder used for holding the mirrors and the spatial filter. The holders are made from a $3\frac{1}{2}$ inch diameter steel bar and weight about 20 lbs. The base of the holder is machined to allow only 3 points to rest on the table, thereby preventing any rocking of the holder due to irregularities in the table surface.

Fig. 87 : Holographic Table Support, Showing Rubber Springs, Steel Plate, and Styrefoam.

D. Plate Clamping Arrangement

There were three primary objectives in designing the plate clamping jig; they are:

1) rigidity of the clamped edge
2) versatility of loading and holding different size plates
3) mass - for stability during the holographic part of the experiment.

The design arrived at for the plate loading system is shown in Figure 88 . It basically consists of 4 parts; the base plate the rear bearing block, the front bearing block, and the loading tower. The base plate is a 14 inch square by 1 inch thick plate of low carbon steel which as been surface ground on both sides. All of the other components are bolted to this plate, which can also be clamped to the table, to prevent movement during the holographic phase of the investigation. The rear bearing block is also low carbon steel which has been surface ground on all sides. It is 12" x 6" by 2 inches thick, and is bolted to the base plate by 14, $\frac{1}{2}$ inch socket head bolts in two rows of 7 each. These two parts are never disassembled, and the bolts are torqued down as tight as possible. The front bearing block is also low carbon steel, surface ground on all sides, being 12" x 3" by 2 inches thick. As can be seen in the figure, it is bolted to both the base plate and the rear bearing block. There are 5 bolts going through the plate to the rear bearing block and 6 bolts holding the front bearing block to the base plate. The plate is held in a vertical position, being clamped at its base. There is two inches of the plate clamped in the fixture, which should result in a satisfactory end condition.

When a plate is placed in the holder, the bolts holding the two bearing blocks together are tightened first. This ensures that the plate is clamped along its whole length. Then the rigidity of the system is improved by bolting the front bearing block to the base plate.

The total weight of the plate holder was 135 lbs., making it difficult to move but very stable. As well, it was clamped to the table to prevent movements during the deflection analysis of the plates.

The loads were applied using a pulley and tower arrangement as shown in Figure 87. The tower has holes on $\frac{1}{2}$ inch centres so that loads can be applied at any height, with an essentially horizontal pull; in fact the maximum error can be expressed as:

$$\Delta P = P\left(1 - \frac{10}{100 + .0625}\right) = 0.0003P \qquad \ldots (D.1)$$

which means there is an error in the load of 0.03% which is negligible. As well, the tower can be moved horizontally and bolted at 1 inch centres; this allows an error which can be expressed as:

$$\Delta P = P\left(1 - \frac{10}{100 + 0.25}\right) = 0.0012\ P \qquad \ldots (D.2)$$

which indicates an error in the load of 0.12%. The maximum loading error can be both of these simultaneously, which gives:

$$\Delta P_{max} = \left\{(1.0003 \times 1.2212) - 1\right\}\ P = 0.0015\ P \qquad \ldots (D.3)$$

or a maximum error of 0.15% which can be safely neglected.

The loads are applied using a U shaped member which is shown in Figure 87. Actually, there are two such members available, one with a 2" clear throat and one with a 6" clear throat. These are used to transfer the load from the rear of the plate to its

front (i. e: hologram side). The actual load is applied by a 1/8" diameter hardened steel ball, pressed into the loading member. It is assumed that this can result in a satisfactory approximation of a point load.

A Point of concern in the overall loading scheme being used here is the friction loss in the pulley used in the loading tower. It is obvious that some loss must exist, and that it is likely significant. It is also likely that the loss is somewhat load dependent. Since there are two major loading ranges involved, it is necessary to consider them separately. With the loads used in the holographic portion of the study, no appreciable friction loss could be determined using a 10 lb. (maximum load) load cell. However, the loads used in the bending moment determination, being much higher (20 x in fact) resulted in a measured friction loss of 5.0 lbs. This factor was of course considered in computing the plate moments.

Fig. 88 : Plate Clamping Jig Shown on Holographic Table, as Used in Experimental Work

VITA

1944 Born in Stekene, Belgium

1967 Received the Degree of Bachelor of Applied Science in Mechanical Engineering from the University of Windsor, Windsor, Ontario.

1969 Received the Degree of Master of Applied Science in Mechanical Engineering from the University of Windsor, Windsor, Ontario.

1971 Presently a Candidate for the Degree of Doctor of Philosophy in Mechanical Engineering at the University of Windsor, Windsor, Ontario.